

THE UNIVERSITY OF OKLAHOMA
GRADUATE COLLEGE

SOLUBILIZATION OF OIL MIXTURES IN ANIONIC SURFACTANT
MICROEMULSIONS

A DISSERTATION
SUBMITTED TO THE GRADUATE FACULTY
In partial fulfillment of the requirements for the
Degree of
Doctor of Philosophy

By
ERIKA SZEKERES
Norman, Oklahoma

2004

UMI Number: 3126141

INFORMATION TO USERS

The quality of this reproduction is dependent upon the quality of the copy submitted. Broken or indistinct print, colored or poor quality illustrations and photographs, print bleed-through, substandard margins, and improper alignment can adversely affect reproduction.

In the unlikely event that the author did not send a complete manuscript and there are missing pages, these will be noted. Also, if unauthorized copyright material had to be removed, a note will indicate the deletion.

UMI[®]

UMI Microform 3126141

Copyright 2004 by ProQuest Information and Learning Company.

All rights reserved. This microform edition is protected against unauthorized copying under Title 17, United States Code.

ProQuest Information and Learning Company
300 North Zeeb Road
P.O. Box 1346
Ann Arbor, MI 48106-1346

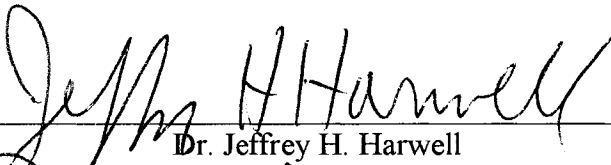
© Copyright by ERIKA SZEKERES 2004

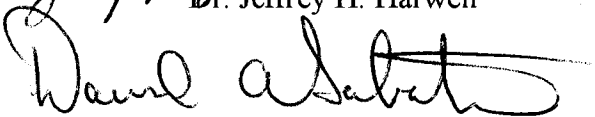
All Rights Reserved

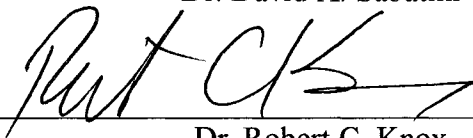
SOLUBILIZATION OF OIL MIXTURES IN ANIONIC SURFACTANT
MICROEMULSIONS

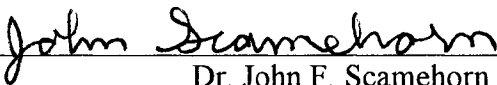
A Dissertation APPROVED FOR THE
SCHOOL OF CHEMICAL ENGINEERING AND MATERIALS SCIENCE

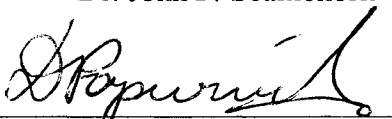
By


Dr. Jeffrey H. Harwell


Dr. David A. Sabatini


Dr. Robert C. Knox


Dr. John F. Scamehorn


Dr. Dimitrios V. Papavassiliou

ACKNOWLEDGEMENT

I wish to express my deepest gratitude and appreciation to my supervisor, Dr. Jeffrey H. Harwell. He has been one of the most supportive people throughout my graduate studies. I would like to thank for his attention, continuous encouragement, and time. His inspiring insights, knowledge, and advice has always provided guidance in my research. I feel very fortunate to have the opportunity to work with him. Without his thoughtful suggestions and support this work could not have been completed.

I would also like to thank Dr. David A. Sabatini for his guidance. He has always been available for discussions of research my results or ideas. I learned from him the skills of a good researcher; planning, carry out, and evaluating experiments, while keeping in mind the big picture. His role was not strictly limited to help in research. He provided a model of a good, “complete” human being. He is a dedicated teacher, a mentor, whose guidance and active involvement has been invaluable.

I also want to thank the help I got from Dr. Robert Knox, my coadvisor for his support and guidance especially at the beginning of my research. I also extend my appreciation to the other members on my committee. Dr. John F. Scamehorn has always been available when I asked for his advice, and was always very supportive, for which I would like to express my special gratitude. I would like to thank Dr. Papavassiliou as well for his time serving on my committee, advice and assistance in completion of this dissertation.

My fellow graduate students, including Edgar Acosta, Twan Doan, Daniel H. Gallo, Anand Upadhyaya, Anuradee Witthayapanyanon also deserve special

acknowledgement for their friendship and encouragement. Working together with them made the atmosphere in the lab fun and enjoyable. My special thanks goes to Edgar for his tremendous help with the experiments, for the stimulating discussions and ideas. In addition, I want to acknowledge the friendship and support from Marjory Rivas and Hose Soto that helped me go through the beginning years of graduate school.

The staff of CEMS and CEES were always kind and helpful. I extend my appreciation to all the staff members.

Finally, my sincerest gratitude is to my husband Dr. Zoltan Laszik for his love, constant encouragement, understanding, and help, which will always be treasured. His confidence gave me strength to complete this work. My gratitude is also to our children, Nandor, Laura, and Aron who make my life complete. I am grateful for the love and encouragement that I received from my family; my parents, Szollosi Maria, and Szekeres Laszlo, and my sister, Szekeres Marta.

TABLE OF CONTENTS

ACKNOWLEDGEMENT.....	IV
TABLE OF CONTENTS	VI
LIST OF TABLES	XII
LIST OF FIGURES	XIII
ABSTRACT.....	XX
CHAPTER 1	1
INTRODUCTION.....	1
REFERENCES.....	8
CHAPTER 2.....	10
THE IMPACT OF ACETONE ON THE SURFACTANT ENHANCED REMEDICATION OF OIL CONTAMINATED AQUIFERS	10
ABSTRACT	10
INTRODUCTION	10
BACKGROUND	12
<i>Phase behavior of oil/water/surfactant system.</i>	12
<i>Surfactant formulations for oil mixtures and polar solvents.</i>	14
MATERIALS AND METHODS.....	17
RESULTS AND DISCUSSION.....	19
<i>Partitioning of acetone and TCE into water in the absence of surfactant.</i>	19
<i>Effect of acetone on the phase behavior.</i>	20
<i>Effect of the electrolyte concentration on the acetone and TCE solubilization.</i>	22
<i>Solubilization of acetone and TCE with changing acetone concentration.</i>	23
<i>Effect of acetone on the surfactant partitioning between the oil and water phases.</i>	26
<i>Interfacial tension studies.</i>	26
IMPLICATIONS FOR REMEDIATION	30
REFERENCES.....	32
FIGURES	35

CHAPTER 3	45
A TWO-STATE MODEL FOR SELECTIVE SOLUBILIZATION OF BENZENE-LIMONENE MIXTURE IN SODIUM DIHEXYL SULFOSUCCINATE MICROEMULSION.....	45
ABSTRACT	45
INTRODUCTION	45
MATERIALS AND METHODS.....	50
MODEL DEVELOPMENT	51
<i>Relationship between the formulation variables and the curvature.....</i>	<i>53</i>
Net-average curvature model for single-component oil.	53
Oil mixtures.	56
<i>Curvature and selectivity relationship.</i>	<i>57</i>
Surface excess model.....	57
Selectivity.....	62
<i>Solution method.....</i>	<i>62</i>
RESULTS AND DISCUSSION.....	64
<i>Optimum salinity and characteristic length.</i>	<i>64</i>
<i>Benzene surface excess.....</i>	<i>65</i>
<i>Selectivity dependence on salinity.....</i>	<i>67</i>
<i>Selectivity dependence on the oil composition.....</i>	<i>70</i>
REFERENCES	72
TABLES	75
FIGURES.....	76
CHAPTER 4	84
PREFERENTIAL SOLUBILIZATION OF DODECANOL FROM DODECANOL-LIMONENE BINARY OIL MIXTURE IN SODIUM DIHEXYL SULFOSUCCINATE MICROEMULSIONS: EFFECT ON OPTIMUM SALINITY AND OIL SOLUBILIZATION CAPACITY	84
ABSTRACT	84
INTRODUCTION	84
BACKGROUND	86
THEORY.....	91
<i>Pseudocomponent assumption.</i>	<i>91</i>
<i>Optimum salinity.</i>	<i>92</i>
<i>Characteristic length.....</i>	<i>94</i>
MATERIALS AND METHODS.....	96
RESULTS AND DISCUSSION.....	97
<i>Pseudocomponent assumption.</i>	<i>97</i>
<i>Surface excess adsorption.</i>	<i>99</i>
<i>Oil solubilization in the low dodecanol concentration range.</i>	<i>101</i>
Surface solubilization.....	101
Core solubilization.....	103
Characteristic length.....	105

Optimum salinity.....	107
<i>Behavior at high dodecanol concentrations</i>	111
Wetting / non-wetting transition.....	111
Disappearance of the three-phase body.....	112
Surfactant partitioning.....	113
Interfacial tension.....	114
CONCLUSIONS.....	115
REFERENCES.....	118
TABLES.....	122
FIGURES.....	124
CHAPTER 5.....	138
MODELING SOLUBILIZATION OF OIL MIXTURES IN ANIONIC MICROEMULSIONS II: MIXTURES OF NON-POLAR AND POLAR OIL COMPONENTS.....	138
ABSTRACT.....	138
INTRODUCTION.....	138
BACKGROUND AND MODEL DEVELOPMENT.....	143
<i>Model description</i>	143
<i>Net-average curvature model</i>	145
<i>Adsorption isotherm</i>	146
<i>Characteristic length model</i>	150
<i>Optimum salinity model</i>	152
<i>Solution method</i>	154
EXPERIMENTAL SECTION.....	157
RESULTS AND DISCUSSION.....	157
<i>Total oil solubilization by the microemulsion</i>	158
<i>Composition of the solubilized oil</i>	161
<i>Excess oil phase composition</i>	163
<i>Selectivity</i>	164
CONCLUSIONS.....	165
REFERENCES.....	167
TABLES.....	170
FIGURES.....	171
CHAPTER 6.....	180
FUTURE RESEARCH.....	180
MATHEMATICAL MODELING OF SOLUBILIZATION OF ACETONE-TCE MIXTURE....	180
CONNECTION BETWEEN THE DIFFERENT OPTIMUM SALINITY AND CHARACTERISTIC LENGTH MODELS USED FOR BENZENE-LIMONENE AND FOR DODECANOL-LIMONENE MIXTURES.....	184
DEPENDENCE OF THE SHELL THICKNESS ON THE ELECTROLYTE CONCENTRATION.....	186
ADSORPTION ISOTHERMS.....	187

RELATIONSHIP BETWEEN THE OPTIMUM SALINITY AND THE CHARACTERISTIC LENGTH AT OPTIMUM.....	188
MIXTURES OF TWO PALISADE LAYER PENETRATING OILS.....	192
SELECTIVE SOLUBILIZATION – COLUMN STUDIES.....	193
FIGURES.....	198
CHAPTER 7.....	210
CONCLUSIONS.....	210
APPENDIX A.....	215
CALCULATION OF THE SHELL THICKNESS FROM SOLUBILIZATION DATA.....	215
APPENDIX B.....	218
EXAMPLE MATHCAD PROGRAM TO CALCULATE BENZENE-LIMONENE MIXTURE SOLUBILIZATION.....	218
APPENDIX C.....	232
GENERAL MATHACAD PROGRAM TO CALCULATE DODECANOL-LIMONENE MIXTURE SOLUBILIZATION.....	232
APPENDIX D.....	244
EXAMPLE MATHCAD PROGRAM TO CALCULATE DODECANOL-LIMONENE MIXTURE SOLUBILIZATION AS A FUNCTION OF SALINITY.....	244
APPENDIX E.....	256
EXAMPLE MATHCAD PROGRAM TO CALCULATE DODECANOL-LIMONENE MIXTURE SOLUBILIZATION AS A FUNCTION OF OIL COMPOSITION.....	256

APPENDIX F.....	273
ACETONE-TCE MIXTURE EXPERIMENTAL DATA.....	273
APPENDIX G.....	277
BENZENE-LIMONENE MIXTURE EXPERIMENTAL DATA.....	277
APPENDIX H.....	283
DODECANOL-LIMONENE MIXTURE EXPERIMENTAL DATA.....	283
APPENDIX I	288
BENZENE-LIMONENE COLUMN STUDY EXPERIMENTAL DATA	288

LIST OF TABLES

Chapter 3

Table 1. Selected parameters of chemicals used in the benzene-limonene experiments.75

Chapter 4

Table 1. Selected properties of the materials used in the dodecanol-limonene experiments..... 122

Table 2. Experimental optimum salinity, middle phase characteristic length, and shell thickness values for different initial dodecanol volume fractions. * Shell thickness values are for $R > 10$ Angstroms. 123

Chapter 5

Table 1. Input data and parameters used in model calculations for dodecanol-limonene mixture..... 170

LIST OF FIGURES

Chapter 1

Figure 1. Molecular structure of d-limonene6

Chapter 2

Figure 1. Partitioning of acetone and TCE in water/TCE/acetone mixture. The volume fraction of water, which is kept constant, is 0.5. Note: 100,000 ppm acetone concentration corresponds to 1.36 mole/liter, and 100,000 ppm TCE concentration corresponds to 1.11 mole/liter.35

Figure 2. Variation of experimental and effective optimum salinity as a function of the initial acetone concentration in the oil. Experimental optimum salinity corresponds to the salinity of the aqueous surfactant solution before contacting with the oil phase, effective optimum salinity is calculated from the average experimental salinity accounting for the dilution of the water pseudo-phase due to acetone partitioning.36

Figure 3.a. Concentration of TCE and acetone in the aqueous surfactant solution as a function of NaCl concentration. The initial acetone concentration in the oil phase was 5 vol. %.37

Figure 3.b. Acetone concentration in the various coexisting phases as a function of salinity. The initial acetone concentration was 5 vol. % in the oil.38

Figure 4. a. Concentration of acetone and TCE in the aqueous surfactant phase as a function of the acetone concentration in the excess oil phase. The salinity was kept constant, 0.89 wt%.....	39
Figure 4. b. Solubilization parameter (SP), and micelle/water partition coefficient (Km) for TCE as a function of the acetone concentration in the excess oil phase. The salinity was constant, 0.89 wt%.	40
Figure 5. Surfactant concentration in the microemulsion phase and excess oil phase as a function of acetone concentration in the oil phase.	41
Figure 6. Variation of the oil/water interfacial tension as a function of the surfactant concentration (AMA).	42
Figure 7. Area per surfactant molecule at the oil/water interface as a function of acetone concentration measured in the excess oil phase.	43
Figure 8. Variation of the specific conductivity as a function of surfactant concentration in acetone free and acetone containing (12.5 % in the oil phase at equilibrium) samples.	44

Chapter 3

Figure 1. Schematic representations of oil solubilizing micelle, and model concept.	76
Figure 2. Optimum salinity and persistence length variation with bulk oil phase composition.	77
Figure 3. Experimental shell thickness variation with salinity for 0.19 volume fraction benzene concentration in bulk oil, optimum salinity 4.4.....	78
Figure 4. Experimental and fitted shell thickness variation with oil phase composition.	78

Figure 5. a. Selectivity dependence on the salinity. Results of four different bulk oil compositions are plotted.....79

Figure 5. b. Dependence of the surface area to volume ratio of the solubilized oil on the salinity. Four different benzene bulk oil volume fractions are plotted.....80

Figure 6. Selectivity plotted with respect to $\ln\left(\frac{S^*}{S}\right)$. Salinity scan data of four different bulk oil benzene volume fractions are included.81

Figure 7. Selectivity dependence on salinity as predicted by the model for seven oil compositions. Corresponding data are also plotted to compare with model..82

Figure 8. a. Selectivity dependence on the oil phase composition. Data and model correspond to no added salt case.83

Figure 8. b. Effect of oil phase composition on the surface area to volume ratio of the solubilized oil. Experimental results are shown for the no added salt case.....83

Chapter 4

Figure 1. a. Average dodecanol volume fraction (C_{ave}) in the solubilized oil, b. Selectivity as a function of bulk oil phase dodecanol volume fraction (C_{bulk}).
..... 124

Figure 2. a. Average dodecanol volume fraction in the solubilized oil versus $(S^*-S)/S^*$, which is a normalized salinity scale, b. selectivity as a function of salinity. Results for different initial bulk dodecanol volume fraction (C_{dode}) in the oil mixture are shown. 125

Figure 3. Shell thickness (d) variation with respect to bulk oil dodecanol volume fraction (C_{bulk}). Data and Langmuir model (fitted) are shown for the no added salt

series, and at higher salinity, where the oil droplet radii were larger than 10 Angstroms.....126

Figure 4. a. Shell thickness (d) variation as a function of salinity, b. shell thickness variation as a function of the oil radius (R). Results of five different initial dodecanol concentrations are presented.127

Figure 5. a. Variation of oil droplet radius as a function of the dodecanol volume fraction in the bulk oil phase (C bulk), b. variation of the total solubilized oil volume and the solubilized oil volume due to the surface solubilization as a function of the dodecanol volume fraction in the bulk oil phase (C bulk). Data with no added salt series are shown.....128

Figure 6. Variation of oil droplet radius as a function of the salinity. Data of five different initial dodecanol volume fractions (C dode) are shown, b. variation of the total solubilized oil volume and the solubilized oil volume due to the surface solubilization as a function salinity. Data of C dode =0.044 initial dodecanol volume fraction series are shown.129

Figure 7. Characteristic length variation in middle phase microemulsion as a function of dodecanol volume fraction in the bulk oil phase (C bulk). Data points calculated from middle phase solubilization results, and the model predictions based on Eq. [20], [22], and [14] are plotted together.....130

Figure 8. Bending rigidity κ (denoted as k eff) variation with respect to the dimensionless adsorption density $\sigma \cdot (R_a^2 + R_b^2)$, denoted as sigma (Ra^2+Rb^2). The bending rigidity is in $k_B T$ units. Data points are fitted with a linear line. The slope of the fitting line is 0.208.....131

Figure 9. a. Variation of the mean curvature (H) as a function of σ/κ (denoted as σ/k_{eff}) at three different salinities, b. variation of the dimensionless curvature with respect to $\xi \cdot \sigma/\kappa$, denoted as $\kappa \cdot \sigma/k_{eff}$. Symbols represent data points calculated from oil solubilization results, linear fitting lines are shown to guide the eye..... 132

Figure 10. a. Variation of the optimum salinity log with respect to the experimental mean curvature, b. variation of the optimum salinity log as a function of the dimensionless curvature. Linear lines are shown only to guide the eye. Results at three different salinities are presented. 133

Figure 11. a. Optimum salinity variation as a function of the oil phase composition (C bulk). Experimentally determined data and model predictions using Eq. [28] are plotted together; b. Variation of the hypothetical dodecanol EACN as a function of the dodecanol mole fraction in the initial oil mixture. Hypothetical EACN values are calculated by using experimental optimum salinities and initial oil phase compositions in Eqs. [2] and [3]...... 134

Figure 12. Variation of the lower critical salinity and the optimum salinity as a function of the dodecanol volume fraction (C bulk) in the bulk oil phase 135

Figure 13. Interfacial tension (IFT) and aqueous phase surfactant concentration (C surf) as a function of the dodecanol volume fraction in the bulk oil phase. 136

Figure 14. Experimental shell thickness (d) and scaled oil solubilization (C oil / C surf) in the aqueous phase as a function of the dodecanol volume fraction in the bulk oil. The scaled oil solubilization is the ratio of the volumetric oil concentration and the surfactant concentration in the microemulsion in ppm..... 137

Chapter 5

- Figure 1. Schematic of the modified pseudo-phase model. 171
- Figure 2. Dependence of the total oil solubilization on the salinity at a fixed initial dodecanol concentration. Experimental data and model predictions are plotted together for six different initial dodecanol concentrations. 172
- Figure 3. Dependence of the total oil solubilization on the initial dodecanol volume fraction in the oil phase at no added salt 173
- Figure 5. Average volume fraction of the dodecanol in the total solubilized oil (C_{ave}) as a function of the initial dodecanol concentration in the oil phase at no added salt. 175
- Figure 6. Variation of the excess oil phase composition (C_{bulk}) as a function of the salinity. The excess oil phase composition is plotted in normalized form, where the basis of the normalization is the initial dodecanol volume fraction in the oil phase. The salinity is normalized by the optimum salinity. Results for five different initial dodecanol concentrations are shown 176
- Figure 7. Variation of the excess oil phase composition (C_{bulk}) as a function of the salinity. The excess oil phase composition is plotted in normalized form, where the basis of the normalization is the initial dodecanol volume fraction in the oil phase 177
- Figure 8. Variation of the selectivity as a function of the salinity at fixed initial dodecanol concentration. The salinity is expressed as NaCl wt %. Selectivity is defined as the ratio of the dodecanol concentration in the solubilized oil and the

dodecanol concentration in the excess oil phase. Results for five different initial dodecanol concentrations are shown.....	178
Figure 9. Variation of the selectivity as a function of the initial dodecanol concentration at no added salt. Selectivity is defined as the ratio of the dodecanol concentration in the solubilized oil and the dodecanol concentration in the excess oil phase.	179
 Chapter 6	
Figure 1. Interfacial tension measured between water and TCE/acetone oil mixture as a function of the initial acetone concentration in the bulk oil.	198
Figure 2. Bending elasticity constant versus benzene volumetric surface excess.	199
Figure 3. Characteristic length for the benzene-limonene mixture as a function of benzene concentration in the bulk oil.	200
Figure 4. Optimum salinity for benzene-limonene mixtures as a function of benzene concentration of the bulk oil mixture.	201
Figure 5. Experimental characteristic length at optimum as a function of shell thickness for the benzene-limonene and the dodecanol-limonene mixture.	202
Figure 6. Experimental optimum salinity as a function of shell thickness for the benzene-limonene and the dodecanol-limonene mixtures.	203
Figure 7. Experimental and model predicted characteristic length at optimum versus optimum salinity for a variety of oil phases.	204
Figure 8. Dodecanol surface excess per mole of surfactant in the middle phase at the optimum formulation as a function of the dodecanol concentration in the	

excess oil phase. Experimental data of the TCE-dodecanol, the PCE-dodecanol, and the limonene-dodecanol mixtures are shown.	205
Figure 9. Limonene and benzene breakthrough curves as a function of flushed pore volume.	206
Figure 10. Variation of the experimental benzene selectivity as a function of flushed pore volume.	207
Figure 11. Interfacial tension between oil and water measured with benzene/limonene mixture as a function of benzene concentration in the bulk oil.	208
Figure 12. Degree of benzene and limonene saturation of the micelles as a function of flushed pore volume.	209

ABSTRACT

Surfactant enhanced aquifer remediation technology has been applied to clean up oil mixtures in which the components have different properties. For oil mixture contaminants the remediation efficiency can vary significantly between the different oil components. To understand this behavior and suggest ways to overcome this problem binary oil mixture solubilization in saturated oil/water/anionic surfactant microemulsion systems has been studied. The oil mixture components were chosen so that their chemical structure be significantly different resulting in differences in water solubility, polarity, molecular volume, etc. Phase behavior, solubilization, and interfacial tension studies have been carried out with three model oil mixtures: TCE-acetone, benzene – limonene, and dodecanol – limonene. The TCE-acetone data suggested that acetone diluted the surfactant monolayer at the oil/water interface reducing its solubilization ability. The optimum salinity remained essentially unchanged upon acetone addition, which was attributed to the almost balanced acetone partitioning between the oil and water phases. Acetone behaved as a very inefficient, balanced cosurfactant, which behavior is related to complete miscibility with TCE and water. The main characteristics of the benzene-limonene and the dodecanol-limonene mixtures are that the semi-polar benzene and amphiphilic dodecanol is solubilized selectively in the oil domain of the microemulsion. Selectivity decreases with increasing electrolyte concentration and with increasing polar oil concentration. Variation of the selectivity with electrolyte concentration and/or oil

phase composition suggests that the excess polar oil be solubilized at the vicinity of the surfactant monolayer. The excess polar oil solubilization was found to follow a Langmuirian adsorption trend. Studies of the dodecanol-limonene system suggest that the amount of oil solubilized at the palisade layer changes the curvature and the bending rigidity of the surfactant film. This in turn affects the optimum salinity and the oil solubilization ability of the microemulsion. These results are used to extend the net-average curvature model to predict solubilization of oil mixtures in microemulsions. Model predictions and experimental data yield excellent agreement. Study and model results are used to explain why significant differences in the SEAR remediation efficiency of individual oil components could occur when the oil contaminant is a complex oil mixture. Possible methods are proposed to improve recovery of the more hydrophobic oils.

CHAPTER 1

INTRODUCTION

Non-aqueous phase liquids (NAPL) are common groundwater contaminants. Because the water solubility of NAPL compounds is usually very low, these chemicals form a separate liquid phase and persist in the subsurface environment for a long time continuously contaminating the ground water (1-3). Frequently these contaminants are mixtures of different organic compounds (2). Surfactant enhanced aquifer remediation (SEAR) using Winsor Type I or Type III microemulsions have been shown to effectively reduce subsurface contamination, thereby decreasing the contaminant level in the groundwater (1, 3). During the process of SEAR an aqueous surfactant solution is injected into the soil which induces a flow of the aqueous phase, and depending on the actual flushing conditions (i.e., interfacial tension, NAPL saturation, and the applied pressure), a flow of the oil phase. The mobilized fluids are extracted from the soil through extraction wells.

Using the SEAR technology the NAPL contamination may be reduced through two mayor routes: (a) mobilization, i.e., flow and extraction of the oil phase if the interfacial tension is low enough, and (b) solubilization, i.e., flow and extraction of the aqueous surfactant phase which contains surfactant solubilized oil molecules (3). It has been found that for DNAPLs that have densities greater than that of water, resulting in a potential of downward migration of the oil phase once the oil phase becomes mobilized.

Therefore instead of the mobilization mechanism, the solubilization mechanism is the preferred method for DNAPLs (3).

The solubilization mechanism in this process includes a mass transfer of the oil molecules from the bulk oil phase into the aqueous phase and the transport of the organic loaded aqueous phase (4-7). It has been suggested that the micellar solubilization is mass transfer rate limited under typical flushing conditions (i.e., slow flow velocity) (7) and the peak local aqueous organic concentration remains below the equilibrium oil solubilization. Nonetheless, a factor that has a major impact on the oil removal is the equilibrium oil solubilization in the aqueous surfactant phase in the absence and in the presence of mass transfer limitations as well. Even if the equilibrium concentration is not attained in the aqueous phase (7-9), it still impacts the remediation process. The mass transfer rate across the oil/water interface depends on the difference between the equilibrium and actual aqueous concentration of the oil species, and is modeled according to a linear driving force model as (5, 7)

$$M_i = K_i \cdot (C_i^{eq} - C_i) \quad [1]$$

where M_i is the mass transfer rate of species i across the interface between the oil phase and the aqueous phase, K_i is the mass transfer coefficient for component i , C_i^{eq} and C_i are the equilibrium and actual concentration of component i in the aqueous phase, respectively.

According to Eq. [1] high equilibrium oil concentration in the aqueous phase promotes high mass transfer rate, especially initially. High equilibrium solubilization is expected to reduce the time/surfactant use required for the remediation. As a consequence, it is important to design the surfactant solution so that the equilibrium oil

solubilization capacity of the aqueous surfactant phase is high. Therefore, it is necessary to know how much the equilibrium oil solubilization in the surfactant system even if it will never be reached.

Typical oil contaminants are mixtures of components, which may have different chemical structures and properties, including alkanes, aromatics, chlorinated solvents, BTEX compounds, ketones, etc (2,10). Significant variation between the remediation efficiency of individual NAPL components has been observed in field studies when the solubilization mechanism was used, and the components had different chemical structure. Rules governing individual species removal efficiency have not yet been studied, and mathematical models have not been proposed to predict realistic variations between the individual oil components.

The primary motivation of this work is to investigate equilibrium solubilization of oil mixtures when the oil components are significantly different from each other. The studied systems, experimental conditions and the proposed models correspond to typical SEAR conditions using solubilization mechanism. Because NAPL as a separate phase is found to persist during the surfactant flush, the studied systems are saturated microemulsions. In saturated Winsor type I microemulsions the surfactant rich phase coexist with excess oil, and Type III microemulsions coexist with excess oil and water phases. Since the mass transfer occurs from the oil phase to the aqueous phase, we are interested in how the conditions in the excess oil phase influence the solubilization in the aqueous surfactant phase. Consequently the studied systems are saturated Winsor-type I or III microemulsions and the models predict the effect of the chemical and compositional conditions in the excess oil phase on the oil solubilization.

In previous research the organic solubilization due to the surfactant aggregates has been correlated to the water solubility of the organic species in molecularly dispersed form (11-13). According to this concept the aqueous surfactant phase is divided into two pseudo-phases: the water and the micellar pseudo-phase. Instead of the impact of the separate NAPL phase conditions, the effect of the concentration of the dissolved oil molecules in the water pseudo-phase on the micellar oil solubilization is studied. Because the individual oil component concentration in the water pseudo-phase itself depends on the composition of the separate phase oil at equilibrium (if present), this concept and the concept of present studies are not fundamentally different, they only work in terms of different composition variables. The present concept seems to be more convenient when using multi-phase flow models as a predicting tool, where the conditions of the separate oil phase are the input variables. Because the oil solubilization models of present studies are developed so that they could be later used in multi-phase flow models, the separate oil phase composition is chosen as the input composition variable.

Design of a surfactant flush is typically based on the pseudo-component assumption (14,15). This means that the NAPL phase is considered as a single component organic phase, which has the averaged properties of the individual NAPL components, obtained by simple mixing rules. Another common assumption is the pseudophase assumption (16). According to this, the surfactant rich phase, which is a single macroscopic phase, may be regarded as composed of three pseudo-phases: the water pseudo phase, the NAPL pseudo phase, and the surfactant rich interfacial pseudo phase. A “completely mixed” assumption applies to all of the phases and pseudo phases. In this approach, for Winsor Type I and III microemulsions the solubilized NAPL

pseudo-phase is assumed to have the same composition as the excess (not solubilized by surfactant) NAPL phase. If these assumptions are valid the oil behaves collectively, resulting in a uniform relative removal of each individual NAPL component during the surfactant flush. These kinds of systems can be regarded “ideal”, and are not studied here, because of the extensive literature available (17-20).

Present work investigates the possibility that non-collective behavior of the NAPL mixture could cause preferential removal of NAPL components. This has been observed in field studies (10). To study non-ideality, the NAPL components are selected based on two important characteristics: the magnitude of their water-NAPL partitioning, and segregation potential within the surfactant solubilized NAPL pseudophase. Phase behavior and oil solubilization studies are carried out in order to establish the effect of these two characteristics of the NAPL components on the phase behavior and on the solubilization capacity of the surfactant system.

Some oil components found at contaminated sites are not only polar but also have high water solubility, i.e., various ketones, including acetone (10,21). Acetone is completely miscible with water and with most oils, hence it is expected to influence not only the properties of the oil but also the water. To study the effect of water miscible organic species the TCE (1,2,3-trichloroethylene) – acetone mixture is used. TCE is a common hydrophobic oil contaminant with low water solubility.

The potential for segregation inside the solubilized oil domain is likely due to the polarity, size, etc. differences between the components (22-26). A mathematical model based on thermodynamic considerations is proposed, which incorporates the results of the phase behavior and solubilization studies. The model can be used to explain and predict

solubilization of the individual oil components and the phase behavior. In this model we build upon the two-state solubilization theory (25), which states that the non-uniform oil component distribution inside the solubilized oil domain is due to the presence of two different solubilization “sites”. Oil molecules solubilized in the core “site” in a “dissolved” state experience chemical environment very similar to the excess oil phase. The other solubilization site is at the surface of the solubilized oil domain, located in the vicinity of the surfactant layer. The oil molecules solubilized at the “surface sites” are solubilized in “adsorbed” state. The environment at the surface sites is very different from the core sites because of the surfactant layer and closeness of the water domain. The two different solubilization sites are expected to cause a radial composition variation perpendicular to the interface inside the solubilized oil domain.

To study segregation, the applicability of the two-state solubilization theory and the impact of potential segregation on the microemulsion properties, we selected two different oil mixtures. The components of the first type of mixture, limonene and benzene have only slight difference in their chemical structure and polarity. Limonene is hydrophobic, and benzene is slightly more polar because of its aromatic ring. The molecular structure of d-limonene ((*R*)-4-isopropenyl-1-methylcyclohexene) is depicted in Figure 1.

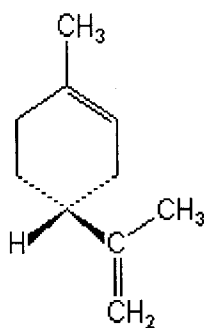


Figure 1. Molecular structure of d-limonene

The components of the second type of oil mixture are limonene and dodecanol, where dodecanol is much more polar than limonene due to its alcohol group. By comparing the results of the two systems the effect of the segregation strength on the microemulsion properties could be evaluated.

Based on the studies and the model results the importance of the non-collective behavior of NAPL mixtures as a reason of the variation between individual component remediation efficiency is discussed. Possible surfactant flush methods are suggested to improve removal of components that usually show lower removal efficiency. Study results provide a better understanding of the limits of the applicability of SEAR technology to clean up real, mixed subsurface NAPL contaminants. The knowledge gained about solubilization of oil mixtures can be used in other surfactant applications as well, where microemulsion microstructure, solubilization of the different oil components and their spatial distribution within the microemulsion plays an important role.

REFERENCES

1. West, C. C.; Harwell, J. H. *Environ. Sci. Technol.* **1992**, *26* (12), 2324-2330.
2. *EPA 542-K-94-003* April **1995** In Situ Remediation Status Report: Surfactant Enhancements
3. Sabatini, D. A.; Knox, R. C.; Harwell, J. H.; Shiau, B. J. In *Soil and Aquifer Pollution: Non-Aqueous Phase Liquids – Contamination and Reclamation*; Rubin, H.; Narkis, N.; and Carberry, J. Eds; 373-391; Springer, New York; **1998**.
4. Abriola, L. M.; Dekker, T. J.; Pennel, K. D. *Environ. Sci. Technol.* **1993**, *27* (12) 2341-2351.
5. UTCHEM 9.0 A Three-dimensional Chemical Flood Simulator Volume II. Technical Documentation, Reservoir Engineering research Program, Center for Petroleum and Geosystems Engineering, The University of Texas at Austin, Austin, Texas; **2000**.
6. Reeves, H. W.; Abriola, L. M. *J. Contaminant Hydrology*, **1994**, *15* (4), 249-276.
7. Powers, S. E., Abriola, L. M, Weber, W. J. *Water Res. Res.* **30**(2), 321-332, **1994**, Kueper, B. H., Mason, A. R. In *Ground Water and Subsurface Remediation. Research Technologies for In-situ Technologies*, Kobus, H.; Barczewski, B.; Koschitzky, H. P., Editors; Springer, Berlin; **1996**, pp. 265-273.
8. Mackay, D. M.; Roberts, P. V.; Cherry J. A. *Environ. Sci. Technol.* **1985**, *19* (5), 384-392.
9. Mercer, J. W.; Cohen, R. M. *J. Contaminant Hydrology* **1990**, *6*, 107-163,.
10. Knox, R. C.; Shiau, B. J.; Sabatini, D. A.; Harwell, J. H. In *Innovative Subsurface Remediation; Field Testing of Physical, Chemical, and Characterization Technologies*; ACS Symposium Series 725; American Chemical Society, Washington, DC.; **1999**, Brusseau, M. L.; Sabatini, D. A.; Gierke, J. S.; Annable, M. D. Eds.; pp. 49-63
11. Edwards, D. A.; Luthy, R. G.; Liu, Z. *Environ. Sci. Technol.* **1991**, *25* (1), 127-133.
12. Knox, R. C.; Shiau, B. J.; Sabatini, D. A.; Harwell, J. H. In *Innovative Subsurface Remediation; Field Testing of Physical, Chemical, and Characterization Technologies*; ACS Symposium Series 725; American Chemical Society,

- Washington, DC.; **1999**, Brusseau, M. L.; Sabatini, D. A.; Gierke, J. S.; Annable, M. D. Eds.; pp.8-23.
13. Shiau, B. J.; Sabatini, D. A.; Harwell, J. H. *Ground Water* **1994**, 32 (4), 561-569.
 14. Vinatieri, J. E.; Fleming, P. D. III. *Soc. Pet. Eng. J.* (Oct. **1979**), 289-300.
 15. Salter, J. S. *SPE paper* 7056; SPE-AIME Fifth Symposium of Improved Methods for Oil Recovery, Tulsa, April 16-19, **1978**.
 16. Biais, J.; Bothorel, P.; Clin, B.; Lalanne, P. *J. Dispersion Sci. Technol.* **1981**, 2 (1), 67-95,
 17. Cayias, J. L.; Schechter, R. S.; Wade, W. H. *SPE Journal*, December **1979**, 351-357.
 18. Salager, J. L.; Bourrel, M.; Schechter, R. S.; Wade, W. H. *SPE Journal*, October, **1979**, 271-278,.
 19. Baran, J. R.; Pope, G. A.; Wade, W. H.; Weerasooriya, V.; Yapa, A. *J. Colloid Int. Sci.* **1994**, 168, 67-72.
 20. Dwarakanath, V.; Pope, G. A. *Environ. Sci. Technol.* **2000**, 34 (22): 4842-4848.
 21. Shiau, B. J.; Hasagawa, M. A.; Brammer, J. M.; Carter, T.; Goodspeed, M.; Harwell, J. H.; Sabatini, D.A.; Knox, R.C.; Szekeres, E. In *Chlorinated Solvent and DNAPL Remediation*; ACS Symposium Series 837; **2003**; pp. 51-72.
 22. Kunieda, H.; Horii, M.; Koyama, M.; Sakamoto, K. *J. Colloid Int. Sci.* **2001**, 236, 78-84.
 23. Kunieda, H.; Ozawa, K.; Huang, K.-L. *J. Phys. Chem. B.* **1998**, 102, 831.
 24. Jonsson, B.; Lindman, B.; Holmberg, K., Kronberg, B. In *Surfactants and Polymers in Aqueous Solution*; Wiley, Chichester, **1998**.
 25. Mukerjee, P.; Cardinal, J. R. *J. Phys. Chem.* **1978**, 82 (14), 1620-1626,.
 26. Rouse, J. D.; Sabatini, D. A.; Deeds, N. E.; Brown, E., Harwell, J. H. *Environ. Sci. Technol.* **1995**, 29 (10), 2484-2498.

CHAPTER 2

THE IMPACT OF ACETONE ON THE SURFACTANT ENHANCED REMEDIATION OF OIL CONTAMINATED AQUIFERS *

ABSTRACT

In field applications of the surfactant enhanced remediation (SEAR) of oil contaminated aquifers the oil contaminant is typically a complex mixture. The objective of this work was to investigate the impact of water-miscible ketones on the surfactant enhanced remediation process. Microemulsion phase behavior, solubilization, and interfacial tension studies were conducted with a representative model system, which contained acetone and trichloroethylene (TCE) as the organic contaminants, and sodium dihexylsulfosuccinate as the surfactant. The optimum salinity was not affected significantly by variations in the oil phase composition. The oil solubilization ability of the surfactant system decreased, however, as the acetone concentration increased. Interfacial tension experiments revealed that as the acetone concentration increased, the area per surfactant molecule appeared to increase, indicating reduced surfactant surface activity. The consequences of these results on the SEAR process are discussed.

INTRODUCTION

A number of laboratory and field studies have demonstrated that surfactant enhanced remediation can be a successful method to clean up organic polluted aquifers (SEAR) (1 - 9). This method employs an aqueous surfactant solution to flush the aquifer

* To be submitted to *Environmental Science and Engineering*

with surfactant concentration above the CMC (critical micelle concentration). The surfactant aggregates solubilize the organic molecules in their hydrophobic interior thereby increasing the apparent aqueous solubility of the organic compound by 1-2 order of magnitude. The oil enriched surfactant solution (i.e., microemulsion) is extracted from the subsurface through extraction wells. As a result, the subsurface oil source can be eventually removed and further contamination of the aquifer water prevented.

Among many factors the success of SEAR depends on the oil/water/surfactant phase behavior and the oil solubilization ability of the surfactant (1, 10-12). The phase behavior and the oil solubilization ability of the surfactant in turn depend on the type of oil (13). The characteristics of the oil that affects the phase behavior and oil solubilization are the polarity, the molecular size, etc. which can be quantified using the equivalent alkane carbon number (EACN) concept (14-16). The EACN of a particular organic compound is equal to the carbon number of a linear alkane that behaves similarly in microemulsions. Hence, a particular surfactant solution may be efficient at one remediation site, but inefficient at another site due to the differences between the contamination at the two sites.

The phase behavior and the oil solubilization with different types of oils have been studied extensively (13). Not only single component oils but also oil mixtures have been of interest because oil contaminants are often composed of a number of components. Mixtures of alkanes with different carbon number (15), mixtures of chlorinated solvents of different degree of chlorination and/or chain length (17), and mixtures of alkanes and aromatic hydrocarbons (15) that have been studied contained components not much different from each other, all of them had low water solubility. It

was found that in the above cases linear mixing rules could be used to characterize the overall hydrophobicity of the oil mixture.

The problem becomes more complicated if the contaminant is a mixture of components, which are significantly different from each other. For example, we have recently reported on a field case study, where the contaminant contained methylene chloride, trichloroethylene, ketones and BTEX compounds (2). A large fraction of the ketones was acetone, a water miscible, polar organic compound, while the other components are sparingly soluble in water. Previous studies did not address the possible effect of the high water solubility of one of the oil components, hence it is not known how the phase behavior and oil solubilization is affected.

The objective of this research is to investigate how the compositional changes of oil mixtures, which contain water miscible organic contaminants affect the phase behavior and the solubilization, and its possible consequences on the remediation process. The surfactant selected for these studies is sodium dihexyl sulfosuccinate, an anionic surfactant. Anionic surfactants are preferred for SEAR because of their relatively low adsorption to the soil compared to non-ionic or cationic surfactants (10).

BACKGROUND

Phase behavior of oil/water/surfactant system.

Microemulsions may have three types of phase behavior, as classified by Winsor (13). The phase behavior changes of anionic surfactant systems can be studied by increasing the electrolyte concentration. With increasing electrolyte concentration a

Winsor Type I – III –II phase behavior transition takes place. In Winsor Type I systems an oil-in-water droplet type microemulsion phase is in equilibrium with an excess oil phase. In Winsor Type III systems the microemulsion phase has a bicontinuous structure and it is in equilibrium with an excess oil and an excess water phase. In Winsor Type II systems a water-in-oil droplet type microemulsion forms, which is in equilibrium with an excess water phase.

Along the salinity scan with increasing electrolyte concentration the solubility of the surfactant in the water decreases and its solubility in the oil increases. Hence, at low salinity the surfactant partitions preferentially into the water, which changes into oil preference with increasing electrolyte concentration. The oil and water solubility of the surfactant and the preference of the surfactant toward oil and water are equal at the midpoint of the Winsor Type III regime, which point corresponds to the optimum formulation. At electrolyte concentrations greater than that of the optimum formulation the surfactant preferentially partitions into the oil. Therefore, the optimum salinity must not be exceeded in SEAR applications.

The change in the oil/water partitioning is accompanied by an increase of the oil concentration in the microemulsion phase (i.e., surfactant rich phase) from very low to almost 100%. Because in SEAR high oil solubilization is required, high salinity is needed to improve process performance. As a result the electrolyte concentration must be optimized to best satisfy the opposing electrolyte concentration requirements due to surfactant partitioning and oil solubilization.

An important parameter that is used guide this optimization is the optimum salinity (18). The optimum salinity is the electrolyte concentration at which optimum

formulation is obtained. At the optimum formulation the solubilization is maximized yet the surfactant solubility in the oil is still low. Hence, by selecting the appropriate electrolyte concentration it is possible to tailor the surfactant formulation for the specific requirements at a remediation site.

Surfactant formulations for oil mixtures and polar solvents.

The effect of polar oil components may be very different depending on the molecular structure, polarity, water solubility, etc. For mixtures in which the components do not differ dramatically from each other, and all of them have low aqueous solubility a linear mixing rule has been proposed to predict the optimum salinity of the mixture as follows (18)

$$\ln S_{mix}^* = K \cdot EACN_{mix} + f(A) - \sigma + a_T (T - T_{ref}) \quad [1.a]$$

where S_{mix}^* is the optimum salinity, K is constant for a given surfactant and oil, $f(A)$ is parameter depending on the alcohol, σ is a parameter depending on the type of surfactant, a_T is the coefficient of the temperature dependence of the optimum salinity, and T and T_{ref} are temperature and the reference temperature, respectively.

$$EACN_{mix} = \sum_i x_i EACN_i \quad [1.b]$$

where $EACN_{mix}$ and $EACN_i$ are the equivalent alkane number of the oil mixture and oil component I, respectively, and x_i is the mole fraction of component i. The $EACN$ of an oil decreases as it becomes less hydrophobic, therefore the above formulas predict an

optimum salinity decrease upon increasing the polar oil concentration. This trend has been verified by experimental results (19).

The effect of alcohols, another type of oils, has also been extensively studied, because they can be used as additives to increase oils solubilization, change phase behavior, improve microemulsion properties (19-21). Alcohols readily mix with hydrophobic oils, and short chain alcohols also mix with the water similarly to acetone. Long chain alcohols primarily stay in the oil domain of the microemulsion. Intermediate chain length alcohols play the role of a cosurfactant because they are likely to enrich in the surfactant monolayer due to the intermediate polarity of this region. Short chain alcohols appear in the water phase, and are not effective cosurfactants. The effect of the alcohol on the phase behavior depends strongly on the alcohol chain length (18-21), as well as the oil and the surfactant and the exact trend must be determined experimentally. Long chain alcohols tend to decrease the optimum salinity, while short chain alcohols may cause the opposite effect. The oil solubilization is expected to increase when long chain alcohols are used, but may decrease for short chain alcohols (24-22).

In the present study we are concerned with the impact of highly water-soluble acetone on the optimum salinity. Equation [1] shows that oil mixture components, alcohols, and cosurfactants can all change the optimum salinity in their own ways, but the effect of the polar organic that partitions into the water is not considered explicitly. Furthermore the alcohol and cosurfactant dependent functions are empirical, and need to be experimentally determined for each system. Hence, Eq. [1] cannot be used directly to elucidate the effect of acetone on the optimum salinity even if we assume that acetone behaves as alcohol.

If acetone behaved as an oil component, the optimum salinity would be expected to sharply decrease with increasing acetone concentration because of its polar character, or even cause Winsor Type II behavior. It is not clear, however, how acetone is distributed within the oil/surfactant film/water regions, and how this distribution contributes to the overall effect of acetone on the microemulsion phase behavior.

To see how the solubilization ability of the microemulsion varies in response to oil phase composition change the solubilization parameters need to be compared at the optimum formulation (25). Research has shown that oils with polar character and/or small molecular size tend to be solubilized more than less polar and/or large ones (17, 26). Hence, one could hypothesize that compositional changes in an oil mixture must change the oil solubilization. If, for example, the concentration of the hydrophobic oil component increases and the other conditions remain unchanged, the oil solubilization is expected to decrease for two reasons. First, the maximum attainable oil solubilization (i.e., solubilization parameter at optimum) decreases as research suggest (25). Second, the formulation shifts farther away from the optimum. This is because even though the electrolyte concentration remains unchanged, the optimum salinity increases as the hydrophobic component concentration increases. A shift away from the optimum causes an additional decrease in the oil solubilization due to critical scaling behavior exhibited by microemulsions (13, 16, 25).

Water soluble alcohols and other non-aqueous polar solvents have been found to push the oil/water/surfactant system towards a tricritical point, destroying the microemulsion microstructure and inhibiting the surfactant aggregation (27, 28-33). For example, small angle neutron scattering experiments with balanced water / formamide /

n-octane / n-alkyl polyglycol ether systems suggested that the amphiphile strength of the surfactant is reduced and the microemulsion becomes disordered with increasing formamide concentration (30).

Other experiments (34, 27) show that the non-aqueous polar solvents like ethylene glycol, formamide, ethanol may increase the CMC, decrease the surfactant aggregation number, and decrease the radius of the micelle. These observations suggest that hydrophilic organic solvents are likely to interfere with the surfactant aggregation. Reduced surfactant aggregation tendency is expected to decrease the oil solubilization.

The objective of this study is to clarify the role of acetone in the system, and its impact on the phase behavior and the oil solubilization in TCE / sodium dihexyl sulfosuccinate / water microemulsion. The results are used to propose an approach for cleaning up oil contamination containing acetone.

MATERIALS AND METHODS

Acetone (99 %+) and Trichloroethylene (TCE, 99%+) were purchased from Aldrich. The surfactant used was sodium dihexyl sulfosuccinate (Fluka, 80% in water). Deionized water was used to prepare the samples. NaCl (99%+) was obtained from Aldrich. All materials were used as received, without further purification.

The water/oil partitioning behavior of acetone was studied in the absence of surfactant. In these studies acetone – TCE mixtures were prepared in the following initial acetone volume %: 0, 1, 2, 5, 7,5, 10, 15, 25. Equal volumes of oil mixtures and water (5 – 5 ml) were contacted in sealed vials. The samples were vigorously shaken for

24 hours in a wrist action shaker, and then left to rest and reach equilibrium at 27 °C. Equilibrium samples were analyzed after 2 weeks for TCE and acetone concentration.

Phase behavior and solubilization experiments were carried out by contacting oil mixtures with surfactant solution in the same way as described above. The same acetone – TCE compositions were used as in the water/oil partitioning studies. The surfactant concentration was kept constant (2 wt %), and the NaCl concentration was varied for each oil phase composition from 0 to 2.237 wt %. After equilibrium was reached the phase volumes were determined, and the concentration of acetone, TCE and surfactant was measured in the various phases.

The acetone and TCE concentration was measured with Varian 3300 gas chromatograph equipped with a flame ionization detector and a 30 m x 0.32 mm Supelcowax 10 capillary column with programmed temperature ramping from 40°C to 250°C at 15 °C/min. The surfactant concentration was measured with ion-coupled chromatography using Dionex chromatograph equipped with reverse phase column (NSI-4mm).

For the interfacial tension experiments the acetone concentration in the oil phase composition was varied similarly to the phase behavior and water solubility experiments. These oil phases were contacted with equal volume of aqueous surfactant solution in a similar manner as described above. In each sample the NaCl concentration was 0.89 wt %. At each oil phase composition the concentration of sodium dihexyl sulfosuccinate was varied increased from 0 to 2 wt %. After equilibrium was reached the interfacial tension between the oil and the aqueous phase was measured in each sample. The interfacial

tension was measured using the spinning drop method (University of Texas spinning drop tensiometer Model 500).

To determine the impact of the acetone on the CMC values the conductivity variation was measured with increasing surfactant concentration using an Orion 710 Aplus conductometer. The CMC was determined in the presence of 12.5 vol. % acetone and also with no added acetone.

RESULTS AND DISCUSSION

Partitioning of acetone and TCE into water in the absence of surfactant.

The oil / water partitioning behavior of acetone and TCE was studied without surfactant at 27 °C in order to find out how their water solubility changes as a function of the oil phase composition. While acetone is completely miscible with water, it is also completely miscible with TCE. In contrast, the water solubility of pure TCE at room temperature is around 1000 ppm. Figure 1 presents the measured acetone and TCE concentrations in the water phase as a function of the acetone concentration in the oil phase at equilibrium with no added surfactant. As the acetone concentration in the oil increases the aqueous acetone concentration increases in a linear fashion. The partition coefficient, which is given by the slope, is constant, with a value around unity. This shows that acetone seems to partition between the oil and the water phases with no apparent preference. This linear behavior suggests no significant acetone aggregation in the water or the oil phase.

The TCE partitioning shows a different behavior. The aqueous TCE concentration seems to be independent from the concentration of TCE in the oil phase. If Raoult's law governed the TCE distribution the TCE concentration would decrease in the water phase as the acetone concentration increases in the oil phase (i.e., with decreasing TCE concentration), due to decreasing TCE chemical potential. Because acetone can be regarded as a cosolvent for the TCE in the water, an increasing acetone concentration is expected to yield increasing aqueous TCE concentration. The two opposite effects appear to neutralize each other, leaving the aqueous TCE concentration essentially unchanged as the TCE concentration increases.

It can be concluded that acetone equipartitions between the oil and water phases. As a result, the properties of both phases must change if acetone is added to the system. The oil phase may become more polar, whereas the water phase becomes more oil-like upon addition of acetone. Furthermore, increasing acetone concentration alone does not yield increased TCE concentration in the water phase.

Effect of acetone on the phase behavior.

If change in the phase behavior of surfactant containing system occurs due to the presence of acetone, the optimum salinity would also change. Hence, the optimum salinity as a function of the acetone concentration was studied. Figure 2 shows the variation of the experimental and the effective optimum salinity as a function of the initial acetone concentration in the oil mixture. The experimental optimum salinity refers to the weight concentration of NaCl in the aqueous surfactant solution before it was

contacted with the oil phase. The NaCl concentration in the aqueous phase decreases after the oil phase is contacted with the surfactant solution because of dilution due to acetone partitioning into the aqueous phase. The initial NaCl concentration decreases due to this dilution effect. We define an effective optimum salinity in which this dilution effect is taken into account.

Figure 2 demonstrates that only slight variation of the optimum salinity occurs, especially in terms of the effective optimum salinity with increasing acetone concentration. The optimum salinity seems to slightly decrease at lower acetone concentrations, and increase above 5 vol. %. This decreasing – increasing trend could indicate a competition between two opposite effects, which almost balance each other. One, which is slightly more important at low acetone concentrations promoting an optimum salinity decrease, and another one with the opposite effect, becoming more important at higher acetone concentrations. Mixing very low EACN polar oil with TCE, such as acetone, is expected to cause a sharp optimum salinity decrease according to Eq. [1]. One may hypothesize that the opposing effect could originate from the high acetone concentration in the water. The optimum salinity results suggest that this effect on the water side almost completely compensates the oil side effect leaving the optimum salinity essentially unchanged.

This suggests that the phase behavior and the optimum salinity are not only affected by the oil side but also by the water side conditions. Hence, the high water solubility of acetone is also important factor in determining the phase behavior.

Effect of the electrolyte concentration on the acetone and TCE solubilization.

Figure 3 demonstrates TCE and acetone concentration changes in the microemulsion phase as the electrolyte concentration is increased. For this data, the initial acetone concentration in the oil phase is 5 volume % and the aqueous surfactant concentration is also constant, at 2 wt%. The optimum salinity in this series is about 1.5 wt%. Acetone and TCE show very different solubilization behavior. Acetone concentration in the microemulsion does not change much with microstructural changes caused by salinity increase. This indicates that acetone is distributed almost uniformly across all phases and pseudophases, and not affected by the surfactant.

In contrast, TCE solubilization is a strong function of the salinity. The TCE solubilization increases slightly at low salinity, but more rapidly closer to the optimum formulation. This behavior is typical of microemulsions, and is related to the decreasing curvature of the surfactant film due to the compression of the electrical double layer around the surfactant head groups. The reduced double layer allows the head groups to move closer, and the curvature towards the oil side decreases. Decreasing curvature yields larger oil droplet sizes, increasing the oil solubilization.

The TCE solubilization data suggest that microemulsion formation occurs at this acetone concentration. The invariance of the acetone concentration shows that the acetone concentration is approximately the same in the water and the oil domain of the microemulsion.

Solubilization of acetone and TCE with changing acetone concentration.

The solubilization performance of different systems needs to be compared at similar physico-chemical state, e.g., at the optimum formulation, because the solubilization depends on the deviation from the optimum state as shown above. According to the phase behavior studies there is no significant variation in the optimum salinity as a function of the acetone concentration. Furthermore, as shown above, TCE solubilization change is small farther away from the optimum. Hence, we assume that at fixed salinity, relatively far away from the optimum, the deviation from the optimum state is about the same at each acetone concentration. Under these conditions changes in the TCE solubilization are not caused by differences in the physico-chemical state, but reflect the effect of the changes in the oil phase composition.

Figure 4. a presents the acetone and TCE solubilization results measured in the microemulsion phase as a function of equilibrium acetone concentration in the excess oil phase at 0.89 wt % NaCl, and constant 2 wt %, surfactant concentration. At 0.89 wt % salinity o/w droplet type microemulsions are formed, coexisting with excess oil phase at each acetone concentration.

We see that the presence of surfactant has little effect on the acetone partitioning. The partition coefficient does not depend on the acetone concentration in the oil, and it is still close to unity, as without surfactant. This result suggests that microemulsion formation had essentially no effect on the partitioning behavior of acetone. Acetone still showed no significant preference for either phase and no association tendency. Solubilization of acetone due to the oil domain and the water domain of the microemulsion makes no difference in its overall concentration in the microemulsion

phase, because the acetone concentration is approximately the same in both oil and water domains. Also, acetone is not accumulated preferentially in the surfactant film, because that would increase its concentration in the microemulsion phase relative to the excess oil phase, which is not seen in Figure 4. a. This seems to further support the idea that acetone is probably distributed uniformly across all phases and pseudophases.

As seen in Figure 4. a the TCE concentration initially increases slightly, then it decreases as the acetone concentration is increased. A TCE concentration decrease is expected because partitioning of the acetone into the water causes dilution of the microemulsion phase, and the TCE chemical potential in the oil phase also decreases. To account for these dilution effects, and see how the ability of the surfactant to solubilize TCE changes we also calculated the solubilization parameters (SP), and the micelle-water partition coefficient (K_m) for the TCE. The solubilization parameter is calculated as follows:

$$SP_{TCE} = \frac{V_{TCE}}{m_{AMA}} \quad [2]$$

where V_{TCE} is the volume of TCE, which is solubilized by the oil domain of the microemulsion, excluding the TCE water solubility, and m_{AMA} is the mass of the surfactant AMA in the microemulsion. The micelle-water partition coefficient for the TCE is calculated as follows (35)

$$K_m = \frac{x_{TCE}^{mic}}{x_{TCE}^{aq}} = \frac{\frac{n_{TCE}^{mic}}{n_{TCE}^{mic} + n_{surf}^{mic}}}{\frac{n_{TCE}^{aq}}{n_{TCE}^{aq} + n_{surf}^{aq} + n_{H_2O}}} \quad [3]$$

where x_{TCE}^{mic} and x_{TCE}^{aq} are the mole fraction of TCE in the micellar and the aqueous phases, respectively, n is the number of moles, the subscript TCE, surf, and H₂O refer to the components TCE, surfactant and water, respectively, the superscripts *mic* and *aq* refer to micellar and aqueous phases. Rearranging Eq. [3] the following expression can be obtained:

$$m_{TCE}^{total} = \frac{K_m M_{H_2O} m_{TCE}^{aq}}{1 - K_m M_{H_2O} m_{TCE}^{aq}} \cdot [m_{surf}^{total} - m_{surf}^{CMC}] + m_{TCE}^{aq} \quad [4]$$

where m_i refers to the mass of component i (TCE or surfactant) expressed as mole per kg water, the superscripts total and CMC refer to the total content and the content at the CMC, respectively, M_{H_2O} is the molar weight of water. Equation [4] was solved for K_m using experimentally determined TCE solubilization data with and without surfactant. The CMC for the surfactant was assumed constant, 0.01 mole / l, and no surfactant partitioning into the oil phase was considered.

The calculated TCE solubilization parameter and micelle – water partition coefficient are plotted in Figure 4.b. The solubilization parameter increases at low acetone concentration, and decreases above 2-3 %. The micelle – water partition coefficient follows the same trend. This indicates that the K_m values change primarily due to the changing oil domain volume in the microemulsion (i.e., the TCE solubilization), and not due to TCE water solubility changes.

It is interesting to note that at low acetone concentrations the TCE solubilization increase is accompanied by a slight optimum salinity decrease. With increasing acetone concentration not only the TCE solubilization but also the optimum salinity trend changes. The change in the optimum salinity and the TCE solubilization trend occurs

around 5 initial vol. % (2-3 equilibrium vol. %) of the acetone in the oil, suggesting that they might have been related. The initial TCE solubilization increase and optimum salinity decrease may be related to the overall oil mixture becoming more polar, giving rise to stronger oil – surfactant tail interactions. This effect becomes overcompensated at higher acetone concentrations by the water side effect of acetone. The water side effect of the acetone may result in reduced surfactant aggregation decreasing the microemulsion solubilization of TCE. The invariance of the optimum salinity may indicate that the pressure changes on the oil side and on the water side of the surfactant membrane are similar when the presence of acetone decreases the surfactant aggregation tendency.

Effect of acetone on the surfactant partitioning between the oil and water phases.

One possible reason for an oil solubilization loss at higher acetone concentrations could be the partitioning of the surfactant into the oil phase. Figure 5 shows the surfactant concentrations measured in the aqueous and oil phase with increasing acetone concentration at 0.89 wt % salinity. According to the data the surfactant partitioning into the oil is small, and is not affected by the acetone concentration within the studied concentration range. Consequently the oil solubilization decrease is not caused by an aqueous surfactant concentration decrease.

Interfacial tension studies.

To elucidate possible reasons explaining the effect of acetone on the optimum salinity and the TCE solubilization variation we studied how the surfactant aggregation is

affected. One possibility is that since acetone was distributed across all phase without preference, it could also be present at the interface. This would cause a dilution of the surfactant monolayer at the oil/water interface. If this in fact happens, the oil / water interfacial area per surfactant molecule increases. We thus determined the area per surfactant molecule at the oil/water interface using interfacial tension experiments.

Figure 6 shows the variation of the o/w interfacial tension as a function of surfactant concentration for several initial acetone concentrations in the oil phase. The NaCl concentration was kept constant, at 0.89 wt % for each series. The results show that adding acetone decreases the interfacial tension even when at zero surfactant concentration. This is expected because acetone has a more polar molecular structure due to its ketone group. The interfacial free energy is reduced since the acetone/water contact is more favorable energetically than the TCE/water contact. As a result it is expected that the free energy gain from formation of a closely packed surfactant monolayer to shield the oil / water contact would also decrease.

As the surfactant concentration is increased the interfacial tension decreases until the CMC is reached. The value of surfactant concentration at which the interfacial tension becomes constant corresponds to the CMC. The area per surfactant molecule at the oil/water interface assuming total dissociation in the presence of 0.89 wt % NaCl is calculated from the slope of the surface tension curve in Figure 6 evaluated at the CMC as follows (36):

$$\Gamma = -\frac{1}{RT} \cdot \frac{d\gamma}{d(\ln c)} \quad [5.a]$$

$$a_s = -\frac{1}{\Gamma \cdot N_{Av}} \quad [5.b]$$

where Γ is the surface excess concentration of the surfactant, γ is the interfacial tension, R is the gas constant, T is the absolute temperature, c is the surfactant concentration in the bulk, a_s is the area per surfactant molecule, and N_{Av} is the Avogadro number.

The variation of the calculated area per surfactant molecule as a function of the acetone concentration is plotted in Figure 7. The area per surfactant molecule seems to increase with increasing acetone concentration. These results suggest that surface activity of the surfactant is reduced at higher acetone concentration. It is likely, that in addition to the surfactant acetone also partitions at the interface. This dilution of the interfacial surfactant film could be attributed to the decreased surface activity of the surfactant in the presence of acetone. Because acetone does not provide interaction with the oil and water due to its small “tail” and “head”, respectively, this leads to a reduced solubilization power. The surfactant is not as tightly packed at the interface because of the very weak “cosurfactant”, acetone. This may explain why the interfacial tension remains higher at saturation when the acetone concentration increases, which is seen in Figure 6.

Determination of the CMC from Figure 6 was complicated by the gradual rather than sharp changes in the interfacial tension as a function of surfactant concentration for acetone containing samples. To confirm that the acetone may increase the CMC, we determined the CMC experimentally with 0 % and 12.5 vol. % acetone from conductivity measurements. The results presented in Figure 8. The CMC corresponds to the surfactant concentration at which the conductivity curve has a “break point”. Without acetone the CMC is about 0.4 wt %, which increases to about 0.9 wt% when acetone is added. This suggests that the aggregate formation becomes less favorable due to the presence of acetone. An important driving force for formation of micelles is to reduce the surfactant

tail / water contact which is unfavorable. Acetone partitioning into the water reduces this driving force, presumably because the acetone/water mixture becomes more compatible with the surfactant tails. Hence the CMC increases.

The above result could explain the almost constant optimum salinity when the acetone concentration changes. The increasing acetone concentration could give rise to two opposing effects as suggested before. The reason why the optimum salinity might decrease and the TCE solubilization increase have already been explained above. The other effect is probably related to the reduced micellization caused by the acetone and the increased area per surfactant molecule at the interface.

At the optimum formulation the pressure on the oil side and on the water side of the surfactant film is equal. As acetone partitions in the interfacial film the distance between the surfactant heads and the tails increases resulting in a pressure decrease on both side of the surfactant film. An invariant optimum salinity might indicate that the pressure decrease is balanced on the oil and the water side, which seems reasonable as acetone was found to exhibit balanced partitioning between the water and the TCE.

The TCE solubilization decrease due to the acetone can be explained due to the increasing area per surfactant molecule. The area is increased due to acetone participation in the interfacial layer. This decreases the average thickness of the interfacial reducing interaction between the surfactant tails and the oil molecules. The surfactant becomes less efficient due to reduced surface activity.

Ultimately it is expected that microemulsion aggregation disappear at high enough acetone concentration, when the surfactant aggregation driving force and the polarity difference between the oil and the water phase is reduced sufficiently.

IMPLICATIONS FOR REMEDIATION

The present study shows the need to design a surfactant system for the specific oil of interest. This is especially important when the oil is comprised of compounds of widely varying properties such as TCE and acetone. The results provide insight to situations where the oil phase composition can vary.

For example, if the oil contaminant contains highly water-soluble organic and more hydrophobic oils such as acetone and TCE, respectively, the surfactant does not provide additional improvement in cleaning up acetone compared to fresh water flush. Both freshwater and surfactant flush would result in the same, relatively fast disappearance of acetone from the oil due to the high water solubility of acetone. In contrast, using fresh water only is not sufficient to remove the hydrophobic oil contamination and using surfactant can significantly improve efficiency. Therefore surfactant flush is still needed for these types of mixtures.

The benefit of using a surfactant depends on whether TCE solubilization improves enough. If the initial acetone concentration is high, TCE solubilization in the microemulsion is low. Therefore the remediation efficiency can not be improved enough using surfactant. In that oil composition range fresh water flush seems appropriate. Freshwater flush helps reduce the acetone concentration. Once the acetone concentration decreased surfactant flush may be started. At reduced acetone concentration the surfactant can increase the TCE removal significantly. Therefore, it is necessary to

monitor the acetone concentration in the extracted flushing solution to determine when to start the surfactant flush.

Another consideration is whether the surfactant formulation remains well optimized as the remediation proceeds. Our studies revealed that because of the balanced partitioning of the acetone between oil and water the oil composition change does not affect the phase behavior significantly. Therefore, the electrolyte concentration does not need to be adjusted during the surfactant flush to reoptimize the formulation for oil mixtures similar to TCE-acetone. We believe, however, that the invariance of the optimum salinity is a result of the balanced oil/water partitioning of the acetone in the present system, and may not apply to other systems where the oil/water partitioning of the water miscible organic component is not balanced.

REFERENCES

1. Sabatini, D. A.; Knox, R. C.; Harwell, J. F.; and Shiau, J. B. In *Soil and Aquifer Pollution. Non-Aqueous Phase Liquids – Contamination and Reclamation*; Rubin, H., Narkis, N., Carberry, J., Eds.; Springer, Berlin; **1998**; pp. 373-391.
2. Shiau BJ, Hasagawa MA, Brammer JM, Carter T, Goodspeed M, Harwell JH, Sabatini DA, Knox RC, Szekeres E In *Chlorinated Solvent and DNAPL Remediation*; ACS Symposium Series 837; American Chemical Society, Washington, D.C.; **2003**, pp. 51-72.
3. Knox, R. C.; Shiau, B. J.; Sabatini, D. A.; Harwell, J. H. In *Innovative Subsurface Remediation. Field Testing of Physical, Chemical, and Characterization Technologies*; ACS Symposium Series 725; Brusseau, M. L.; Sabatini, D. A.; Gierke, J. S.; Annable, M. D., Eds.; American Chemical Society, Washington, D.C.; **1999**; pp. 49 – 63.
4. Brown, C. L.; Delshad, M.; Dwarakanath, V.; Jackson, R. E.; Londergran, J. T.; Meinardus, H. W.; McKinney, D. C.; Oolman, T.; Pope, G. A.; Wade, W. H. In *Innovative Subsurface Remediation. Field Testing of Physical, Chemical, and Characterization Technologies*; ACS Symposium Series 725; Brusseau, M. L.; Sabatini, D. A.; Gierke, J. S.; Annable, M. D., Eds.; American Chemical Society, Washington, D.C.; **1999**; pp. 64 – 85.
5. Knox, R. C.; Sabatini, D. A.; Harwell, J. H.; Brown, E.; West, C. C.; Blaha, F.; Griffin, C. *Ground Water* **1997**, 35 (6), 948-953.
6. Sabatini, D. A.; Knox, R. C.; Harwell, J. H.; Soerens, T.; Chen, L.; Brown, R. E.; West, C. C. *Ground Water* **1997**, 35 (6), 954-963.
7. Londergan, J. T.; Meinardus, H. W.; Mariner, P. E.; Jackson, R. E.; Brown, C. L.; Dwarakanath, V.; Pope, G. A.; Ginn, J. S.; Taffinder, S. *Ground Water Monitoring and Remediation* **2001**, 21 (4), 57-67.
8. Dwarakanath, V.; Pope, G. A. *Env. Sci. Technol.* **2000**, 34 (22), 4842-4848.
9. Boving, T. B.; Brusseau, M. L. *J. Contaminant Hydrology* **2000**, 42 (1): 51-67.
10. Harwell, J. H. In *Transport and Remediation of Subsurface Contaminants. Colloidal, Interfacial, and Surfactant Phenomena*. ACS Symposium Series 491; Sabatini, D. A.;

- Knox, R. C., Eds.; American Chemical Society, Washington, D. C.; **1992**; pp. 124 – 132.
11. West, C.; Harwell, J. H. *Environ. Sci. Technol.* **1992**, 26 (12), 2324-2330.
 12. Sabatini, D. A.; Knox, R. C.; Harwell, J. H.; Wu, B. J. *Contaminant Hydrol.* **2000**, 45 (1-2), 99-121
 13. Bourrel, M., Schechter, R. *Microemulsions and Related Systems*. Marcel Dekker, New York, **1988**.
 14. Wade, W. H, Morgan, J.C., Jacobson, J., Salager, R. S., and Schechter, R. S. *Soc. Pet. Eng. J.* Aug **1978**, 242-252.
 15. Cayias, J. L., Schechter, R. S., and Wade, W. H. *Soc. Pet. Eng. J.* 351-357, Dec **1976**
 16. Cash, L., Cayias, J. L., Fournier, G., McAllister, D., Sharz T., Schechter, R. S., Wade, W. H. *J. Colloid Int. Sci.* **1977**, 59, 39.
 17. Baran, J. R.; Pope, G. A.; Wade, W. H.; Weerasooriya, V.; Yapa, A. *Environ. Sci. Technol.* **1994**, 28, 1361-1366.
 18. Salager, J. L.; Anton, R. E. In *Handbook of Microemulsion Science and Technology*; Kumar, P.; Mittal, K. L., Eds.; Marcel Dekker, New York, **1999**; pp. 247-308
 19. Salager, J L.; Bourrel, M.; Scechter, R. S.; Wade, W. H. *Soc. Pet. Eng. J.* **1979**, 19, 271-278.
 20. Kegel, W. K.; Lekkerkerker, H. N. *Colloids and Surfaces A.* **1993**, 76, 241-248.
 21. Bellocq, A. M. In *Handbook of Microemulsion Science and Technology*; Kumar, P.; Mittal, K. L., Eds.; Marcel Dekker, New York, **1999**; pp. 139-184.
 22. Strey, R.; Jonstromer, M. *J. Phys. Chem.* **1992**, 96, 4537.
 23. Kahlweit, M.; Strey, R.; Busse, G. *J. Chem. Phys.* **1991**, 95, 5344.
 24. Graciaa, A.; Lachaise, J., Cucuphat, C.; Bourrel, M.; Salager, J. L. *Langmuir* **1993**, 3371.
 25. Salager, J. L. In *Microemulsions in Handbook of detergents. Part A: Properties, surfactant science series, Volume 82*, Broze, G.; editor; Marcel Dekker, New York, **1999**; pp. 253-302.
 26. Uchiyama, H.; Acosta, E.; Tran, S.; Sabatini, D. A.; Harwell, J. H. *Ind. Eng. Chem. Res.* **2000**, 39 (8), 2704-2708.

27. Aramaki, K.; Olsson, U.; Yamaguchi, Y.; Kunieda, H. *Langmuir* **1999**, *15* (19), 6226-6232.
28. Strey, R.; Jonstromer, M. *J. Phys. Chem.* **1992**, *96* (11), 4537-4542.
29. Ruiz, C. C.; Molina-Bolivar, J. A.; Aguiar, J.; MacIsaac, G.; Moroze, S.; Palepu, R. *Colloid Polymer Sci.* **2003**, *281* (6), 531-541.
30. Schubert, K. V.; Strey, R. *J. Chem. Phys.* **1991**, *95* (11), 8532-8545.
31. Nagarajan, R.; Wang, C. C. *Langmuir* **2000**, *16* (12), 5242-5251.
32. Kahlweit, M.; Strey, R.; Aranoto, M.; Busse, G.; Jen, J.; Schubert, K. V. *J. Chem. Phys.* **1991**, *95* (4), 2842-2853.
33. Rao, V.; Ruckenstein, E. *J. Colloid Int. Sci.* **1986**, *113* (2), 375-387.
34. Carnero Ruiz, C.; Molina-Bolivar, J. A.; Aguiar, J.; MacIsaac, G.; Moroze, S.; Palepu, R. *Colloid Polym Sci.* **2003**, *281*, 531-541.
35. Hoiland, H.; Kvammen, O.; Backlund, S.; Rundt, K. In *Surfactants in Solution*; Volume 2; Mittal, K. L.; Lindmann, B., Eds.; **1984**, pp. 949-962.
36. Hiemenz, P. C. *Principles of Colloid and Surface Chemistry*; 2nd Edition; Marcel Dekker; New York; **1986**; pp. 381-398.

FIGURES
Chapter 2

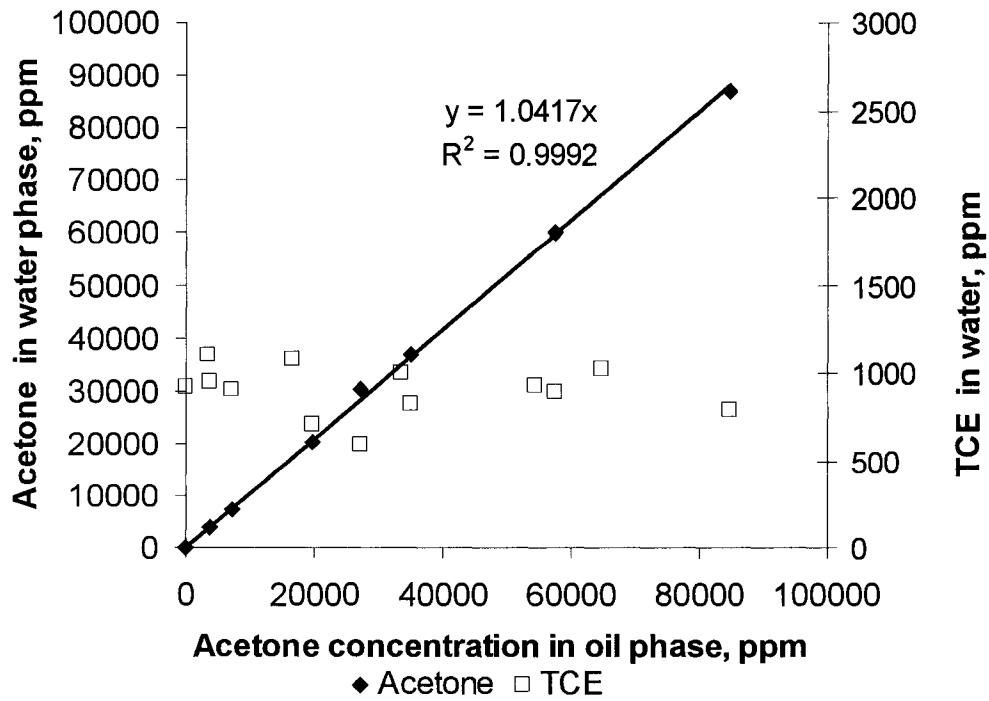


Figure 1. Partitioning of acetone and TCE in water/TCE/acetone mixture. The volume fraction of water, which is kept constant, is 0.5. Note: 100,000 ppm acetone concentration corresponds to 1.36 mole/liter, and 100,000 ppm TCE concentration corresponds to 1.11 mole/liter.

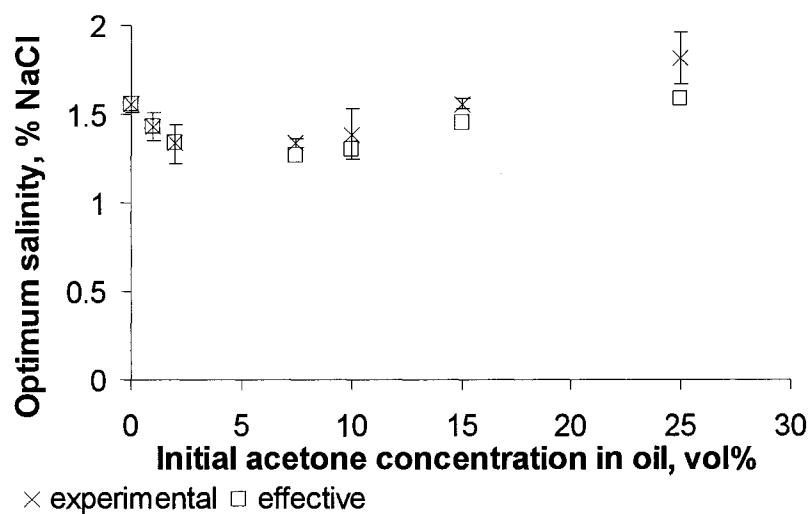


Figure 2. Variation of experimental and effective optimum salinity as a function of the initial acetone concentration in the oil. Experimental optimum salinity corresponds to the salinity of the aqueous surfactant solution before contacting with the oil phase, effective optimum salinity is calculated from the average experimental salinity accounting for the dilution of the water pseudo-phase due to acetone partitioning.

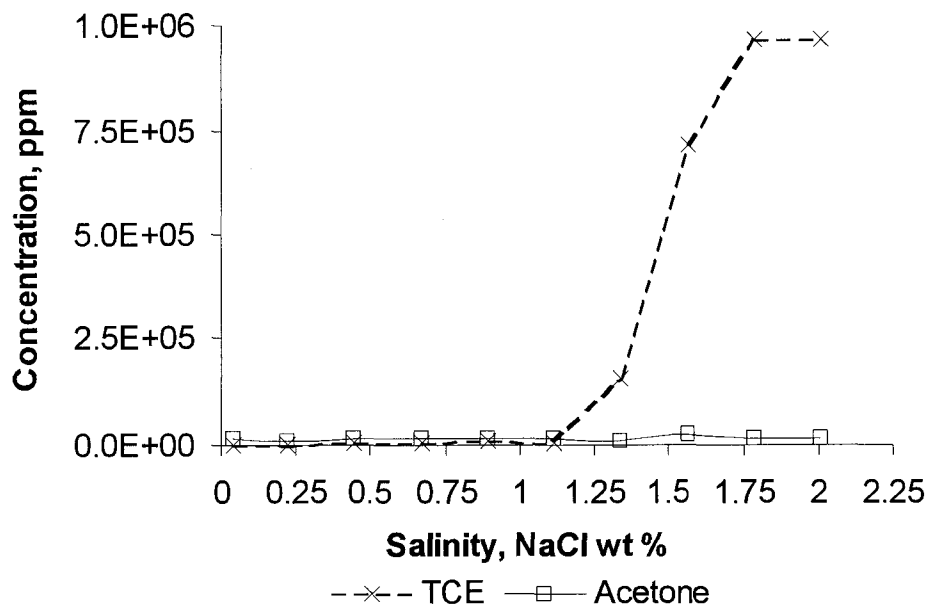


Figure 3.a. Concentration of TCE and acetone in the aqueous surfactant solution as a function of NaCl concentration. The initial acetone concentration in the oil phase was 5 vol. %.

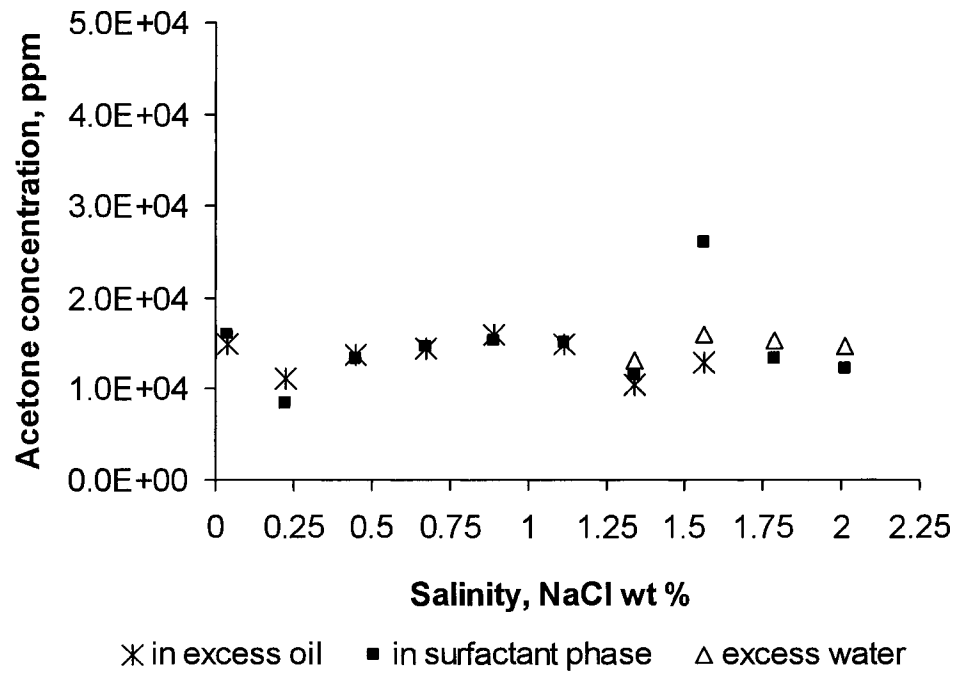


Figure 3.b. Acetone concentration in the various coexisting phases as a function of salinity. The initial acetone concentration was 5 vol. % in the oil.

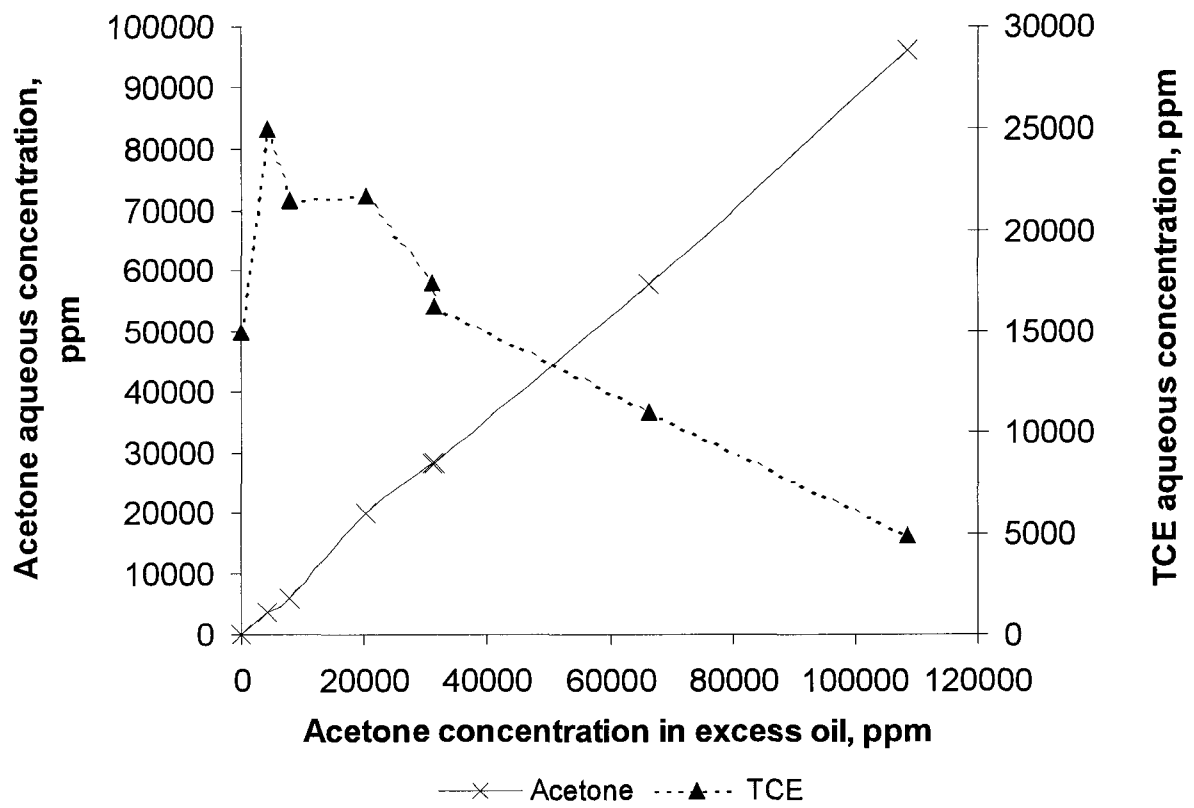


Figure 4. a. Concentration of acetone and TCE in the aqueous surfactant phase as a function of the acetone concentration in the excess oil phase. The salinity was kept constant, 0.89 wt%

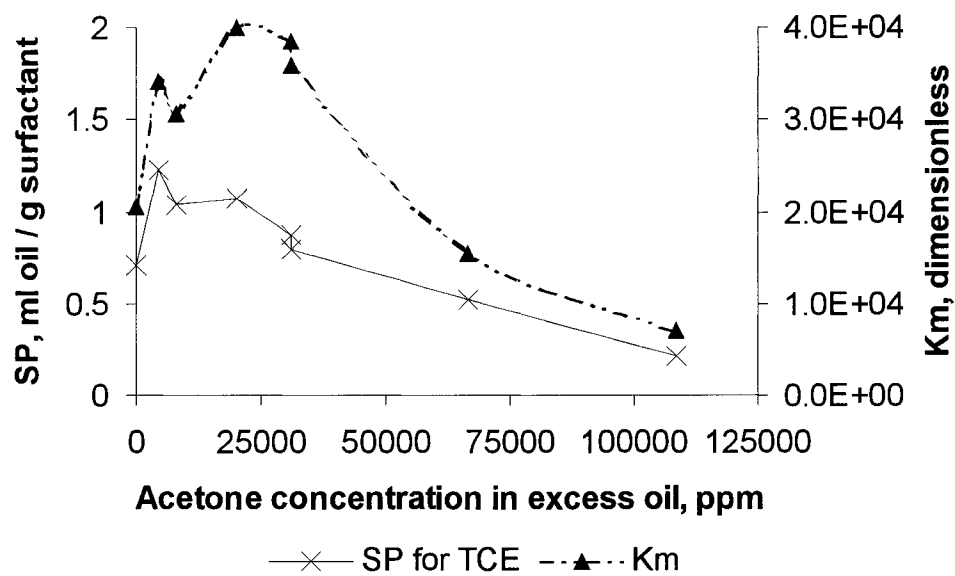


Figure 4. b. Solubilization parameter (SP), and micelle/water partition coefficient (Km) for TCE as a function of the acetone concentration in the excess oil phase. The salinity was constant, 0.89 wt%.

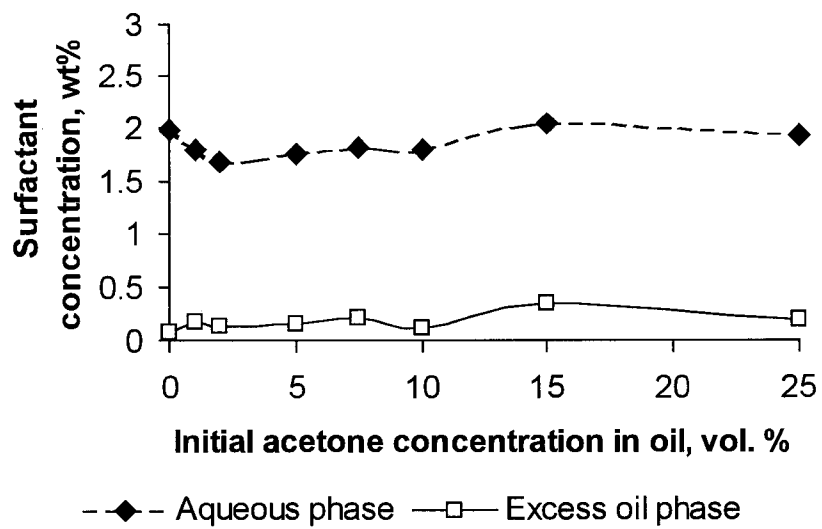


Figure 5. Surfactant concentration in the microemulsion phase and excess oil phase as a function of acetone concentration in the oil phase.

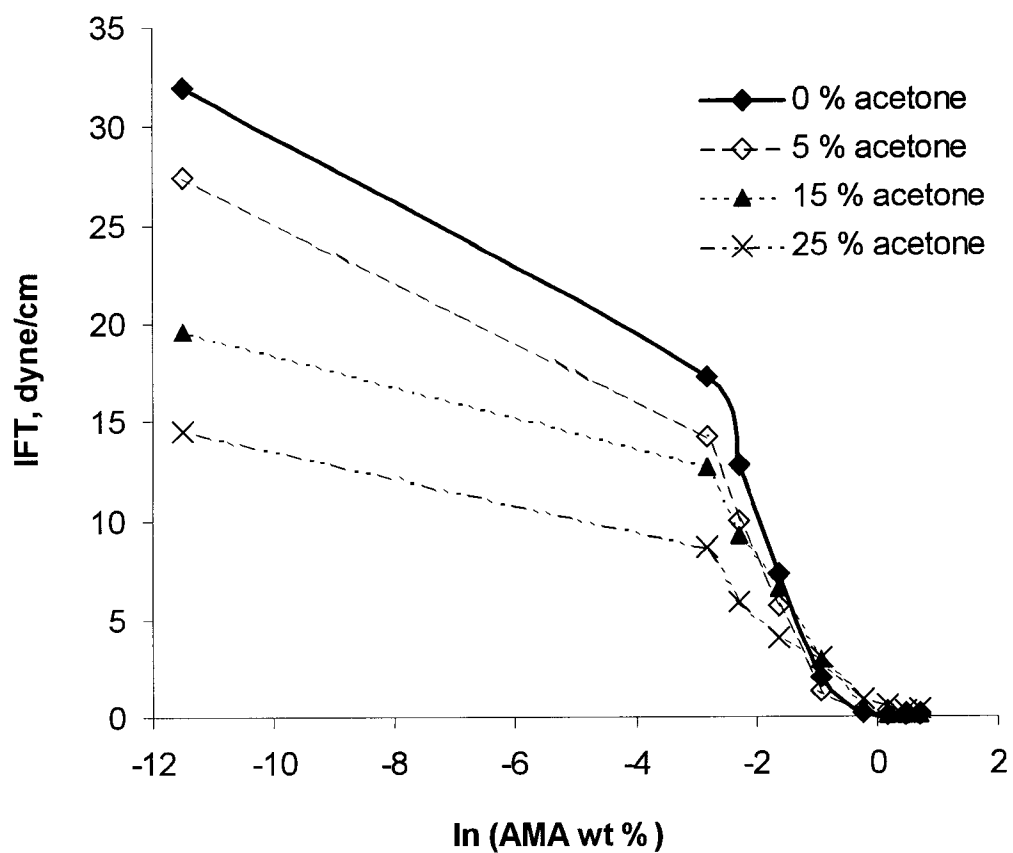


Figure 6. Variation of the oil/water interfacial tension as a function of the surfactant concentration (AMA).

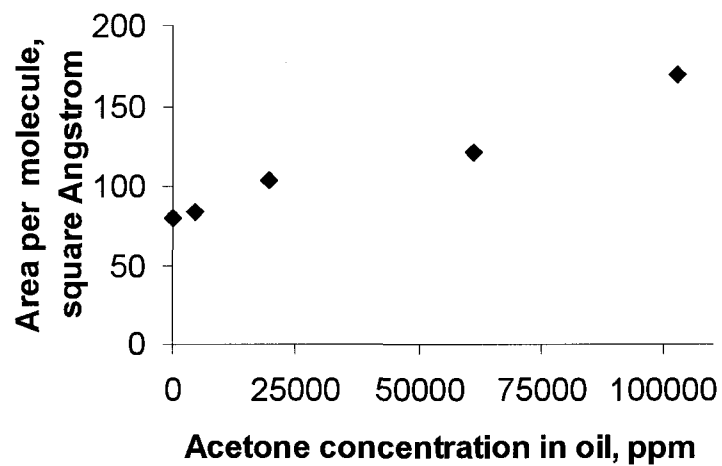


Figure 7. Area per surfactant molecule at the oil/water interface as a function of acetone concentration measured in the excess oil phase.

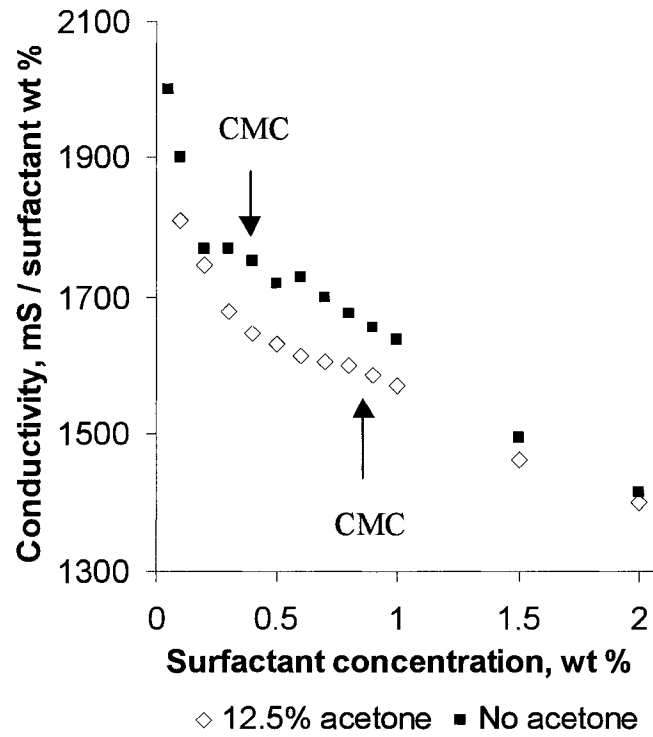


Figure 8. Variation of the specific conductivity as a function of surfactant concentration in acetone free and acetone containing (12.5 % in the oil phase at equilibrium) samples.

CHAPTER 3

A TWO-STATE MODEL FOR SELECTIVE SOLUBILIZATION OF BENZENE-LIMONENE MIXTURE IN SODIUM DIHEXYL SULFOSUCCINATE MICROEMULSION*

ABSTRACT

When surfactants are used to solubilize oil the oil to be solubilized is often a mixture of components with differing properties, e.g., solubilization of drug molecules in microemulsion formulations, remediation of organic polluted aquifers using surfactants, etc. Previous research has demonstrated that the more polar components are solubilized selectively under certain conditions. Even though it is important to know the composition of the solubilized oil from the application point of view, only a few studies can be found on the subject and simple mathematical model for the selectivity is not available. In this research we studied microemulsion systems containing water, sodium dihexyl sulfosuccinate as the surfactant, and limonene-benzene mixture as the oil. It was found that the selectivity towards benzene was highest at low electrolyte and benzene concentrations, and decreased as the electrolyte concentration or the benzene concentration in the oil increased. This result is discussed on the basis of the microstructural changes in the microemulsion and the two-state solubilization theory proposed by Mukerjee. These findings led to a simple mathematical model for the selectivity, which is sensitive to oil composition and electrolyte concentration variations. The model combines the two-state solubilization theory and the net-average curvature model of microemulsion solubilization to yield close agreement with the experimental data.

INTRODUCTION

Surfactants are often used to increase the water solubility of organic compounds. Solubilization increase is due to incorporation of the organic compound into the

* Submitted to *Langmuir* December, 2003

hydrophobic domain of the microemulsion, formed by the surfactant (1-3). Increased organic solubility is particularly important in a number of applications, e.g. remediation of organic contaminant polluted aquifers, drug delivery formulations, cosmetics, detergency, etc. In many of these applications the oils are mixtures of different types of components, and one is interested in how oil mixtures, rather than single component oils are solubilized in microemulsions.

A typical example for the subsurface organic contaminant remediation applications, the Chemical Disposal Pit / Fire Training Area at the Hill Air Force Base, Utah, was studied our research group. This site was contaminated with chlorinated solvents and fuel hydrocarbons, including trichloroethylene (TCE), tetrachloroethylene (PCE), chlorinated and non-chlorinated aromatics, decane and undecane (4). These organic compounds are different in their molecular structure, flexibility, and polarity.

In drug delivery applications, microemulsion are used to make water-soluble formulations from hydrophobic drug compounds (5-8). These microemulsions usually contain not only the hydrophobic drug molecules but also other oils to aid the preparation and/or the formulation. In these applications the oils to be solubilized are also mixtures, and the oil components may have significantly different properties.

Previous research (1-3, 9-16) has shown that, depending on the nature of the oil molecule, it can be solubilized at different locations in the surfactant micelles. Non-polar oils are preferentially solubilized in the micellar core. Amphiphilic oils also accumulate in the palisade layer. Polar oils locate close to the polar surface of the micelles. In unsaturated micellar solutions, differences in the preferred solubilization loci lead to different solubilization behaviors for non-polar, amphiphilic, and polar oils. For example,

as the mole fraction of the oil in the micelles increases, the micelle-water partition coefficient increases for non-polar oils, but decreases for polar oils.

Mukerjee and his coworkers (17-19) found that polar oils are solubilized preferentially compared to non-polar oils. They studied solubilization of various benzene derivatives and naphthalene in Triton X-100 surfactant micelles. They proposed a qualitative two-state solubilization model to explain this solubilization difference. According to their model an oil molecule can be solubilized in two states. Oils are solubilized in the micellar core in a “dissolved state” due to the solvent power of the hydrophobic core. Both polar and non-polar oils can be solubilized in this state. The other solubilization state is the “adsorbed state” solubilization, which occurs close to the micelle-water interface. Adsorbed state solubilization is favored for polar oils compared to non-polar oils due to their surface-active behavior at the micelle-water interface. In this case the oil/water interfacial tension for the polar oil is less than that for the hydrocarbon liquid corresponding to the tail of the surfactant. This explains the increased adsorption tendency at the interface. There is equilibrium between the two solubilization states, even if only one kind of oil is solubilized. The distribution of the oil between the “adsorbed” and the “dissolved” states depends strongly on the surface activity of the oil at the interface. Polar oils have greater surface activity than non-polar oils. Therefore the more polar the oil, the larger the fraction in the “adsorbed” state according to this theory.

The origin of the observed higher solubilization for the polar oils is explained as follows. While non-polar oils can be solubilized only in the micellar core both the core and the palisade layer is available for solubilization for polar oils. This means, that there is an extra solubilization region available for the polar oils. Furthermore, adsorption of

the polar oils at the interface decreases the surfactant tail/water interfacial tension. This tends to decrease the Laplace pressure, changing the curvature of the surfactant layer. As a result, the curvature towards the oil side decreases, and the volume of the micellar core increases. Consequently the preferential solubilization of the polar oils over non-polar oils results from both palisade layer solubilization and Laplace pressure effects.

Solubilization of single component oils and mixtures of similar components has been investigated extensively (1-3). Solubilization of oil mixtures of significantly different components received much less attention. Measurable oil fractionation has been evidenced in Type III systems (1) for a number of oil mixtures, which was attributed primarily to an interfacial effect. Nagarajan et al. (20) studied selective solubilization from several binary oil mixtures in ionic surfactant systems. They found that the selectivity towards the more polar oil varied significantly, depending on the type of the oil components. When the difference between the polarities and/or molar volumes of the oil components was more significant, the selectivity was greater. They studied the effect of the oil phase composition. The selectivity was highest, on the order of 10, at low polar component concentration in the oil, which decreased as the concentration increased. However, the effect of the electrolyte concentration and the resultant structural changes of the microemulsion on the selectivity have not been studied.

Nagarajan and Ruckenstein (20-23) developed a mathematical model for microemulsions, based on molecular thermodynamics. The model was able to predict the basic features of the observed selectivity trends in ionic surfactant systems (20). The disadvantage of this model is the difficulty of obtaining the necessary thermodynamic

parameters to accurately represent molecular interactions in the microemulsion. A simple model, which uses parameters that are easy to obtain, is still needed.

The Salager group studied the ethyl-oleate and hexadecane oil mixtures / non-ionic surfactant systems (24). In this oil mixture ethyl-oleate is much more polar than the hexadecane. It was observed that the solubilized oil at the interfacial layer contains more polar ethyl oleate than the excess oil. Ethyl-oleate segregation occurs in the oil layer located near the interface.

The effect of the variation of oil phase composition and the ethylene oxide number (EON) of the surfactant on the segregation parameter have been analyzed. The segregation decreased in a non-linear fashion when the mole fraction of the ethyl-oleate in the oil increased. It has been demonstrated that variation in the surfactant EON affected the microstructure of the microemulsion. With decreasing surfactant EON the average oil droplet size increased. This was paralleled by a linear decrease of the segregation. They clearly demonstrated that there is a connection between the segregation and the microemulsion microstructure and the oil phase composition.

In this research the objective is to study the origin of the sensitivity of the selectivity to the microstructure and the oil phase composition in anionic surfactant systems. The polar and non-polar oil mixture components are benzene and limonene, respectively. Benzene has a polar character due to the high polarizability of the aromatic ring. Limonene is the hydrophobic oil component, which behaves similarly to hexane in microemulsions. The surfactant is sodium dihexyl sulfosuccinate, and the additive is NaCl. The microemulsions are saturated systems, in which o/w droplet type or middle phase microemulsion coexists with excess oil phase. The effect of the oil phase

composition is studied by varying the benzene volume fraction from 0 to 1. The effect of the microstructural changes is studied by varying the electrolyte concentration. We propose that a simple mathematical model can be developed for the selectivity, which takes into account the effect of structural changes and incorporates the two-state solubilization theory.

MATERIALS AND METHODS

Chemicals. (R)-(+)-Limonene (98+ %), benzene (99+ %) and sodium chloride (99+ %) were purchased from Aldrich (Milwaukee, WI) and used without further purification. Sodium dihexyl sulfosuccinate (AMA, 80 wt % in water) was obtained from Fischer Chemicals (Fluka brand). Selected properties of the above materials are listed in Table 1.

Methods. Phase behavior studies were carried out by contacting equal volumes (5 ml) of oil, and aqueous solution of 4 wt % AMA with varying salinity at room temperature. Samples were gently shaken several times a day for one week, and then left to equilibrate for two more weeks. Salinity was varied between no added salt to salinities high enough to reach the optimum formulation. Salinity scans were performed for nine different oil compositions between pure benzene and pure limonene. Additionally, water solubility of benzene and limonene for the same nine oil mixtures were also determined, with no surfactant and NaCl.

After equilibration, phase volumes were measured. Limonene and benzene concentrations in the various phases were determined with Shimadzu GC-17A Gas Chromatograph equipped with Tekmar 700 Headspace Autosampler and a 0.52mm x 30m Supelco DB 25 column. Samples were spiked with 10 wt % AMA solution to avoid problems of surfactant background effect. Samples were analyzed in triplicates, the error in benzene and limonene concentration measurements being less than $\pm 5\%$.

Benzene and limonene concentration data obtained from aqueous surfactant phases include contributions due to organic water solubility and microemulsion solubilization. To obtain the microemulsion solubilization only the concentrations measured in surfactant containing samples were reduced by the water solubilities measured in surfactant free aqueous phase samples.

MODEL DEVELOPMENT

As mentioned before the selectivity is sensitive to the microemulsion microstructure (24). The microstructural changes are caused by changes in the curvature of the surfactant membrane. Curvature change occurs if the microemulsion formulation changes (25). In ionic microemulsions, for example, increasing the salinity reduces the electrostatic repulsion between the similarly charged surfactant head groups. As a result the pressure on the water-side decreases and the head groups can move closer to each other, while the oil side pressure remains unchanged. Therefore the shape of the surfactant film changes: the curvature towards the oil decreases. The polar character of

the oil also affects the curvature with a similar result. Polar oils tend to penetrate between the tails of the surfactant more than non-polar oils as discussed in the introduction. Penetration increases the pressure in the surfactant tail region, while the pressure on the water-side is not affected. As a consequence the curvature of the surfactant film towards the oil decreases.

Based on the two-state solubilization theory we assume that the total solubilization can be split into two contributions: due the interface and the core. The polar oil mole fraction in the interfacial oil is higher than in the core oil or in the excess oil phase. Then, the overall solubilized oil composition is richer in the polar oil if the interfacial oil solubilization dominates. In contrast, the mole fraction of the polar oil in the total solubilized oil decreases as the core solubilization contribution becomes dominant.

Curvature changes impact the volume of the solubilized oil in the two regions in a different way. Decreasing curvature causes core solubilization to increase, because the droplets become bigger. In contrast the total surface area of the solubilized oil is not affected significantly by the curvature changes as long as the type and concentration of the surfactant remains the same. The total surface area is fixed by the amount of surfactant in the system. Therefore the volume of oil solubilized in the interfacial layer is not expected to vary significantly as the curvature is changed with constant oil phase composition. When the curvature is large (i.e., small droplets) the contribution of the interfacial layer solubilization to the total solubilization dominates. As the curvature decreases (i.e., large droplets), the interfacial layer contribution remains the same, but the contribution from core solubilization increases rapidly. It is expected that the core

contribution becomes dominant even at moderate droplet radii, because the volume depends on the radius on the third power. Therefore the selectivity is large for formulations promoting large curvature (i.e. small radius), and is expected to decrease rapidly for formulations promoting curvature decrease.

To develop a mathematical model for the selectivity, one has to find a relationship first between the formulation variables (e.g., type and concentration of components in the microemulsion, and temperature) and the curvature of the surfactant film. The next step is to find a relationship between the curvature and the selectivity. This way the selectivity can be predicted as a function of the formulation variables, which the formulator can change to manipulate the selectivity.

Relationship between the formulation variables and the curvature.

The net-average curvature model can be utilized to provide the relationship between the formulation variables and the curvature. Detailed description of the model for single component oils can be found in reference 26, but is briefly reviewed below.

Net-average curvature model for single-component oil.

The model considers saturated microemulsions, in which the microemulsion is in equilibrium with an excess oil and/or water phase(s). The microemulsions are regarded as a collection of oil and water droplets of various geometry and size distribution, corresponding to an average equivalent oil radius and water radius, respectively. The net-average curvature model combines the surfactant affinity difference (SAD) concept (25),

and the critical scaling approach (27) to predict the radius and volume of oil and water solubilized by the microemulsion as a function of a selected formulation variable.

For anionic surfactants SAD is given by

$$-\frac{SAD}{RT} = \ln S - K \cdot EACN + \sigma - f(A) - a_T \cdot (T - T_{ref}) \quad [1]$$

where S is the salinity in NaCl %, $EACN$ is the equivalent alkane number of the oil, σ is a characteristic parameter of the surfactant, $f(A)$ is a function of the lipophilic alcohol/cosurfactant, a_T is a positive coefficient for the temperature effect, T is the temperature in Kelvin, T_{ref} is the reference temperature, and R is the gas constant. When the formulation variable is the salinity, and the optimum salinity is known, SAD is expressed as

$$-\frac{SAD}{RT} = \ln \frac{S^*}{S} \quad [2]$$

where S^* is the optimum salinity, the NaCl concentration necessary to obtain balanced formulation.

The net curvature of the oil and water is zero (28-30) at the balanced point which is considered as the critical point. The net curvature of the surfactant film is scaled to the distance from the optimum formulation as follows

$$\left| \frac{1}{R_o} \right| - \left| \frac{1}{R_w} \right| = \frac{1}{L} \cdot \ln \left(\frac{S^*}{S} \right) \quad [3]$$

where R_o and R_w are the equivalent droplet radii corresponding to the oil and water domain in the microemulsion, respectively, L is an adjustable scaling parameter dependent on the length of the surfactant tail.

The average of the water curvature $\left(\frac{1}{R_w}\right)$ and the oil curvature $\left(\frac{1}{R_o}\right)$ reaches a minimum value in the Type III regime (28-30). This limiting value is equated with the inverse of the characteristic length scale of the microemulsion as

$$\frac{1}{2}\left(\left|\frac{1}{R_o}\right| + \left|\frac{1}{R_w}\right|\right) = \frac{1}{\xi} \quad [4]$$

where ξ is the characteristic length, introduced by de Gennes and Taupin (31). The characteristic length depends on the type of surfactant/cosurfactant and oil, and calculated from middle phase solubilization data as

$$\xi = \frac{6\phi_o\phi_w V_m}{A} \quad [5]$$

where ϕ_o and ϕ_w are the volume fractions of oil and water respectively in the middle phase, and V_m is the volume of the middle phase.

In Winsor Type I microemulsions all of the water is contained in the microemulsion, and the radius of water is computed as

$$R_w = \frac{3V_w}{A} \quad [6]$$

where V_w is the volume of water added to the system, and A is the total internal surface area provided by the surfactant monolayer separating the oil and water domains of the microemulsion. In Winsor Type II systems all of the oil is contained in the microemulsion, therefore the oil radius is given by

$$R_o = \frac{3V_o}{A} \quad [7]$$

where V_o is the known volume of the oil added to the system.

For Winsor Type I systems Eqs. [3] and [6] are solved for the radius of the oil and water as a function of the salinity. For Winsor Type III systems the oil and water droplet radii are computed by solving Eqs. [3] and [4], and for Winsor Type II systems Eqs. [3] and [7] are used.

The volume of solubilized oil (V_o) and water (V_w) are be calculated as

$$V_o = \frac{R_o \cdot A}{3} \quad [8]$$

and

$$V_w = \frac{R_w \cdot A}{3} \quad [9]$$

Oil mixtures.

The optimum salinity and the characteristic length are expected to vary as the oil phase composition varies. If the dependence of the optimum salinity and the characteristic length on the oil phase composition is known the net-average curvature model can be applied to oil mixtures.

Salager et al. (32) and Baran et al. (33, 34) have introduced linear mixing rules for the optimum salinity as follows:

$$\ln S_{mix}^* = \sum_i x_i \ln S_i^* \quad [10]$$

where S_{mix}^* is the optimum salinity of the oil mixture, S_i^* and x_i are the optimum salinity and mole fraction of component i , respectively. This model choice was corroborated by our experimental data, which showed no significant departure from the linear mixing rule.

To our knowledge, no relationship has been proposed for the characteristic length dependence on the oil composition. Based on our experimental data we found that a linear mixing rule yields a reasonable fit according to

$$\xi_{mix} = \sum_i x_i \xi_i \quad [11]$$

where ξ_{mix} and ξ_i are the characteristic lengths of the mixture and pure component i , respectively.

For oil mixtures Eqs. [3], and [4] need to be modified by incorporating Eqs.[10], and [11] to introduce the dependence of the core solubilization on the oil phase composition.

Curvature and selectivity relationship.

Surface excess model.

The concepts of the two-state solubilization theory are applied to develop the curvature-selectivity relationship. Because selectivity can be defined only in Type I and III microemulsions, Type II systems are not considered below. Microemulsions are thermodynamically stable, macroscopically single-phase solutions. According to the pseudophase model (35) the microemulsion phase can be divided into three pseudophases: oil pseudophase, water pseudophase, and the surfactant film, which separates the oil and water pseudophases. In saturated microemulsions the microemulsion coexists with the excess oil phase in Type I systems, and with both excess oil and excess water in Type III systems. At equilibrium, the chemical potentials of an oil component

(i) in the excess oil phase (μ_i^{oil}), in the water pseudophase ($\mu_i^{mic,water}$), and in the oil pseudophase ($\mu_i^{mic,oil}$) are equal.

$$\mu_i^{oil} = \mu_i^{mic,water} = \mu_i^{mic,oil} \quad [12]$$

Oil is not allowed in the surfactant layer as long as it cannot be considered as a cosurfactant. The main criteria we used to decide if a component is considered an “oil” or a “cosurfactant” was its ability to change the neutral area per surfactant molecule at the oil/water interface. Oils do not pull apart the surfactant molecules and do not locate themselves between the surfactant molecules at the interface, therefore the area per surfactant molecule is not affected in the presence of oils. In contrast, cosurfactants enter the surfactant film, increasing the total interfacial area. This results in an increased “apparent” area per surfactant molecule if the co-adsorbed cosurfactant molecules are not accounted for. The oils employed in this research behaved as oils, as they did not change the area per surfactant molecule. As a conclusion, in our simplified model all of the oils are assumed to be located in the oil pseudophase, including the core or the interfacial oil regions. The surfactant film therefore contains no oil molecules.

The composition distribution in the oil droplet is assumed to be non-homogenous as depicted in Figure 1. The oil pseudophase is divided into two sub-phases according to the two-state solubilization theory: the interfacial and the core regions. Inside the real oil droplets, the oil composition is uniform up to a certain radius, $R_{uniform}$. The oil within this radius contains both polar and non-polar components. At equilibrium the chemical potentials in this core ($\mu_i^{uniform}$), the interfacial oil region, (μ_i^{int}), and in the excess oil phase (μ_i^{oil}) are equal:

$$\mu_i^{oil} = \mu_i^{uniform} = \mu_i^{int} \quad [13]$$

It is reasonable to assume that because the environment of the liquid-like interior of the core is very similar to the environment in the excess oil phase, both the uniform core and the excess oil phase have the same bulk composition (c_{bulk})

$$c_{uniform} = c_{oil} = c_{bulk} \quad [14]$$

where $c_{uniform}$ and c_{oil} are the volume fractions of the polar component in the uniform core and the excess oil phase, respectively.

The interfacial oil region of thickness d is located close to the micelle /water interface. Because of its mild surface activity, the polar component is enriched in the interfacial region. The benzene concentration increases gradually within this thickness from c_{bulk} to 1 as the surface of the droplets is approached.

Using solubilization data it is not possible to compute neither $R_{uniform}$ nor d . However, we can compute a different arrangement of a core and a shell in a simplified manner using our model, while keeping the total amount of the solubilized oil components the same as in the real system. This is depicted in Figure 1. In the model arrangement the shell accounts for the benzene surface excess, and contains only benzene:

$$c_{int} = 1 \quad [15]$$

where c_{int} is the volume fraction of benzene in the model interfacial oil. The volume of the interfacial region of the model therefore is given by the surface excess of the polar component. The thickness of this layer, denoted as q , is necessarily smaller than the real thickness of the concentration gradient, d .

In the simplified model all of the hydrophobic oil is located inside a “core”, with a radius of R_c . Here the composition is equal to the excess oil phase composition. This concept is similar to the Gibbs’ surface excess model (36), where the interface is assumed to have zero thickness, and the bulk phase composition is extrapolated up to the interface. The adsorbed material is then accounted for as surface excess per unit area.

The radius of the model core (R_c) and the thickness of the model shell (q) of this model arrangement are easily computed based on the knowledge of the volumetric solubilization of the two oils as single component oils, the composition of the excess oil phase, and the total interfacial area. However, both R_c and d must be regarded as parameters rather than real sizes of different real physical regions in the microemulsion.

An appropriate adsorption isotherm can be employed to relate the surface excess to the bulk oil concentration. We used a Langmuir isotherm-type relation (36) in terms of volume as

$$q = \frac{Kc_{bulk}}{B + c_{bulk}} \quad [16]$$

where q is the volume of the surface excess of the polar oil per unit surface area, c_{bulk} is the volume fraction of the polar oil in the core of the solubilized oil droplets, which is the same as that in the excess oil phase, and K and B are the Langmuir parameters, related to the maximum adsorption and the energy of adsorption per molecule. We are using the Langmuir model in a phenomenological way, since the "adsorption" in our case is likely more of a mobile type. Other restrictions of the Langmuir isotherm (e.g. monolayer assumption, no interaction between adsorbates and the surfactant tails, neglecting oil mixture non-idealities, etc.) may also not fully apply to our system. Future research

should analyze these aspects in more detail. We believe, however, that the Langmuir model is a reasonable assumption for solubilization in the polar region of the interface in that there are a limited number of solubilization sites for fixed surfactant concentration. Polar oil solubilization in this region is thus competitive solubilization.

In Eq. [16] q has length dimension, and corresponds to a shell thickness, which increases the radius of the core solubilized oil droplets. Therefore the total radius of the oil droplet becomes

$$R_t = R_c + q \quad [17]$$

where R_c is the radius of the core.

We expect that the value of q is less than the molecular size of the benzene molecule (~ 5.5 Angstroms) for different reasons. If the model shell were one benzene molecular size thick, it would be an indication of a saturated monomolecular adsorption at the interface. These kinds of films develop when surfactants adsorb at the interface as the only interfacial components. Benzene is not a surfactant, so we do not anticipate saturated adsorption. Furthermore, the “adsorbed” benzene molecules are located probably between some of the surfactant tails. Hence, in reality, the excess benzene does not necessarily fill the total interfacial area, even at high adsorption. In the model the interfacial oil and the surfactant layer are separated, the total volume of the excess benzene molecules are distributed over the entire interfacial area, and the real thickness of the interfacial oil region is reduced. These simplifications cause the model shell thickness (q) to remain well below the molecular size of benzene.

Selectivity

We define the selectivity as

$$Sel = \frac{c_{ave}}{c_{bulk}} \quad [18]$$

where c_{ave} is the volume fraction of the polar component in the oil pseudophase averaged over the core and interfacial oil regions. The average polar component volume fraction is given by

$$c_{ave} = \frac{\frac{4}{3}\pi R_c^3 \cdot c_{bulk} + \frac{4}{3}\pi((R_c + q)^3 - R_c^3) \cdot c_{int}}{\frac{4}{3}\pi(R_c + q)^3} \quad [19]$$

Combining Eqs. [18] and [19] yields

$$Sel = \left(\frac{R_c}{R_c + q}\right)^3 + \frac{1}{c_{bulk}} \left(\frac{(R_c + q)^3 - R_c^3}{(R_c + q)^3}\right) \quad [20]$$

Equation [20] provides relationship between the curvature and the selectivity.

Solution method.

The first step in the solution method is to calculate the core oil droplet radius using Eqs. [3] –[7]. Calculation of the shell thickness, the average solubilized oil composition, and the selectivity requires the knowledge of the bulk oil concentration, which can be very close to the initial oil concentration, but is strictly not the same. The bulk oil concentration is computed by solving the material balance of the polar oil:

$$V_o \cdot y = (V_o - V_t) \cdot c_{bulk} + V_t \cdot c_{ave} \quad [21]$$

where V_o is the total volume of oil added to the system, y is the volume fraction of the polar oil in the initial oil phase, and $V_t = A \frac{R_c + q}{3}$ is the total volume of oil solubilized in the microemulsion. The shell thickness and selectivity are calculated using Eqs. [16] and [20], respectively.

The selectivity model requires several parameters. The length parameter, L is the scaling parameter of the net curvature equation (Eq. [3]). It is an empirically adjustable determined parameter, which is the same for systems with the same surfactant. The characteristic length and optimum salinity models use pure component characteristic lengths and optimum salinities. These parameters are not empirically fitted, but rather are experimentally obtained directly from salinity scans with pure component oils. The Langmuir model contains two more parameters. Although these parameters are treated as empirical ones, they have thermodynamic origins as indicated before. The Langmuir parameters are obtained by fitting the average solubilized oil concentration and the experimental selectivity data to Eqs. [19] and [20], respectively.

There are several simplifications introduced in the selectivity model other than the ones previously discussed. The optimum salinity and characteristic length of the mixture was calculated based on the initial oil composition rather than the equilibrium oil phase composition. This simplification could be used because the difference between the equilibrium oil phase composition and the initial oil phase composition was small and the optimum salinity and characteristic length was not affected significantly.

The model considers spherical droplets of oil and water. The shape of the droplets may increasingly deviate from the sphere with increasing salinity. Neglecting the shape variation possibly causes some error in the predicted shell thickness. It is not expected to

yield large error for ionic surfactants because the shell thickness is at least one order of magnitude smaller than the core radius.

The variation of the CMC with changing electrolyte concentration is also neglected, because the CMC of the sodium dihexyl sulfosuccinate surfactant is two orders of magnitude less than the concentration used. All of the surfactant in excess of the CMC is assumed to reside at the internal interface in the microemulsion.

The contribution of the water solubility of the oil components to the total amount of oil in the microemulsion phase is taken same as measured without surfactant. It was assumed that the water solubilities of the oil components remain the same in the presence of surfactant aggregates. While this may not be correct, the error resulting from this simplification should be negligible, since micellar solubilization tends to be at least 1-2 orders of magnitude larger than water solubility.

RESULTS AND DISCUSSION

Optimum salinity and characteristic length.

Figure 2 shows the experimental and model predicted optimum salinity and characteristic length as a function of the oil phase composition. The optimum salinity decreased as the benzene volume fraction increased in the bulk oil. This agrees with the expected trend. In systems with high optimum salinity the surfactant interaction with the water is much stronger than its interaction with the oil. Therefore a large amount of electrolyte is needed to decrease the water-side interaction enough to reach balanced surfactant interactions with the oil and water side. As the benzene concentration increases

in the oil mixture, the oil becomes slightly more hydrophilic. The oil side interaction increases. Consequently less decrease of the surfactant-water interaction is enough to reach balance. Hence the optimum salinity decreases. The close agreement between the experimental and estimated optimum salinities support the linear mixing rules employed in Eq.10.

The characteristic length increases linearly with increasing benzene mole fraction. An increasing trend is expected, because polar oils are solubilized better than more hydrophobic oils (17-19, 26, 33, 37).

Benzene surface excess.

Shell thicknesses have been computed to verify the presence of benzene surface excess. The computed shell thickness values are greater than zero, therefore benzene is present in excess in the solubilized oil compared to the excess oil. If the presence of excess benzene in the micelles is due to adsorption from the bulk oil of the core, the amount of adsorption depends on the surface area and the bulk oil concentration. The shell thickness is not expected to vary as the salinity varies, because the surface area and the bulk oil concentration is not dependent on the salinity. However, the shell thickness is expected to depend on the bulk oil composition in the core according to a Langmuirian or another type of adsorption isotherm. Therefore, the idea of surface excess adsorption is justified if the experimental results show these expected trends.

“Experimental” shell thickness data (q) were obtained in the following way. First, the total solubilized limonene and benzene volume was computed from measured organic concentrations in the surfactant phase. The average benzene volume fraction in

the total solubilized oil is computed from the solubilization data. Then, the equivalent oil droplet radius (R_t) is calculated according to Eq. [8]. This radius contains both core and interfacial oil solubilization, but no surfactant. The shell thickness is obtained by solving Eq. [19] for q , substituting $R_c = R_t - q$, and using the experimental average benzene volume fraction of the solubilized oil. “Fitted” shell thicknesses were obtained by fitting our selectivity model to the selectivity data through each salinity scan series for all seven initial oil concentrations.

The shell thickness typically showed only negligible variation with increasing salinity at constant benzene concentration in the oil phase as shown in Figure 3. The shell thickness appears to be slightly less at low salinity than at higher salinity. This might be due to the small droplet radius. At low salinity the oil droplets are probably too small to separate a core and an interfacial region well. Limonene is likely to spend more time close to the micelle/water interface on a statistical basis when the oil droplets are very small, even if it is energetically not favored. Consequently benzene shares the interfacial layer more with limonene. This could reduce the apparent benzene surface excess. However, in the selectivity model shell thickness variation with changing salinity is neglected, because the salinity dependence was found to be weak.

The dependence of the shell thickness on the oil phase composition at constant salinity (no added salt) is presented in Figure 4. “Experimental” and “fitted” shell thicknesses are plotted together. It is seen that both experimental and fitted shell thicknesses depend on the benzene concentration in the bulk oil according to a Langmuirian isotherm. It was possible to fit the shell thickness (for all oil concentrations and salinities) using the same Langmuir parameters, $K = 0.94$ and $B = 0.35$. These

variations of the shell thickness with the salinity and the oil phase composition indicate that the benzene enrichment in the solubilized oil could be due to accumulation at the interface.

It is seen on Figure 4 that “experimental” and “fitted” shell thickness points are very close to each other. Therefore, experimental and fitted data points yield about the same Langmuir parameters. This is encouraging, because the two Langmuir parameters could also be determined from an adsorption isotherm instead of fitting several salinity scan selectivity data. Fitting one adsorption isotherm requires significantly less experimental effort than obtaining the parameters through fitting several salinity scans.

The computed shell thickness values were below 1 Angstrom for all experimental series as we see in Figures 3 and 4. These very small values indicate that the benzene adsorption is not strong, and does not produce a saturated monomolecular layer, as surfactants would do. Shell thickness values less than the molecular size of benzene (~5.5 Angstrom) result necessarily as discussed earlier. Hence, our shell thickness values reflect only a “swelling” rather than a true thickness where benzene segregation occurs. The shell thickness parameter accounts for any benzene volumetric surface excess per unit interfacial area. For benzene in this system the surface excess is small, and it is evenly distributed over the large total interfacial area, so very small shell thickness values result.

Selectivity dependence on salinity.

Figure 5. a shows variation of the experimental selectivity with increasing salinity, at constant bulk oil concentration. The selectivity is highest at low salinity, and

decreases as the salinity increases. Figure 5. b demonstrates the accompanying changes in the surface area to volume ratio of the solubilized oil as a function of salinity. It is seen that the surface area to volume ratio decreases as the salinity increases. Because the surface area is fixed by the amount of the surfactant, the core solubilization must become increasingly dominant as the salinity increases. Selectivity is highest at low salinity, when the interfacial solubilization is more dominant. Consequently the interfacial region must be rich in benzene. Selectivity approaches unity upon increasing salinity, when the core solubilization becomes dominant. This is an indication that the oil composition in the core is similar to the excess oil phase composition. We conclude then that benzene accumulation at the interface is responsible for the selective benzene solubilization, and the structural changes due to salinity variation strongly affect the selectivity.

We next analyze the relationship between the selectivity and the surface area to volume ratio. Figure 6 shows the selectivity as a function of $\ln\left(\frac{S^*}{S}\right)$. This salinity scale transformation is instructive because $\ln\left(\frac{S^*}{S}\right)$ is a linear function of the net curvature, as seen from Eq. 3. In the Winsor Type I phase behavior region, the contribution of the water droplet radius to the net curvature is negligible, because the water droplets are very large. Consequently the new salinity scale will be essentially linear with respect to the inverse oil radius $\left(\frac{1}{R_o}\right)$. The surface area-volume ratio of the oil droplets is also linear in the curvature, because

$$\frac{A}{V} = \frac{4\pi R^2}{\frac{4}{3}\pi R^3} \propto \frac{1}{R} \quad [22]$$

Figure 6 shows that the selectivity is a linear function of $\ln\left(\frac{S^*}{S}\right)$ with some deviation at low salinities (i.e., high $\ln\left(\frac{S^*}{S}\right)$ values). Therefore the selectivity is essentially a linear function of the surface area /volume ratio of the droplets.

This result also seems to support idea that the total solubilization has two contributions: one due to the interfacial excess (M_{int}):

$$M_{int} = V_{int} \quad [23]$$

where V_{int} is the volume of the solubilized oil at the interface, composed of only benzene, and another contribution due to the bulk solubilization by the micellar core (M_{core}):

$$M_{core} = c_{core} \cdot V_{core} \quad [24]$$

where c_{core} is the volume fraction of benzene in the micellar core, V_{core} is the solubilized oil volume in the cores. The selectivity is given by

$$Selectivity = \frac{[V_{int} + c_{core} \cdot V_{core}]/[V_{int} + V_{core}]}{c_{core}} = \frac{1}{c_{core}} \cdot \left[c_{core} \cdot \frac{V_{core}}{V_{int} + V_{core}} \right] + \frac{1}{c_{core}} \cdot \left[\frac{V_{int}}{V_{int} + V_{core}} \right] \quad [25]$$

When the droplets are sufficiently large, $V_{core} + V_{int} \cong V_{core}$, which yields

$$Selectivity \cong 1 + \frac{1}{c_{core}} \cdot \left[\frac{V_{int}}{V_{core}} \right] \quad [26]$$

The total volume of the interfacial solubilization contribution of N droplets is

$$V_{int} \cong q \cdot A_{droplets} = N \cdot q \cdot 4\pi R_{core}^2 \quad [27]$$

and the volume of the core solubilization is given as

$$V_{core} = N \cdot \frac{4}{3} \pi R_{core}^3 \quad [28]$$

Hence, the selectivity can be approximated as

$$Selectivity \cong 1 + \frac{3q}{c_{core}} \cdot \left[\frac{1}{R_{core}} \right] \quad [29]$$

If the salinity is changed while the initial oil composition is constant, the shell thickness and the equilibrium bulk oil concentration remain constant. Hence, the selectivity follows a linear dependence on the inverse oil radius according to Eq. 29. The same linear dependence is demonstrated on Figure 6. The slight deviation from linearity at low salinity (high $\ln\left(\frac{S^*}{S}\right)$) values especially for low benzene concentrations may result from the fact that the droplet sizes are probably not large enough to apply $V_{core} + V_{int} \cong V_{core}$ and $V_{int} \cong q \cdot A_{droplets}$.

Figure 7 presents results of model predictions for the selectivity dependence on the salinity for seven oil compositions. There is a good agreement between model and data results over the complete salinity range. The good fit suggests that the model concepts discussed above are realistic.

Selectivity dependence on the oil composition.

Figure 8. a shows the dependence of the selectivity on the benzene concentration in the bulk oil at no added salt. Experimental data and model predictions are plotted together. The selectivity decreases with increasing benzene volume fraction. This is a somewhat surprising result, because one would think, that higher benzene concentration in the bulk oil should increase the surface excess adsorption. Consequently the selectivity

should increase. On the contrary, the results show an opposite trend. This indicates that another effect may also be important, which tends to decrease the selectivity.

The surface area to volume ratio is useful parameter, which indicates whether the interfacial or the core solubilization dominates the overall solubilization. If the surface area to volume ratio is large, the surface solubilization is more important, and if it is small, the core solubilization dominates. Figure 8. b demonstrates the variation of the surface area to volume ratio of the solubilized oil. We see a decreasing trend of this ratio as the benzene concentration in the bulk oil phase increases. This is expected, because as the benzene concentration increases, the overall oil phase becomes more polar. Polar oils are known to be solubilized better than non-polar oils. Larger solubilized volume corresponds to larger droplet radius and smaller area to volume ratio. Decreasing surface area to volume ratio tends to decrease the selectivity as discussed before. Because the selectivity decreases with increasing benzene concentration, the effect of surface area to volume ratio appears to dominate over the increasing shell thickness. The model provided good agreement with the experimental data in predicting this trend.

REFERENCES

1. Bourrel, M.; Schechter, R. S. *Microemulsions and Related Systems: Formulation, Solvency and Physical Properties*; Marcel Dekker; New York, **1988**.
2. Rosen, M. *Surfactants and Interfacial Phenomena*; 2nd ed; John Wiley & Sons; New York, **1989**.
3. Dunaway, C. S; Christian; S. D., Scamehorn, J. F. In *Solubilization in Surfactant Aggregates*; Surfactant Sciences Series 55; Christian, S. D., and Scamehorn, J. F. Eds; Marcel Dekker; New York, **1995**; pp. 3-31.
4. Knox, R. C., Shau, B. J., Sabatini, D. A., Harwell, J. H. In *Innovative Subsurface Remediation, Field Testing of Physical, Chemical, and Characterization Technologie*; ACS Symposium Series 725; Brusseau, M. L., Sabatini, D. A., Gierke, J. S., and Annable, M. D., Eds., American Chemical Society, Washington, D.C., **1999**; pp. 49-63.
5. Kreilgaard, M. *Advanced Drug Delivery Reviews* **2002**, *54*, Suppl. 1, S77-S98.
6. Malcolmson, C., Satra, C., Santaria, S., Sidhu, A., Lawrence, M. J. *J. Pharm. Sci.* **1998**, *87* (1), 109-16.
7. Malcolmson, C., Lawrence, M. J. *J. Pharm. Pharmacol.* **1993**, *45* (2), 141-3.
8. Lawrence, M. J., Rees, G. D. *Adv. Drug. Deliv. Rev.* **2000**, *6*, 45 (1), 89-121
9. Jonsson, B; Landgren, M; Olofsson, G. In *Solubilization in Surfactant Aggregates*; Surfactant Sciences Series 55; Christian, S. C. and John F. Scamehorn, J. F., Eds.; Marcel Dekker, New York; **1995**; pp. 115-141.
10. Lee, B-H.; Christian, S. H.; Tucker, E. E.; Scamehorn, J. F. *Langmuir* **1990**, *6*, 230-235.
11. Mahmoud, F. Z.; Higazy, W. S.; Christian, S. D.; Tucker, E. E; Taha, A. A. *J. Colloid Interface Sci.* **1989**, *131*, 96-102.
12. Uchiyama, H.; Tucker, E. E.; Christian, S. D.; Scamehorn, J. F. *J. Phys. Chem.* **1994**, *98*, 1714-1718.
13. Smith, G. A.; Christian S. D.; Tucker, E. E.; Scamehorn, J. F. *J. Solution Chemistry* **1986**, *15* (6), 519-529.
14. Tucker, E. E.; Christian, S. D.; *J. Colloid and Interface Sci.* **1985**, *104* (2), 562-568.

15. Rouse, J. D.; Sabatini, D. A.; Deeds, N. E.; Brown, R. E. *Env. Sci. Technol.* **1995**, *29*, 2484-2498.
16. Harwell, J. H. In *Transport and Remediation of Subsurface Contaminants. Colloidal, Interfacial and Surfactant Phenomena*; ACS. Symposium Series 491; Sabatini, D. A.; Knox, R. C., Eds.; American Chemical Society, Washington, D. C.; **1992**; pp. 124-132.
17. Mukerjee, P.; Cardinal, J. R. *J. Phys. Chem.* **1978**, *82* (14), 1620.
18. Mukerjee, P. In *Solution Chemistry of Surfactants*; Volume 1; Mittal, K. L., Editor; Plenum, New York; **1979**; pp. 153.
19. Mukerjee, P. *Pure & Appl. Chem.* **1980**, *52*, 1317-1321.
20. Nagarajan, R.; Ruckenstein, E. In *Surfactants in Solutions*; Volume 2; Mittal, K.L. and Lindman, B., Eds.; Plenum Press, New York; **1984**; pp. 923-947.
21. Ruckenstein, E. *Fluid Phase Equilibria* **1985**, *20*, 189-206.
22. Ruckenstein, E. In *Handbook of Microemulsion Science and Technology*; Kumar, P., and Mittal, K.L., Eds; Marcel Dekker, New York; **1999**; pp. 45-58.
23. Nagarajan, R.; Ruckenstein, E. *Langmuir* **2000**, *16*, 6400-6415.
24. Graciaa, A; Lachaise, J.; Cucuphat, C.; Bourrel, M.; Salager, J. L. *Langmuir* **1993**, *9*, 1473-1478.
25. Salager, J. L. In *Handbook of Detergents, Part A, Properties*; Surfactant Science Series 82; Zoller, U.; Editor in Chief; Broze, G.; Editor ; Marcel Dekker, New York; **1999**; pp. 253-302.
26. Acosta, E., Szekeres, E., Sabatini, D. A., Harwell, J. H. *Langmuir* **2003**, *19* (1), 186-195.
27. Strey, R. *Colloid Polym. Sci.* **1994**, *272*, 1005.
28. Adelman, D.; Cates, M. E.; Roux, D.; Safran, S. A. *J. Chem. Phys.*, **1987**, *87* (12), 7229-7241.
29. Bellocq, A. M. In *Emulsions and Emulsion Stability*; Surfactant Science Series 61; Sjoblom, J.; Schick, M. J.; and Fowkes, F. M.; Eds.; Marcel Dekker, New York; **1996**; pp. 181-236.

30. Auvray, L. in *Micelles, Membranes, Microemulsions and Monolayers*; Gelbart, W. M.; Ben – Shaul, A.; and Roux, D.; Editors; Springer-Verlag, New York; **1994**; pp. 347-393.
31. De Gennes, P. G.; Taupin, C. *J. Phys. Chem.* **1982**, *86*, 2294.
32. Salager, J. L.; Bourrel, M.; Schechter, R. S.; Wade, W. H. *Soc. Pet. Eng. J.* **1979**, 271-277.
33. Baran, J. R.; Pope, G. A.; Wade, W. H.; Weerasooriya, V.; Yapa, A. *Environ. Sci. Technol.* **1994**, *28*, 1381-1388.
34. Baran, J. R.; Pope, G. A.; Wade, W. H.; Weerasooriya, V. *Langmuir* **1994**, *10*, 1146-1150.
35. Biais, J; Bothorel, P; Clin, B; Lalanne, P. *J. Dispersion Sci. Technol.* **1981**, *2* (1), 67-95.
36. Lyklema, J. In *Liquid-Fluid Interfaces*; Fundamentals of Interface and Colloid Science, Volume III.; Academic Press, San Diego; **2000**; pp. II. 4.1- II. 4.33.
37. Shiau, B. J.; Sabatini, D. A.; Harwell, J. H. *Ground Water* **1994**, *32*, 561-569.

TABLES

Chapter 3

Sodium dihexyl sulfosuccinate	CMC ^a , mole / l	0.01
	Area per surfactant molecule ^{a,d} , Angstroms ²	100
	Length parameter ^d , Angstroms	10
Benzene	Optimum salinity ^b , %	2.04
	Characteristic length at optimum ^b , Angstroms	79
(R)- (+)- Limonene ((R)-4-Isopropenyl-1- methyl-1- cyclohexene)	Optimum salinity ^b , %	6.1
	Characteristic length at optimum ^b , Angstroms	38

Table 1. Selected parameters of chemicals used in the benzene-limonene experiments.

^a Ref. 2, ^b Determined experimentally as part of this research, ^d Ref. 26.

FIGURES

Chapter 3

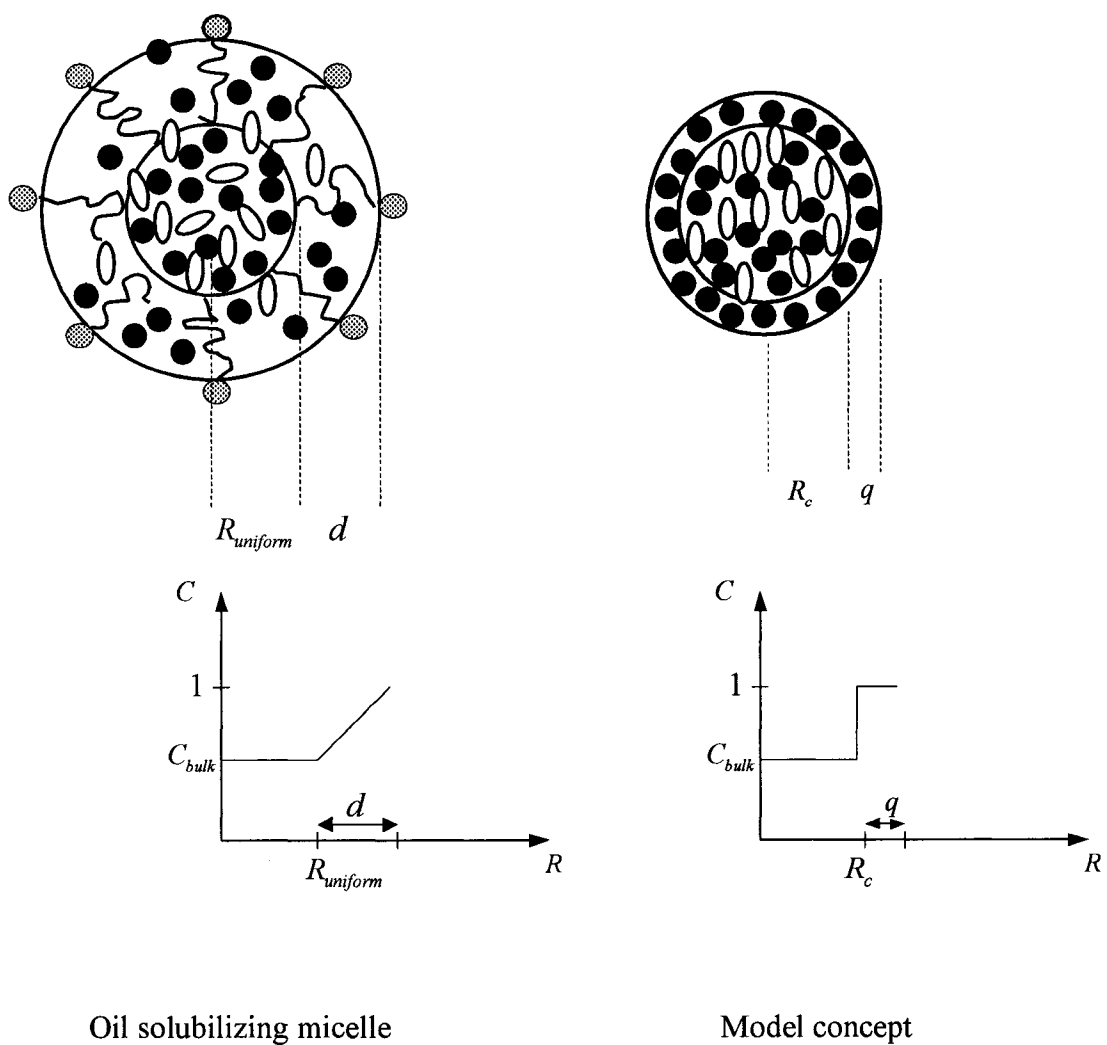


Figure 1. Schematic representations of oil solubilizing micelle, and model concept.

The figures show the volume fraction variation of the more polar oil component in the solubilized oil (C) as a function of the radius (R) for the real oil solubilizing micelle and for the model.

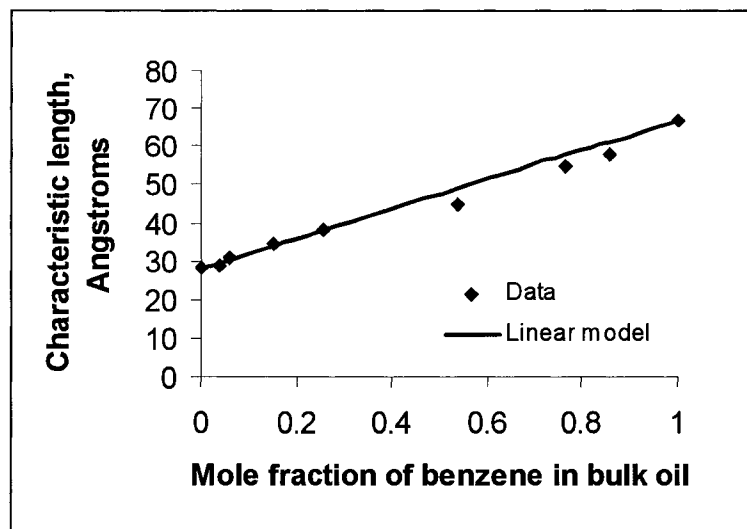
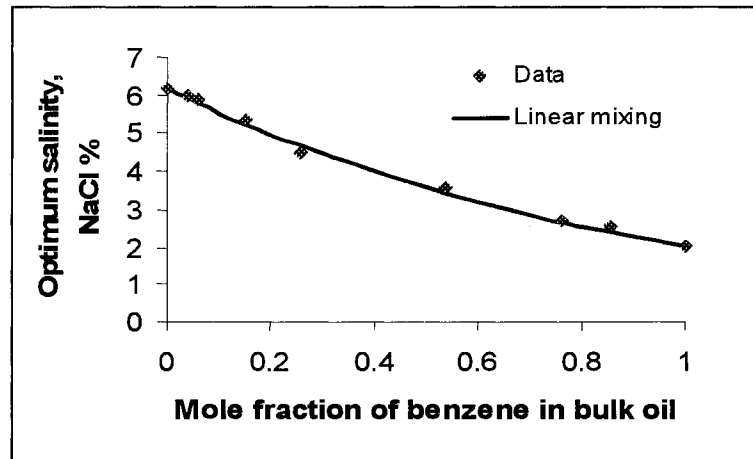


Figure 2. Optimum salinity and persistence length variation with bulk oil phase composition.

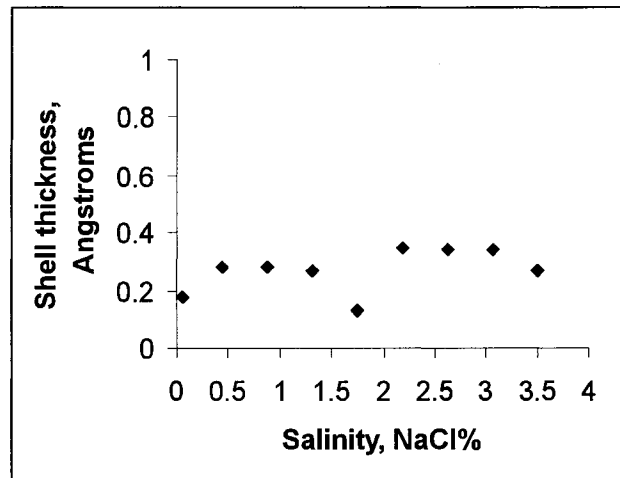


Figure 3. Experimental shell thickness variation with salinity for 0.19 volume fraction benzene concentration in bulk oil, optimum salinity 4.4.

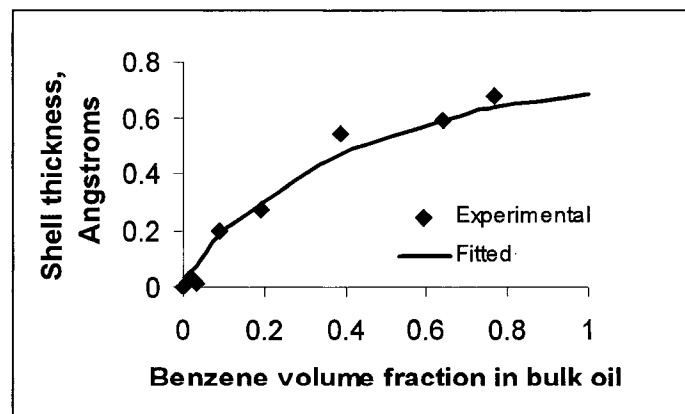


Figure 4. Experimental and fitted shell thickness variation with oil phase composition.

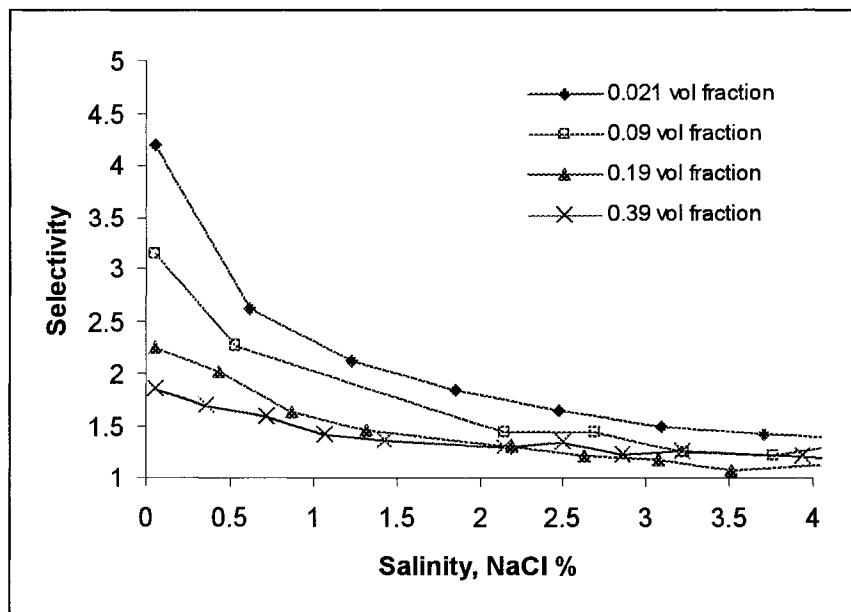


Figure 5. a. Selectivity dependence on the salinity. Results of four different bulk oil compositions are plotted.

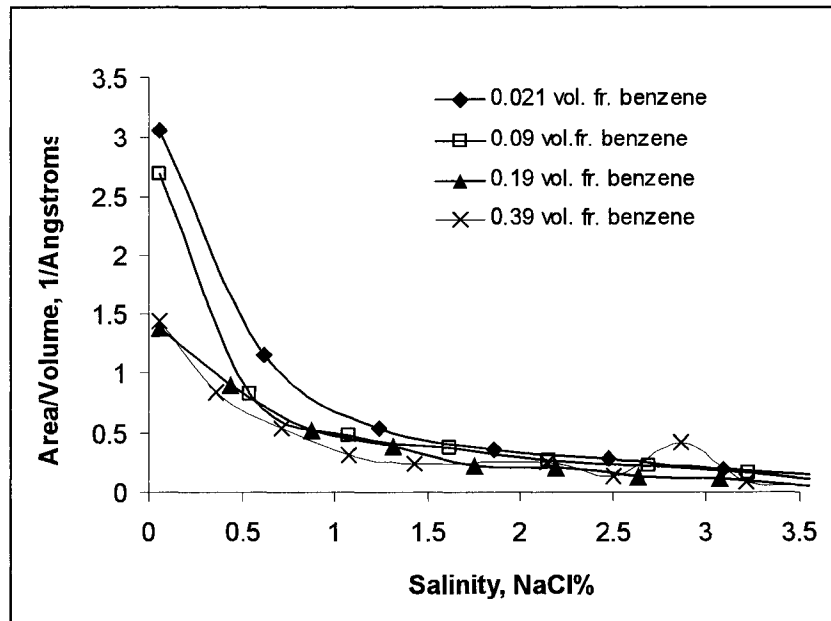


Figure 5. b. Dependence of the surface area to volume ratio of the solubilized oil on the salinity. Four different benzene bulk oil volume fractions are plotted.

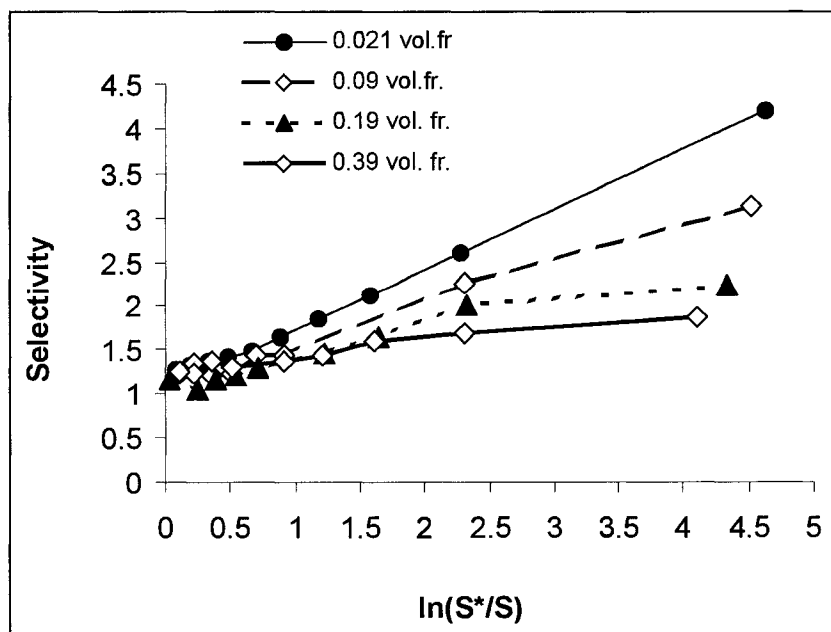


Figure 6. Selectivity plotted with respect to $\ln\left(\frac{S^*}{S}\right)$. Salinity scan data of four different bulk oil benzene volume fractions are included.

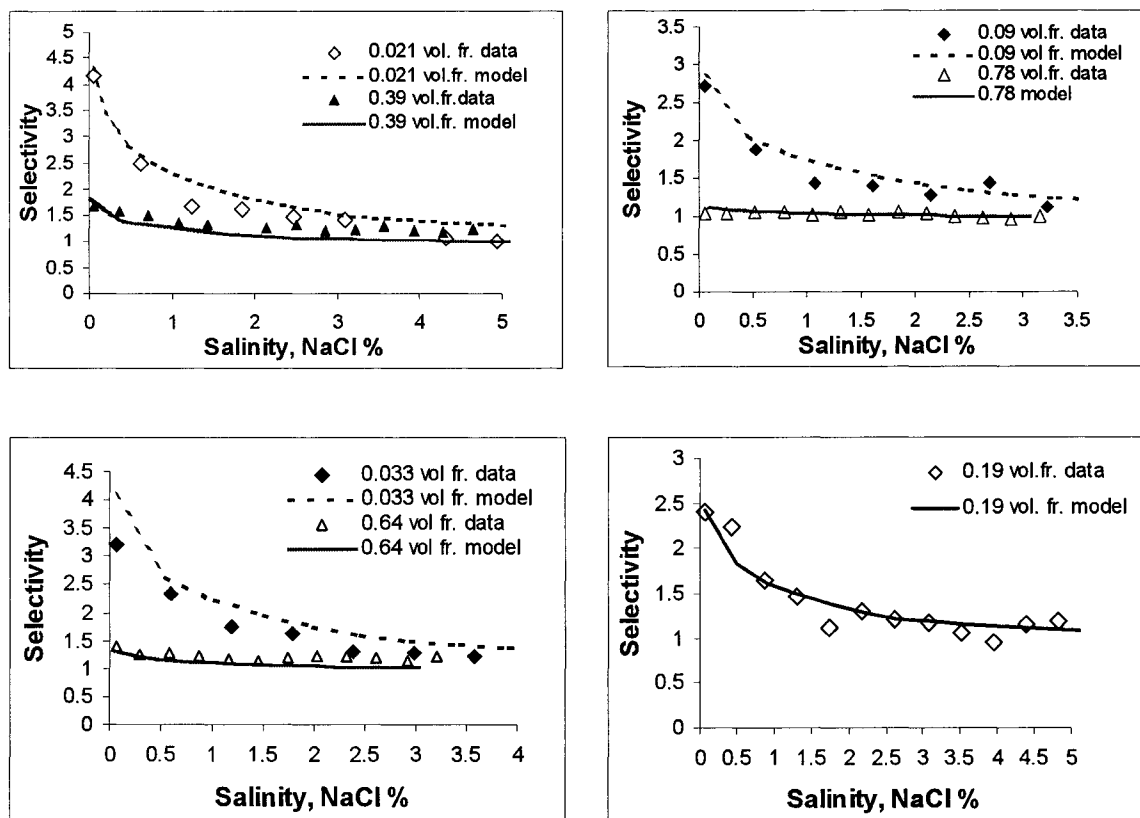


Figure 7. Selectivity dependence on salinity as predicted by the model for seven oil compositions. Corresponding data are also plotted to compare with model.

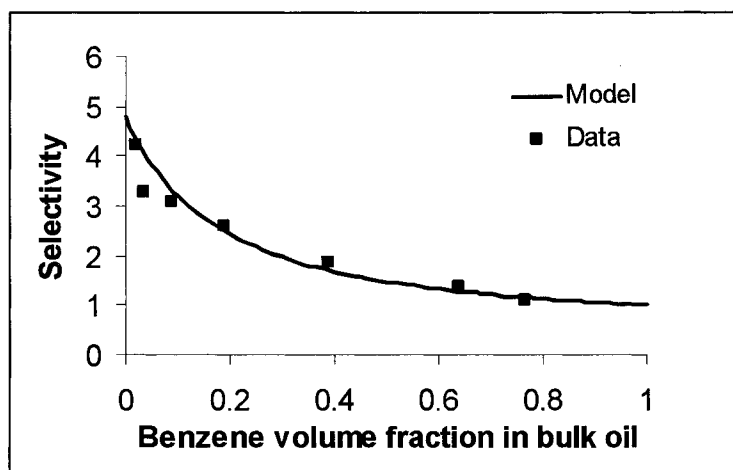


Figure 8. a. Selectivity dependence on the oil phase composition. Data and model correspond to no added salt case.

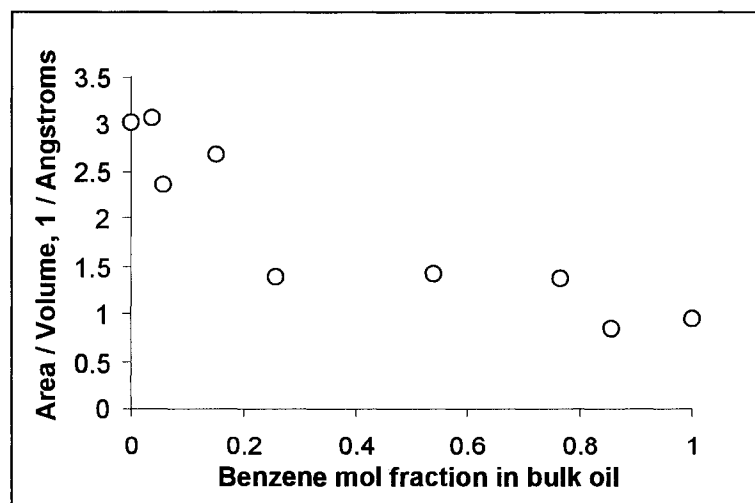


Figure 8. b. Effect of oil phase composition on the surface area to volume ratio of the solubilized oil. Experimental results are shown for the no added salt case.

CHAPTER 4

PREFERENTIAL SOLUBILIZATION OF DODECANOL FROM DODECANOL-LIMONENE BINARY OIL MIXTURE IN SODIUM DIHEXYL SULFOSUCCINATE MICROEMULSIONS: EFFECT ON OPTIMUM SALINITY AND OIL SOLUBILIZATION CAPACITY *

ABSTRACT

Solubilization of a dodecanol-limonene binary oil mixture has been studied in saturated Winsor type I and III sodium dihexyl sulfosuccinate microemulsions. The system showed different oil solubilization behavior below and above 0.2 dodecanol volume fraction. Below 0.2 dodecanol volume fraction regular Winsor type microemulsions formed. The oil solubilization was characterized in this concentration range by the optimum salinity and the characteristic length. Dodecanol showed a Langmuirian-type adsorption at the palisade layer. Variation of the optimum salinity and middle phase characteristic length with increasing dodecanol concentration could be linked to the dodecanol surface excess variation. These relationships were used to develop new mathematical models for the optimum salinity and characteristic length as a function of oil phase composition. Both models yielded excellent agreement with the data. Above 0.2 dodecanol volume fraction regular Winsor type microemulsions did not form but rather the surfactant partitioned between the water rich and oil rich phases. Under these circumstances the role of dodecanol as a cosolvent for the surfactant in the oil phase was important, and microemulsion formation became less favorable. Therefore our new models were not applicable in this concentration range.

INTRODUCTION

Solubilization of oil mixtures in microemulsions is encountered in surfactant enhanced aquifer remediation (SEAR) processes for two main reasons. Oil contamination

* To be submitted to *Journal of Colloid and Interface Science*

at a remediation site is likely an oil mixture (1-4), both polar and non-polar (e.g., hydrocarbons, aromatics, chlorocarbons, ketones, etc.). Polar oil (e.g. dodecanol) may also be introduced intentionally into the surfactant solution as an additive in order to increase solubilization of a more hydrophobic oil contaminant by the surfactant solution (5-8). Solubilization of single component oils and oil mixtures containing similar oil components has been well studied. In contrast oil mixtures with components of differing polarities have received much less attention. In the present study, we investigate the solubilization of binary non-polar and polar oil mixtures in microemulsions formed using an anionic surfactant.

To assess the remediation performance of SEAR, it is necessary to know how much oil is solubilized in the microemulsion (4, 9-12). However, comparing two microemulsions is difficult, because solubilization depends on a number of factors (13), including the type/concentration of oil, surfactant, additives (electrolyte, alcohol), and temperature. Salager suggested (14) comparing the solubilization ability of different microemulsions at a common reference point. For this purpose, a convenient reference point is the optimum formulation. At the optimum formulation equal volumes of oil and water are solubilized, the solubilization parameter is maximum, and the interfacial tension between the oil/microemulsion and water/microemulsion phases reach a minimum. Therefore two items of information are needed to characterize a microemulsion: (1) the set of independent variables (e.g. composition, and temperature) that is necessary to produce the optimum formulation, and (2) the solubilization capacity of the surfactant at the optimum formulation (15,16).

In this study, NaCl additive is used to fine-tune the surfactant formulation to reach optimum. The concentration of NaCl at which optimum formulation is achieved is called optimum salinity (16). The characteristic length (17) at optimum formulation gives information about the solubilization ability of the surfactant. The characteristic length is essentially equal to the average radius of the oil droplets in direct (o/w droplet type) microemulsions. At the optimum formulation, the characteristic length is equal to the average half thickness of the oil (or water) domain that can be correlated to one surfactant layer. The larger the optimum characteristic length, the more efficient the surfactant is in solubilizing oil (or water).

Both optimum salinity and optimum characteristic length depend on the type of oil to be solubilized, if all other conditions are kept constant. To decide whether a surfactant could efficiently solubilize specific oil mixture at a certain formulation, knowledge is necessary of these two parameters as a function of the oil phase composition. Our objectives are to study the dependence of the optimum salinity and characteristic length at optimum on the oil phase composition.

BACKGROUND

In order to find the optimum formulation for an oil/ionic surfactant pair at a fixed temperature experimental phase behavior studies are carried out (9,18-20). First the aqueous surfactant solution is contacted with the oil. The surfactant forms direct (oil-in-water type), oil swollen micelles. If there is enough oil, two phases are formed, the microemulsion phase and the excess oil phase. Next, additives are introduced (e.g.,

electrolyte, alcohol) in increasing concentration. This causes a continuous change in the curvature of the surfactant layer, resulting in an increase of the micellar radius. Approaching the optimum formulation, an excess water phase starts to phase separate. At this point the discrete droplet type microstructure changes into bicontinuous. The salinity at which excess water separation starts is called lower critical point. Above this salinity the two phase system changes into a three phase system. The microemulsion phase is located in the middle phase, and the excess oil/water phases occur in the upper/lower phases depending on their densities. The formulation is called “optimum” when the solubilized oil volume and the water volume in the microemulsion become equal. At the optimum formulation the natural curvature of the surfactant membrane is zero. Upon further salinity increase, the upper critical point is reached, at which point the excess oil phase disappears and the mixture becomes a two phase system again. One phase is the microemulsion phase with w/o micelles, and the other phase is the excess water phase.

In this research we use electrolytes as additives. In this case, optimum salinity refers to the electrolyte concentration which produces the optimum formulation. Optimum salinity for single component oil can be calculated using the surfactant affinity difference (SAD) concept, introduced by Salager et al. (14-16). For anionic surfactants SAD is given as

$$\frac{SAD}{RT} = \mu_s^{*,o} - \mu_s^{*,w} = \ln S - K \cdot EACN - f(A) + \sigma - a_T \Delta T \quad [1]$$

where R is the gas constant, T is the absolute temperature, $\mu_s^{*,o}$ and $\mu_s^{*,w}$ are the chemical potentials of the surfactant in the oil and in the water, respectively; S is the salinity, K is a constant, depending on the type of the surfactant, $EACN$ is the equivalent alkane carbon number of the oil, $f(A)$ is a function which depends on the alcohol, σ is a

constant which depends on the surfactant, and a_T is the coefficient of the temperature effect on the SAD. At the optimum formulation $SAD = 0$, and the optimum salinity is given as

$$\ln S^* = K \cdot EACN + f(A) - \sigma + a_T \Delta T \quad [2]$$

Baran et al. (21) proposed an optimum salinity model for oil mixtures using the pseudocomponent assumption for the oil. When the pseudocomponent assumption (13, 22-23) is valid, the oil behaves in a collective way. The composition of the solubilized oil is equal to the initial oil phase composition. If there is excess oil phase in equilibrium with the microemulsion, the solubilized oil composition and the excess oil phase composition are equal. The $EACN_{mix}$ of the oil mixture is computed applying a linear mixing rule as follows:

$$EACN_{mix} = \sum_i x_i EACN_i \quad [3]$$

where $EACN_{mix}$ and $EACN_i$ are the equivalent alkane carbon numbers of the mixture and component i , respectively, and x_i is the mole fraction of component i in the oil mixture. Combining Eqs. [2] and [3] yields the following expression for the optimum salinity of the oil mixture:

$$\ln S_{mix}^* = \sum_i x_i \cdot \ln S_i^* \quad [4]$$

where S_i^* is the optimum salinity of single component oil i .

One finds however, that the solubilized oil composition deviates from the initial oil composition when the polarity and/or molecular volume of the oil components are different (24, 25). For these mixtures, the pseudocomponent assumption is not valid, and

it is not clear how the mixture optimum salinity should be computed. The experimentally determined optimum salinity was also found to deviate from the one predicted by Eq. [4].

To our knowledge, a mathematical model to predict the middle phase characteristic length of oil mixtures as a function of oil composition has not been proposed. However, instead of the characteristic length, the optimum solubilization parameter has been used to describe the oil solubilization ability of the surfactant. For example, an optimum solubilization parameter model for oil mixtures has been developed and used in UTCHEM (26). UTCHEM is a multi-phase, multi-component flow simulator developed at the University of Texas, at Austin. The solubilization parameter is defined as the solubilized oil volume per unit volume of surfactant. Similarly to the characteristic length it provides information about the solubilization ability of the surfactant. It is a linear function of the mixture EACN as

$$\beta(S) = s(S) \cdot EACN_{mix} + h(S) \quad [5]$$

where $\beta(S)$ is the solubilization parameter at salinity S , $s(S)$ and $h(S)$ are salinity dependent empirical parameters, which are not dependent on the oil composition. To calculate the oil mixture EACN the pseudophase assumption is applied, with a linear mixing rule according to Eq.[3]. As the polar component mole fraction is increased, the mixture EACN decreases linearly. This results in a linear solubilization parameter increase at constant salinity.

Examples can be found in the literatures that demonstrate when this model can not be accurate (21). Deviations may come from two sources: (1) the EACN mixing rule is not linear, or (2) the solubilization parameter is not a linear function of the mixture EACN. Graciaa and Salager present an example of when the EACN mixing rule is not

linear (25). In their system the solubilization parameter did not follow a simple linear dependence on the concentration of the polar component in the oil phase. Rather, while solubilization increased linearly at first when the polar component mole fraction was increased, it reached a constant value at about 0.5 mole fraction.

The failure of the solubilization parameter to be a linear function of the mixture EACN may also result from approaching the tricritical point because of increased oil polarity (i.e. EACN decrease). The tricritical point is defined as the point at which three conjugate phases become simultaneously identical (27), resulting in a single-phase system. The single phase point can be reached by increasing the surfactant concentration in optimum middle phase microemulsion until the microemulsion phase (i.e., middle phase) incorporates all of the excess oil and water. Single phase system could also be brought about if the lower and upper critical end-points merge in balanced systems, while the surfactant concentration is sufficiently large (28, 29). The latter condition corresponds to tricritical systems as it is associated with the weakening of the structure (30). It has been observed that merging the two critical end points may take place, for example, when the oil polarity is increased (29, 31). If the oil polarity is such that the two critical points merge, the microemulsion changes from o/w to w/o droplet type without middle phase formation as the salinity is increased. Close to the tricritical point, the amphiphilicity of the surfactant is decreased (29), which leads to reduced solubilization.

As a general trend the solubilization parameter rises with increasing oil polarity (i.e., decreasing oil EACN) for systems with strong surfactants, in agreement with the UTCHEM model. However, the optimum solubilization parameter increase with decreasing EACN is limited. This is because at sufficiently high oil polarity the surfactant

may start to behave as a weak surfactant, resulting in a system, which approaches a tricritical state. When this point is close, the solubilization parameter starts to decrease. This behavior is not accounted for in the UTCHEM model, hence the model is valid only up to a certain oil polarity. For mixtures of polar and non-polar oils it is therefore necessary to develop new models for the optimum salinity and the solubilization parameter dependence on the oil phase composition. Furthermore, it is important to determine the oil composition limits where the models can be used.

We propose that polar oil components may be enriched in the solubilized oil because of their surface activity at the vicinity of the surfactant film. If this happens, it causes deviation from the pseudocomponent assumption. The question is whether the degree of the deviation from the pseudocomponent assumption or the surface excess adsorption itself dictates optimum salinity and the characteristic lengths. In the proposed new models, the optimum salinity and the solubilization parameter depend explicitly on the surface excess of the surface active component, and only implicitly on the initial oil phase composition. The new models will be evaluated against experimental data.

THEORY

Pseudocomponent assumption.

Previous research results help explain the deviation from the pseudocomponent assumption in polar – non-polar oil mixtures. It is well known that oils are solubilized in different locations in the micelles, depending on their polarity (13, 32 - 34). There are

basically three different locations for oil solubilization: the polar surface region, the palisade layer (between the surfactant tails), and the hydrophobic core. Non-polar oils are solubilized only in the micellar core. In saturated micellar solutions semi-polar and polar oils may be solubilized not only in the core but and also in the palisade and surface regions. It has been proposed that the surface active behavior of a polar oil and the favorable entropy of mixing effects are responsible for oil molecules entering the palisade layer and the surface region (24, 32,34).

When binary mixtures of polar and non-polar oils are solubilized, the non-polar component is restricted to the core, but the polar oil is solubilized in both the core and in the palisade layer. Therefore, the polar oil is solubilized preferentially (24, 25). As a result, the concentration of the polar oil is greater in the solubilized oil than in the excess oil phase and the pseudocomponent assumption will no longer apply.

Optimum salinity.

The presence of the oil molecules in the palisade layer is expected to influence the optimum salinity. In the optimum formulation the surfactant film curves neither to the oil nor to the water side, but has a mean curvature of zero. Upon solubilization of the oil, at constant salinity, the shape (i.e., curvature) of the surfactant film changes (35). The greater the tendency of the oil to partition into the palisade layer, the greater the decrease of the curvature of the surfactant film towards the oil. When the oil solubilization already decreases the curvature, less electrolyte concentration is needed to reach zero mean curvature at the optimum. Hence, reduction of the optimum salinity is expected as the oil penetration tendency increases.

For binary oil mixtures of polar and non-polar oils, the oil penetrating into the palisade layer is expected to be more representative of the polar oil than the initial oil mixture. Therefore, the curvature change caused by the solubilization of the oil mixture might also resemble an oil mixture that is more polar than the initial oil.

The SAD concept can be used to relate the curvature change upon oil solubilization and the optimum salinity. At a salinity below the optimum salinity (S), in the absence of alcohols and when temperature effects are neglected, SAD is given as

$$\frac{SAD}{RT} = \ln(S) - K \cdot EACN + \sigma \quad [6]$$

At the optimum salinity, when EACN is kept constant

$$0 = \ln S^* - K \cdot EACN + \sigma \quad [7]$$

Combining Eqs. [6] and [7] yields

$$\frac{SAD}{RT} = \ln S - \ln S^* \quad [8]$$

In a recent paper (36) it has been proposed, that

$$\frac{SAD}{RT} \propto H_{net}(S) \quad [9]$$

where $H_{net}(S) = \left| \frac{1}{R_o} \right| - \left| \frac{1}{R_w} \right|$ is the net curvature at a salinity S , R_o and R_w are the radii of oil and water droplets, respectively. Introducing a proportionality constant, L , and combining Eqs. [7] and [8] we arrive at

$$\ln S^*(C) - \ln S = L \cdot H_{net}(S, C) \quad [10]$$

The optimum salinity in equation [10] is a function of only the oil composition (C) if the temperature and the type and concentration of surfactant is fixed, whereas the net curvature is the function of both the salinity and the dodecanol concentration.

For oil composition 1:

$$\ln \frac{S^*_1}{S} = L \cdot H_{net,1}(S) \quad [11]$$

For oil composition 2:

$$\ln \frac{S^*_2}{S} = L \cdot H_{net,2}(S) \quad [12]$$

Combining Eqs. [10] and [11] at constant salinity we arrive at

$$\ln S^*_2 = \ln S^*_1 + L \cdot [H_{net,1} - H_{net,2}] \quad [13]$$

where $H_{net,1}$ and $H_{net,2}$ are net curvatures of composition 1 and composition 2, respectively, evaluated at the same salinity. Equation [13] suggests that the logarithm of the optimum salinity is a linear function of the net curvature. If a relation between the curvature and the palisade layer solubilization (and oil phase composition) was available, the optimum salinity could be predicted as a function of the composition.

Characteristic length.

The characteristic length of the microemulsion can characterize the oil/water solubilization ability of the surfactant. The larger the characteristics length, the better the solubilization ability of the surfactant. According to De Gennes and Taupin, the characteristic length is given (17)

$$\xi = \alpha \cdot \exp\left(\frac{2\pi\kappa}{k_B T}\right) \quad [14]$$

where α is a molecular length, κ is the bending elasticity of the surfactant film, k_B is the Boltzmann constant and T is the absolute temperature. The characteristic length can be inferred from solubilization data (37) using

$$\xi = \frac{6\phi_{oil}\phi_{water}V_m}{A_s} \quad [15]$$

where ϕ_{oil} and ϕ_{water} are the volume fractions of oil and water domain in the microemulsion, respectively, V_m is the volume of the microemulsion, and A_s is the total surface area of the surfactant film. The bending elasticity values have been estimated from excess dispersed phase/microemulsion interfacial tension data and small-angle neutron scattering (38, 39). Using Eqs. [14] and [15] the bending elasticity values may also be inferred from middle phase solubilization data. Equation [14] predicts that increasing the bending rigidity yields increasing optimum characteristic length, and greater oil solubilization.

We propose that the bending rigidity and the characteristic length may be increased by the penetration of the polar oil in the palisade layer. Salager and Graciaa also attributed the oil solubilization boosting caused by the lipophilic linkers to their segregation in an oriented fashion near the interface (25). Amphiphilic block co-polymers that adsorb on the surfactant membrane have also been shown to boost solubilization (38,40). The solubilization boosting was linked to the increase in the bending rigidity. A linear relationship between the bending rigidity and the adsorption was derived theoretically and confirmed experimentally.

In this research we investigate how the surface excess of the polar oil is related to the bending rigidity and the characteristic length of the system. Bending rigidity values will be estimated from solubilization data using Eqs. [14] and [15].

MATERIALS AND METHODS

Materials. The anionic surfactant sodium dihexyl sulfosuccinate (80 w% solution in water) was purchased from Aldrich Chemical (Fluka Brand). (R)-(+)-Limonene (98+ %), n-dodecanol (98+ %) and NaCl (99+ %) were obtained from Aldrich (Milwaukee, WI) and were used without further purification. Table 1 shows selected properties of the materials used.

Methods. Batch solubilization studies were performed by mixing equal volumes (5 ml) of aqueous surfactant solution and oil mixture. The test tubes were kept at constant temperature at 23° C, and shaken several times a day for three days. After the samples were left to equilibrate for two weeks, phase volumes were recorded, and concentration of limonene, dodecanol and surfactant were measured in each phase. In selected series the interfacial tension between the coexisting phases was also measured.

The concentration of limonene and dodecanol was measured with Varian 3300 gas chromatograph using FID detector and SPB 20 capillary column with programmed temperature. The sodium dihexyl sulfosuccinate concentration was measured with a Dionex ion chromatograph using an NS1 column. The interfacial tension was measured by the spinning drop method, with a Model 500 University of Texas tensiometer. The 300

μl capillary test vial was filled with the denser phase. 1-5 μl of the lighter phase was injected into the filled vial, and droplet size readings were taken after equilibration.

Two experimental series were carried out. In experimental series 1 the surfactant concentration was kept constant at 4 wt %. No electrolyte was added to the surfactant solution. Therefore, in this series the salinity was also kept constant. The volume fraction of dodecanol in the oil phase was varied from 0 to 1 throughout the series. In this series all mixtures yielded two phase systems at equilibrium

In experimental series 2 the surfactant concentration was also kept constant at 4 wt % in each vials. The dodecanol concentration in the oil phase was varied between 0 and 0.2 volume fraction. At each dodecanol concentration, salinity scans were performed. Through the salinity scan the salinity was varied so that Winsor Type I – III – II phase behavior transitions could be generated. Additionally, water solubility of the two oil components was measured as a function of oil phase composition.

RESULTS AND DISCUSSION

Pseudocomponent assumption.

Figure 1 shows how preferential solubilization varies with changes in dodecanol concentration at constant salinity. In Figure 1.a, the average dodecanol volume fraction in

the solubilized oil (C_{ave}) is plotted with respect to the dodecanol volume fraction in the excess oil phase (C_{bulk}). The salinity was kept constant (no added salt) in this series. We computed C_{ave} from:

$$C_{ave} = \frac{C_{dodecanol}}{C_{dodecanol} + C_{limonene}} \quad [16]$$

where $C_{dodecanol}$ and $C_{limonene}$ are the measured dodecanol and limonene volumetric concentrations in the microemulsion. Figure 1.b presents the corresponding selectivity variation trend. The selectivity is defined as

$$Selectivity = \frac{C_{ave}}{C_{bulk}} \quad [17]$$

If the oil behaved in a collective way, the compositions of the solubilized oil and the excess oil phase should be the same. Consequently the selectivity should be equal to unity for all bulk dodecanol concentrations. However, it is seen that the surfactant solubilized oil contains more dodecanol than the excess oil phase and the selectivity values are greater than 1 for all oil concentrations. This means that dodecanol is solubilized preferentially in the microemulsion, and the oils do not behave collectively. Therefore the pseudocomponent assumption is not valid.

The next question is whether changes in salinity affect this trend. Figure 2.a and 2.b demonstrates that the surfactant system solubilizes dodecanol preferentially even when the salinity increases. Figure 2.a reveals that the average dodecanol concentration remains greater in the solubilized oil than in the excess oil phase when salinity increases at constant bulk oil composition. In Figure 2.b it is seen that the selectivity is largest at

low salinity and decreases with salinity increase but remains greater than 1, even when optimum salinity is reached.

It can be concluded that the salinity increase and the dodecanol concentration increase affect the overall oil solubilization in the same way. The question arises, what causes the average dodecanol concentration in the solubilized oil to decrease?

Surface excess adsorption.

In our model we assume that the oil concentration distribution inside the micelles is not uniform. The non-uniform concentration is caused by the dodecanol surface activity. To account for this, the total volume of the oil droplet is divided into two regions as in the two-state model of Mukerjee (32): the surface shell, and the core. Therefore, the total oil solubilization has two contributions: (a) the surface solubilization, and (b) the core solubilization. Because of its surface excess, the concentration of dodecanol is high in the surface shell region, and lower in the core. If the surface solubilization contribution is important, strong deviations from the pseudocomponent assumption can be expected. On the contrary, if the core solubilization becomes dominant, the oil may behave as a pseudocomponent. It is therefore necessary to study how the surface and core solubilization varies compared to each other if the mixture composition and the salinity changes.

The surface excess of the polar oil (i.e., dodecanol in our model system) is defined as

$$n_i^\sigma = n_i - c_i^\alpha V^\alpha - c_i^\beta V^\beta \quad [18]$$

where n_i^σ is the moles of dodecanol surface excess, n_i is the total number of moles of dodecanol in the microemulsion, c_i^α and V^α are the dodecanol concentration and the volume of the water pseudophase, respectively, and c_i^β and V^β are the dodecanol concentration and the volume of the core solubilized oil in the oil pseudophase, respectively. The pseudophase theory (13, 41) is utilized to define phases α , β , and the surface σ . The microemulsion is a macroscopically single phase system, which can be divided into three sub-phases: (1) the water pseudophase, α , the (2) the oil pseudophase, β , and (3) the interface, or C-layer σ . The C-layer contains the surfactant film, and any excess oil due to its surface activity. Our oils are assumed to remain in the oil side of the surfactant and not to be affected the adsorption of the surfactant film in the C-layer. The effect of the surfactant on the oil surface excess is taken as constant, when the oil composition is changed. Therefore, the presence of the surfactant in the C-layer is accounted for only by providing a constant total interfacial area (A_s) between α and β pseudophases.

Our experimental series consist of saturated microemulsions. In saturated microemulsions the microemulsion phase is in equilibrium with excess dispersed phase. We assume, that the water side contribution in Eq. [18] can be neglected because the dodecanol solubility is very low in water compared to its solubility in the limonene. The dodecanol concentration in the core oil pseudophase (in the core of the micelles) was taken to be the same as the dodecanol concentration in the excess oil phase.

The moles of surface excess were then converted into volume basis (v_i^σ), and divided by the total interfacial area:

$$d = \frac{V_i^\sigma}{A_s} \quad [19]$$

The resultant volume based surface excess (d) corresponds to a shell thickness. The moles of surfactant in the system fix the total interfacial area. The shell thickness slightly increases the total radius and volume of the solubilized oil droplets. The geometry of the curved surfactant layer deviates from a plane surface, affecting the computed shell thickness results, but this deviation is neglected, because generally shell thickness values were an order of magnitude smaller than the core oil radii even when the radius is small.

Variation in the shell thickness as a function of the bulk concentration of dodecanol is presented in Figure 3. It is seen that below C_{bulk} of 0.2 the shell thickness increases as the dodecanol concentration in the bulk oil increases. Shell thicknesses seem to approach saturation between 0.1 and 0.2 volume fraction. Above 0.2 dodecanol volume fraction this trend changes, and the shell thickness decreases. These results indicate that the overall solubilization pattern is different below and above 0.2 volume fraction.

Oil solubilization in the low dodecanol concentration range.

Surface solubilization.

It is possible to fit the shell thickness data in Figure 3 at no added salt with a Langmuir adsorption isotherm below 0.2 volume fraction.

$$d = \frac{k \cdot C_{bulk}}{b + C_{bulk}} \quad [20]$$

where $k = 0.75$ Angstroms, and $b = 0.05$ are fitting parameters related to the maximum possible adsorption and the energy of adsorption per molecule, respectively.

The shell thickness variation (d) with respect to the salinity is presented in Figure 4a. We expected that the shell thickness would remain essentially constant as a function of salinity. On the contrary, the results show an increasing trend. It is interesting to see these results also on Figure 4.b, where the salinity scale is replaced by the radius of the solubilized oil. A well-known consequence of the salinity increase is the increase of the radius of the oil-swollen micelles (14, 19, 32). The radius is calculated from the experimental solubilization data according to

$$R = \frac{3V_{oil}^{mic}}{A_s} \quad [21]$$

where V_{oil}^{mic} is the total oil volume that is solubilized in the micelles, and we assumed spherical micelles. Figure 4.b shows that the shell thickness increases linearly as the radius of the oil increases up to about 10 Angstroms. Above that size, shell thickness seems to remain essentially constant if the salinity changes.

Our experiments cannot explain why the shell thickness is small at low salinity. We believe, however, that below 10 Angstrom there is probably not enough room for a separate core oil and surface region inside the micelles. The surfactant tails are likely to be present in the “core”, which might cause the dodecanol chemical potential to decrease. Decreased chemical potential leads to surface excess decrease. Another possible reason may be related to the water pseudo phase contribution to the surface excess adsorption. The electrolyte concentration increase in the water could cause increased dodecanol salting out and increasing shell thickness. Deviation of the shape of the micellar

aggregate from a sphere, and polydispersivity also cause uncertainties in the calculation of the shell thickness.

Shell thickness variation as a function of concentration for $R > 10$ Angstroms is shown in Figure 3. The data points could be fitted with a Langmuir type isotherm using coefficients $k = 1.25$ and $b = 0.04$. Experimental optimum salinities, middle phase characteristic lengths and shell thicknesses are listed in Table 2.

We conclude, that the dodecanol surface excess increases with increasing dodecanol concentration in the bulk oil. It is not affected significantly by the salinity, when the radius of the oil droplet is larger than ~ 10 Angstroms. Both changes could explain only an increase or invariant selectivity trend with increasing bulk oil concentration or salinity. Consequently, the observed decreasing selectivity has to be caused by the other contribution (core solubilization) to the total oil solubilization.

Core solubilization.

The other location for solubilization of oil is the micellar core. Mukerjee, who also divides the total solubilized oil into two regions, proposed that the oil solubilized in the adsorbed state is in equilibrium with the oil solubilized in the core (32). At equilibrium the chemical potential of an oil component is the same in each phases and pseudophases. Hence, the chemical potential of a component is the same in the excess oil, in the micellar oil, and also in the core and in the adsorbed state. It follows that because the chemical environment in the core and in the excess oil is very similar (42), the equality of the chemical potentials translates to equal concentrations. Therefore it seems reasonable to assume that the composition of the excess oil and the core is the same.

The volume of the oil solubilized in the core is related to the curvature of the surfactant membrane. The smaller the curvature towards the oil, the larger the radius of the micelles. This results in larger solubilized oil droplets, which means that the core volume increases. Any change in the formulation that promotes curvature decrease causes core oil solubilization to increase. It is our assumption that the dodecanol volume fraction is the same in the micellar core and in the excess oil phase. Therefore, if the core solubilization becomes dominant over the surface solubilization, the average micellar concentration of the dodecanol should approach its excess oil phase concentration. This trend is paralleled by the selectivity approaching unity. The fact that these trends are exhibited in our system supports the assumption that $C_{core} = C_{bulk}$.

Increasing the electrolyte concentration or increasing the polarity of the oil can generate curvature decrease. Figure 5. a demonstrates how the radius of the solubilized oil droplet increases as the bulk oil phase concentration increases. Figure 5.b shows that this translates to an increase in the total solubilized oil volume. We also plotted the volume variation of the surface solubilization contribution with the radius increase on Figure 5.b. Surface solubilization was obtained from computing the volumetric dodecanol surface excess as described before. The difference between the total solubilization and the surface solubilization is assigned as core solubilization. Data for the no-added-salt case are presented. It is seen on Figure 5.b that the core solubilization increase is overwhelming compared to the surface solubilization as the bulk concentration (or radius) increases. Consequently the selectivity must decrease, and the average micellar oil composition must approach the bulk oil phase composition. This is in good agreement

with the experimental trends. Figure 6.a and 6.b suggest the same result, when the curvature change is generated by the increasing electrolyte concentration as expected.

In conclusion, we have shown that the selectivity decreased towards unity and the overall micellar oil composition approached the bulk oil composition, as the core solubilization became more dominant. As a result, treating the oil mixture as a pseudocomponent may seem to be appropriate even if one component is surface active. Since the core radius tends to be large at the optimum formulation the core solubilization is large. It follows that the optimum salinity and solubilization parameters should vary with the oil composition according to ideal mixing rules. However, these rules did not seem to work well in our system. Therefore we tried to link the optimum salinity and the oil solubilization capacity to the shell thickness rather than the deviation from the pseudocomponent assumption.

Characteristic length.

We use the characteristic length to quantify the solubilization capacity as explained before. Characteristic lengths are estimated from the solubilization data of the middle phases in experimental series 2. Presented on Figure 7, the characteristic length increases with increasing dodecanol concentration. The variation is essentially linear with the oil phase composition below 0.04 volume fraction. Departure from linearity is observed at higher concentration. Above 0.04 volume fraction the characteristic length does not increase as fast as below 0.04 volume fraction with increasing the dodecanol concentration.

Equation [14] suggests that the characteristic length is an exponential function of the bending elastic rigidity. It has been shown (38, 40, 43, 44) that adsorption of amphiphilic block co-polymers at the surfactant film increases the bending rigidity. Theoretically, the effect of adsorbed polymer on the bending moduli was found to be:

$$\kappa = \kappa_0 + \frac{k_B T}{12} \left(1 + \frac{\pi}{2}\right) \sigma (R_a^2 + R_b^2) \quad [22]$$

where κ_0 is the bending rigidity of the surfactant film without adsorbed polymer, σ is the number density of the polymer in the membrane, R_a and R_b are the end-to-end distance of the hydrophilic and the hydrophobic block, respectively.

We found a similar behavior in our system. First we computed the bending rigidity from the characteristic length by applying Eq. [14]. A surfactant molecular size of $a = L + d$ was used, where $L = 10$ Angstroms is the extended length of the tail of the surfactant, and d is the shell thickness, calculated from solubilization data. In order to get a good fit between experimental bending rigidities and Eq. [22], the adsorption was evaluated at higher salinities where the shell thickness is not affected by the salinity variation. Furthermore, to get a good fit, the end-to-end distance of the hydrophobic and hydrophilic segment was set as $R_b = 15$ Angstroms and $R_a = 3$ Angstrom, respectively. These values for dodecanol seem realistic. In Figure 8 the experimental bending rigidities are plotted together with model predictions as a function of the dimensionless adsorption, $\sigma(R_a^2 + R_b^2)$. The data points could be fitted with a linear function. The slope of the fitting equation is about 0.2, which agrees very well with the theoretical value of 0.21 given in (40). This is an encouraging result, because Eq. [14], [20] and [22] could be employed as a model to relate the characteristic length and the oil phase composition.

The model to compute characteristic length as a function of dodecanol concentration can be set up as follows. First, we need to experimentally determine the characteristic length of the system with the reference oil (i.e. pure limonene), form a middle phase microemulsion, according to Eq. [15]. The corresponding bending rigidity is computed from Eq. [14], providing a value for κ_0 . The Langmuir adsorption isotherm parameters k and b are obtained experimentally at higher salinities (1% NaCl), where the salinity dependence of the adsorption can be neglected. The characteristic length as a function of dodecanol concentration is then calculated using Eqs. [14], [20], and [22]. This characteristic length model uses several parameters. The Langmuirian parameters are empirical, although with thermodynamic meaning. The other parameters corresponding to the molecular sizes of the surfactant (L), and the dodecanol (R_a and R_b) are not empirical. Therefore, if the characteristic length of the limonene and the adsorption isotherm are measured experimentally, the characteristic length variation with dodecanol concentration in the oil phase can be computed. Figure 7 demonstrates that the model agrees closely with the data and captures the non-linear trend observed experimentally.

Optimum salinity.

We demonstrated that increasing the dodecanol concentration, the dodecanol adsorption increases, and the curvature of the surfactant film towards the oil side tends to decrease. Indeed, the mean curvature change upon increasing amphiphilic block copolymer adsorption has also been observed experimentally (40, 44, 45). The mean curvature is obtained by averaging the curvatures of the surfactant film in the x and y

directions (46). The influence of the polymer on the mean curvature is predicted according to

$$H = H_0 + \frac{1}{4} \left(\sqrt{\frac{\pi}{6}} \right) \cdot \frac{k_B T}{\kappa} \cdot \sigma (R_a - R_b) \quad [23]$$

where H_0 is the natural curvature of the surfactant without polymer adsorption, and

$F = \frac{1}{4} \left(\sqrt{\frac{\pi}{6}} \right) (R_a - R_b)$ is a constant multiplier, if the same polymer is used. The term $\frac{\sigma}{\kappa}$

is a function of the surface adsorption. It is interesting to see if combining Eqs. [23] and [13] could be applied to calculate optimum salinity.

Figure 9.a demonstrates that at fixed salinity the experimentally obtained mean curvature (equal to the inverse equivalent oil droplet radius) decreases linearly with increasing $\frac{\sigma}{\kappa}$ as predicted by Eq. [23]. The slope seems to depend on the salinity, which may be caused by the slight salinity dependence of the shell thickness. This is not expected from Eq. [23]. However, when a normalized radius scale is used, and the dimensionless curvature \bar{H} is plotted against $\xi \cdot \sigma / \kappa$, the slopes become independent from the salinity, with a value of about -10 , as demonstrated in Figure 9.b.

The use of \bar{H} is explained as follows. In the absence of added electrolyte the free electrolyte concentration in the microemulsion corresponds to about the CMC for monovalent surfactants, and the mean curvature of the surfactant film is approximately equal to the local curvature. The local curvature is the inverse of the actual domain size (i.e., $H_{CMC} \approx 1/R_{o,CMC}$). When the optimum formulation is reached by adding electrolyte, the electrolyte concentration increases from the CMC to the optimum salinity (S^*). As a

result the mean curvature of the surfactant film decreases from $H_{CMC} \approx 1/R_{o,CMC}$ to zero. However, when the optimum condition is reached, the surfactant layer is not flat, and its local curvature is not zero. The characteristic domain size grows from $\sim R_{o,CMC}$ to only up to ξ . Hence the local surfactant membrane curvature changes from $H_{CMC} \approx 1/R_{o,CMC}$ to $1/\xi$. Therefore the radius (and local curvature) scale is different for the different oil compositions. This is taken into account by introducing the normalized oil radius. The radius is normalized as

$$\bar{R}_j = \frac{R_j}{\xi_j} \quad [24]$$

The dimensionless curvature becomes

$$\bar{H}_j = H_j \cdot \xi_j \quad [25]$$

where the j subscript refers to oil composition j .

Equation [23] could therefore be used at any salinity with the same slope, if the dimensionless curvature is used in the following form:

$$\bar{H} = \bar{H}_0 + F \cdot \frac{k_B T}{\kappa} \cdot \sigma \cdot \xi \quad [26]$$

where, in our system, $F \approx 10$ was found for the slope.

The next step is to check the linear relationship between the optimum salinity log and the curvature predicted by Eq. [10]. Deviation from linearity is expected at low salinities due to the palisade layer solubilization. It can be explained as follows. In Eq. [10] only the core radius is considered as the basis of the curvature. At the same time, experimental solubilization data includes both core and palisade layer solubilization,

resulting in a larger radius. The difference between the core radius and experimental radius is greater at low salinities, when the droplets are small. Consequently using the experimental curvature in Eq. [10] could cause significant deviation at low salinities. In Figure 10.a $\ln S^*$ is plotted against the experimental curvature, evaluated at three different salinities. The results clearly demonstrate non-linearity. In contrast, in Figure 10.b we see a linear dependence of $\ln S^*$ on the dimensionless curvature for the three salinities. The relationship is of the form

$$\ln S^* = \ln S^*_0 + B \cdot (\bar{H} - \bar{H}_0) \quad [27]$$

with slopes of about $B = -0.2$. Combining Eqs. [26] and [27] and recognizing that

$F \cdot B \approx \frac{1}{4} \left(\sqrt{\frac{\pi}{6}} \right) \cdot (R_a - R_b)$, we arrive at

$$\ln S^* = \ln S^*_0 + \frac{1}{4} \cdot \left(\sqrt{\frac{\pi}{6}} \right) \cdot k_B T \cdot (R_a - R_b) \cdot \left(\frac{\sigma}{\kappa} \cdot \xi \right) \quad [28]$$

Equation [28] yields very good predictions for the optimum salinity according to Figure 11. a. This relationship can be used to calculate optimum salinity of the mixture, if the optimum salinity and the characteristic length of the pure limonene is known, and the two Langmuir isotherm parameters are determined experimentally. It should be noted that the model of Baran et al. (Eq. [2] and [3]) is not expected to work well for this mixture. This is because in order to obtain the measured optimum salinities, one has to use different EACN values for the dodecanol for different dodecanol concentrations, as shown in Figure 11.b.

Behavior at high dodecanol concentrations.

At dodecanol concentrations above 0.12 volume fraction another source of non-ideal behavior becomes evident. With increasing dodecanol concentration at constant salinity, the overall polarity of the bulk oil increases. This tends to increase the solubilization efficiency of the surfactant, because the interaction between the surfactant tails and the oil become stronger. However, above a certain concentration, the increased compatibility between the surfactant and the oil phase also leads to a surfactant partitioning into the oil phase. As a result some of the surfactant may be lost to the oil phase. Less surfactant remaining in the water phase yields decreased oil solubilization.

Solubilization may further be affected if the microemulsion becomes near-tricritical. It has been (29, 30) suggested that near-tricritical mixtures are weakly structured. When the mixture becomes weakly structured, one would expect a change in the oil solubilization mechanism. Composition of liquid mixtures, which have no structure, is mainly governed by cosolvent effects. Consequently the rules of microemulsion solubilization are expected to break down. In our systems, increasing the dodecanol concentration the overall polarity of the oil mixture increases. Increasing the oil polarity is known to push the system towards the tricritical point. Several signs of approaching a tricritical point have been observed in system of this research.

Wetting / non-wetting transition.

The progression from strongly to weakly structured mixtures can be detected by non-wetting / wetting transition (47, 48). This transition precedes the tricritical point. When the dodecanol volume fraction in the oil increases to about 0.1 the interface

between the middle phase and the excess phases become fuzzy. This is an indication that the system is at a non-wetting / wetting transition (29). At 0.2 volume fraction, at 0.6 wt % salinity the interfaces became so unstable that the phase boundaries of the middle phase could no longer be defined well. As a result, we could not estimate the characteristic lengths from solubilization data, and only the salinity of the balanced state could be determined. Salinity scan above this concentration yielded only two-phase systems. Both oil and water rich phases looked bluish, which is the indication of the presence of large aggregates in both phases. Similar behavior has also been observed by other researchers (28). The classical Winsor type I – III – II phase behavior disappeared, because regular middle phase no longer formed.

Disappearance of the three-phase body.

Variations of the lower critical salinity and the optimum salinity with dodecanol concentration could also be a good indication of approaching tricritical points (28, 29). It is seen on Figure 12 that the lower critical salinity (the salinity of the lower critical point) and the optimum salinity merge. At 0.2 dodecanol volume fraction the system approached the tricritical point so closely, that the regular middle phase disappeared. At this concentration Type I – II transition occurs at 0.6 % salinity, which signals the balanced state. It has been found, that in order to form bicontinuous microemulsions with ionic surfactants, a minimum amount of salt (~0.5 %) is required to efficiently reduce the repulsion between adjacent surfactant layers, which is caused by the head group charge (46). At 0.2 dodecanol volume fraction the optimum salinity approached this minimum

salinity requirement, and stable middle phase could not be formed. Above this dodecanol concentration our model breaks down.

Surfactant partitioning.

Figure 13 shows measured surfactant concentrations in the aqueous phase as a function of dodecanol concentration in the oil at no added salt. The surfactant concentration is constant up to 0.2 volume fraction. Above 0.2 volume fraction, the surfactant increasingly starts to partition in a stepwise fashion into the oil rich phase. At around 0.4 volume fraction a balanced state is reached when the surfactant equipartitions between the two phases. Above that dodecanol concentration the surfactant partitioning into the oil phase is even more pronounced. However, a still significant fraction of the surfactant remains in the water.

From this behavior we conclude that dodecanol behaves as a cosolvent for the surfactant in the oil phase. This effect becomes important only above 0.2 volume fraction. Because of the surfactant partitioning into the oil phase, less surfactant remains available to form aggregates in the aqueous phase. This causes reduced oil solubilization.

The oil solubilization is affected by not only the surfactant concentration present in the aqueous phase, but also by the shell thickness. The combined effect of the shell thickness variation and the surfactant partitioning on the oil solubilization is represented by the non-scaled solubilization. Just above 0.2 volume fraction the shell thickness still slightly, which tends to increase the oil solubilization. This may be able to counter balance the effect of the decreasing surfactant concentration when the surfactant loss is not too large. As a result, the solubilization may not decrease immediately as the

surfactant concentration in the aqueous phase starts to decrease. To separate the effect of shell thickness, we also plotted the scaled solubilization. Scaled solubilization is the ratio of the solubilized oil concentration and the surfactant concentration in the aqueous phase. It is seen in Figure 14 that approaching 0.4 volume fraction the shell thickness also decreases suggesting a weakening structure, and probably increasing cosolvency. Accordingly the scaled oil solubilization decreases as well, following the same trend as the shell thickness.

Interfacial tension.

We could verify the decreasing solubilization trend by measuring the interfacial tension between the two coexisting phases. Interfacial tension as a function of dodecanol concentration is presented on Figure 13. The interfacial tension and the curvature are related. High curvature corresponds to high tension between the macroscopic aqueous/oil interface, and small solubilization. On the contrary, if the curvature is small, the interfacial tension tends to be small too, and the solubilization large. Recall that the curvature (at constant salinity) is affected by the shell thickness. As the shell thickness increases, the curvature of the surfactant film decreases. With increasing dodecanol concentration, the shell thickness increases fast at first, slowing down at higher concentrations because it is approaching an adsorption saturation. The interfacial tension on Figure 13 seems to follow this trend. It decreases fast at low dodecanol concentrations, slowing down as the concentration increases. The lowest IFT value was measured at about 0.4 dodecanol volume fraction. At this point the surfactant partitioning between the oil and the water is almost balanced, indicating, that the affinity of the surfactant towards

the water and the oil are close. This condition should result in a minimum IFT. As the dodecanol concentration is further increased, the system goes away from this balance, the affinity of the surfactant becomes greater for the oil phase than for the water phase, and the IFT increases.

The oil solubilization, IFT and surfactant concentration results indicate that in the high dodecanol concentration regime a microemulsion solubilization is no longer the only important process. The cosolvency must also be taken into account, which is beyond the scope of this research. We conclude that the optimum salinity and characteristic length models may be applicable only below 0.2 dodecanol volume fraction, where the cosolvent effects are not important.

CONCLUSIONS

Solubilization of limonene-dodecanol binary oil mixtures has been studied in aqueous sodium dihexyl sulfosuccinate surfactant solution. NaCl was used as an additive. The effect of oil phase composition on the oil solubilization characteristics of the microemulsion was analyzed. It was found that the oil mixtures did not behave collectively, and the microemulsion preferentially solubilized dodecanol. This trend did not change when NaCl was added. Therefore, the pseudocomponent assumption is not valid for the oil mixture used in this study, and prior models for optimum salinity and solubilization parameter cannot give accurate predictions.

In the low dodecanol concentration range (below 0.2 volume fraction), oil solubilization by the strongly structured microemulsion was the dominating solubilization mechanism. The optimum salinity and the characteristic length variation with increasing dodecanol concentration did not follow ideal mixing rules. Deviation from the ideal mixing rules could be explained by taking into account the surface activity of the dodecanol at the surfactant layer. The dependence of the dodecanol surface excess on the bulk oil phase composition followed a Langmuirian adsorption trend. In the newly developed mathematical model for the characteristic length we linked the characteristic length to the dodecanol surface excess. The dodecanol surface excess is solubilized in the palisade layer of the micelles by penetrating between the surfactant tails. This increases the bending rigidity of the surfactant film. Because the bending rigidity increases, the characteristic length increases too. Our characteristic length model uses the following input data: (1) characteristic length of the non-polar oil component, determined experimentally, (2) fitted Langmuir parameters of the dodecanol adsorption isotherm, also obtained experimentally. We found excellent agreement between characteristic length model predictions and experimental data.

The presence of dodecanol surface excess not only increases the rigidity, but also decreases the curvature of the surfactant membrane towards the oil side. In the new model, the optimum salinity is related to the surface excess adsorption. This model requires (1) measured optimum salinity of the non-polar oil component, (2) experimentally obtained characteristic length for the non-polar oil, and (3) the two fitted Langmuir adsorption isotherm parameters. The model yielded good predictions for the optimum salinity.

Above 0.2 dodecanol volume fraction, dodecanol behaved as a cosolvent for the surfactant in the oil phase. Because of the cosolvent effect, the surfactant increasingly partitioned into the oil phase as the dodecanol concentration increased. Increasing dodecanol cosolvency caused reduced micellar oil solubilization. Additionally, around 0.4 dodecanol volume fraction the efficiency of the surfactant remaining in the aqueous phase also decreased. This was attributed to approaching the tricritical point and a transition from strongly structured microemulsion to weakly structured mixture, and the disappearance of the regular Winsor-like behavior. The new optimum salinity and the characteristic length models do not include these effects, and therefore break down above 0.2 dodecanol volume fraction.

REFERENCES

1. Knox, R. C.; Shau, B. J.; Sabatini, D. A.; Harwell, J. H. In *Innovative Subsurface Remediation. Field testing of Physical, Chemical, and Characterization Technologies*; ACS Symposium Series 725; Brusseau, M. L.; Sabatini, D. A.; Gierke, J. S.; Annable, M. D., Eds.; Washington, D.C.; **1999**; pp 49-63.
2. Bedient, P. B.; Holder, A. W.; Enfield, C. G.; Wood, A. L. In *Innovative Subsurface Remediation. Field testing of Physical, Chemical, and Characterization Technologies*; ACS Symposium Series 725; Brusseau, M. L.; Sabatini, D. A.; Gierke, J. S.; Annable, M. D., Eds.; Washington, D.C.; **1999**; pp 36-48.
3. Fountain, C. J. *EPA Ground-Water Remediation Technologies Analysis Center; Publication Document Number TE-98-02*; Pittsburg, P. A.; **1998**.
4. Katherine A. Bourbonais, K. A.; Compeau, G. S.; MacClellan, L. K. In *Surfactant – Enhanced Subsurface Remediation*; ACS Symposium Series 594; Harwell, J. H.; Sabatini, D. A., Eds.; American Chemical Society, Washington, D.C.; **1995**; pp. 161-176.
5. Uchiyama, H.; Acosta, E.; Tran, S.; Sabatini, D. A.; Harwell, J. H. *Ind. Eng. Chem. Res.* **2000**, *39*, 2704-2708.
6. Graciaa, A.; Lachaise, J.; Cucuphat, C.; Bourrel, M.; Salager, J. L. *Langmuir*, **1993**, *9*, 669-672.
7. Graciaa, A.; Lachaise, J.; Cucuphat, C.; Bourrel, M.; Salager, J. L. *Langmuir*, **1993**, *9*, 3371-3374.
8. Salager, J. L.; Graciaa, A.; Lachaise, J. *J. Surfactants Detergents*, **1998**, *1* (3), 403-406.
9. Shiau, B. J.; Rouse, J. D.; Sabatini, D. A.; Harwell, J. H. In *Surfactant – Enhanced Subsurface Remediation*; ACS Symposium Series, Vol. 594; Harwell, J. H.; Sabatini, D. A. Eds.; American Chemical Society, Washington, D.C.; **1995**; pp. 64-79.
10. Pope, G. A.; Wade, W. H. In *Surfactant – Enhanced Subsurface Remediation*; ACS Symposium Series 594; Harwell, J. H.; Sabatini, D. A. Eds.; American Chemical Society, Washington, D.C.; **1995**; pp.142-160.

11. Harwell, J. H. In *Transport and Remediation of Subsurface Contaminants. Colloidal, Interfacial, and Surfactant Phenomena*; ACS Symposium Series 491; Sabatini, D. A.; Knox, R. C. Eds.; Washington, D.C.; **1992**; pp. 124-132.
12. Sabatini, D. A.; Knox, R. C.; Harwell, J. H.; Shiau, B. J.: In *Soil and Aquifer Pollution. Non-Aqueous Phase Liquids – Contamination and Reclamation*; Rubin, H.; Harkis, N.; Carberry, J., Eds.; **1998**; 373-391.
13. Bourrel, M.; Schechter, R. S. *Microemulsions and Related Systems*; Marcel Dekker, Inc., New York, **1988**, pp. 335-392.
14. Salager, J. L. In *Handbook of Detergents. Part A: Properties*; Surfactant Science Series 82; Zoller, U., Editor-in-Chief; Broze, G., Editor.; Marcel Dekker, New York, **1999**, pp. 253-302.
15. Reed, R. L.; Healy, R. N. in *Improved Oil Recovery by Surfactant and Polymer Flooding*; Shah, D. O.; Schechter, R. S., Eds.; Academic Press, New York, **1977**.
16. Salager, J. L.; Vasquez, E.; Morgan, J. C.; Schechter, R. S.; Wade, W. H. *Soc. Pet. Eng. J.* April, **1979**, 107-115.
17. De Genes, P. G.; Taupin, C. *J. Phys. Chem.* **1988**, 86 (13), 2294-2305.
18. Miller, C. A; Neogi, P. *Interfacial Phenomena. Equilibrium and Dynamic Effects*; Surfactant Science Series 17; Marcel Dekker, New York; **1985**; pp. 140-183.
19. Salager, J. L.; Anton, R. E. In *Handbook of Microemulsion Science and Technology*; Kumar, P.; Mittal, K. L., Eds.; Marcel Dekker, New York; **1999**; pp. 247-280.
20. Weerasoroiya, V.; Yeh, S. L.; Pope, G. A.; Wade, W. H. In *Surfactant-Based Separations. Science and technology*; ACS Symposium Series 740; American Chemical Society, Washington, D.C.;**1999**; pp. 23-34.
21. Baran, J. R.; Pope, R.G. A.; Wade, W. H.; Weerasooriya, V.; Yapa, A. *J. Colloid and Interface Science* **1994**, 168, 67-72.
22. Provoust, L.; Pope, G. A.; Rouse, B. A. *Soc. Pet. Eng. J.* Oct. **1985**, 693-703.
23. Provoust, L.; Satoh, T.; Pope, G. A.; Sepehrnoori, K.. *SPE 13031*; In *Proceedings of the 59th Annual Meeting of the Society of Petroleum Engineers*, Houston, TX, Sept.; **1984**.
24. Nagarajan,R.; Ruckenstein, E.: In *Surfactants in Solution, Vol. 2*; Mittal, K.L.; Lindman, B., Eds.; Plenum Press, New York; **1984**; pp. 923-947.

25. Graciaa, A.; Lachaise, J.; Cucuphat, C.; Bourrel, M.; Salager, J. L. *Langmuir*, **1993**, *9*, 1473-1478.
26. UTCHEM-9.0 A Three-Dimensional Chemical Flood Simulator. Volume II: Technical Documentation, The University of Texas at Austin, **2000**.
27. Griffith, R. B.; Widom, B. *Phys. Rev.* **1973**, *18*, 2173.
28. Yamaguchi, Y.; Aoki, R.; Azemar, N.; Solans, C.; Kuneida, H.: *Langmuir*, **1999**, *15*, 7438-7445.
29. Kahlweit, M.; Busse, G.. *J. Phys. Chem. B.* **2000**, *104*, 4939-4943.
30. Schubert, K. -V.; Strey, R.; Kline, S. R.; Kaler, E. W. *J. Chem. Phys.* **1994**, *101*, 5343.
31. Baran, J.R; Pope, G. A.; Wade, W. H.; Weerasooriya, V.; Yapa, A. *Environ. Sci. Technol.* **1994**, *28*, 1361-1366.
32. Mukerjee, P.; Cardinal, J. R.: *J. Phys. Chem.* **82**, *1978*, *14*, 1620.
33. Rouse, J. D.; Sabatini, D. A.; Deeds, N. E.; Brown, R. E. *Env. Sci. Technol.* **1995**, *29*, 2484-2498.
34. Jonsson, B.; Landgren, M.; Olofsson, G. In *Solubilization in Surfactant Aggregate*; Christian, S. D.; Scamehorn, J. F., Eds.; Surfactant Science Series 55; Marcel Dekker, New York, **1995**, pp. 115-139.
35. Ezrahi, S.; Aserin, A.; Garti, N. In *Handbook of Microemulsion Science and Technology*; Kumar, P.; Mittal, K. L., Eds.; Marcel Dekker, New York, **1999**, pp. 185-246.
36. Acosta, E.; Szekeres, E.; Sabatini, D. A.; H. Harwell, J. H. *Langmuir* **2003**, *19*, 186-195.
37. Safran, A. In *Micelles, Membranes, Microemulsions, and Monolayers*; Gelbart, W. M.; Ben-Shaul, A.; Roux, D., Eds.; Springer-Verlag, New York; **1994**; pp. 427-474.
38. Gompper, G.; Endo, HMihailescu, M.; Allgaier, J.; Monkenbush, M.; Richter, D.; Jakobs, B.; Scottmann, T.; Strey, R. *Europhys. Lett.* **2001**, *56* (5), 683-689.
39. Sottmann, T.; R. Strey, R. *J. Chem. Phys.* **1997**, *106* (22), 8606-6815
40. Sottmann, T: *Current Opinion in Colloid and Interface Science* **2002**, *7*, 57-65.

41. Biais, J.; Bothorel, P.; Clin, B.; Palanne, P. *J. Dispersion Science and Technology* **1981**, 2 (1), 67-95.
42. Ruckenstein, E. *In Handbook of Microemulsion Science and Technology*, Kumar, P.; Mittal, K. L., Eds; Marcel Dekker, New York; **1999**; pp. 45-58.
43. Endo, H.; Allagier, J.; Gompper, G.; Jakobs, B.; Monkenbush, M.; Richter, D.; Scottmann, T.; Strey, R. *Phys. Rev. Lett.* **2000**, 85 (1), 102-105.
44. Gompper, G.; Richter, D.; Strey, R. *J. Phys. Condens. Matter* **2001**, 13, 9055-9074.
45. Breidenich, M.; Netz, R. R.; Lipowski, R. *Europhys. Lett.* **2000**, 49 (4), 431-437.
46. Evans, D. F.; Wennerstrom, H. *The Colloidal Domain. Where Physics, Chemistry, and Biology Meet*, 2nd Edition, Wiley-VCH, New York; **1999**; pp. 559-561.
47. Widom, B. *Langmuir* **1987**, 3, 12.
48. Gompper, G.; Schick, M. *Phys. Rev. Lett.* **1990**, 65,1116.

TABLES

Chapter 4

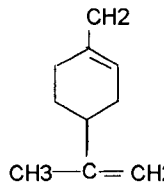
	Sodium dihexyl sulfosuccinate	1-Dodecanol	(R)-(+)-Limonene
Structure	$(\text{CH}_3(\text{CH}_2)_5\text{OOC}-$ $\text{H})_2(\text{SO}_3\text{Na})$	$\text{CH}_3(\text{CH}_2)_{11}\text{OH}$	
Molecular weight	388	186	136
Density g/ml		0.82	0.84
Area per molecule Angstrom ²	100		
CMC	0.014		
Mole/liter			
EACN			~ 6

Table 1. Selected properties of the materials used in the dodecanol-limonene experiments.

Dodecanol vol. fraction	Optimum salinity NaCl %	Characteristic length Angstrom	Shell thickness* Angstrom
0	6.3	39	0
0.0092	5.5	44.7	0.22
0.0183	3.8	54.8	0.36
0.03	3.1	61.6	0.5
0.044	2.59	75.2	0.64
0.113	1.15	105	0.88

Table 2. Experimental optimum salinity, middle phase characteristic length, and shell thickness values for different initial dodecanol volume fractions. * Shell thickness values are for $R > 10$ Angstroms.

FIGURES
Chapter 4

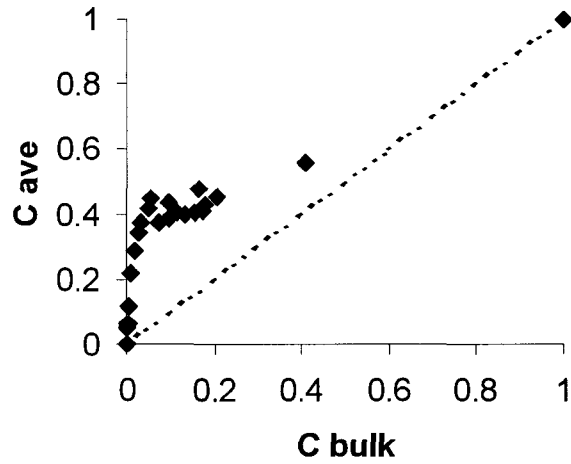


Figure 1.a

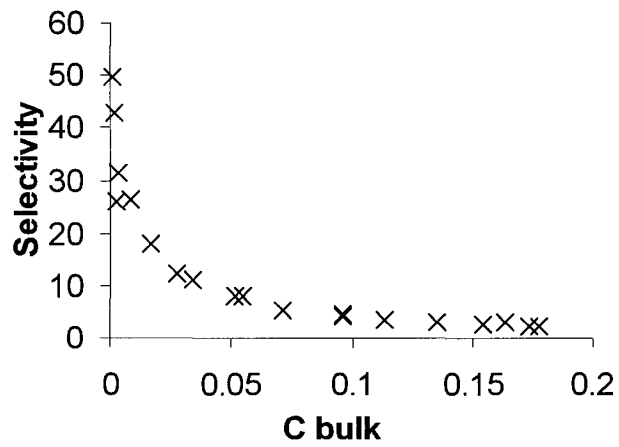


Figure 1.b

Figure 1. a. Average dodecanol volume fraction (C_{ave}) in the solubilized oil, b. Selectivity as a function of bulk oil phase dodecanol volume fraction (C_{bulk}).

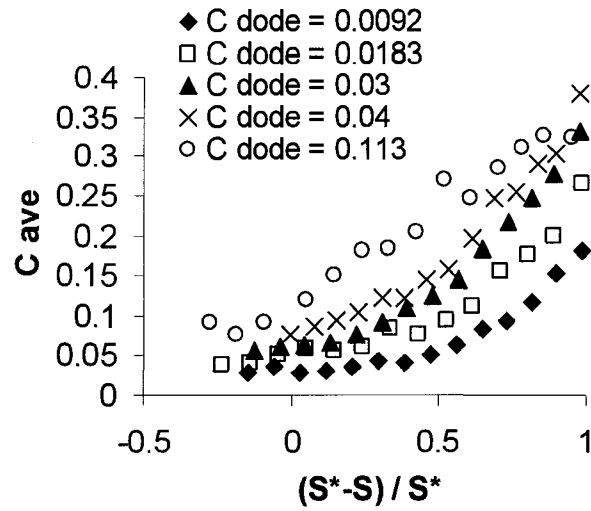


Figure 2.a

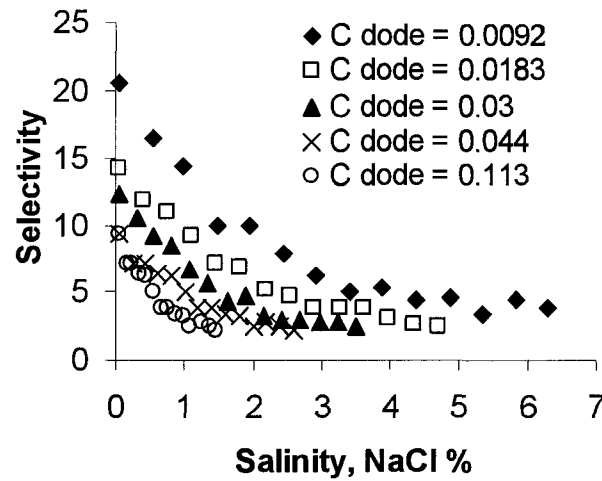


Figure 2.b

Figure 2. a. Average dodecanol volume fraction in the solubilized oil versus $(S^*-S)/S^*$, which is a normalized salinity scale, b. selectivity as a function of salinity. Results for different initial bulk dodecanol volume fraction (C dode) in the oil mixture are shown.

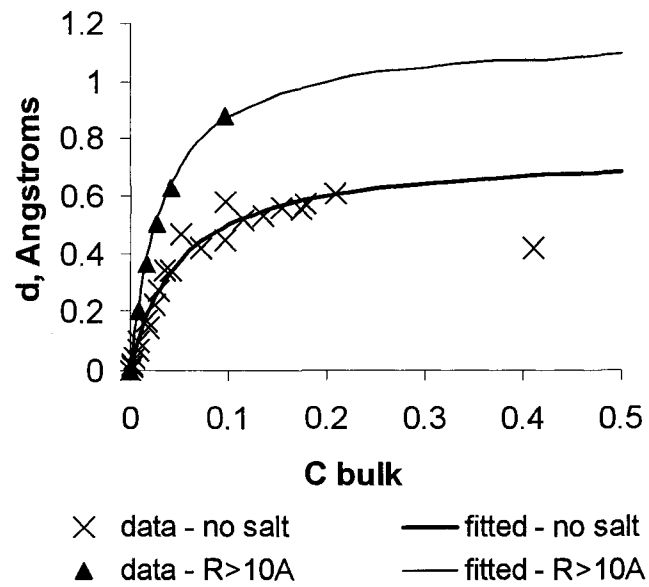


Figure 3. Shell thickness (d) variation with respect to bulk oil dodecanol volume fraction (C_{bulk}). Data and Langmuir model (fitted) are shown for the no added salt series, and at higher salinity, where the oil droplet radii were larger than 10 Angstroms.

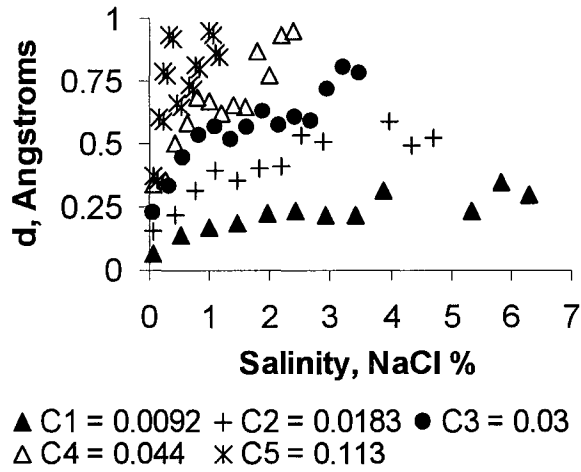


Figure 4. a

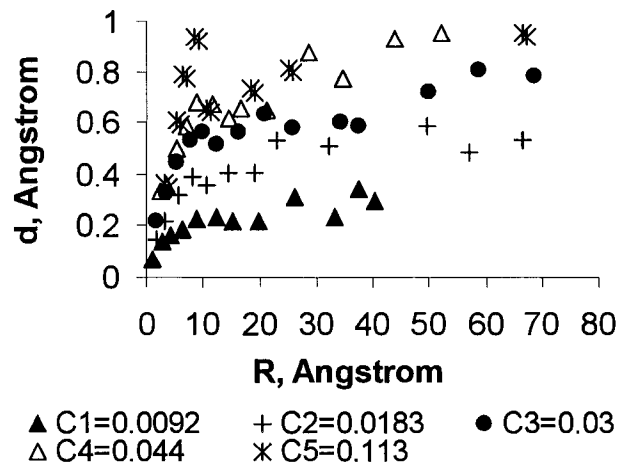


Figure 4. b

Figure 4. a. Shell thickness (d) variation as a function of salinity, b. shell thickness variation as a function of the oil radius (R). Results of five different initial dodecanol concentrations are presented.

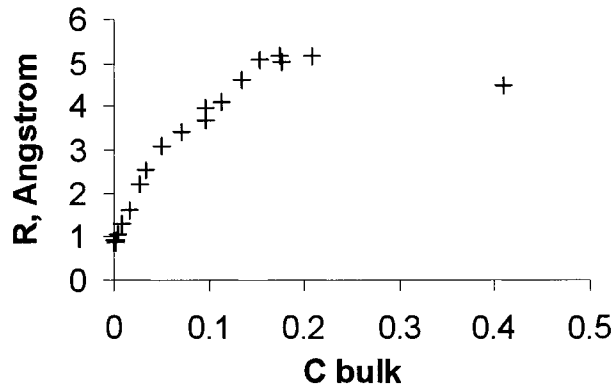


Figure 5. a

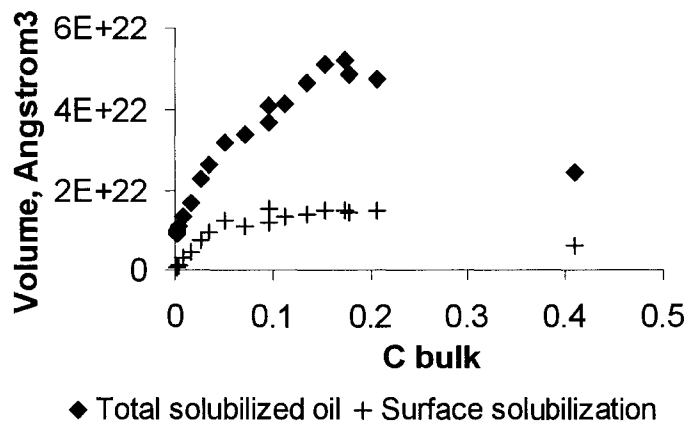


Figure 5.b

Figure 5. a. Variation of oil droplet radius as a function of the dodecanol volume fraction in the bulk oil phase (C bulk), b. variation of the total solubilized oil volume and the solubilized oil volume due to the surface solubilization as a function of the dodecanol volume fraction in the bulk oil phase (C bulk). Data with no added salt series are shown.

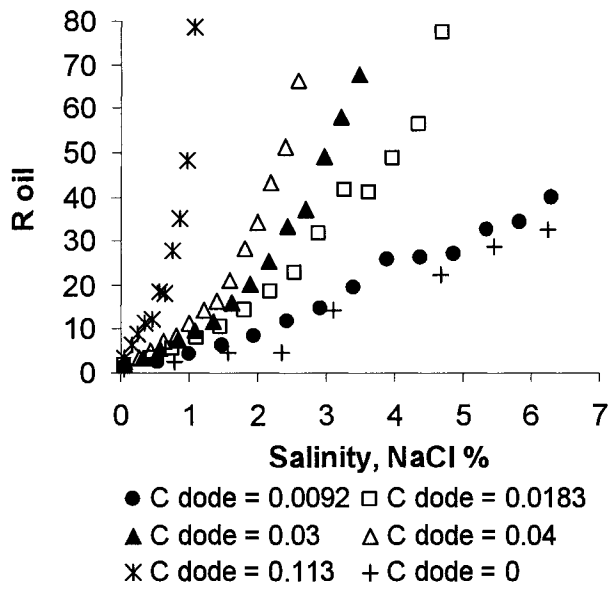


Figure 6. a

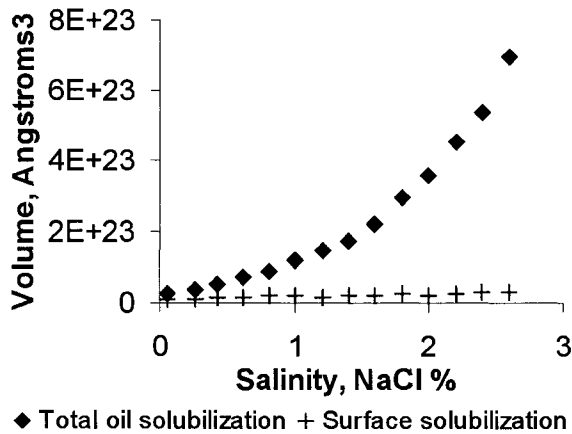


Figure 6. b

Figure 6. Variation of oil droplet radius as a function of the salinity. Data of five different initial dodecanol volume fractions (C dode) are shown, b. variation of the total solubilized oil volume and the solubilized oil volume due to the surface solubilization as a function salinity. Data of C dode = 0.044 initial dodecanol volume fraction series are shown.

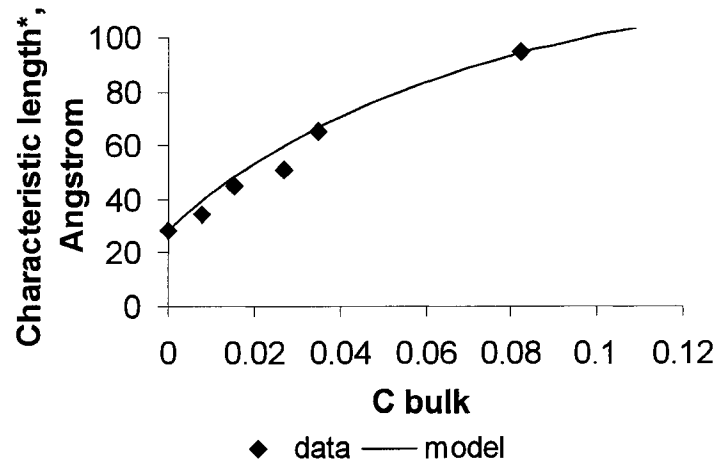


Figure 7. Characteristic length variation in middle phase microemulsion as a function of dodecanol volume fraction in the bulk oil phase (C bulk). Data points calculated from middle phase solubilization results, and the model predictions based on Eq. [20], [22], and [14] are plotted together.

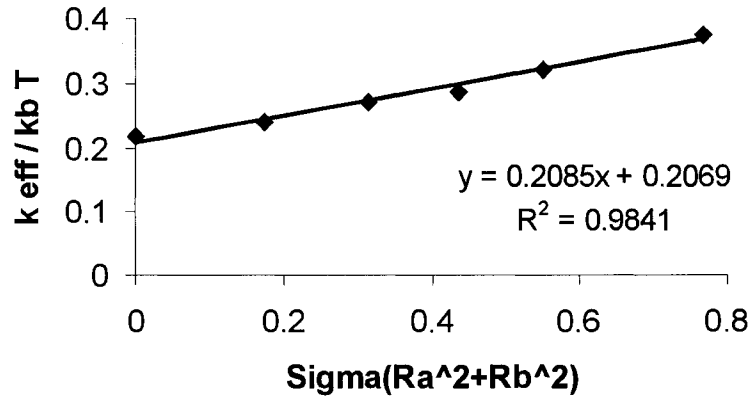


Figure 8. Bending rigidity κ (denoted as k_{eff}) variation with respect to the dimensionless adsorption density $\sigma \cdot (R_a^2 + R_b^2)$, denoted as $\text{sigma}(Ra^2 + Rb^2)$. The bending rigidity is in $k_B T$ units. Data points are fitted with a linear line. The slope of the fitting line is 0.208.

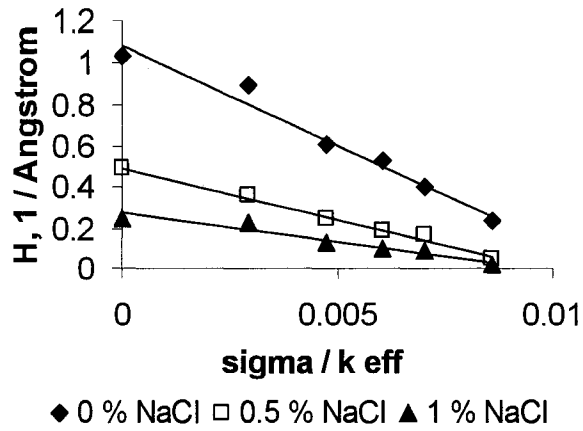


Figure 9.a

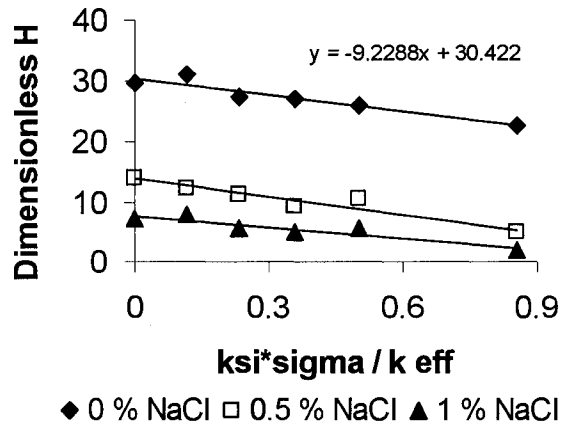


Figure 9. b

Figure 9. a. Variation of the mean curvature (H) as a function of σ/κ (denoted as σ/k eff) at three different salinities, b. variation of the dimensionless curvature with respect to $\xi \cdot \sigma/\kappa$, denoted as $\text{ksi} \cdot \sigma/k$ eff. Symbols represent data points calculated from oil solubilization results, linear fitting lines are shown to guide the eye.

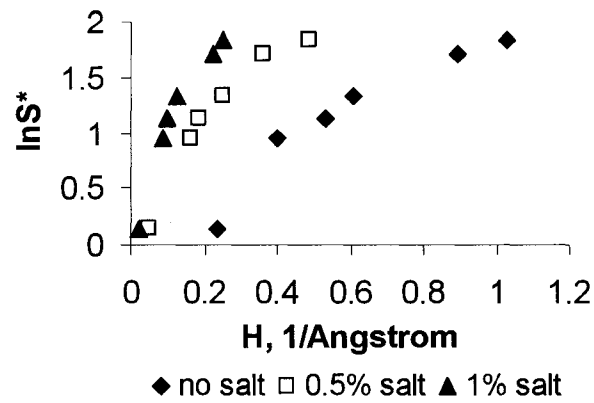


Figure 10.a

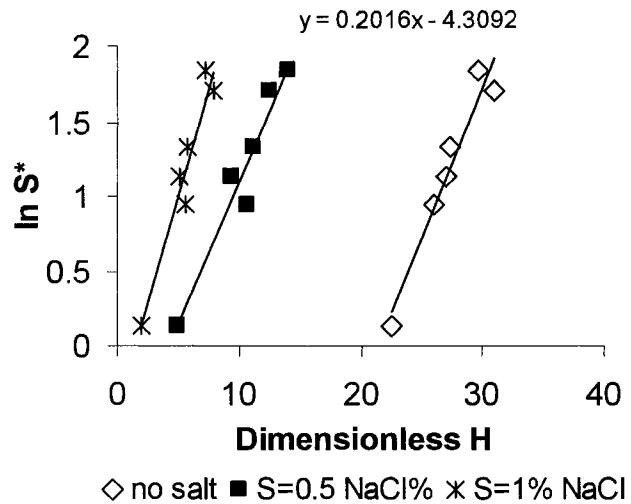


Figure 10. b

Figure 10. a. Variation of the optimum salinity log with respect to the experimental mean curvature, b. variation of the optimum salinity log as a function of the dimensionless curvature. Linear lines are shown only to guide the eye. Results at three different salinities are presented.

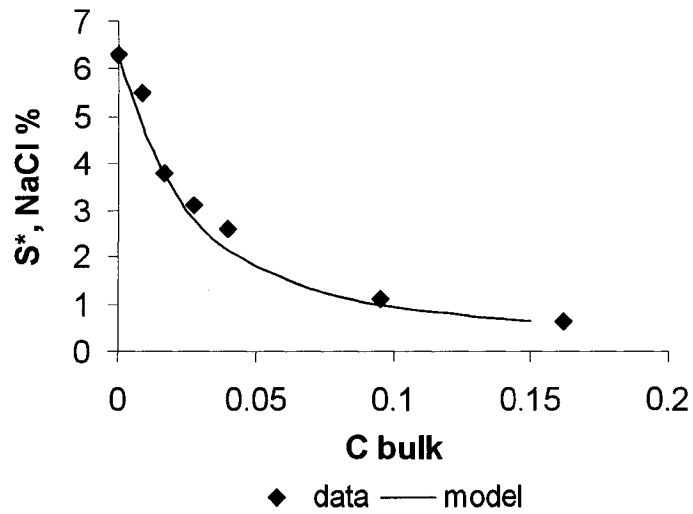


Figure 11.a

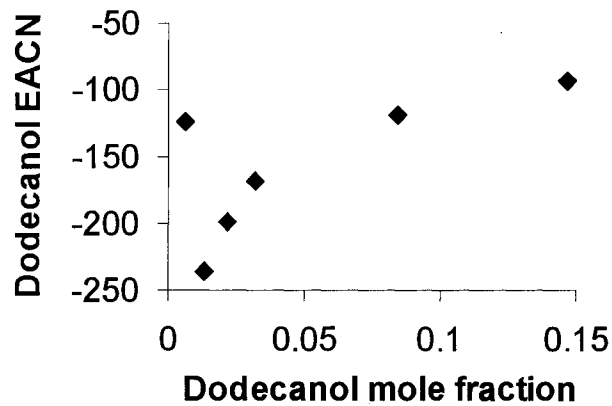


Figure 11. b

Figure 11. a. Optimum salinity variation as a function of the oil phase composition (C_{bulk}). Experimentally determined data and model predictions using Eq. [28] are plotted together; b. Variation of the hypothetical dodecanol EACN as a function of the dodecanol mole fraction in the initial oil mixture. Hypothetical EACN values are calculated by using experimental optimum salinities and initial oil phase compositions in Eqs. [2] and [3].

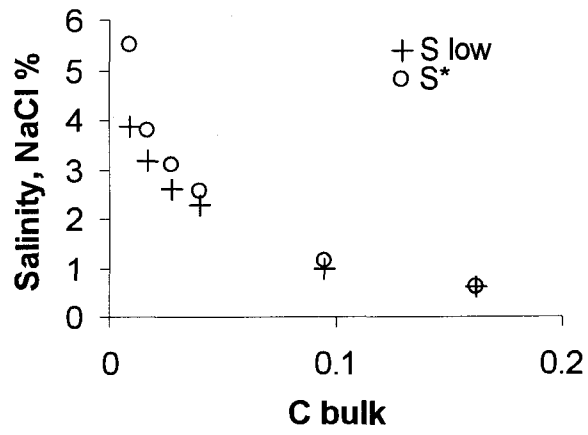


Figure 12. Variation of the lower critical salinity and the optimum salinity as a function of the dodecanol volume fraction (C bulk) in the bulk oil phase

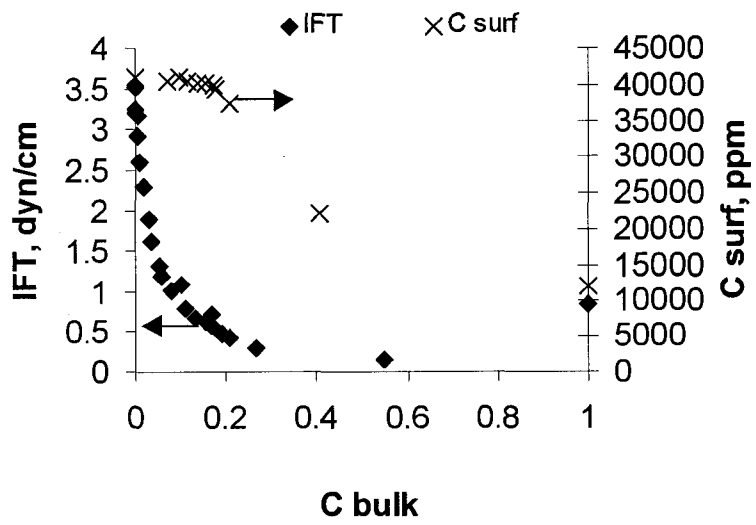


Figure 13. Interfacial tension (IFT) and aqueous phase surfactant concentration (C surf) as a function of the dodecanol volume fraction in the bulk oil phase.

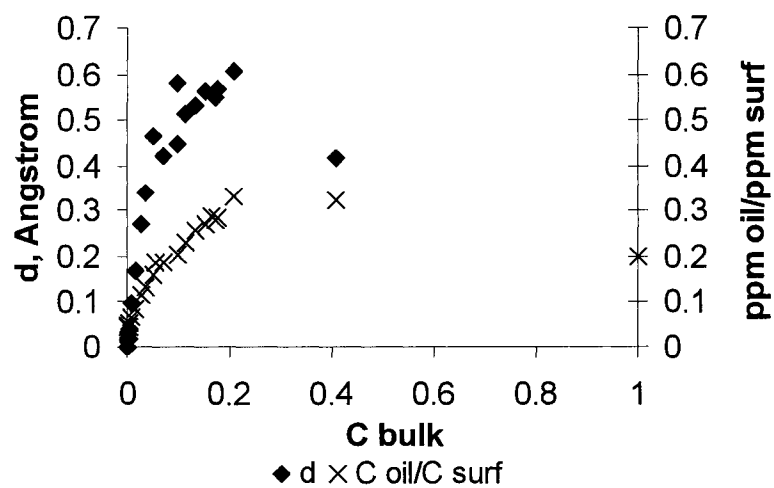


Figure 14. Experimental shell thickness (d) and scaled oil solubilization (C_{oil} / C_{surf}) in the aqueous phase as a function of the dodecanol volume fraction in the bulk oil. The scaled oil solubilization is the ratio of the volumetric oil concentration and the surfactant concentration in the microemulsion in ppm.

CHAPTER 5

MODELING SOLUBILIZATION OF OIL MIXTURES IN ANIONIC MICROEMULSIONS II: MIXTURES OF NON-POLAR AND POLAR OIL COMPONENTS*

ABSTRACT

Polar/amphiphilic oils, called lipophilic linkers are sometimes added to oil – water – ionic surfactant microemulsions in order to increase the solubilization of hydrophobic oils. The solubilization increase has been well documented for a number of systems. However, models to calculate the solubilization increase have been proposed only for optimum microemulsions (i.e., middle phase microemulsions solubilizing equal volumes of oil and water). In this paper we propose a mathematical model to predict solubilization enhancement for non-optimum microemulsion systems. The model is an extension of the net-average curvature model of microemulsion. The net average curvature model is combined with a surface activity model to account for the increased palisade layer solubilization due to the presence of the polar/amphiphilic oil component. New non-linear mixing rules are also incorporated to account for the optimum salinity and the characteristic length variation as a function of the concentration of the lipophilic linker. The model predicts the effect of the variation in the lipophilic linker concentration and the electrolyte concentration on the oil solubilization in accordance with the experimental results.

INTRODUCTION

We have recently developed a new mathematical model (the net-average curvature model) to predict the solubilization of single-component-oils in

* To be submitted to *Journal of Colloid and Interface Science*

microemulsions (1). However, in practical applications the oil to be solubilized is often a mixture, and one is interested in predicting the solubilization of oil mixtures rather than single component oils. One particular case of oil mixture solubilization is when long chain alcohols, called lipophilic linkers, are added to the microemulsion in order to boost the solubilization of a hydrophobic oil (2) – (6). These lipophilic linkers must also be considered as oils because they are not miscible with water. Hence we are dealing with oil mixtures when lipophilic linkers are used. In this research we extend the net-average curvature model for these kinds of oil mixtures and see if it can predict the lipophilic linker effect on the oil solubilization.

Previous modeling of the lipophilic linker effect concentrated on the prediction of the solubilization enhancement only at the optimum formulation (i.e., in middle phase microemulsions solubilizing equal volumes of oil and water). Acosta et al. (2) found that for anionic microemulsions at the optimum formulation the solubilization parameter increased as a linear function of the linker concentration at low concentrations. They proposed a model for the solubilization enhancement at the optimum formulation, which applies in the linear regime (2). However, above a certain linker concentration the solubilization enhancement declined. They suggested that this decline is related to a change in the partitioning of the linker molecules between the excess oil phase and the middle phase microemulsion (3). It was also demonstrated that the linker effect depends on the type of the oil. The linker effect diminishes if the oil component is more polar.

Linkers were also found to affect the optimum salinity. The optimum salinity corresponds to the electrolyte concentration necessary to achieve optimum formulation. The occurrence of the optimum formulation appeared to shift towards lower salinity as

the linker concentration increased in the low concentration regime (3). The logarithm of the optimum salinity was found to be proportional to the concentration of the linker in the studied concentration range. This observation was used to develop a model for the variation of the optimum salinity as a function of the linker concentration (3). More recent results also evidenced that it is the interfacial linker content rather than the initial dodecanol concentration that dictates the optimum salinity and the optimum solubilization in these systems (4, 5).

Salager and coworkers (6-8) investigated the lipophilic linker effect in non-ionic surfactant microemulsions. They reported that the solubilization enhancement was proportional to the linker concentration (6). Research by Graciaa et al. (9) evidenced that both the optimum EON (i. e., the ethylene oxide number of the surfactant, which produces optimum microemulsion) and the solubilization capacity of the optimum microemulsion is affected by the linker additive. At low linker concentrations a linear dependence of the optimum EON and solubilization parameter on the linker concentration was demonstrated. Above a certain concentration, however, the solubilization at the optimum formulation and the optimum EON became less sensitive to the additive concentration (9). In this linker concentration regime the solubilization enhancement did not improve upon further linker concentration increase.

These results imply that the linker effect may change depending on the linker concentration in both ionic and non-ionic surfactant systems. From the practical standpoint it is important to know at what concentration will the solubilization enhancement diminish. Current models cannot make such predictions, because they apply only for low linker concentrations. Lipophilic linker molecules are expected to influence

the microstructure and solubilization at formulations other than optimum as well. However, the existing models, do not apply for non-optimum formulations.

Our objective is to develop a new model that applies for the non-linear regime and for non-optimum formulations as well, and is sensitive to the type of oil.

The net-average curvature model predicts solubilization of single component oils for not only optimum but also non-optimum formulations. A detailed description of the net-average curvature model can be found elsewhere (1). To predict solubilization of oil mixtures the net-average curvature model must be extended to incorporate additional features. One such extension has already been proposed, for the mixture of benzene and limonene (10). When the oil mixture composition varies the overall characteristic of the oil phase is also expected to change. Two parameters are used in the net-average curvature model to take into account the characteristics of the oil (1), the optimum salinity and the characteristic length at optimum. The optimum salinity refers to the concentration of electrolyte needed to obtain a balanced microemulsion, in which equal volumes of oil and water are solubilized. The characteristic length is a parameter that is related to the microstructure and the solubilization ability of the surfactant. Further discussion of these parameters can be found elsewhere (11-17).

Ruckenstein and Nagarajan (18) found that even mild polarity difference between the oil components (i. e., benzene and hexane) could result in preferential solubilization of the more polar component. They suggested that the selectivity towards the more polar oil is the consequence of its enrichment close to the surface of the solubilized oil domain. We found similar behavior with benzene / limonene oil mixture in a sodium dihexyl sulfosuccinate surfactant system (10). In that oil mixture the difference in the molecular

structure and the polarity between the oil components is not large, but benzene was still solubilized preferentially. The benzene segregation could be treated as surface excess phenomenon. For that system the single oil net-average curvature model was modified in two ways: by incorporating an expression to account for the benzene surface excess and by using linear mixing rules for the optimum salinity and the optimum characteristic length for the oil mixture.

In the current work the properties of the two oil components, the lipophilic linker and the hydrophobic oil, are more significantly different from each other. To study such a system we selected dodecanol as the linker, and limonene as the hydrophobic oil, and sodium dihexyl sulfosuccinate as surfactant. Dodecanol-limonene mixtures differ from the benzene-limonene system in that the component polarities and molecular structures are significantly different, and the dodecanol has a strong tendency to segregate near the interface (4,10). It has been shown that simple linear mixing rules cannot be used to calculate mixture properties (2-4, 9) especially at high concentrations of linker. The solubilization parameter is linear only at low linker concentrations. Similarly, the linear mixing rule for the optimum salinity applies only at low polar oil concentrations (4, 9, 19).

Therefore in our new solubilization model for the lipophilic linker – hydrophobic oil system, not only does the surface excess model need to be utilized as in the case of the benzene-limonene mixture but also the linear mixing rules must be modified to calculate the oil properties.

BACKGROUND AND MODEL DEVELOPMENT

Model description.

The model considers saturated o/w type as depicted in Figure 1. In saturated o/w microemulsions two macroscopic phases are in equilibrium: the microemulsion phase and the excess oil phase. The excess oil phase contains the oil, which is rejected by the microemulsion. The microemulsion is modeled according to the pseudo-phase theory (20). According to this theory the microemulsion is divided into three pseudo-phases: the water pseudophase, the oil pseudophase, and the surfactant film. The water pseudo-phase contains all of the water, the molecularly dispersed surfactant at its CMC, and the electrolyte. The oil pseudo-phase contains the two oil components that are solubilized. All of the surfactant in excess of the CMC is assumed to adsorb at the oil-water interface, making up the surfactant film. By using this treatment we have neglected the following factors: (a) the water pseudo-phase contains molecularly dispersed oil molecules at their water solubility, (b) under certain conditions the oil pseudo-phase may also contain some surfactant in a molecularly dispersed form, according its CMC in the oil, (3) water and oil might interpenetrate the surfactant film in a random manner, causing the surfactant layer not to be pure surfactant.

In our new model we further divided the oil pseudo-phase into two sub-regions: the interfacial (or shell) oil, and the core oil. The necessity of this treatment is explained as follows. In real microemulsions the composition distribution within the solubilized oil is not homogenous. The concentration of the polar oil gradually increases from the core of the solubilized oil towards the surface. Exact functionality between the distance from

the core and the composition has not been proposed so far. In addition, the geometry of the oil pseudo-phase is also complex, because oil is solubilized in the hydrophobic core and also between the surfactant tails, in the palisade layer. This makes it even more difficult to propose such a relationship.

We simplify the composition – distance functionality in two ways. First, the shape of the solubilized oil domain is taken as spheres, which include both the core oil and the palisade layer oil. Second, the concentration gradient is replaced by a step function with two values. With that the total volume of the spheres is divided into two regions where the oil composition is different, but constant within each region.

It is now well established by previous research that polar oil is solubilized in excess of the more hydrophobic component. Furthermore, the polar oil excess is correlated to the interfacial area of the microemulsion. Therefore it is treated in our model as surface excess. Because of this treatment the two regions of the solubilized oil are the one in the center with bulk oil composition, and another one at the surface where the surface excess is located. We call these regions core and surface layer (or shell), respectively. In the core the oil composition equals that of the excess oil phase. Because the chemical environment in the excess oil phase and in the core oil portion of the oil pseudo-phase is similar, this assumption seems reasonable. The surface layer is envisioned as a shell whose thickness equals the volumetric surface excess per unit surface area. This shell contains only polar oil. The sizes of these two regions are such that they yield the same total solubilized oil volume and overall oil composition as that in the real microemulsion. Hence a convenient model is created, which provides the same overall oil solubilization, as a more complicated model would do.

It is important to note, however, that the compositions, the geometry, and the sizes of the model regions are hypothetical, they do not exist in the real microemulsion. Therefore the model is not able to give precise information about the composition distribution within the microemulsion.

The same pseudophase model, described above, applies for bicontinuous microemulsions as well.

Net-average curvature model

We use the net-average curvature model to compute the solubilization in the core. As discussed elsewhere in detail (1), the net-average curvature model is able to predict average oil/water domain sizes and the volume of solubilized oil/water as a function of a selected formulation variable. The selected formulation variable in this study is the electrolyte concentration. The ability of the net-average curvature model to predict microemulsion properties derives from its use of oil and water drops, which are assumed to exist simultaneously in the microemulsion. The drops may not actually exist, in which they are fictitious.

For o/w droplet microemulsions the equivalent radius of the continuous phase (R_w) is computed based on the conservation of the surfactant volume and assuming constant surfactant density at the oil/water interface, and uniform, spherical droplet shapes as follows:

$$R_w = \frac{3V_w}{A_s} \quad [1]$$

where V_w is the volume of the water added to the system, A_s is the total interfacial area of the surfactant film.

The equivalent radius of the dispersed phase (R_o) is then simply computed from the net curvature of the surfactant film. The net curvature is calculated as

$$\frac{1}{R_o} - \frac{1}{R_w} = \frac{1}{L} \ln \frac{S^*}{S} \quad [2]$$

where L is a parameter related to the length of the surfactant tail, S^* is the optimum salinity, and S is the salinity.

The minimum value of the average curvature, which depends on the characteristic length of the bicontinuous microemulsion, is calculated according to:

$$\frac{1}{2} \left(\left| \frac{1}{R_o} \right| + \left| \frac{1}{R_w} \right| \right) \geq \frac{1}{\xi^*} \quad [3]$$

where ξ^* is the characteristic length of the bicontinuous microemulsion. For bicontinuous microemulsions Eqs. [2] and [3] are solved simultaneously to obtain the equivalent radii of the oil and the water domain.

Adsorption isotherm

An adsorption isotherm is applied to compute the solubilization in the surface layer. It is well known that oil molecules of varying polarity are incorporated in the surfactant aggregates at different locations (21-25). Polar oils have been observed to segregate near the surfactant layer (9, 21-25). In this way the interfacial tension is reduced due to the surface excess of the polar component (24, 25). Segregation may also be entropy driven, which favors enrichment of the smaller oil molecules in the palisade

layer. However, we assume, that in the present system the surface-active behavior dominates. Several surface adsorption isotherm equations have been proposed in the literature (26, 27), which relate the surface excess to the concentration of the bulk phase. In this work we use a Langmuir isotherm (Eq. [4]) to model this behavior:

$$d = \frac{K \cdot c_{bulk}}{B + c_{bulk}} \quad [4]$$

where d is the volumetric surface excess of the polar oil per unit surface area, K and B are adsorption parameters related to the maximum surface excess that would fill the surface sites and the energy of adsorption, and c_{bulk} is the volume fraction of the polar oil in the bulk oil.

Analyzing the solubilization data of dodecanol-limonene mixture in sodium dihexyl sulfosuccinate we found that the shell thickness values are typically very small, in some cases even below 1 Angstrom (4). This is an expected result, which originates from the simplification of the oil domain geometry and the concentration distribution function in the model. It is anticipated that in the dodecanol-limonene system even though dodecanol has a great tendency to go to the interface, but still does not adsorb at the interface as aggressively as a surfactant. That is why dodecanol is considered as a lipophilic linker and not as a surfactant. Consequently, we do not really see a total surface saturation leading to a monomolecular layer, like in the case of the surfactants. Only if dodecanol behaved as a surfactant, would we be able to realize a shell thickness equal to the length of one dodecanol molecule.

Treating the solubilized dodecanol excess as surface excess quantity is another reason that yields small shell thickness values. Because the surface excess depends on the bulk oil concentration, at low concentration the adsorption is low. If we want to distribute

those few oil molecules over the whole surface area, we necessarily get a very small shell thickness.

What we really calculate as shell thickness is the surface excess moles of the polar oil, according to the standard Gibbs treatment (28). The excess occurs across a certain thickness, but, following the Gibbs convention, it is simplified by taking the physical interface thickness zero (i.e. the bulk concentration is extrapolated up to the interface), and only the material balance is considered to compute the surface excess. Then we convert the surface excess moles into volume in the model. The total volume of these molecules is divided by the whole interfacial area to get the volumetric surface excess. This must necessarily yield very small thickness at lower concentrations.

We have also checked the possible effect of deviation from the spherical shape on the model shell thickness values. Because we analyze only Type I and Type III, and all of the oils are contained in the oil droplets, the shell is located on the outer surface of the oil droplets, and the hypothetical water droplets are not affected by the shell. (This is probably also a simplification, as the shell could be located somewhat "in between" the water and the oil core.) We keep the surface excess constant, no matter how the shape changes. For the same droplet volume, the sphere has the smallest surface area. Because the shell volume should also be kept constant, the sphere should have the largest shell thickness. This causes a decrease of the shell thickness if the microemulsion contains more elongated shapes instead of spheres. This shell thickness deviation, however, must be very small because the shell thickness is usually 1-2 order of magnitude less than the radius of the droplet. So it appears that using spheres in the model instead of the actual non-spherical shapes is not responsible for the small shell thickness values.

The model shell thickness is not equivalent with the thickness over which the oil composition varies, as one goes from the center of the oil droplets towards the interface. The model is not designed to do that. The model only computes, how much of the different kinds of oils are solubilized. To carry this out, it uses a parameter, "shell thickness", which is of course hypothetical. It only means the surface excess (mole/area) in a volumetric form.

We use the volumetric form, because we plan to incorporate this model into a flow model for porous media. Porous media flow models (e.g. UTCHEM by the University of Texas (29)) are more convenient, if volumes are used. Furthermore, when we analyzed data for two different oil mixtures, the benzene-limonene (10) and the dodecanol-limonene (4) data, we saw that both the optimum salinity and the characteristic length depended on the shell thickness the same way, no matter if benzene or dodecanol excess produced the shell. This is an interesting result, and we decided to keep the volumetric treatment so that this feature is not lost. Of course, for dodecanol, a lot less concentration is enough to produce a similar effect as in the benzene case, and it can go well beyond the affect of benzene, because dodecanol adsorbs more. This is why dodecanol is a linker, while benzene is not. But it looks like, the same shell thickness (if exist) produces the same characteristic length and optimum salinity for both dodecanol – limonene and benzene – limonene mixtures.

In the sodium dihexyl sulfosuccinate surfactant system limonene is not expected to penetrate appreciably into the palisade layer due to its hydrophobicity. In this special case, when the amount of hydrophobic oil solubilized in the palisade layer is negligible, almost all of the oil solubilized in the palisade layer is the polar oil. Therefore, the surface

excess and the palisade layer solubilization can be assumed to coincide. Furthermore, the core, as defined in our model, must also coincide with the core that can be calculated with the net-average curvature model. This special case applies to the system of the research reported here, allowing us to combine the net-average curvature model with the surface excess model to predict the total oil solubilization.

To calculate the radius corresponding to the total oil solubilization the volumetric surface excess (i.e., shell thickness) has to be added to the core radius:

$$R_o = R_c + d \quad [5]$$

where R_c is the core oil solubilization as computed by the net-average model, and d is the shell thickness as calculated from the surface adsorption model (Eq. [4]).

Characteristic length model

The characteristic length in bicontinuous microemulsions is also expected to depend on the oil type. Indeed, it has been found experimentally that oils with shorter chain yield larger characteristic length (30).

To explain this, one needs to consider the optimum formulation. In an optimum formulation the net curvature of the surfactant film is zero, because the average curvature towards the oil and the water are equal but with opposite sign. However, the surfactant film is locally bent, rather than flat, due to thermal fluctuation effects. Two bending rigidity parameters have been introduced (31) to characterize the resistance of the surfactant film against bending: the bending rigidity and the saddle splay rigidity. These parameters represent the resistance against bending and saddle splay deformations, respectively. The rigidity of the film affects the deviation of the local curvature from the

preferred curvature of the surfactant film. Rigid films are bent less by thermal fluctuation effects than softer ones, resulting in smaller local curvature deviations. Therefore the length over which the surfactant layer remains essentially flat at the optimum formulation, where the preferred curvature is zero, is larger. As a consequence, microemulsions with rigid surfactant film have larger characteristic lengths.

The type of oil can influence the rigidity. In the balanced state (i.e., at the optimum formulation) the pressure on the water side and on the oil side of the surfactant film is equal. Due to entropy effects, oil molecules tend to penetrate between the tails of the surfactant (18, 25). The penetration tendency is greater for oils with low EACN, because these oils are usually smaller, and experience less conformational restrictions in the palisade layer. The penetration tendency is also expected to be greater for polar oils than for non-polar oils. Polar oils could reduce the interfacial tension between the water and the surfactant tails if they locate themselves close to the micelle/water interface (18, 24). This could also be a driving force for the penetration. Penetration causes the pressure on the oil side of the surfactant film to increase, increasing the bending rigidity (32). To compensate (maintain the mean curvature at zero), the pressure on the water side also has to increase. In order to increase the water side pressure one has to reduce the screening of the electrostatic repulsion between the ionic surfactant head groups by adding less electrolyte, hence the optimum salinity decreases. The increased pressure on the water side also affects the saddle splay rigidity (33). As a result, the overall rigidity of the surfactant film increases. The more rigid film will bend less in response to thermal fluctuation effects. This explains why oil penetration between the surfactant tails tends to

decrease the optimum salinity and increase the characteristic length of the bicontinuous microemulsion.

In a recent paper (4) we proposed that the characteristic length dependence on the oil surface excess could be computed adopting the relationship between the bending rigidity and the adsorption density of amphiphilic copolymers (34):

$$\kappa = \kappa_0 + \left(1 + \frac{\pi}{12}\right) \cdot (R_a^2 + R_b^2) \cdot \sigma \quad [6]$$

$$\xi^* = a \cdot \exp \frac{2\pi \cdot \kappa}{k_B T} \quad [7]$$

where κ and κ_0 are the bending rigidity of the surfactant layer in the presence and in the absence, respectively, of the adsorbing oil component, R_a and R_b are the length of the hydrophilic and the hydrophobic segment of the adsorbing oil molecule, respectively, and σ is the number density of the adsorbed oil at the interface, ξ^* is the characteristic length, $a = L + d$ is a length parameter, which combines the molecular length of the surfactant (L), and the shell thickness (d), k_B is the Boltzmann constant, and T is the absolute temperature.

Optimum salinity model

In the net-average curvature model, the droplet radii are sensitive to the type of oil, because S^* and ξ^* are dependent on the type of oil. The equivalent alkane carbon number (EACN) has been introduced to characterize the type of oil (19). Oils with larger

EACN are more hydrophobic than oils with low EACN. Salager and coworkers proposed that the optimum salinity depends linearly on the EACN of the oil according to (35)

$$\ln S^* = K \cdot EACN - \sigma + f(A) + a_T (T - T_{ref}) \quad [8]$$

where S^* is the optimum salinity, K is a constant, depending on the type of the surfactant, $f(A)$ is a function which depends on the alcohol, σ is a constant which depends on the surfactant, T is the absolute temperature, and a_T is the coefficient of the temperature effect on the optimum salinity.

If the oil is a mixture, an overall EACN may be defined according to

$$EACN_{mix} = \sum_i x_i EACN_i \quad [9]$$

where $EACN_{mix}$ and $EACN_i$ are the equivalent alkane carbon numbers of the mixture and component i , respectively, and x_i is the mole fraction of component i in the oil mixture.

Combining Eq.[8] and Eq.[9] yields

$$\ln S^*_{mix} = x_i \ln S^*_i \quad [10]$$

Equation [10], which is based on linear mixing rule, has been shown to work well for a number of oil mixtures composed of similar oil components (19, 36, 37).

We observed, as did Baran et al. (19) and Salager et al. (9), that mixtures of components with differing polarities do not closely follow Eq.[10]. To account for the deviation we previously introduced a different model for the optimum salinity (4). In that model we account for the affect of the polar component surface excess (34). A more detailed explanation of this model can be found elsewhere (4). The optimum salinity is given as

$$\ln S^*_{mix} = \ln S^*_0 + \frac{1}{4} \cdot \left(\sqrt{\frac{\pi}{6}} \right) \cdot (R_a - R_b) \cdot \frac{\sigma}{\kappa} \cdot \xi \quad [11]$$

where S^*_{mix} and S^*_0 are the optimum salinity in the presence and in the absence of the polar oil, respectively. Equation [11] is incorporated in the present model to account for the optimum salinity dependence on the oil phase composition.

Solution method

The proposed model predicts the solubilization of oil and water as a function of the selected formulation variable (i.e. electrolyte concentration) and the concentration of the lipophilic linker. Additionally, the model also computes the compositions of the solubilized oil and the excess oil. The input parameters include the optimum salinity (S^*_0) and the characteristic length at optimum (ξ_0) of the pure hydrophobic oil/ surfactant system, the Langmuir parameters (K and B), and the surfactant length parameter (L). The optimum salinity and the characteristic length are experimentally determined from a salinity scan experiment with the carried out with the water/surfactant/hydrophobic oil system. The surfactant length parameter (L) may be approximated with the extended length of the surfactant tail. The Langmuir parameters are obtained by fitting experimental adsorption isotherm at intermediate salinity (i.e. below the lower critical salinity).

Because the polar oil was shown to partition considerably into the microemulsion (9), the linker concentration in the bulk oil is expected to decrease from the initial value once solubilization has reached equilibrium. The proposed model takes this effect into

account by applying the conservation of the linker in the system as a constraint in the following way:

$$V_o \cdot c_{ini} = (V_o - V_t) \cdot c_{bulk} + V_t \cdot c_{ave} \quad [12]$$

where V_o is the volume of the oil in the system including all phases, V_t total volume of oil solubilized in the microemulsion, c_{ini} is the initial volume fraction of the dodecanol in the oil mixture, c_{bulk} is the dodecanol volume fraction in the bulk oil, c_{ave} is the average dodecanol volume fraction in the solubilized oil.

The first task is to find the optimum salinity and optimum characteristic length for a given initial linker concentration. To do so Eqs. [4], [11], [6], and [12] are solved iteratively for the bulk oil concentration at the optimum formulation. Once the equilibrium bulk oil composition under optimum conditions is known, the volumetric surface excess (i.e. shell thickness), optimum salinity, and characteristic length are calculated as a function of bulk oil composition.

The next step is to calculate the equilibrium bulk oil phase composition as a function of the salinity (at fixed initial oil composition). This is carried out iteratively by solving Eqs. [1] – [5] and [12]: knowing the bulk oil phase compositions we calculate the shell thickness, and solve the net-average curvature model for the oil and water radii. Given the calculated radii of the fictitious oil and water droplets and the shell thickness the model calculates the volume of the total solubilized oil and water employing Eq. [2].

Our model is based on certain simplifications. (a) The oil dissolved in molecularly dispersed form in the water is neglected. While our experimental results suggested that in the case of limonene/dodecanol mixture this assumption is reasonable, water solubility may be more significant for other types oil components. (b) The CMC of the surfactant

and the counterion binding is taken as a constant and is assumed independent from the type of oil. All of the surfactant above its aqueous CMC is assumed to reside at the oil/water interface. (c) The adsorbed surfactant layer is considered as a two-dimensional incompressible liquid. Therefore, the area per surfactant molecule (a_s) at the oil/water interface is taken to be a constant as a function of the curvature. (d) Segregation of the linker at the adsorbed surfactant layer does not change the adsorption of the surfactant. This appears in the model by virtue of using a constant area per surfactant molecule (a_s) as a function of oil phase composition. (e) The change in the oil phase characteristics does not affect the amphiphilicity and oil/water partitioning characteristics of the surfactant. (f) The surface excess of the linker at the palisade layer is not affected by the curvature of the surfactant film. We found that the latter assumption is not completely satisfied over the total curvature range in a salinity scan. However, significant variations were found only at the highest curvature values, and the assumption proved reasonable for all other curvature values. We expect some deviation between model and experimental data due to this simplification at very low salinity. (g) The microemulsion is saturated. This means that when bicontinuous microemulsion forms, there are always excess oil and water phases present, which are in equilibrium with the microemulsion phase. As a result, the microstructure and solubilization are mainly determined by the curvature effects, and interlayer interactions are not important.

It is anticipated that the above simplifications could cause some deviation between the predictions and the data, but the model can still predict the observed trends correctly.

EXPERIMENTAL SECTION

Laboratory experiments have been carried out in order to test the performance of the proposed model. The model system contained a binary oil mixture, anionic surfactant, water, and electrolyte. The surfactant type and concentration, the temperature, and the water-to-oil ratio were kept constant. The polar oil component is 1-dodecanol, the hydrophobic oil component is (R)-(+)-Limonene ((R)-4-Isopropenyl-1-methyl-1-cyclohexene). The surfactant is sodium dihexyl sulfosuccinate. NaCl was used as an additive to vary the formulation. Salinity scan experiments were carried out with different oil phase compositions. Concentration of the oil components, and the surfactant were measured GC, and liquid chromatography, respectively in each phases after equilibrium was reached. For more detailed description of the materials, methods, and experimental solubilization results the reader is referred to a previous paper (4).

RESULTS AND DISCUSSION

Input data used in the model are shown in Table 1. The adsorption isotherm, the optimum salinity and optimum characteristic length values are presented and discussed in detail in a previous paper (4). Here only the oil solubilization results are presented and compared to the data.

The dodecanol was always below 0.2 volume fraction, because above that value the system closely approaches a tricritical point and some of the assumptions of our model become invalid. For example, between 0.12- 0.2 volume fraction the middle phase

wets its interfaces with the excess phases, which indicates that the amphiphilicity of the surfactant decreases (38). Above 0.2 volume fraction the regular Winsor I-III-II type phase behavior transition with increasing salinity disappears and is replaced by the gradual, stepwise transition of the surfactant from the water phase into the oil phase. As a result, no middle phase microemulsion is found. When this phenomenon occurs, our model will necessarily break down.

Total oil solubilization by the microemulsion

As discussed above, the total oil solubilization varies both with changes in the salinity and in the dodecanol concentration. In Figure 2 model results and experimental solubilization data are presented for the solubilized oil concentration in the microemulsion phase at several fixed initial dodecanol concentrations as a function of salinity. For a fixed initial dodecanol concentration the solubilized oil volume increases as the salinity increases as expected. This is attributed to the decrease of the curvature of the surfactant film (39). A sudden increase in the total oil volume fraction in the microemulsion phase is seen after passing the Winsor Type I-III transition boundary. The salinity corresponding to the Type I-III transition is the lower critical salinity. The large increase in the oil solubilization occurs above the lower critical salinity because in the Type III region excess water phase is expelled from the microemulsion.

Figure 2 shows that the model provides a close estimate of the lower critical salinities and the total oil solubilization for all series, except for the highest dodecanol concentration (0.12 volume fraction). At 0.12 dodecanol volume fraction the predicted

optimum salinity is about 0.4 wt % higher than the data. Because of this shift the model tends to underpredict the oil solubilization at a fixed salinity.

This deviation could be attributed to some simplifications that may become inappropriate around 0.12 dodecanol volume fraction. It is beyond the scope of this research to investigate these deviations, which should be addressed in another study. However, some of our findings could provide a basis for a qualitative explanation of such a trend. At around 0.12 dodecanol volume fraction a non-wetting / wetting transition was detected. This indicates that the microemulsion shifted towards a weakly structured mixture because the oil phase polarity increased (40). At the same time we found that almost 100 % of the surfactant remained in the aqueous phase up to 0.2 initial dodecanol volume fraction. Partitioning of the surfactant into the oil phase started only above 0.2 volume fraction. Therefore, it is likely that around 0.12 volume fraction the fraction of the molecularly dispersed surfactant increased at the expense of the organized surfactant due to the weakening of its amphiphilicity. This is equivalent to increasing the CMC in the water phase. This would cause the solubilization due to the organized surfactant to decrease only slightly.

The unorganized surfactant (at the actual CMC) could also increase the effective salinity of the solution, without adding more salt. Even a small effective salinity increase might cause a significant decrease of the surfactant layer curvature in this system, because the optimum salinity is already very small (predicted around 1.5 wt % for this oil composition), and the system is very sensitive to salinity changes. Hence the bulk oil solubilization is expected to significantly increase and the optimum formulation could be reached with less added salt.

Neglecting these effects could cause our model to overestimate the optimum salinity, thereby underestimating the oil solubilization and overestimating the average dodecanol concentration in the solubilized oil. We conclude, therefore, that our model works well before the non-wetting / wetting transition is reached, but when this transition occurs, predictions become inaccurate.

The total oil solubilization as a function of the bulk oil phase composition is presented in Figure 3. The total oil solubilization is expressed as the concentration of both oil components in the microemulsion phase in ppm. Figure 3 shows model results and experimental data at fixed salinity (at no added salt). According to the figure the model predicts that the solubilization will increase as the dodecanol concentration increases. The same trend was observed experimentally as well. The model slightly overpredicts the solubilization at low salinity. This is expected because the shell thickness is assumed to be constant in the model. However, we found that for very small oil droplet sizes, the shell thickness appeared to be slightly less (4). At no added salt the droplet sizes are in fact very small when the dodecanol concentration is low. If the shell thickness is overestimated, the oil solubilization is also overestimated. When the dodecanol concentration increases, the droplet size increases as well, even if the salinity is kept constant. That is why the shell thickness estimates appear to improve at intermediate dodecanol concentrations, as seen in Figure 3. At high dodecanol concentration (above 0.12 initial volume fraction, which corresponds to about 0.1 bulk oil volume fraction) the deviation between the model and the data becomes again slightly greater. This time, however, the model underpredicts the solubilization. We believe that

this is caused by the closeness to the tricritical point and the non-wetting / wetting transition as explained above.

To extend our model to the non-wetting / wetting transition regime, one would have to allow for changes in the amphiphilicity of the surfactant and incorporate cosolvent effects due to the molecularly dispersed surfactant. But by analyzing the variation of the interfacial tension between the coexisting phases it should be possible to identify the non-wetting / wetting transition point (41). Beyond the wetting regime, when the tricritical point is reached along this path, the bicontinuous microemulsion structure is lost (42). To predict this point for ionic surfactant systems, the observation that ionic microemulsions can only be formed above a certain electrolyte concentration (43) might be a starting point. If the predicted optimum salinity is less than the minimum salinity required for microemulsion formation, the microemulsion regime might be terminated. Extensive studies on microemulsions near tricritical points are required before such adjustments to the model could be developed.

Composition of the solubilized oil

The dodecanol volume fraction in the solubilized oil varies as a function of the excess oil composition and the salinity. Figure 4 shows the salinity dependence at fixed initial bulk oil composition. For a fixed initial oil composition the dodecanol concentration in the solubilized oil is higher at lower salinity, decreasing as the salinity approaches the optimum salinity. This could be attributed to the increasing contribution of the core solubilization as the salinity increases (1). Because dodecanol is enriched only in the shell and not in the core, increasing core solubilization necessarily reduces the

overall dodecanol concentration in the solubilized oil. Since the model reproduces this trend, we can conclude that the two-state solubilization appears to be a correct approach for these systems.

The fit between data and model is excellent for initial dodecanol volume % of 0.92, 1.82, 3.1, and 4.4. At low salinity, however, the model seems to slightly overestimate the dodecanol volume fraction. This is expected if one considers the shell thickness variation at low salinity as discussed above. The model is shifted towards higher salinity compared to the experimental data for the 12 volume % series. This deviation is expected because of the error in the prediction of the optimum salinity. The optimum salinity shift is clearly demonstrated in Figure 2.

The dependence of the average dodecanol concentration of the solubilized oil (c_{ave}) on the bulk oil composition is presented in Figure 5. Both concentrations are in terms of dodecanol volume fractions. In general dodecanol concentration increases rapidly at low dodecanol concentrations. The increase slows down considerably, reaching a constant slope as the dodecanol concentration in the bulk oil increases. The model is able to reproduce this trend correctly. However, the model overpredicts the dodecanol concentration in the solubilized oil, at initial dodecanol concentrations above 0.12 volume fraction (~ 0.1 bulk oil volume fraction). Here the oil composition is richer in the limonene than predicted, yet the total oil solubilization is higher, as seen in Figure 3. This means that the larger total oil solubilization is due to factors other than the dodecanol surface excess. We believe that the reduced amphiphilicity of the surfactant plays an important role in this trend as described above.

Excess oil phase composition

The new model is able to calculate the composition not only of the solubilized oil, but also of the excess oil. The excess oil composition as a function of salinity is presented in Figure 6. The initial oil composition and the optimum salinity are used to normalize the dodecanol concentration and salinity data, respectively, in Figure 6. Data and model results show good agreement. The dodecanol concentration in the excess oil phase is expected to be less than the initial value, because dodecanol is solubilized preferentially. Therefore the normalized dodecanol concentration values are less than unity. Because the surfactant concentration is very low (only 4 wt %), the amount of solubilized oil is small compared to the total amount of the oil in the system. Consequently, depletion of the dodecanol is marginal. For this reason the dimensionless dodecanol concentration values are around 0.85-0.9, remaining close to unity. We also see that the salinity appears to have only a small effect on the depletion of dodecanol from the oil. This is expected because the shell thickness is not affected strongly by the salinity variation.

Figure 7 demonstrates the variation of the excess oil phase with varying initial oil composition for no added salt. Data and model results are presented in normalized form. The dimensionless bulk dodecanol concentration tends towards unity as the initial dodecanol concentration increases, which is captured by the model. This trend can be understood if we recall that increasing the dodecanol concentration the shell thickness follows a saturation trend. This means, that above a certain dodecanol concentration the shell contribution to the total oil solubilization does not increase very much. At the same time oil droplet sizes at fixed salinity increase because the oil becomes more polar. Therefore the contribution from the bulk core solubilization to the total oil solubilization

increases. As a result the average composition of the solubilized oil, which leaves the oil phase, approaches the excess oil composition. Hence, the excess oil composition at equilibrium approaches the initial composition. Figure 7 suggests that overall the dodecanol depletion decreases as the initial dodecanol concentration increases.

Selectivity

The selectivity is defined as the ratio of the dodecanol concentration in the solubilized oil (c_{ave}) and in the excess oil phase (c_{bulk}):

$$Selectivity = \frac{c_{ave}}{c_{bulk}} \quad [13]$$

Figure 8 shows the variation of the selectivity as a function of salinity. The model follows the experimental trends closely. The selectivity decreases as the salinity increases. This behavior is discussed in greater detail in a companion paper (4). The excellent fit between data and model at dodecanol concentrations below 12 volume % further supports that the basic model concepts are realistic. There is a larger deviation between data and model at 12 % dodecanol. This is expected, because the model does not take into account the closeness to the tricritical point and the non-wetting/wetting transition. In Figure 9 we plot the selectivity variation as a function of the initial dodecanol concentration with no added salt. Again, the model closely follows the trend of the data. The model slightly overpredicts the experimental selectivities. This is not surprising because the total oil solubilization dominated by the bulk oil composition exceeds the predicted values.

CONCLUSIONS

A mathematical model has been developed to predict solubilization enhancement of hydrophobic oils in anionic microemulsions. The net-average curvature model has been extended to binary oil mixtures by accounting for not only the oil solubilization in the core but also for the preferential polar oil solubilization in the palisade layer. A Langmuir type adsorption isotherm is introduced to account for the palisade layer solubilization. As a new feature, the polar oil component depletion in the excess oil phase is accounted for as well. Furthermore, new relationships have been introduced to describe the dependence of the optimum salinity and the characteristic length dependence on the oil phase composition. Required input parameters include the interfacial area per surfactant molecule, surfactant tail length parameter, optimum salinity without the linker, characteristic length without the linker, molecular sizes of the hydrophobic and the hydrophilic part of the linker molecule, and the two parameters of the Langmuir isotherm. All of these may be calculated or determined experimentally, except for the Langmuir parameters, which require curve fitting.

Results of experimental solubilization studies presented in a previous paper were used to evaluate the model predictions. The model provided good agreement with the experimental data for those oil mixtures, which were able to form middle-phase microemulsions. By using this model, it is for the first time possible to calculate the solubilization enhancement, the composition of the solubilized oil and the excess oil phase not only at optimum formulations but also in non-optimum formulations (i.e. over the course of Winsor Type I – III microemulsions). The model provided excellent

predictions for oil mixtures below 0.12 initial dodecanol volume fraction, and when the droplet sizes are not very small.

At 0.12 volume fraction the model seems to deviate from the experimental data. This deviation is manifested in overprediction of the optimum salinity, and underprediction of the oil solubilization. While a thorough study is needed to reveal the exact reason(s) for this deviation, we believe that the closeness of the surfactant system to the tricritical point, and weakening of the amphiphilic strength of the surfactant play an important role. This change is not accounted for in the model, and thus deviations between model and data increase above 0.12 dodecanol volume fraction.

At very low salinity, when the micellar sizes are small, the model also seems to slightly depart from the data. Under these conditions the shell thickness is overpredicted, because the model neglects the slight dependence of the shell thickness on the salinity in this regime. As a consequence the dodecanol concentration in the solubilized oil and the total oil solubilization are slightly overpredicted.

Based on the model predictions we can conclude that the solubilization enhancement appears to be directly related to the dodecanol surface excess in the oil droplets. An increase of the surface excess increases the characteristic length and decreases the optimum salinity. Both of these changes tend to increase the oil solubilization at a fixed salinity. The dependence of the surface excess on the dodecanol concentration follows a Langmuirian trend. Therefore the efficiency of the solubilization enhancement diminishes as the “saturation” is approached. Linker molecules are observed to be most efficient in concentrations before the “saturation” is approached.

REFERENCES

1. Acosta, E.; Szekeres, E.; Sabatini, D. A.; and Harwell, J. H. *Langmuir* **2003**, *19*, 186-195.
2. Uchiyama, H.; Acosta, E.; Tran, S.; Sabatini, D. A.; Harwell, J. H. *Ind. Eng. Chem. Res.* **2000**, *39*, 2704-2708.
3. Acosta, E.; Tran, S.; Uchiyama, H.; Sabatini, D. A.; Harwell, J. H. *Environ. Sci. Technol.* **2002**, *36*, 4618-4624.
4. *Chapter 4 of this Dissertation*
5. Uchiyama, H.; Acosta, E.; Tran, S.; Sabatini, D. A.; Harwell, J. H. *Ind Eng. Chem. Res.* **2000**, *39*, 2704-2708.
6. Graciaa, A.; Lachaise, J.; Cucuphat, C.; Bourrel, M.; Salager, J. L. *Langmuir* **1993**, *9*, 669-672.
7. Graciaa, A.; Lachaise, J.; Cucuphat, C.; Bourrel, M.; Salager, J. L. *Langmuir* **1993**, *9*, 3371-3374.
8. Salager, J. L.; Graciaa, A.; Lachaise, J. *J. Surf. Det.* **1998**, *1* (3), 403-406.
9. Graciaa, A.; Lachaise, J.; Cucuphat, C.; Bourrel, M.; Salager, J. L. *Langmuir*, **1993**, *9*, 1473-1478.
10. Szekeres, E.; Acosta, E.; Sabatini, D. A.; Harwell, J. H. A Two-State Model for Selective Solubilization of Benzene-Limonene Mixture in Sodium Dihexyl Sulfosuccinate Microemulsion; *Submitted to Langmuir*, **2003**.
11. De Gennes, P. G.; Taupin, C. *J. Phys Chem.* **1982**, *86* (13), 2294.
12. Auvray, L. in *Micelles, Membranes, Microemulsions and monolayers* Eds. Gelbart, W. M.; Ben-Shaul, A.; Roux, D. **1994**, Springer-Verlag, New York, pp. 337-393.
13. Bellocq, A. M. pp. In *Emulsions and Emulsion Stability, Surfactant Science Series, Vol. 61*, Editor Sjoblom, J.; Marcel Dekker, New York, **1996**, 181-235.
14. Nagarajan, R.; Ruckenstein, E. *Langmuir* **2000**, *16*, 6400-6415.
15. Safran, S. A. *Statistical Thermodynamics of Surfaces, Interfaces, and Membranes*, Addison-Wesley Pub., Reading, Massachusetts, **1994**, pp. 247-253

16. Bourrel, M.; Schechter, R. S. *Microemulsions and Related Systems* Marcel Dekker, New York, **1988**.
17. Salager, J. L.; Anton, R. E. in *Handbook of Microemulsion Science and Technology*, Kumar, P.; Mittal, K. L. Eds., Marcel Dekker, New York, **1999**, pp. 247-280.
18. Nagarajan, R.; Ruckenstein, E. in *Surfactants in Solution*, Vol.2. **1984**, pp.923-947.
19. Baran, J.; Pope, G.; Wade, W. H.; Weerasooriya, V.; Yapa, A. *J. Colloid and Interface Sci.* **1994**, *168*, 67-72.
20. Biais, J., Bothorel, P., Clin, B., and Lalanne, P. *J. Dispersion Sci. Tech.* **1981**, *2* (1), 67-95.
21. Harwell, J. H. in *Transport and Remediation of Subsurface Contaminants. Colloidal, Interfacial, and Surfactant Phenomena*, ACS Symposium Series, 491. Sabatini, D. A.; Knox, R. C. Editors, Washington, D.C., American Chemical Society, **1991**, pp. 124-132.
22. Rouse, J. D.; Sabatini, D. A.; Deeds, N. E.; Brow, R. E. *Environ. Sci. Technol.* **1995**, *29* (10), 2484-2489.
23. Kunieda, H.; Horii, M.; Koyama, M.; Sakamoto, K. *J. Colloid Int. Sci.* **2001**, *236*, 78-84.
24. Mukerjee, P.; Cardinal, J. R. *J. Phys. Chem.* **1978**, *82* (14), 1620-1627.
25. Jonsson, B.; Landgren, M.; Olofsson, G. in *Solubilization in Surfactant Aggregates*, Surfactant Science Series, Vol. 55. Christian, S.; Scamehorn, J. F. editors, Marcel Dekker, New York, **1995**, pp.115-142.
26. Danov, K. D.; Kralchevsky, P. A.; Ivanov, I. B. in *Handbook of Detergents, Part A: Properties*, Surfactant Science Series, Vol. 82, Broze, G. Editor, Marcel Dekker, New York, **1999**, pp. 303-418.
27. Lyklema, J. *Fundamentals of Colloid and Interface Science. Volume 3. Liquid-Fluid Interfaces*. Academic Press, London, **1991**.
28. Kakiuchi, T. in *Liquid Interfaces in Chemical, Biological, and Pharmaceutical Applications*, Volkov, A. G. Editor; Marcel Dekker, New York; **2001**; pp.106-122.
29. UTCHEM 9.0 A Three-dimensional Chemical Flood Simulator Volume II. Technical Documentation, Reservoir Engineering research Program, Center for Petroleum and Geosystems Engineering, The University of Texas at Austin, Austin, Texas; **2000**.

30. Sottmann, T.; Strey, R. *J. Chem. Phys.* 1997, *106* (20), 8606-8615.
31. Helfrich, W. *Z. Naturforsch.* 1973, *28c*, 693.
32. Binks, B. P.; Kelay, H.; Meunier, J. *Europhys. Lett.* 1991, *16*, 53.
33. Maugey, M.; Bellocq, A. M. *Langmuir* 1999, *15*, 8602-8608.
34. Sottmann, T. *Current Opinion in Colloid and Interface Science*, 2002, *7*, 57-65.
35. Salager, J. L.; Bourrel, M.; Schechter, R. S.; Wade, W. H. *SPE Journal*, 1979, *19*, 271-278.
36. Cash, R. L., Cayias, J. L., Fournier, L. L., McAllister, D., Schares, T., Schechter, R. S., Wade, W. H. *J. Colloid and Interface Sci.* 1977, *59*, 39.
37. Cayias, J. L., Schechter, R. S., Wade, W. H. *Soc. Pet. Eng. J.* 1976, *16*, 351.
38. Gompper, G.; Schick, M. in *Handbook of Microemulsion Science and Technology*, Kumar, P.; Mittal, K. L. Eds., Marcel Dekker, New York, 1999, pp. 59-104.
39. Salager, J. L. in *Handbook of Detergents, Part A: Properties*, Surfactant Science Series, Vol. 82, Broze, G. Editor, Marcel Dekker, New York, 1999, pp. 253-302.
40. Strey, R. *Ber. Bunsenges. Phys. Chem.* 1993, *97*, 742.
41. Kahlweit, M., Busse, G. *J. Phys. Chem. B.* 2000, *104*, 4939-4943.
42. Yamaguchi, Y., Aoki, R., Azemar, N., Solans, C., Kuneida, H. *Langmuir* 1999, *15*, 7438-7445.
43. Evans, D. F., Wennerstrom, H. In *The Colloidal Domain. Where Physics, Chemistry, and Biology meet.* 2nd Edition, Wiley-VCH, New York, 1999, pp. 543-599.
44. Perry *Chemical Engineer's Handbook*, Seventh Edition; McGraw-Hill, New York, 1997.
45. Rosen, M. J. *Surfactants and Interfacial Phenomena*, 2nd ed., Wiley, New York, 1989.

TABLES

Chapter 5

Input data	Surfactant concentration	wt %	4
	Volume of oil	ml	5
	Volume of water+surfactant	ml	5
Surfactant properties	Molecular weight ^a	g/mole	388
	CMC ^b	mole/l	0.01
	Area per surfactant molecule (a) ^c	Angstrom ²	100
	Surfactant tail parameter (L) ^c	Angstrom	10
Dodecanol properties	Density ^a	g/ml	0.82
	Molecular weight ^a	g/mole	136
	Hydrophilic length, R _a ^{d,e}	Angstrom	3
	Hydrophobic length, R _b ^{d,e}	Angstrom	15
	Langmuir parameter, K ^d	Angstrom	1.25
	Langmuir parameter, B ^d	-	0.04
Limonene properties	Density ^a	g/ml	0.842
	Molecular weight ^a	g/mole	136
	Optimum salinity ^d	w % NaCl	6.2
	Optimum characteristic length ^d	Angstrom	39

Table 1. Input data and parameters used in model calculations for dodecanol-limonene mixture

^{a)} Ref. 44, ^{b)} Ref. (45), ^{c)} Ref. (1), ^{d)} Ref. (4). ^{e)} Calculations suggested in Ref. (45).

FIGURES

Chapter 5.

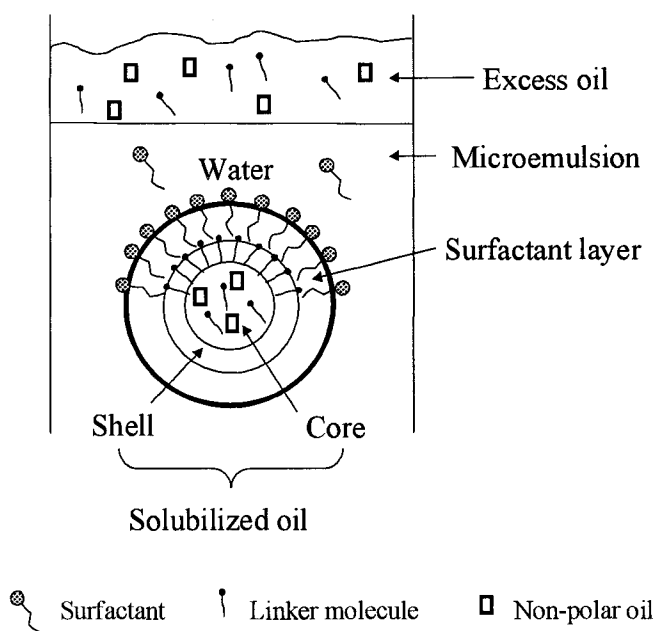


Figure 1. Schematic of the modified pseudo-phase model.

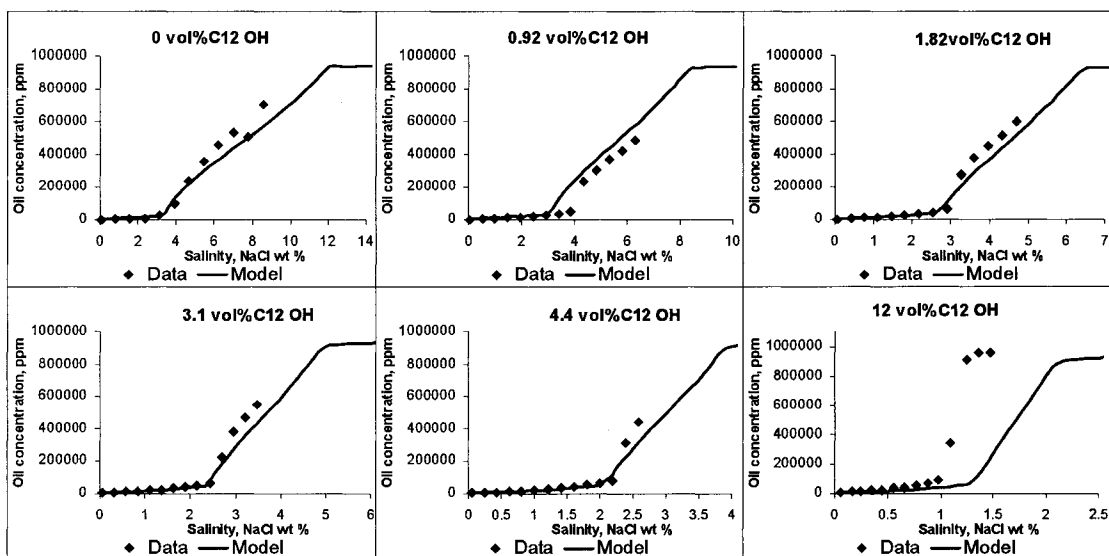


Figure 2. Dependence of the total oil solubilization on the salinity at a fixed initial dodecanol concentration. Experimental data and model predictions are plotted together for six different initial dodecanol concentrations.

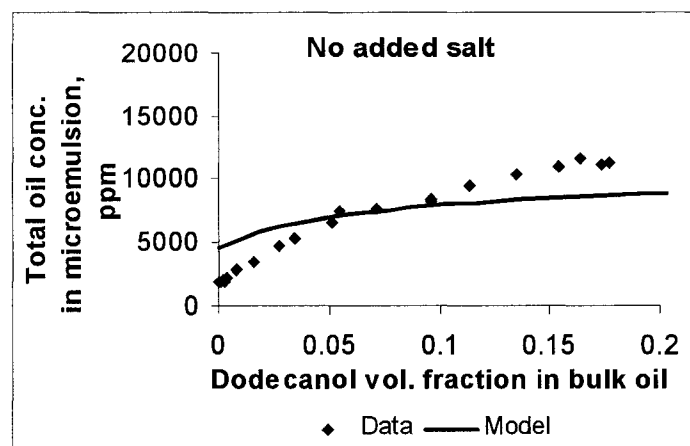


Figure 3. Dependence of the total oil solubilization on the initial dodecanol volume fraction in the oil phase at no added salt

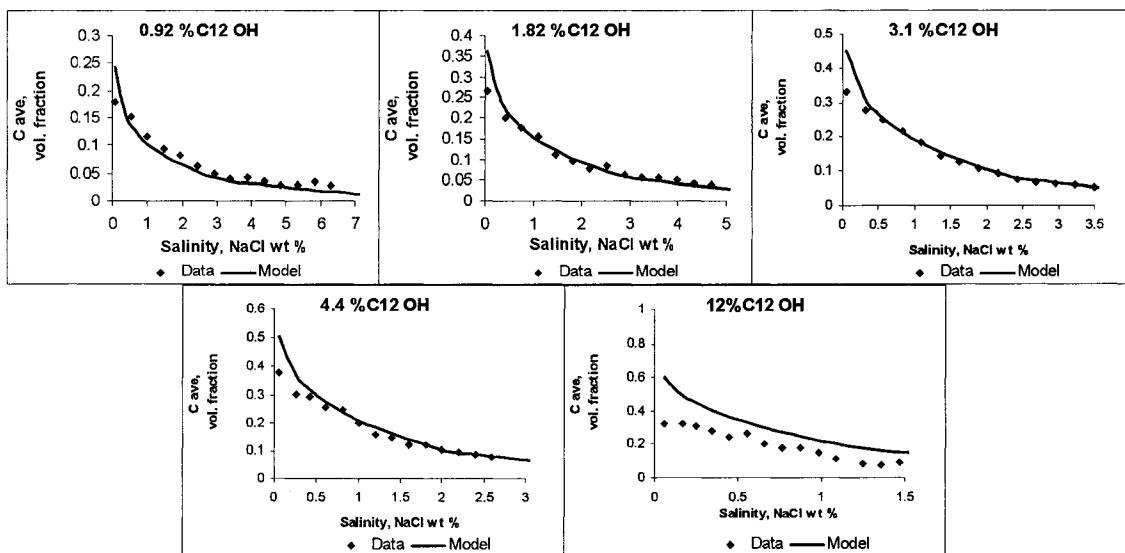


Figure 4. Average volume fraction of the dodecanol in the total solubilized oil (C_{ave}) as a function of the salinity at fixed initial dodecanol concentration. Results for five different initial dodecanol concentrations are shown.

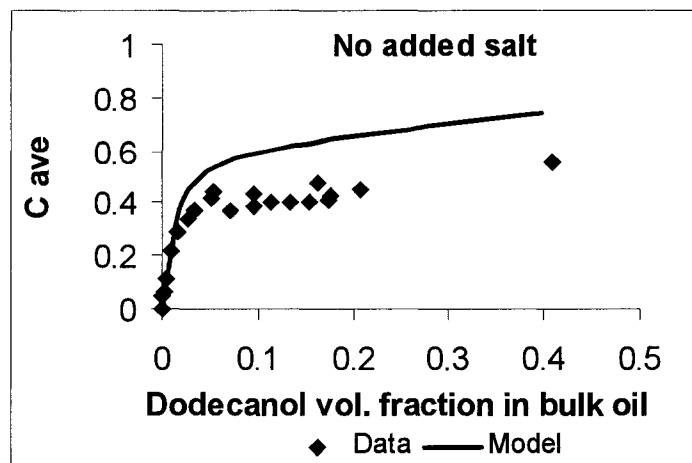


Figure 5. Average volume fraction of the dodecanol in the total solubilized oil (C_{ave}) as a function of the initial dodecanol concentration in the oil phase at no added salt.

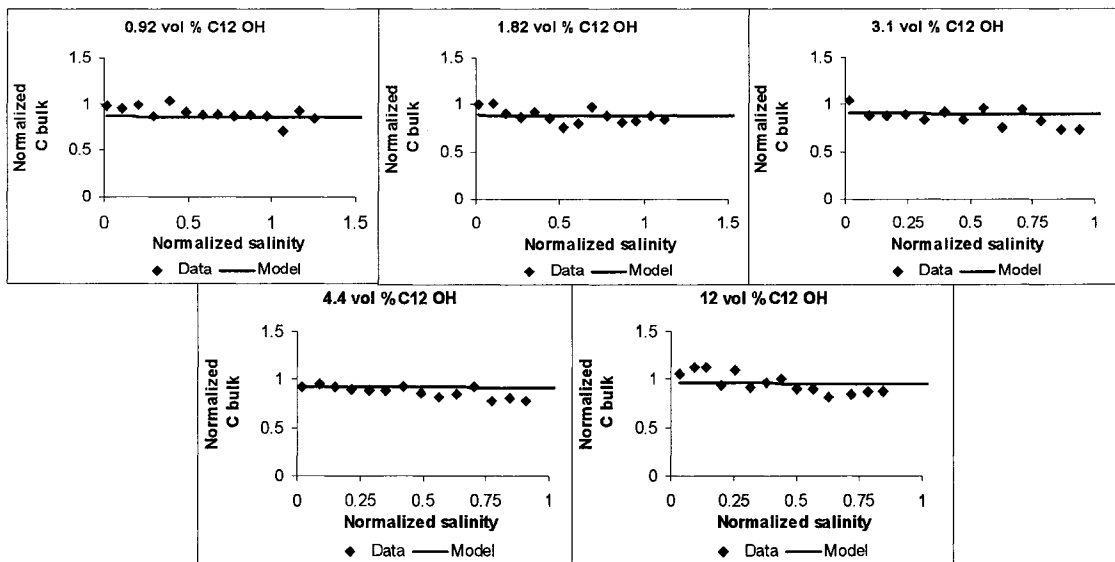


Figure 6. Variation of the excess oil phase composition (C_{bulk}) as a function of the salinity. The excess oil phase composition is plotted in normalized form, where the basis of the normalization is the initial dodecanol volume fraction in the oil phase. The salinity is normalized by the optimum salinity. Results for five different initial dodecanol concentrations are shown

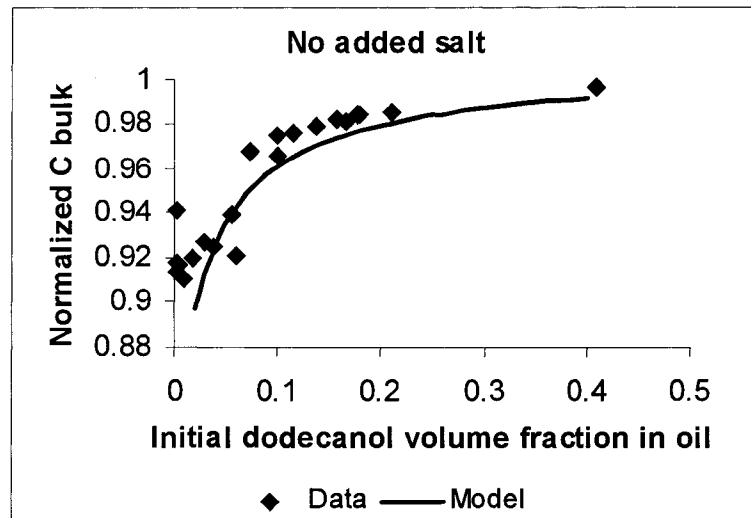


Figure 7. Variation of the excess oil phase composition (C bulk) as a function of the salinity. The excess oil phase composition is plotted in normalized form, where the basis of the normalization is the initial dodecanol volume fraction in the oil phase

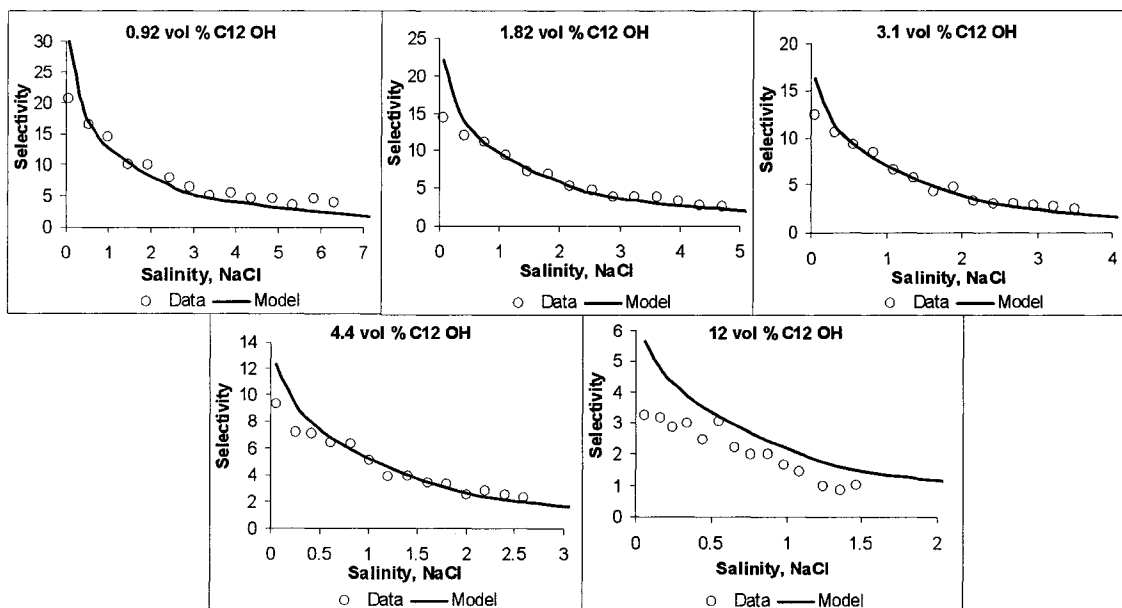


Figure 8. Variation of the selectivity as a function of the salinity at fixed initial dodecanol concentration. The salinity is expressed as NaCl wt %. Selectivity is defined as the ratio of the dodecanol concentration in the solubilized oil and the dodecanol concentration in the excess oil phase. Results for five different initial dodecanol concentrations are shown

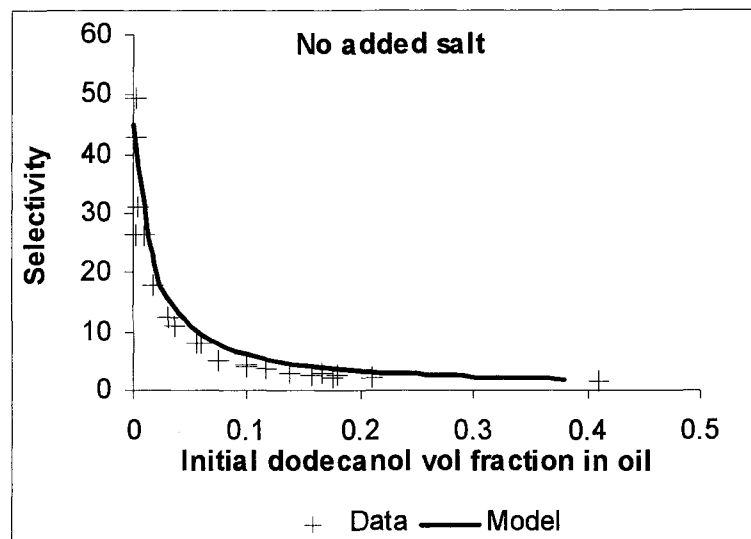


Figure 9. Variation of the selectivity as a function of the initial dodecanol concentration at no added salt. Selectivity is defined as the ratio of the dodecanol concentration in the solubilized oil and the dodecanol concentration in the excess oil phase.

CHAPTER 6

FUTURE RESEARCH

The experimental and modeling studies presented in the preceding chapters contribute to an increased understanding of oil mixture solubilization phenomena in microemulsions. Evaluating the results it is seen that future research would be beneficial in several areas. Some of these areas are discussed below.

MATHEMATICAL MODELING OF SOLUBILIZATION OF ACETONE-TCE MIXTURE

The first study evaluated the solubilization and phase behavior of sodium dihexyl sulfosuccinate microemulsion with acetone-TCE mixture. A mathematical model, however, has not been proposed, because for that more research is needed. It can be hypothesized, however, that the net-average curvature model could be applied for this type oil mixture as well, after incorporating the special effect of the acetone on the system. The current results suggest that these special effects contribute to:

- an oil solubilization decrease with increasing acetone concentration, and
- an optimum salinity, which is more-or less independent from the oil mixture composition.

These trends are different from what would be expected for a typical oil mixture of polar / non-polar oils, both components having low water solubility.

The experimental results in Chapter 2 suggested that the solubilization decrease upon acetone addition is probably due the dilution of the surfactant monolayer by acetone. This is different from the effect of benzene or dodecanol in that these compounds do not pull apart the surfactant molecules and the effective area per surfactant molecule remains essentially unchanged. In order to model the monolayer dilution effect of acetone first a relationship should be developed between the oil phase composition and the interfacial dilution in terms of the area per surfactant molecule. Then other relationships are needed which relate the area per surfactant molecule with the characteristic length at the optimum formulation and with the optimum salinity.

It is not known at this point how the polar oil (i.e., acetone) partitioning into the surfactant layer can be quantified and its dependence on the system variables and the oil composition could be mathematically formulated. This aspect requires further theoretical and experimental work. It can be hypothesized that for a polar oil component like acetone to partition between the surfactant layer, the bulk oil and the water phases in a more or less balanced way it is necessary to exhibit complete miscibility with water and the hydrophobic oil at the same time. This behavior is accompanied with no interfacial activity of acetone in the hydrophobic oil/water system. The acetone / TCE / water system satisfy this requirement as seen in Figure 1, where the IFT versus concentration relationship with no surfactant is linear, suggesting no acetone interfacial activity.

The optimum salinity and the characteristic length variation as a function of the oil phase composition has been developed for mixtures from which the polar component is enriched at the interface in Chapter 4. The equations were based on the similarity of dodecanol and adsorbing amphiphilic diblock copolymers. In the acetone-TCE system, however, acetone behaves similarly to non-adsorbing polymers rather than adsorbing diblock copolymers. Hence, it is questionable how the correlations based on polar oil adsorption could be applied for TCE-acetone mixtures. A more appropriate approach could be to link the area per surfactant molecule variations and the balanced oil/water partitioning with the characteristic length and the optimum salinity.

A possible characteristic length decrease could originate from the decreased average surfactant layer thickness as acetone inserts itself between surfactant molecules. The overall thinning of the surfactant layer (decreasing a in Eq. [1] below) can be explained due to the small molecular size of acetone. A thin surfactant layer is expected to have decreased rigidity. The DeGennes-Taupin equation predicts a decreased characteristic length in this case, which results in small oil solubilization:

$$\xi = a \cdot \exp \frac{2\pi \cdot \kappa}{k_B T} \quad [1]$$

The bending elasticity would also decrease if the overall surfactant membrane becomes thinner. These effects together reduce the characteristic length according to Eq. [1].

The optimum salinity is expected to decrease with increasing polar oil concentration as discussed in the previous chapters. The increased penetration of the polar oil between the surfactant tails results in an increased pressure on the oil side of the surfactant film, which at the optimum formulation needs to be balanced by an increased pressure on the water side. The increased pressure requirement is fulfilled at lower

electrolyte concentration, where the electrical double layer repulsion is greater. Hence the optimum salinity is lowered.

This trend applies only when the adsorption of the oil molecules results in an increased “effective” surfactant layer thickness at the interface. In this case the area per surfactant molecule remains constant. For the acetone-TCE mixture, however, the effective layer thickness, and the pressure on the oil and water sides decreases rather than increase due to the dilution of the surfactant film. Hence the optimum salinity model based on polar oil adsorption is questionable.

The water side effects of adsorbing diblock copolymers are considered mainly due to steric effects. In anionic surfactant systems, when the polar oil appears on the water side, electric interactions in the head group region also need to be considered. When the oil is hydrophobic enough it would not modify the electric repulsion between the surfactant head groups, because it remains essentially on the oil side. In contrast, acetone appears on the water side, and is expected to modify the effective head group repulsion depending on its concentration. This again complicates the application of adsorption based optimum salinity models to the acetone-TCE mixture.

In conclusion, it is expected that a significant acetone “surface excess” does not appear at the oil/water interface in the acetone-TCE system. Instead of the surface excess adsorption some other quantities must be found that dictate the characteristic length and the optimum salinity variation for developing oil solubilization model.

CONNECTION BETWEEN THE DIFFERENT OPTIMUM SALINITY AND CHARACTERISTIC LENGTH MODELS USED FOR BENZENE-LIMONENE AND FOR DODECANOL-LIMONENE MIXTURES

The second and third systems containing limonene-benzene and limonene-dodecanol mixtures, respectively, could be both modeled using the net-average curvature model combined with the surface excess adsorption model. The optimum salinity and characteristic length model equations used for the two mixtures, however, were not the same. For the benzene-limonene mixture a simple linear mixing rules were applied. For the dodecanol-limonene system new models were developed based on the experimental observation that the bending rigidity and the curvature of the surfactant film is affected by the polar oil penetration into the palisade layer.

It is interesting to see if the models based on the polar oil surface excess adsorption could also be extended for the benzene-limonene system. First we checked if the linear relationship between the bending rigidity and the shell thickness (i.e., benzene volumetric surface excess) is valid for the benzene-limonene mixture. Figure 2 demonstrates that the linearity seems to apply. Next the optimum salinity and the characteristic length as a function of the oil phase composition are calculated using the surface excess based models as described in Chapter 4 for the dodecanol-limonene system. In order to get good fit between data and model predictions using Langmuir parameters $K = 0.94$ Angstroms and $B = 0.35$ the molecular size of the benzene needs to be fitted. With hydrophilic segment size $R_a = 2$ Angstrom and hydrophobic segment size $R_b = 13$ Angstroms a good fit between data and the model is reached. Figure 3

shows the characteristic length data and model predictions versus oil phase composition with these parameters.

Figure 4 shows the experimental and model predicted optimum salinity as a function of oil phase composition. The characteristic length model captures the slight non-linearity that is visible in the data points. The linear mixing rule based model does not follow this trend. The optimum salinity predictions are just as good with the linear mixing rule model as with this model. We can conclude that the surface excess adsorption based models work well, if the molecular sizes that are obtained by the fitting are reasonable. The segment sizes seem somewhat large, and it is also questionable whether assigning two different segments in one molecule of benzene is realistic. Benzene does not have a linear molecular structure, for which the above models were developed, which may be a reason of the large molecular sizes. To decide about these questions more studies are needed, evaluating and comparing different types of oil mixtures.

It is likely, that the linear mixing rules used in Chapter 3 to model the solubilization of benzene-limonene mixture provided a good fit with the data, because benzene surface excess adsorption is not large. On the other hand, the models based on the polar oil surface excess adsorption predict the same linear mixing behavior because the benzene surface excess adsorption is small.

DEPENDENCE OF THE SHELL THICKNESS ON THE ELECTROLYTE CONCENTRATION

In the net-average curvature model as applied for the benzene-limonene and the dodecanol-limonene mixtures it was assumed that the shell thickness (i.e., polar oil surface excess) is independent from the electrolyte concentration. However, when the shell thickness was calculated from the solubilization data it showed a slight but consistent dependence on the salinity for a fixed oil phase initial composition for both oil mixtures at low electrolyte concentrations. The dependence was more pronounced for the dodecanol than for the benzene containing mixtures. Typically the shell thicknesses were increasing with increasing salinity and decreasing curvature. The origin of this behavior needs to be investigated, which could further improve the solubilization model at low salinity.

Reduced shell thickness at low salinity could be related to configuration constraints due to very small droplet sizes, simplifying the adsorption phenomena by using a Langmuir isotherm, neglecting a decreased salting out effect, or the origin could simply be the method of calculating the shell thickness from the solubilization data.

Recent preliminary SANS data suggests that the assumption of constant area per surfactant molecule is not strictly satisfied when the electrolyte concentration is increased. It has been found that the area per molecule is largest at the optimum formulation and smaller at low salinity which yield slightly smaller interfacial area at low salinity than at optimum. In the solubilization model the area per surfactant molecule is assumed to be constant when the salinity varies. When evaluating the shell thickness values from the solubilization data, the area per molecule was also taken constant. This

could cause the experimental shell thickness to appear smaller than it really is because the volume of the excess polar oil is divided by an overestimated area to compute the shell thickness.

The net-average curvature model predictions are also affected by using a constant area per surfactant molecule instead of allowing for variations with salinity. Future studies are needed to examine this aspect in more detail, and whether the model could be improved to provide better predictions at low salinity if area per surfactant molecule variation is allowed.

ADSORPTION ISOTHERMS

The use of a realistic adsorption isotherm is an important element of the solubilization model for oil mixtures. In the current model formulation of the adsorption isotherm needs to be determined experimentally for each system. We expect that the isotherm changes depending on the oil components, the surfactant type temperature, etc. Therefore, applying the solubilization model requires considerable experimental work.

In future research it would be interesting to study what kinds of adsorption isotherms apply to systems with different oil components, and surfactants. Even though the adsorption isotherm is treated in an empirical manner in the present research, it has thermodynamic basis. For example, the Langmuir isotherm parameters are related to the enthalpy of adsorption and the maximum possible monolayer adsorption. These parameters might be calculated using thermodynamic properties without doing experiments, which would make using the solubilization model more convenient.

Another interesting area would be to study whether the real concentration distribution within the solubilized oil domain could be obtained from the adsorption isotherm. In such applications, where it is important to know the actual interfacial composition, this model improvement would be very advantageous.

RELATIONSHIP BETWEEN THE OPTIMUM SALINITY AND THE CHARACTERISTIC LENGTH AT OPTIMUM

The shell thickness is defined as the polar oil excess solubilized in the microemulsion in terms of volume per unit interfacial area. The shell thickness is different from the usual surface excess quantities in that the surface excess is defined on the volume instead of the molar basis. The use of volumes instead of moles was chosen because the solubilization model was developed with a next future plan in mind: to incorporate it into a multiphase porous media flow model, and use it for designing surfactant enhanced subsurface remediation. Porous media flow models are frequently formulated in terms of volume, thus it seemed convenient to develop a volume-based solubilization model. This explains why the volume-based definition is retained for convenient future model compatibility.

The use of volume turned out to be interesting from another point of view. It is apparent that for both the dodecanol-limonene and the benzene-limonene system the characteristic length increases, and the optimum salinity decreases as the shell thickness increases as shown in Figure 5 and Figure 6, respectively. It appears that for these two systems it does not matter, what is the polar oil. The important parameter that determines

the characteristic length and the optimum salinity is the shell thickness. Figure 5 and Figure 6 demonstrates that the characteristic length and the optimum salinity as a function of the shell thickness, respectively, fall on the same line for both systems. It is a quite interesting result especially considering the significant difference between benzene and dodecanol in their chemical structure, polarity, and molecular weight, and amphiphilicity. Future research should address the question whether this kind of behavior is of general validity, and might be exhibited by other oils too.

As a consequence the above observation the optimum salinity and the characteristic length are not independent from one another for a given surfactant. The optimum salinity vs. characteristic length relationship does not depend on the type of oils in the microemulsion formed with a given surfactant. We demonstrate this in Figure 7, by plotting the characteristic length – optimum salinity pairs for a series of different oils, all with the same surfactant. The oils include single component oils and binary oil mixtures. Figure 7 suggests that if one knows for example the optimum salinity with a certain type of oil, the characteristic length can be calculated using the general optimum salinity-characteristic length relationship which is characteristic for the surfactant.

The shell thickness may turn out to be a useful parameter in characterizing the influence of specific oil on the microemulsion system. So far the most practical parameter characterizing the oil has been the EACN (equivalent alkane carbon number). Its value in formulating microemulsions has been proven over many years. However, for oil mixtures with components that are different in polarity, the EACN concept does not apply well, as demonstrated in Chapter 4. In contrast, the shell thickness parameter seems to work well not only for pure oils, but even for polar/non-polar oil mixtures as well.

The question arises how can we obtain the shell thickness parameter for a single component oil? Pure oils produce no composition difference within the solubilized oil, and the shell thickness loses its physical meaning, and cannot be directly obtained from solubilization studies. However, pure oils can penetrate into the palisade layer to varying degree depending on their polarity/molecular size, etc. A hypothetical shell thickness value for pure oils could be obtained from its mixtures with a hydrophobic oil, which is expected to not penetrate significantly the palisade layer. Then the shell thickness of the pure polar oil can be inferred from an adsorption isotherm through extrapolation to 100 % polar oil. Using this method, for example, the shell thickness of pure benzene is estimated about 0.7 Angstroms. This value could be treated as a measure of the oil effect on the microemulsion properties.

The extrapolated pure “shell thickness” values obtained this way may also be used in the net-average model to estimate the “palisade layer radius” (Acosta et al. *Langmuir*, 2003, 19 (1), 186-195). The palisade layer radius is the difference between the equivalent oil droplet radius that corresponds to the oil solubilized in the core plus and in the palisade layer and the equivalent oil droplet radius accounting only for the core solubilization. In order to predict interfacial tension values the core and the palisade layer radii need to be known.

It is also a question how the type of the hydrophobic oil affects the adsorption isotherm and the shell thickness values when one wants to determine the pure component shell thickness parameter. In order to get a meaningful shell thickness parameter for pure oils it is important, that the hydrophobic oil has very small penetration between the surfactant tails. The system with this kind of oil could be used as a reference system,

providing a “zero” shell thickness. A small shell thickness was inferred for limonene in sodium dihexyl sulfosuccinate microemulsion. This assumption was based on the negligible deviation between the experimental and model predicted IFT values, when the predicted IFT was calculated using only the oil core radius (Acosta et al. *Langmuir*, 2003, 19 (1), 186-195).

Preliminary results indicate that the surface excess adsorption is stronger when there is a greater polarity difference between the oil components. Dodecanol surface excess as a function of bulk oil phase composition is presented in Figure 8 for dodecanol-TCE, dodecanol-PCE, and dodecanol-limonene mixtures. We see decreasing adsorption of dodecanol when the hydrophobic oil is changed in the order limonene → PCE → TCE. Note that limonene is more hydrophobic than PCE, and PCE is more hydrophobic than TCE. This result suggests that limonene is the best candidate in the group of limonene, PCE, TCE, benzene, dodecanol to use as reference “zero” shell thickness. The other implication of this result is that the polar oil produces greater synergistic effect on the solubilization if the other oil component is more hydrophobic.

The result in Figure 8 is not surprising, because one driving force for the polar oil to approach the water/oil interface is to reduce the contact between the water and the hydrophobic components in the system, thereby reducing the interfacial energy. It has been found in spectroscopic studies (Hunter, R. J. *Introduction to Modern Colloid Science*; Oxford University Press, 1994) that even unfavorable water/hydrophobic oil contact occurs for certain time duration at the oil/water interface. Not only surfactant tail/water contact, but also hydrophobic oil / water contact was shown to occur. On a statistical basis, however, these contacts last much shorter time than the more favorable

polar oil/water contact at the interface. Consequently, it is likely that the more hydrophobic the oil component, the less time it spends in contact with the water if polar oils are also present in the mixture. Hence, we can expect that the polar oil adsorption be enhanced in the presence of a more hydrophobic oil.

MIXTURES OF TWO PALISADE LAYER PENETRATING OILS

Using the dodecanol-limonene and the benzene-limonene mixtures we studied oil mixtures, with one, essentially non-penetrating oil (limonene), and another, penetrating oil (benzene or dodecanol). When using the term “penetrating” we mean the tendency for the oil molecules to be solubilized in between the tails of the surfactant, in the palisade layer. On non-penetrating oil we mean the type of oils, that are solubilized in the hydrophobic core of the oil swollen surfactant aggregate, but not between the surfactant tails. Non-penetrating oils spend very little time in the palisade layer. Because limonene is assumed to be a non-penetrating oil, there was no need to develop a mixing rule for the palisade layer. The palisade layer was filled with the polar oil only.

Oil mixtures with components, which each have some tendency to penetrate the palisade layer, have not been studied. It would be interesting to see how the solubilization model can be applied for these oils. For these oils some sort of mixing rule needs to be developed for the palisade layer. This mixing rule would take into account that a portion of the palisade layer is filled with an oil mixture of bulk composition, and only the other portion of the palisade layer solubilization is due to surface excess of the more polar oil.

The hypothetical pure component shell thickness parameters would be necessary in developing these mixing rules.

These kinds of studies may help explain why synergism occurs in some oil mixtures and why not in other mixtures. It might also be possible to explain why the lipophilic linkers are not as effective in increasing the solubilization of polar oils as hydrophobic oils. The solubilization boosting effect of the lipophilic linker is related to its excess solubilization. If the linker has reduced surface-active behavior because the other oil component is rather polar its solubilization boosting is reduced. Therefore, a certain polarity difference is needed between the oil and the linker in such a way, that the linker is more hydrophilic than the other oil. If the linker becomes too hydrophobic, its solubilization enhancing effect again decreases.

SELECTIVE SOLUBILIZATION – COLUMN STUDIES

Finally, future research should apply the solubilization model under flow conditions. Preliminary experiments demonstrate that selective solubilization may occur not only in equilibrium, but also under flow conditions. Figure 9 presents breakthrough curves obtained from a column study, in which the column was contaminated with a benzene-limonene oil mixture containing 0.1 volume fraction benzene. The column was subsequently flushed with 4 wt % aqueous sodium dihexyl sulfosuccinate solution with no added NaCl. The conditions of the experiment are shown in Appendix I. The organic removal mechanism was primarily solubilization. Very small mobilization occurred in three points at the maximum of the breakthrough curve. The concentration of benzene

and limonene measured in the effluent is plotted as a function of pore volume. The concentration of benzene and limonene increases after flushing the column with one pore volume. After one pore volume there is a small peak on both benzene and limonene breakthrough curves. This might be attributed to the observed small mobilization or local benzene enrichment at the oil/water interface. After this regime, the concentration of benzene and limonene seems to reach a constant level. This indicates that probably steady state has been reached, and the oil pool behaved more-or-less as a constant contamination source.

Figure 10 shows the benzene selectivity as a function of the pore volume. The selectivity values are between 2.5 and 1.5, averaging around 2. These experiments demonstrate that some selectivity occurs in flow systems even with the benzene-limonene mixture, which contain components that are not very different from each other. The selectivity is somewhat lower under flow conditions than at equilibrium. Certain selectivity decrease could be due to evaporation losses occurred before the samples were analyzed. The selectivity under equilibrium conditions would be about 3.

We may hypothesize that the high initial selectivity seen in Figure 10 results from the initial benzene enrichment at the surface of the oil pool, which is in contact with the flushing phase. It is also apparent from the high solubilization of limonene after the first pore volume, that the rate limiting step is the transfer of the oil molecules from the oil phase into the surfactant micelles at the macroscopic oil/water interface rather than by diffusion of the single oil molecules from the oil /water interface to the micelles which are distributed throughout the aqueous phase. If diffusion of the oil molecules across the water were the rate-limiting step, limonene concentration would be much less than

benzene in the flushing solution, because the water solubility for limonene is much less than for benzene.

If the oil/water interface is locally enriched in benzene, the micelles may solubilize more benzene. This would yield higher selectivity values because of the method selectivity is computed. To explain this, let's first consider what happens when the empty micelle solubilizes the oil mixture at the macroscopic interface. The interface which interacts with the adsorbing micelles has relatively high overall benzene concentration. The oil/water IFT measured without surfactant as a function of benzene concentration depicted in Figure 11 seems to support this idea. The IFT variation is non-linear suggesting that benzene is slightly enriched at the oil/water interface. The high local benzene concentration determines the overall oil composition solubilized by the micelles, which will be rich in benzene. Even its core benzene composition is likely higher than the bulk composition of the oil pool far away from the interface. The selectivity, computed as the ratio of the benzene concentration in the solubilized oil and the benzene concentration in the oil mixture that was used to contaminate the column, will also appear higher initially because the solubilized overall oil is rich in benzene, and the bulk benzene concentration used to compute the selectivity is lower than that in the micellar core.

After the flow/concentration conditions reach steady state, the interfacial benzene concentration may drop because of developing a benzene supply / removal balance at the interface. This would decrease the selectivity.

Figure 12 shows how to what degree the micelles became saturated with the oil molecules during the flush. To compute the micellar saturation we normalized the

benzene and limonene concentration measured under flow condition with the respective concentrations under equilibrium conditions. The micellar saturation by benzene and limonene are plotted as a function of pore volume. Figure 12 shows, that the micelles do not become saturated. This is expected, and other researchers also found similar behavior. In general the saturation level reached is expected to depend on the flow conditions, and the column length. If the column is too short, and/or the flow rate is too low, there is not enough time for the oil mass transfer between the phases. Our results indicate that the flow was too fast compared to the oil mass transfer, and only a fraction of the equilibrium solubilization capacity of the surfactant was used.

Interestingly, the limonene saturation was relatively higher than the benzene saturation. While the reason of this result is not known, it must be noted, that evaporation loss was found more severe for benzene than for limonene during the solubilization experiments. The low dynamic selectivity may also be related to the unsaturated micellar conditions. For unsaturated microemulsions not only the thermodynamics of the surfactant membrane but also the availability of the oil components play an important role. In that case not all of the oil is available to attain the interfacial curvature dictated by the energetic of the surfactant film. Hence, the aggregates become more strongly curved, than in a saturated system. As a result, the free energy of the aggregates could be reduced more if the system becomes more similar to the saturated system. This might be best accommodated if the core solubilization is increased on the expense of the palisade layer solubilization because the tail region is too crowded to allow additional oil uptake between them. This results in a selectivity that is lower than the equilibrium value. A

solubilization model applicable for unsaturated microemulsion systems would have to consider these effects in detail.

It is concluded, that selective solubilization occurs under flow conditions just like in equilibrium systems, even with slight polarity difference between the oil components. In order to model the selectivity accurately, the current solubilization model needs to be modified to account for the interfacial mass transfer limitations, and unsaturated microemulsion conditions.

FIGURES

Chapter 6

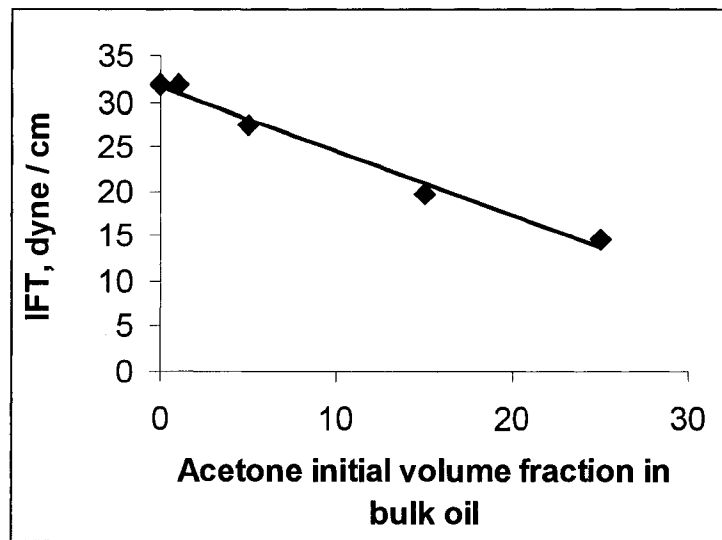


Figure 1. Interfacial tension measured between water and TCE/acetone oil mixture as a function of the initial acetone concentration in the bulk oil.

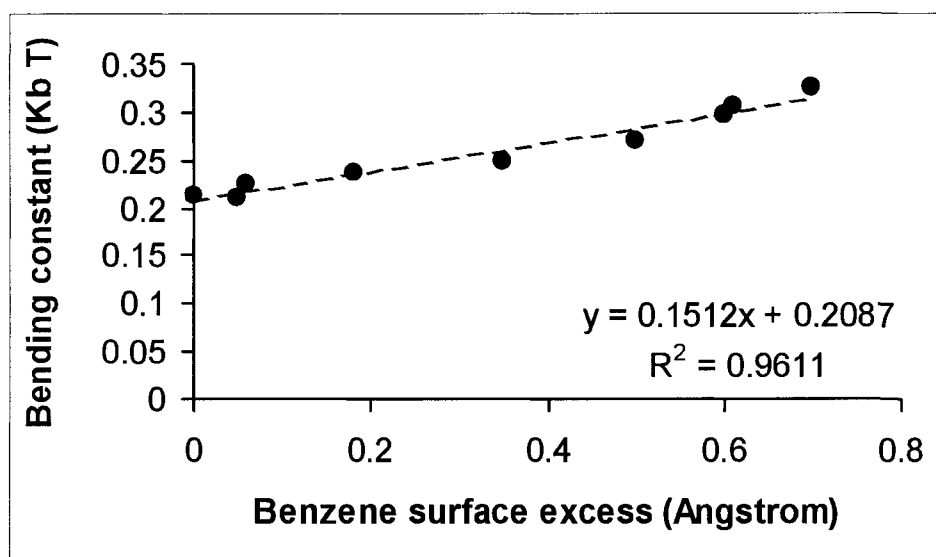


Figure 2. Bending elasticity constant versus benzene volumetric surface excess.

Bending elasticity constants are estimated from experimental middle phase volumes and surfactant concentration from the benzene-limonene solubilization experiments. The benzene surface excess in the solubilized oil is calculated from solubilization data as described in Appendix A.

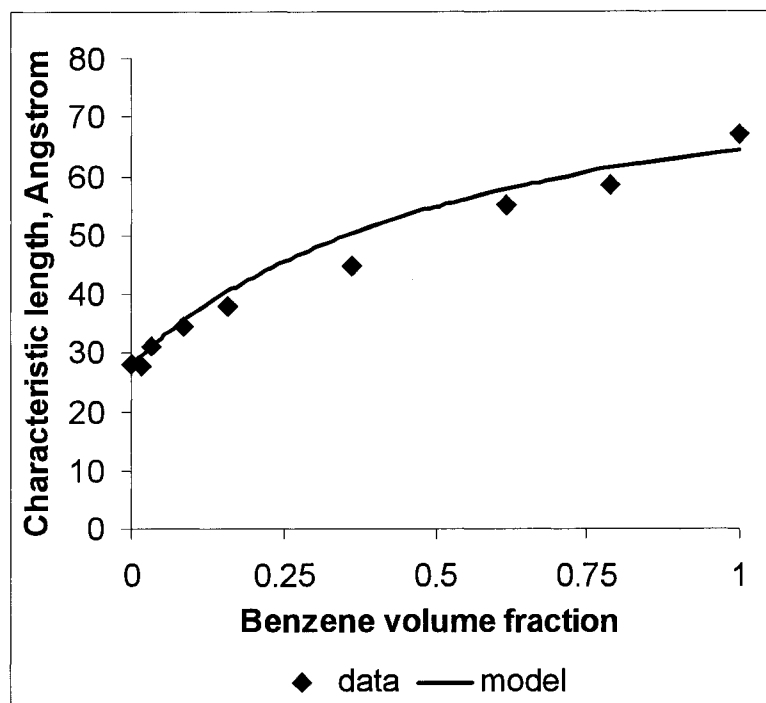


Figure 3. Characteristic length for the benzene-limonene mixture as a function of benzene concentration in the bulk oil.

Data points are estimated from middle phase solubilization results. The model predicted values are calculated using the surface excess adsorption based model for the characteristic length instead of the linear mixing rule introduced in Chapter 4.

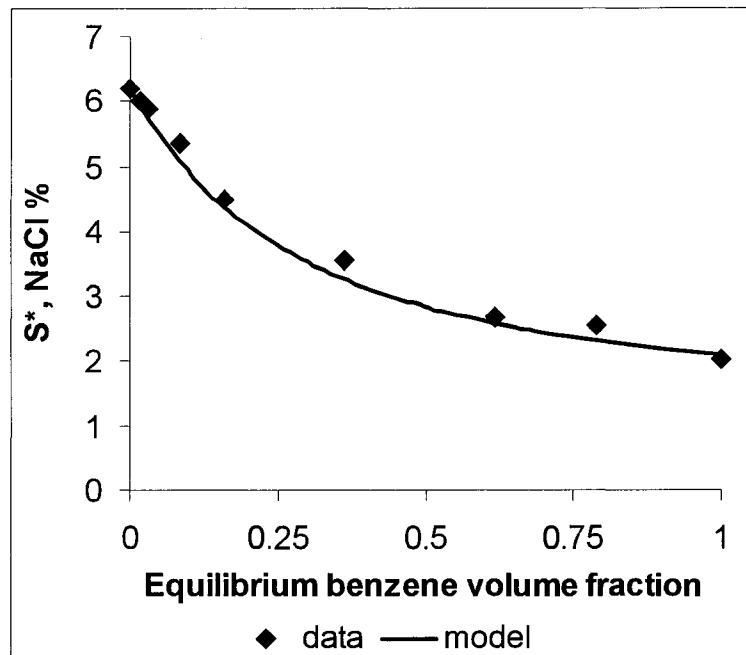


Figure 4. Optimum salinity for benzene-limonene mixtures as a function of benzene concentration of the bulk oil mixture.

Data points are experimentally obtained from salinity scans, and Model predictions are based on the surface excess adsorption model for the optimum salinity instead of the linear mixing rule used in Chapter 4.

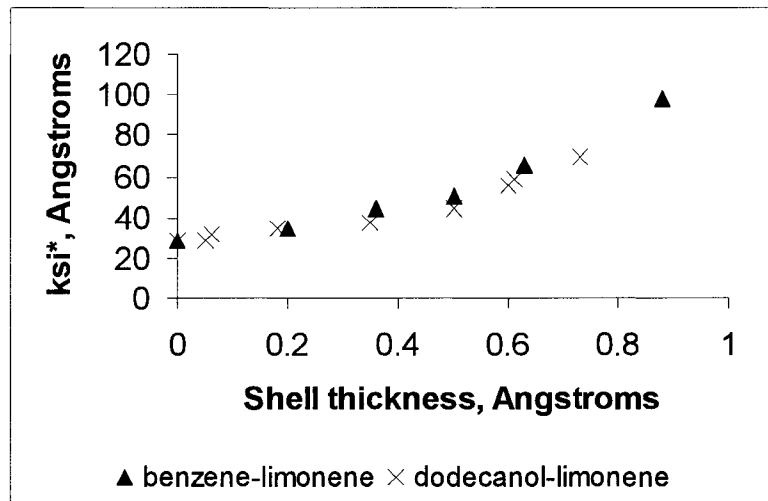


Figure 5. Experimental characteristic length at optimum as a function of shell thickness for the benzene-limonene and the dodecanol-limonene mixture.

Data points for both mixtures seem to fall on the same curve.

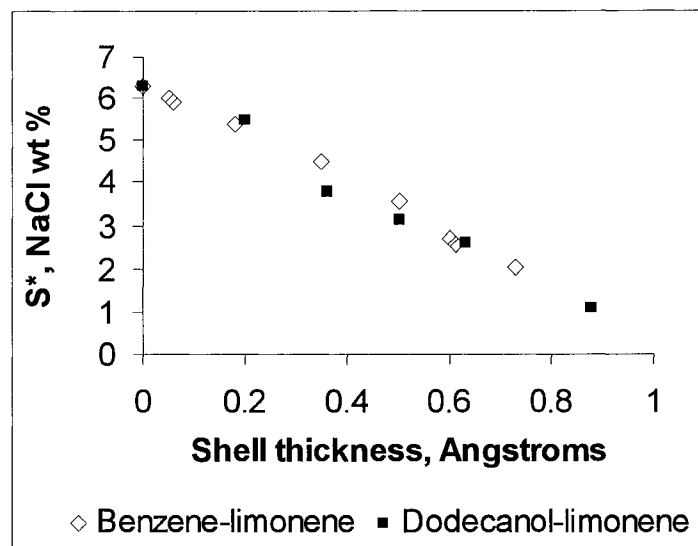


Figure 6. Experimental optimum salinity as a function of shell thickness for the benzene-limonene and the dodecanol-limonene mixtures.

Data points seem to fall on the same line.

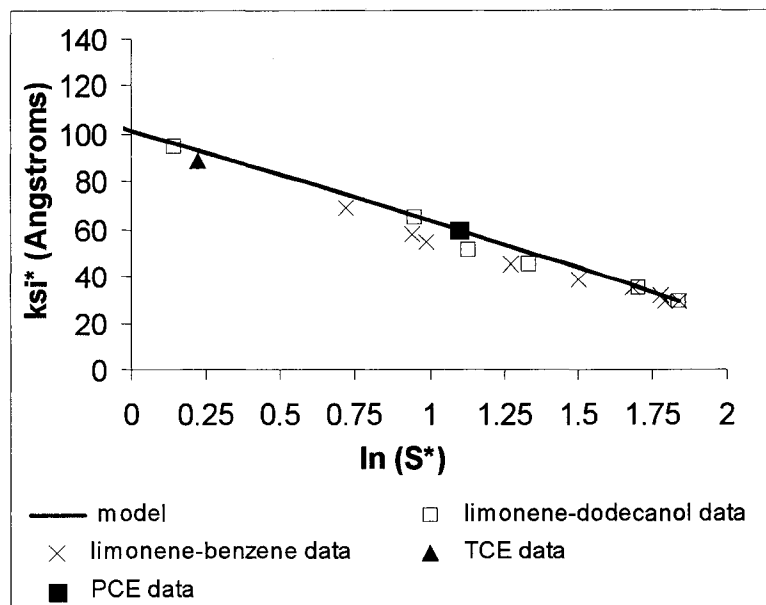


Figure 7. Experimental and model predicted characteristic length at optimum versus optimum salinity for a variety of oil phases.

Model characteristic length at optimum and model optimum salinity value pairs are calculated using the polar oil surface excess adsorption models for the benzene-limonene and dodecanol-limonene mixtures as described in Chapter 4.

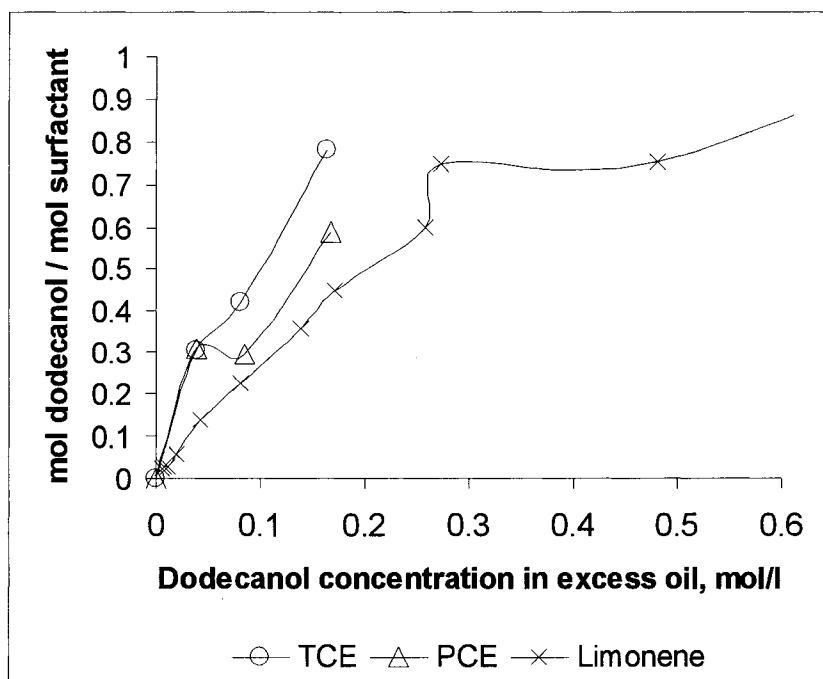


Figure 8. Dodecanol surface excess per mole of surfactant in the middle phase at the optimum formulation as a function of the dodecanol concentration in the excess oil phase. Experimental data of the TCE-dodecanol, the PCE-dodecanol, and the limonene-dodecanol mixtures are shown.

The lines connecting the corresponding data points are included only to guide the eye.

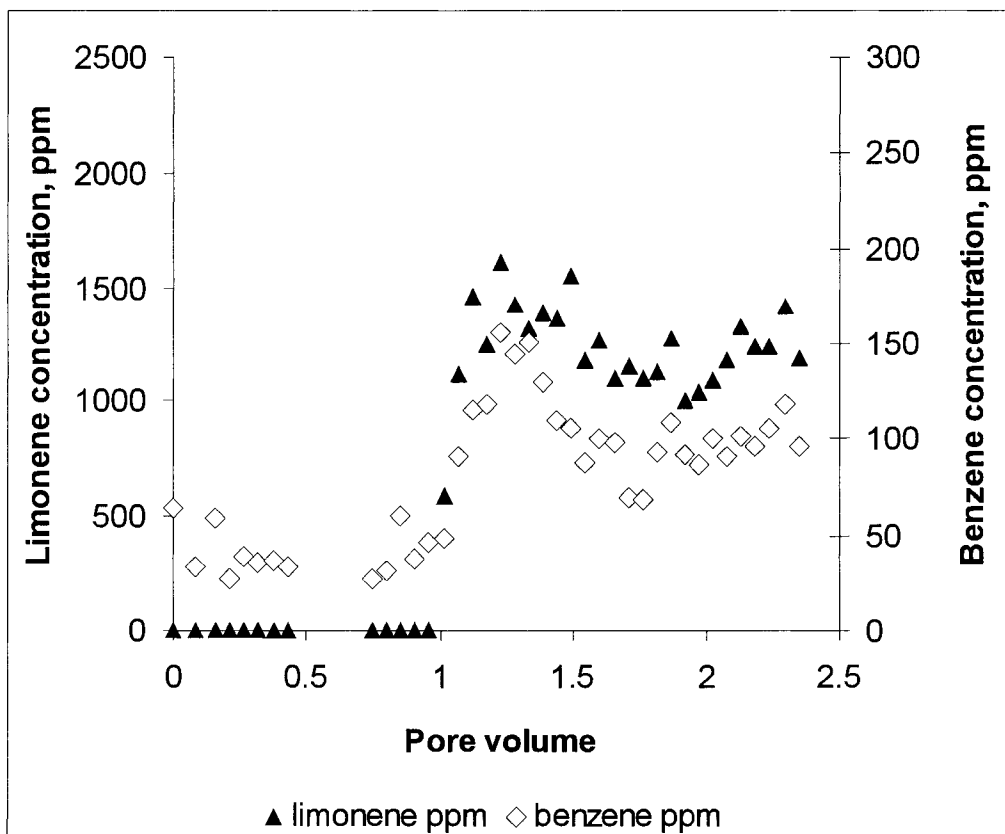


Figure 9. Limonene and benzene breakthrough curves as a function of flushed pore volume.

Organic concentrations are measured after 24 hours of the column experiment, hence evaporation losses likely reduced the original concentration values.

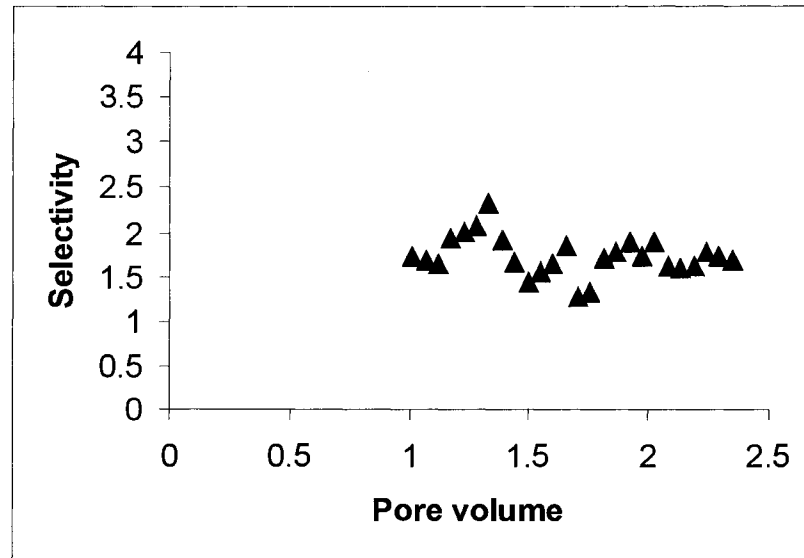


Figure 10. Variation of the experimental benzene selectivity as a function of flushed pore volume.

The selectivity is defined as the ratio of the benzene volume fraction in the solubilized oil and the benzene volume fraction in the initial oil contamination in the column.

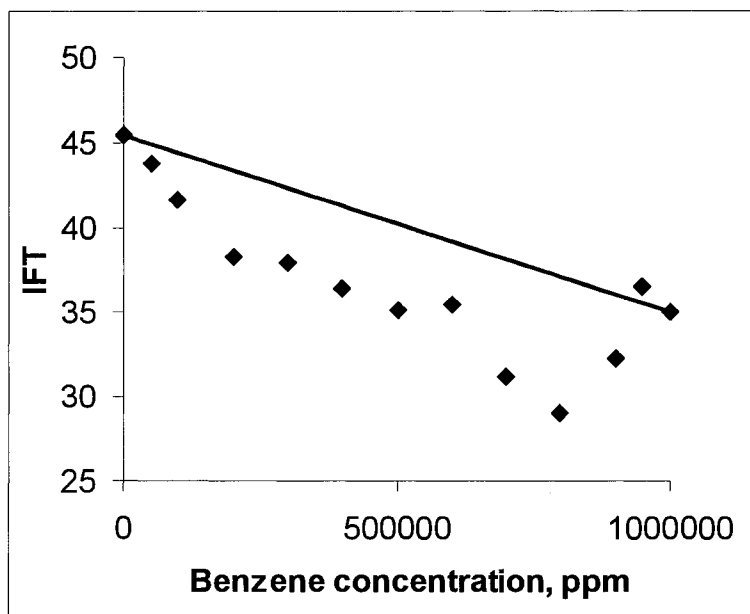


Figure 11. Interfacial tension between oil and water measured with benzene/limonene mixture as a function of benzene concentration in the bulk oil.

The linear line correspond to an IFT variation if benzene and limonene would exhibit ideal mixing in the bulk and at the oil/water interface.

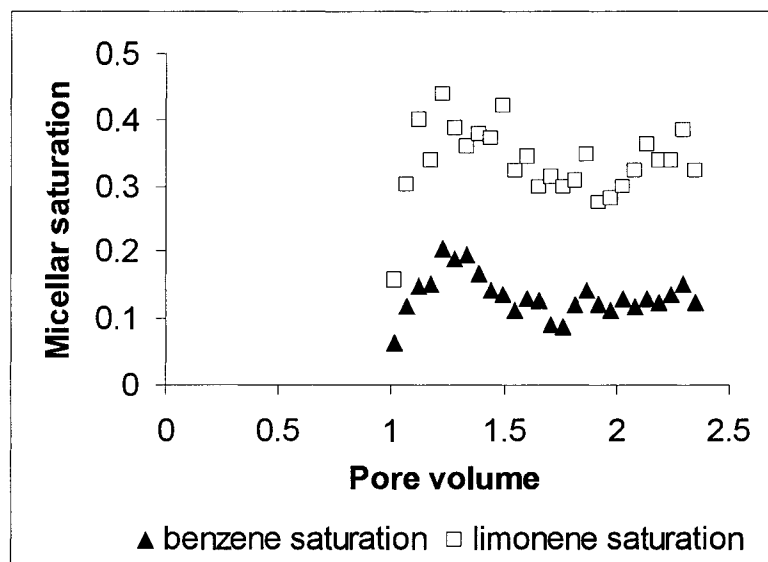


Figure 12. Degree of benzene and limonene saturation of the micelles as a function of flushed pore volume.

To compute the degree of micellar benzene and limonene saturation the experimentally measured benzene and limonene solubilization data were normalized by the equilibrium benzene and limonene solubilization measured for the initial oil mixture that was used to contaminate the column.

CHAPTER 7

CONCLUSIONS

The experimental and modeling studies presented contribute to an increased understanding of oil mixture solubilization phenomena, important in SEAR processes. The objective set forth was to study “non-ideal” oil mixtures of polar and non-polar oil components with respect to the relationship between the microemulsion properties and the oil phase composition. A new mathematical model has been proposed for the solubilization of studied binary oil mixtures based on study results. The new models are formulated in a way that allows for incorporation into a multi-component multi-phase flow model. Three different binary oil mixtures were evaluated in which the nature of the polar oil was varied from slightly polar, to strongly polar, and amphiphilic.

The first study evaluated mixtures of a hydrophobic and a strongly polar oil component, the polar oil being completely miscible in both water and the hydrophobic oil. The effect of such polar oil on the microemulsion was evaluated using the water / acetone – TCE mixture / sodium dihexyl sulfosuccinate system. It was found that the conditions required for the optimum formulation were essentially independent from the acetone concentration. In contrast, the oil solubilization ability of the surfactant decreased as the acetone concentration increased. Solubilization experiments and interfacial tension studies were used to help explain this behavior. It was shown that the area per surfactant molecule increases, especially at higher acetone concentration, when the acetone

concentration increases. This was attributed to acetone partitioning into the surfactant layer, pushing away the surfactant molecules from one another. The weak “cosurfactant” acetone in the surfactant layer provides poor interaction with the oil and the water because of its small hydrophobic “chain” and hydrophilic “head” size, reducing the overall solubilization ability of the mixed surfactant layer. Acetone was shown to have essentially balanced partitioning between the oil and the water, with and without surfactant. The balanced partitioning indicates that acetone as a cosurfactant is “optimized” in this system, having equal preference for both oil and water. As a result the optimum salinity does not change with changing acetone concentration.

The above behavior has implications for SEAR design. If the organic pollutant contains a lot of component behaving similar to acetone in this system, at the beginning of SEAR simple fresh water flush seems appropriate. During the fresh water flush the polar component solubilization is high but the hydrophobic contaminant removal is low. Surfactant flush can start when the polar oil component concentration decreased enough so that the polar oil doesn't interfere with the microemulsion solubilization. The surfactant flush is able to increase the removal of the hydrophobic oil component at this point. In a particular system that is similar to the system of this study, there is no need to adjust the electrolyte concentration as the removal process progresses. Evaluating the contaminant mixtures from this standpoint may help increase overall contaminant removal efficiency, and reduce remediation time and cost of surfactant.

The second study addressed oil mixture solubilization with only small polarity difference, with both oil components having low water solubility. The model system was

the saturated microemulsion of water / limonene-benzene / sodium dihexyl sulfosuccinate. In the oil mixture benzene is the more polar component, its slightly polar nature is due to its delocalized aromatic π - electrons. It was demonstrated that benzene is selectively solubilized in the microemulsion. The selectivity decreased with increasing salinity and/or benzene concentration. Based on this result it was hypothesized that the solubilization has contributions from the hydrophobic core and from the interfacial layer. The concentration of benzene is lowest in the center of the core, and highest at the interfacial layer. With increasing salinity and benzene concentration the core contribution becomes more dominant and the selectivity decreases.

A mathematical model has been proposed, which used the experimental solubilization results. The core solubilization contribution is modeled using the net-average curvature model. The interfacial layer solubilization is conceptualized as surface excess of the polar oil, and modeled with a Langmuirian adsorption isotherm. The model provided excellent solubilization predictions for the oil solubilization, selectivity, and the solubilized oil composition.

The third model system was water / limonene-dodecanol mixture / sodium dihexyl sulfosuccinate. In the limonene-dodecanol mixture dodecanol has polar and amphiphilic character. Essentially the same trends were seen with this system as in the second study, except that the surface-active behavior of dodecanol was more pronounced.

The results suggested that the surface excess of the polar oil rather than the initial oil phase composition dictated the microemulsion properties. It was found that the change of the rigidity and the surfactant film curvature is related to the surface excess of the

polar oil. Through this relationship, the conditions necessary for the optimum formulation and the oil solubilization ability of the microemulsion changed depending upon the surface excess. Increasing bulk polar oil concentration increased the surface excess, which in turn decreased the optimum salinity and increased the oil solubilization. New models for the optimum salinity and the optimum characteristic length were proposed based on these results, and incorporated into the net-average curvature model. The two-state solubilization model combined with the net-average curvature model provided again excellent solubilization predictions.

Studies of the second and third system shed light on the origin of synergism observed during oil mixture solubilization. The bicontinuous microemulsion characteristic length of the oil mixtures was found to depend linearly on the polar oil surface excess for both studied oil mixture systems. If the surface excess is a linear function of the bulk oil composition, no synergism is expected. This kind of mixture would correspond to a “polar” oil, that is even less surface active than benzene in the second study. The surface excess of the polar oil in such a mixture may develop, because the polar oil is allowed to approach the oil/water interface closer than a non-polar one, The surface excess is dependent on the chemical potential of the polar oil in the core.

For more polar oils, the surface excess vs. bulk oil composition shows a positive deviation from linearity, depending on the polarity difference between the oils. The greater this deviation, the more pronounced the solubilization synergism. It appears that

the deviation of the surface excess from linearity as a function of bulk oil composition dictates the synergism.

The results of the second and third study suggest that the composition of the oil phase may vary with time during surfactant flush in a SEAR process, when the polar oil has low water solubility. Because of the selective solubilization of the polar oil, the unsolubilized excess oil pool becomes more and more rich in the hydrophobic oil. Consequently, if the surfactant solution was optimized for the initial oil composition, it becomes unoptimized later as the surfactant flush progresses. In order to maximize the oil solubilization, the surfactant formulation needs to be adjusted accordingly, e.g., increase the electrolyte concentration, switch to more hydrophobic surfactant, etc.

Appendix A

Calculation of the shell thickness from solubilization data

Symbols used

c_{ini} initial concentration of component 1 in the oil (volume fraction)

V_{ini} total initial volume of oil (L^3)

V_{eq} volume of excess oil phase at equilibrium (L^3)

v_{1sol} volume of component 1 in the surfactant aggregates at equilibrium (L^3)

v_{2sol} volume of component 2 in the surfactant aggregates at equilibrium (L^3)

V_w volume of water in the system (L^3)

V_s volume of surfactant in the system (L^3)

A_s total neutral interfacial area of the surfactant monolayer at the oil/water interface,
(L^2)

Experimentally measured solubilization data

c_{1w} and c_{2w} concentration of component 1 and component 2, respectively, measured in the surfactant phase, (volume fraction)

S_1 and S_2 water solubility of component 1 and component 2, respectively, measured without surfactant, (volume fraction)

c_{eq} concentration of component 1 in the excess oil phase measured at equilibrium.
(volume fraction)

Calculation of the surface excess

The systems contain a microemulsion phase and an excess oil phase. The oil phase contains two components, component 1 and component 2. Component 1 is solubilized in excess in the surfactant phase over component 2. The total amount of oil solubilized in the microemulsion phase is due to (1) the molecularly dispersed organic in the water, and (2) the solubilization due to incorporation into the surfactant aggregates (i.e. microemulsion). The experimental data contains both contributions.

The concentration of component 1 and component 2 in the surfactant phase due to solubilization only, respectively, is given by:

$$c_{1s} = c_{1w} - S_1 \quad \text{and} \quad c_{2s} = c_{2w} - S_2 \quad [1]$$

These concentrations can be written as

$$c_{1s} = \frac{v_{1sol}}{v_{1sol} + v_{2sol} + V_w + V_s} \quad \text{and} \quad c_{2s} = \frac{v_{2sol}}{v_{1sol} + v_{2sol} + V_w + V_s} \quad [2]$$

The total volume of solubilized oil is

$$v_t = v_{1sol} + v_{2sol} \quad [3]$$

Combining Eqs. [2] and [3] yields the total solubilized oil volume as

$$v_t = \frac{(V_w + V_s) \cdot (c_{1s} + c_{2s})}{1 - (c_{1s} + c_{2s})} \quad [4]$$

The average concentration of component 1 in the solubilized oil is obtained as

$$c_{ave} = \frac{c_{1s}}{c_{2s} + c_{2s}} \quad [5]$$

The surface excess of component 1 is

$$v_{1excess} = (v_1 - v_{disp}) - v_{1sol} - v_{1eq} \quad [6]$$

where $v_1 = V_{ini} \cdot c_{ini}$ is the total amount of component 1 in the system,

$v_{disp} = S_1 \cdot (V_w + V_s + V_{1+2})$ is the volume of component 1 in the aqueous phase in

molecularly dispersed form, $V_{1+2} = \frac{(c_{1w} + c_{2w}) \cdot (V_w + V_s)}{(1 - c_{1w} - c_{2w})}$ is the total volume of

component 1 and 2 in the surfactant phase, $v_{1sol} = v_t \cdot c_{ave}$ is the volume of solubilized

component 1, and $v_{1eq} = V_{eq} \cdot c_{eq}$ is the volume of component 1 remaining in the excess oil

phase.

Because of the inherent difficulties in measuring V_{eq} accurately, it is evaluated from mass

balance on component 1.

$$V_{eq} = V_{ini} - (c_{1w} + c_{2w}) \cdot (V_w + V_s + V_{1+2}) \quad [8]$$

Calculation of the shell thickness

The excess component 1 volume is distributed on the surface of the oil droplets of average radius R_o . The radius of the oil droplets are computed as

$$R_o = \frac{3 \cdot v_t}{A_s} \quad [9]$$

The shell thickness is obtained by solving Eq. 10 for d .

$$v_{1excess} = \frac{4}{3} \pi \cdot [(R_o + d)^3 - R_o^3] \quad [10]$$

Appendix B

Example Mathcad Program to Calculate Benzene-Limonene Mixture Solubilization

Example Mathcad program to calculate oil/water radius, solubilized oil composition, selectivity, and total oil solubilization as a function of salinity and initial oil phase composition is presented. When the salinity is the variable the initial oil phase composition is fixed. The example calculations are carried out for the 0.021 benzene volume fraction. When the oil phase composition is the variable the salinity is fixed. Example calculations are carried out at no added salt. The model predictions are compared to experimental data. Water solubility of benzene is accounted for in the computations of experimental solubilization.

Data

<u>Surfactant properties:</u>	Area per surfactant molecule (Angstroms ²)	a := 100
	Molecular weight (g/mole)	MWs := 388
	Concentration in water (g/100ml)	Cs := 4
	CMC (%)	CMC := 0.0588
	Length parameter (angstroms)	L := 10

Water phase initial data: Initial surfactant+water volume (ml) Vw0 := 5

Oil phase properties:

Component 1	Benzene	density (g/ml)	ρ1 := 0.879
		molecular weight (g/mole)	MWo1 := 78.11
		EACN	EACN1 := 0 not used
		Optimum salinity (%)	S1 := 2.04
		Characteristic length (Angstroms)	ξ1 := 67
		initial oil volume fraction	c1ini := 0.021
Component 2	Limonene	density (g/ml)	ρ2 := 0.842
		molecular weight (g/mole)	MWo2 := 136.24
		EACN	EACN2 := 6.3 not used
		Optimum salinity (%)	S2 := 6.2
		Characteristic length (Angstroms)	ξ2 := 28.8
		Initial oil volume fraction	c2ini := 1 - c1ini
Initial oil volume (ml)		Vo0 := 5	

Adsorption parameters:

$$K := 0.94 \quad (\text{Angstrom})$$

$$B := 0.35 \quad (\text{dimensionless})$$

Parameters are empirically evaluated from solubilization data at intermediate salinity.

Calculations :

1. Calculate the mixture properties:

Benzene initial volume fraction in the oil phase: $y := 0,0.02.. 1$

Oil mixture mole fraction:
$$n1(y) := \frac{\frac{y \cdot \rho1}{MWo1}}{\frac{y \cdot \rho1}{MWo1} + \frac{(1 - y) \cdot \rho2}{MWo2}}$$

Mixture optimum salinity:
$$OS(y) := e^{n1(y) \cdot \ln(S1) + (1 - n1(y)) \cdot \ln(S2)}$$

Mixture maximum characteristic length: $\xi(y) := y \cdot \xi1 + (1 - y) \cdot \xi2$ $\xi = \text{function}$

Note : Changes in the oil mixture composition due to oil solubilization do not have a significant effect on the optimum salinity and the characteristic length, and are neglected.

2. Conversions:

Initial surfactant volume (angstroms³):

$$Vs := Vw0 \cdot 10^{24} \cdot \frac{Cs}{100} \quad Vs = 2 \times 10^{23}$$

Initial water volume (angstroms³):

$$Vw := Vw0 \cdot 10^{24} \cdot \frac{100 - Cs}{100} \quad Vw = 4.8 \times 10^{24}$$

Total surfactant surface area (angstroms²):

$$A := Vw0 \cdot \left(\frac{Cs}{100}\right) \cdot \left(\frac{1}{MWs}\right) \cdot 6.022 \cdot 10^{23} \cdot a \quad A = 3.104 \times 10^{22}$$

Total initial oil volume (angstroms³):

$$V_o := V_{o0} \cdot 10^{24}$$

4. Calculate oil and water droplet sizes:

Radius of oil and water if all of the water (or oil) is solubilized:

$$R_o := 3 \cdot \frac{V_o}{A} \qquad R_w := 3 \cdot \frac{V_w}{A} \qquad \text{constants}$$

Type I systems:

$$RRc(x,y) := \frac{1}{\left(\frac{1}{L}\right) \cdot \ln\left(\frac{OS(y)}{x}\right) + \frac{1}{R_w}} \qquad \text{core oil radius in Type I phase behavior}$$

$$ksi1(x,y) := \frac{1}{\left(\frac{1}{2}\right) \cdot \left[\left(\frac{1}{RRc(x,y)}\right) + \frac{1}{R_w}\right]} \qquad \text{variable characteristic length in Type I systems}$$

$$\text{lower critical salinity:} \qquad x1(y) := OS(y) \cdot e^{-2 \cdot L \cdot \left[\left(\frac{1}{\xi(y)}\right) - \left(\frac{1}{R_w}\right)\right]}$$

Type III systems:

$$RRRc(x,y) := \frac{1}{\left(\frac{1}{2 \cdot L}\right) \cdot \ln\left(\frac{OS(y)}{x}\right) + \left(\frac{1}{\xi(y)}\right)} \qquad \text{oil radius in Type III systems}$$

$$RRw(x,y) := \frac{1}{\left(\frac{1}{\xi(y)}\right) - \left(\frac{1}{2 \cdot L}\right) \cdot \ln\left(\frac{OS(y)}{x}\right)} \qquad \text{water radius in Type III systems}$$

Type II systems:

$$RRRw(x,y) := \frac{1}{\left(\frac{1}{Ro}\right) - \left(\frac{1}{L}\right) \cdot \ln\left(\frac{OS(y)}{x}\right)} \quad \text{water radius in Type II}$$

$$x2(y) := OS(y) \cdot e^{-2 \cdot L \cdot \left[\left(\frac{1}{Ro}\right) - \left(\frac{1}{\xi(y)}\right)\right]} \quad \text{upper critical salinity}$$

Discretize salinity values (x): $x := 0.0588, 0.2.. 13$

Combined core oil droplet radius piecewise function:

$$rc(x,y) := \begin{cases} RRc(x,y) & \text{if } x < x1(y) \\ RRRc(x,y) & \text{if } x1(y) \leq x \leq x2(y) \\ Ro & \text{otherwise} \end{cases}$$

Combined water droplet radius piecewise function:

$$rw(x,y) := \begin{cases} Rw & \text{if } x < x1(y) \\ RRRw(x,y) & \text{if } x1(y) \leq x \leq x2(y) \\ RRRw(x,y) & \text{otherwise} \end{cases}$$

5. Calculate benzene concentration in excess oil at equilibrium:

Calculations are done for the given fixed initial benzene concentration (y) in the oil.

Initial equilibrium concentration guess for solve block: $C_{eq} := 0.05$

Solve block:

Given

$$C_{eq} = \frac{V_o \cdot y - \left[rc(x,y) + K \cdot \left(\frac{C_{eq}}{B + C_{eq}} \right) \right] \cdot \left(\frac{A}{3} \right) \cdot \left[1 + \frac{rc(x,y)^3 \cdot (C_{eq} - 1)}{\left[rc(x,y) + K \cdot \left(\frac{C_{eq}}{B + C_{eq}} \right) \right]^3} \right]}{\left[V_o - \left[rc(x,y) + K \cdot \left(\frac{C_{eq}}{B + C_{eq}} \right) \right] \cdot \frac{A}{3} \right]}$$

$FF(x,y) := \text{Find}(C_{eq})$

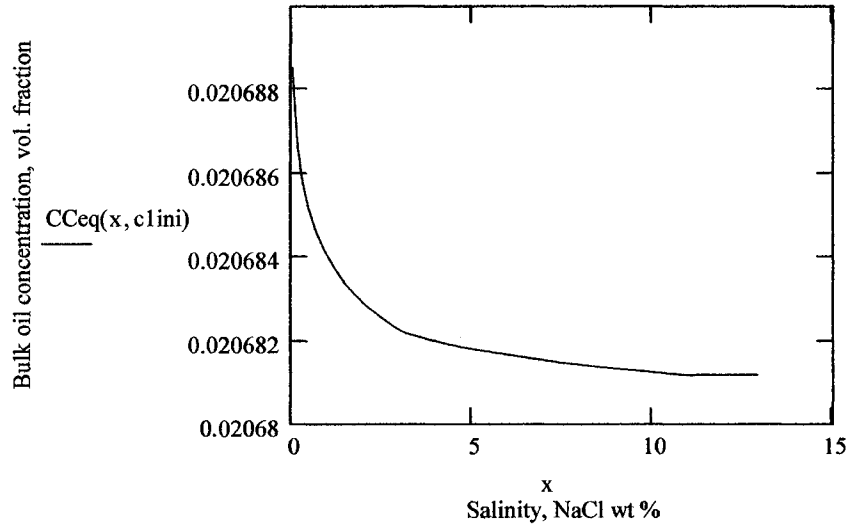
$CC_{eq}(x,y) := FF(x,y)$ $CC_{eq}(3, c1ini) = 0.021$

Here $CC_{eq}(x,y)$ is the calculated equilibrium oil concentration in the excess oil for initial concentration of y .

At initial concentration $y = c1ini$ and at no added salt: $CC_{eq}(0.058, c1ini) = 0.021$

Plot of excess oil concentration at equilibrium, as a function of salinity, at $y = c1ini$:

$c1ini = 0.021$



Notice that bulk oil concentration decreases very slightly as salinity increases, the decrease is not measurable. This was found to be valid experimentally.

6. Calculate shell thickness:

$$d(x,y) := \frac{K \cdot CCEq(x,y)}{B + CCEq(x,y)}$$

$$d(3, c1ini) = 0.052$$

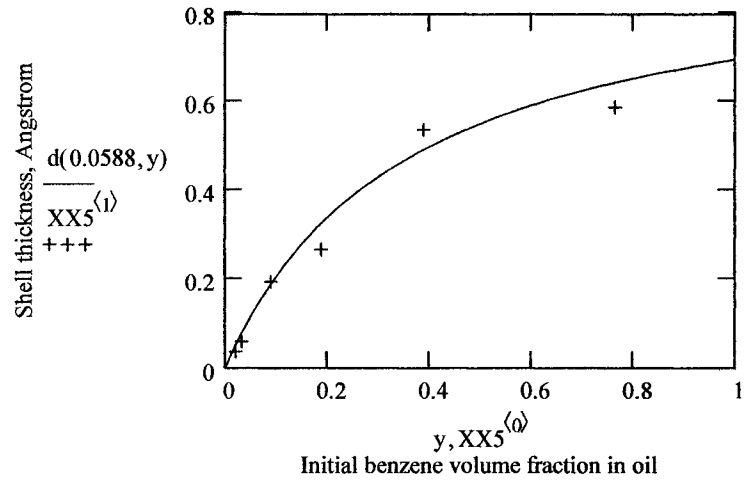
$$d(0.058, 0.5) = 0.552$$

Experimental data :

From d data averaged over the salinity scan: first column is initial benzene concentration (vol. fraction) , second column is shell thickness (Angstrom)

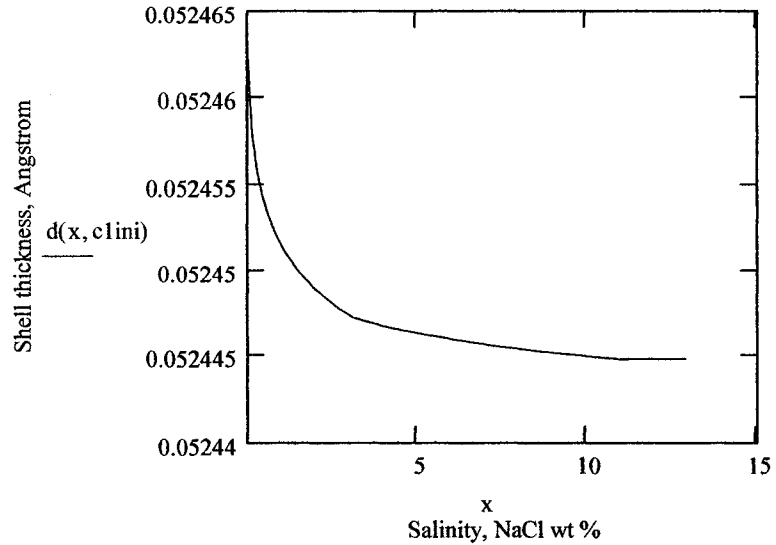
$$XX5 := \begin{pmatrix} 0 & 0 \\ 0.021 & 0.037 \\ 0.033 & 0.06 \\ 0.09 & 0.196 \\ 0.19 & 0.27 \\ 0.39 & 0.54 \\ 0.766 & 0.59 \end{pmatrix}$$

Shell thickness model prediction and data as a function of initial benzene concentration:



Shell thickness variation (predicted) as a function of salinity, at initial benzene volume fraction $y = c1ini$:

$c1ini = 0.021$



Shell thickness variation with the salinity is negligible. The slight apparent decrease is predicted because the benzene concentration in the bulk phase decreases as salinity increases (interfacial shape change).

7. Calculate average benzene concentration in the solubilized oil:

$$C_{ave}(x,y) := \left[1 + \frac{rc(x,y)^3 \cdot (CC_{eq}(x,y) - 1)}{\left[rc(x,y) + K \cdot \left(\frac{CC_{eq}(x,y)}{B + CC_{eq}(x,y)} \right) \right]^3} \right]$$

Experimental Cave vs. salinity for $y = c1ini$ (first column is salinity, second column is Cave):

0.0588	0.089138585
0.618174133	0.047742055
1.236348266	0.034745802
1.854522398	0.034738945
2.472696531	0.03074643
3.090870664	0.02789318
3.709044797	0.029304857
4.327218929	0.025076307
4.945393062	0.019633938
5.563567195	0.02290634
6.181741328	0.022836381
6.79991546	0.025075889
7.418089593	0.021976419
8.036263726	0.024360397

XX2 :=

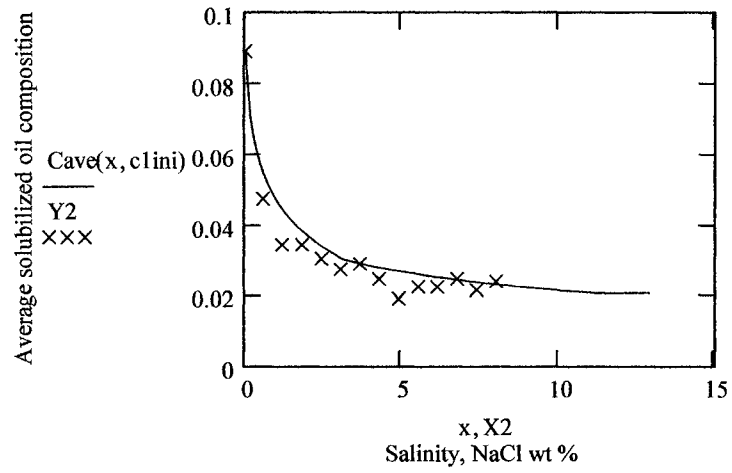
Experimental salinity:

X2 := XX2⁽⁰⁾

Experimental Cave:

Y2 := XX2⁽¹⁾

Plot of predicted and experimental average benzene volume fraction in the solubilized oil:

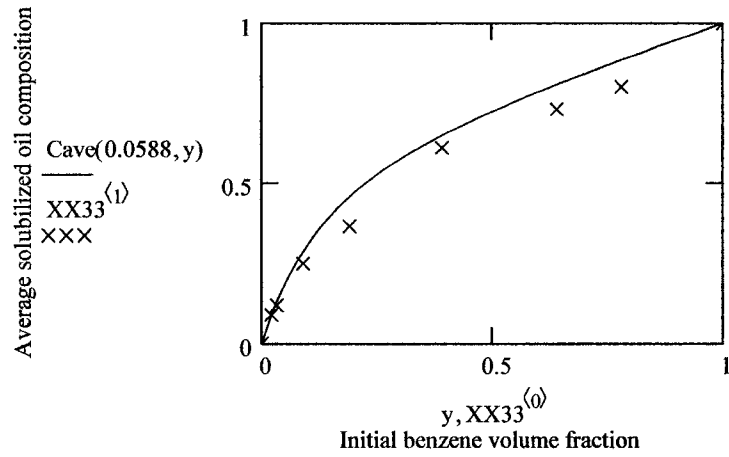


Average benzene concentration in the solubilized oil as a function of initial concentration:

Experimental C_{ave} vs. concentration, no salt (first column is initial concentration, second column is experimental C_{ave}):

0	0
0.021	0.09
0.033	0.12
0.09	0.25
0.19	0.365
0.39	0.61
0.64	0.73
0.78	0.8
1	1

Plot of Cave model predictions and experimental data as a function of initial concentration:



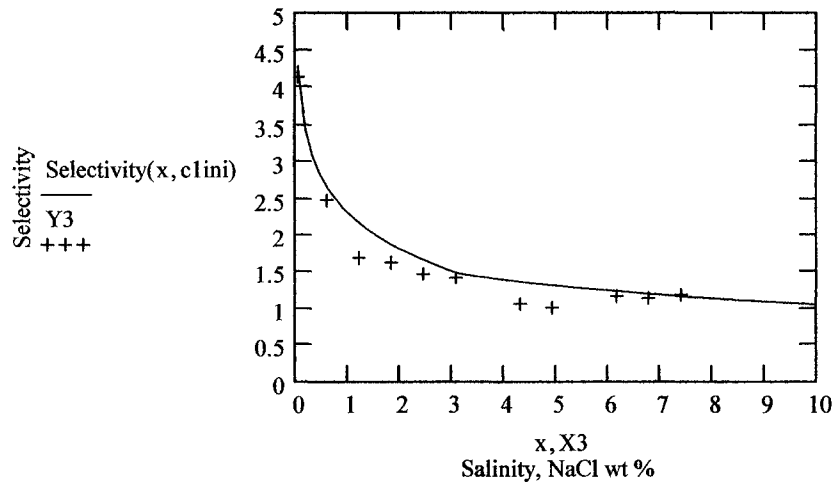
8. Calculate selectivity :

$$\text{Selectivity}(x,y) := \frac{\text{Cave}(x,y)}{\text{CCeq}(x,y)}$$

Experimental Selectivity vs. salinity for $y = c1ini$ (first column is salinity, second column is selectivity) :

0.0588	4.149134049		
0.618174133	2.479874949		
1.236348266	1.689243979		
1.854522398	1.630040547		
2.472696531	1.477404615		
3.090870664	1.425536113		
4.327218929	1.062220066		
4.945393062	1.011614449		
6.181741328	1.165656796	X3 := XX3 ⁽⁰⁾	Y3 := XX3 ⁽¹⁾
6.79991546	1.142377813		
7.418089593	1.189911709		

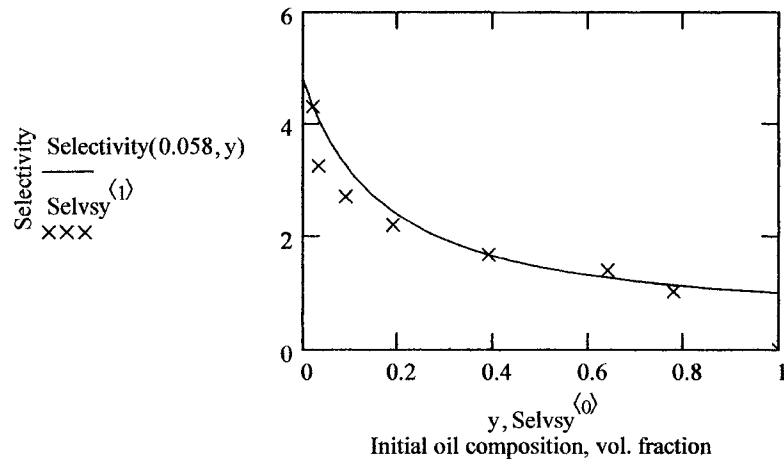
Plot of selectivity as a function of salinity, for initial oil concentration of $y = c1ini$:



Experimental selectivity variation as a function of initial oil concentration for no added salt (first column is benzene volume fraction in oil, second column is selectivity) :

Selvsy :=	0.021	4.3
	0.033	3.25
	0.09	2.7
	0.19	2.2
	0.39	1.67
	0.64	1.39
	0.78	1.02
	1	0

Plot of selectivity versus initial oil composition - model prediction and experimental data



Selectivity at no added salt and $y = c1ini$:

$$\text{Selectivity}(0.0588, c1ini) = 4.294$$

9. Calculate total oil solubilization :

Total solubilized water in surfactant macro phase:

$$vw(x,y) := rw(x,y) \cdot \frac{A}{3}$$

Total solubilized oil in the macroscopic surfactant phase:

$$vo(x,y) := (rc(x,y) + d(x,y)) \cdot \frac{A}{3}$$

Total volume of macroscopic surfactant phase:

$$vs(x,y) := vw(x,y) + vo(x,y) + Vs$$

Combined oil concentration in surfactant macro phase:

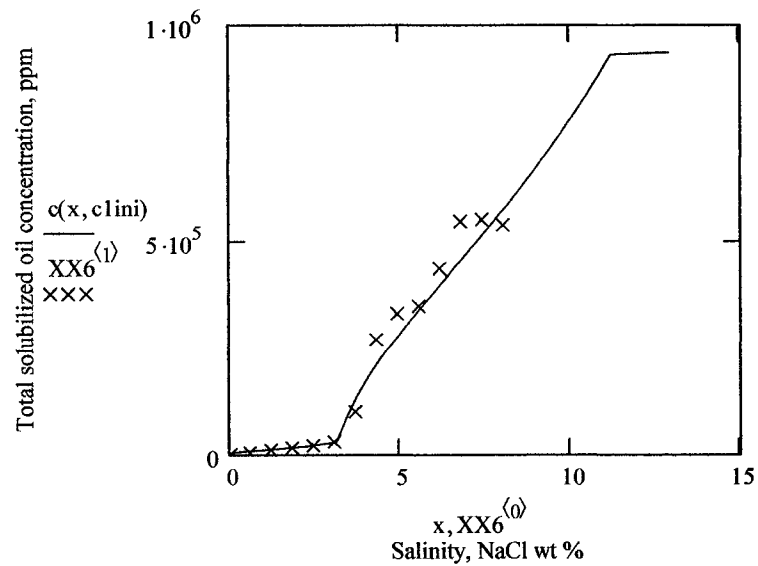
$$c(x,y) := \frac{vo(x,y) \cdot 10^6}{vs(x,y)}$$

Experimental total oil concentration in surfactant phase as a function of salinity, at $y = c1ini$
 (first column is salinity, second column is total oil ppm in the surfactant phase) :

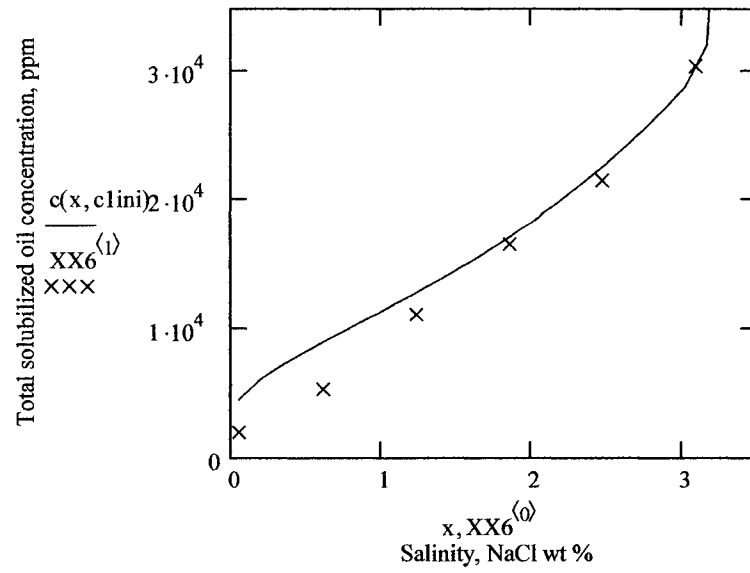
XX6 :=

0.0588	2011.171316
0.618174133	5356.37633
1.236348266	11219.78115
1.854522398	16682.84657
2.472696531	21571.20049
3.090870664	30470.14246
3.709044797	100941.5148
4.327218929	272945.7697
4.945393062	334068.985
5.563567195	350979.2997
6.181741328	437701.8576
6.79991546	546420.6258
7.418089593	551090.9192
8.036263726	538167.645

Plot of experimental and model surfactant phase total oil concentrations in vol ppm, as a function of salinity:



Total oil solubilization in the low solubilization regime :



Appendix C

General Mathcad Program to Calculate Dodecanol-Limonene Mixture Solubilization

Mathcad model to calculate the solubilization of dodecanol-limonene oil mixture in the microemulsion phase as a function of both initial dodecanol concentration and salinity.

Data

<u>Surfactant properties:</u>	Area per surfactant molecule (Angstroms ²)	a := 100
	Molecular weight (g/mole)	MWs := 388
	Concentration in water (g/100ml)	Cs := 4
	CMC (%)	CMC := 0.0588
	Length parameter (angstroms)	L := 10

<u>Water phase initial data:</u>	Initial surfactant+water volume (ml)	Vw0 := 5
----------------------------------	--------------------------------------	----------

Oil phase properties:

Component 1	density (g/ml)	ρ1 := 0.82
Dodecanol	molecular weight (g/mole)	MWo1 := 186
	length of hydrophilic segment	Ra := 3
	length of hydrophobic segment	Rb := 17
Component 2	density (g/ml)	ρ2 := 0.842
Limonene	molecular weight (g/mole)	MWo2 := 136.24
	Optimum salinity (%)	S2 := 6.2
	Characteristic length (Angstroms)	ξ2 := 28.8

Initial oil volume (ml)	Vo0 := 5	
-------------------------	----------	--

Adsorption parameters:

Saturation thickness (angstroms): $K := 1.25$

Slope denominator: $B := 0.04$

Conversions

Initial surfactant volume (angstroms³):

$$V_s := V_w0 \cdot 10^{24} \cdot \frac{C_s}{100} \qquad V_s = 2 \times 10^{23}$$

Initial water volume (angstroms³):

$$V_w := V_w0 \cdot 10^{24} \cdot \frac{100 - C_s}{100} \qquad V_w = 4.8 \times 10^{24}$$

Total surfactant surface area (angstroms²):

$$A := V_w0 \cdot \left(\frac{C_s}{100} \right) \cdot \left(\frac{1}{MWS} \right) \cdot 6.022 \cdot 10^{23} \cdot a \qquad A = 3.104 \times 10^{22}$$

$$V_o := V_o0 \cdot 10^{24} \qquad R_o := 3 \cdot \frac{V_o}{A} \qquad R_w := 3 \cdot \frac{V_w}{A}$$

Calculate optimum salinity and optimum characteristic length:

Discretize the dodecanol concentration for easier computations.

$$m := 10 \qquad j := 0..m$$

Initial dodecanol concentration in the oil (in volume fraction) y_j :

$$y_j := 0.0092 + 0.0092 \cdot j \cdot 4$$

Calculate bending rigidity with no dodecanol (κ_2):

$$\kappa_2 := \frac{\ln\left(\frac{\xi_2 + L}{L}\right)}{2 \cdot \pi} \quad \kappa_2 = 0.216$$

shell thickness $d_j := \frac{K \cdot y_j}{B + y_j}$ use initial concentration

number density $\sigma_j := d_j \cdot (10)^{-24} \cdot \left(\frac{\rho_1}{MW_{o1}}\right) \cdot 6.022 \cdot 10^{23}$

bending constant $\kappa_j := \kappa_2 + \left(\frac{1}{12}\right) \cdot \left(1 + \frac{\pi}{2}\right) \cdot (Ra^2 + Rb^2) \sigma_j$

characteristic length $\xi_j := L \cdot e^{(2 \cdot \pi \cdot \kappa_j)}$

optimum salinity $OS_j := e^{\left[\ln(S_2) + \left(\frac{1}{4}\right) \cdot \sqrt{\frac{\pi}{6}} \cdot (Ra - Rb) \cdot \frac{\sigma_j}{\kappa_j} \right]}$

Calculate equilibrium bulk oil concentration at optimum (C_{eq}):

$$RRo_j := \xi_j + d_j$$

$$vo_j := \frac{A \cdot RRo_j}{3}$$

$$C_{eq,j} := \frac{Vo \cdot y_j - vo_j \cdot \left[1 - \frac{(\xi_j)^3}{(RRo_j)^3} \right]}{Vo - vo_j \cdot \left[1 - \frac{(\xi_j)^3}{(RRo_j)^3} \right]}$$

Continue with iterations until equilibrium excess oil phase composition does not change :

$$\begin{aligned}
 \text{final}(\text{Ceq}, j) := & \left. \begin{array}{l}
 p \leftarrow \text{Ceq}_j \\
 y \leftarrow y_j \\
 \text{for } k \in 1..4 \\
 \quad d \leftarrow \frac{K \cdot p}{B + p} \\
 \quad \sigma \leftarrow d \cdot (10)^{-24} \cdot \left(\frac{\rho l}{\text{MWo}l} \right) \cdot 6.022 \cdot 10^{23} \\
 \quad \kappa \leftarrow \kappa_2 + \left(\frac{1}{12} \right) \cdot \left(1 + \frac{\pi}{2} \right) \cdot (\text{Ra}^2 + \text{Rb}^2) \cdot \sigma \\
 \quad \xi \leftarrow L \cdot e^{(2 \cdot \pi \cdot \kappa)} \\
 \quad \text{OS} \leftarrow e^{\left[\ln(\text{S}2) + \left(\frac{1}{4} \right) \cdot \sqrt{\frac{\pi}{6}} \cdot (\text{Ra} - \text{Rb}) \cdot \frac{\sigma}{\kappa} \right]} \\
 \quad \text{RRo} \leftarrow \xi + d \\
 \quad \text{vo} \leftarrow \frac{A \cdot \text{RRo}}{3} \\
 \quad p \leftarrow \frac{\text{Vo} \cdot y - \text{vo} \cdot \left[1 - \frac{(\xi)^3}{(\text{RRo})^3} \right]}{\text{Vo} - \text{vo} \cdot \left[1 - \frac{(\xi)^3}{(\text{RRo})^3} \right]}
 \end{array} \right| p
 \end{aligned}$$

the solution:

$$\text{final}(\text{Ceq}, j) =$$

$7.931 \cdot 10^{-3}$
0.042
0.078
0.115

Convert the solution function into discretized form to continue the computations:

$$p_j := \text{final}(\text{Ceq}, j)$$

$$p_j =$$

$7.931 \cdot 10^{-3}$
0.042
0.078

Final iterated values at optimum conditions for different initial concentrations (j):

shell thickness

$$d_j := \frac{K \cdot p_j}{B + p_j}$$

number density

$$\sigma_j := d_j \cdot 10^{-24} \cdot \left(\frac{\rho l}{MW_{o1}} \right) \cdot 6.022 \cdot 10^{23}$$

bending constant

$$\kappa_j := \kappa_2 + \left(\frac{1}{12} \right) \cdot \left(1 + \frac{\pi}{2} \right) \cdot (Ra^2 + Rb^2) \sigma_j$$

characteristic length

$$\xi_j := L \cdot e^{(2 \cdot \pi \cdot \kappa_j)}$$

optimum salinity

$$OS_j := e^{\left[\ln(S_2) + \left(\frac{1}{4} \right) \cdot \sqrt{\frac{\pi}{6}} \cdot (Ra - Rb) \left(\frac{\sigma_j \cdot \xi_j}{\kappa_j} \right) \right]}$$

Experimental data:

initial oil concentration vs.
characteristic length without
the surfactant length

$$X_{133} := \begin{pmatrix} 0 & 28.8 \\ 0.0092 & 34.6 \\ 0.0182 & 45 \\ 0.03 & 51 \\ 0.044 & 65 \end{pmatrix}$$

initial oil concentration vs.
characteristic length with
the surfactant length

$$X_{13} := \begin{pmatrix} 0 & 39 \\ 0.009 & 44.7 \\ 0.0183 & 54.8 \\ 0.031 & 61.6 \\ 0.044 & 75.2 \\ 0.113 & 100 \end{pmatrix}$$

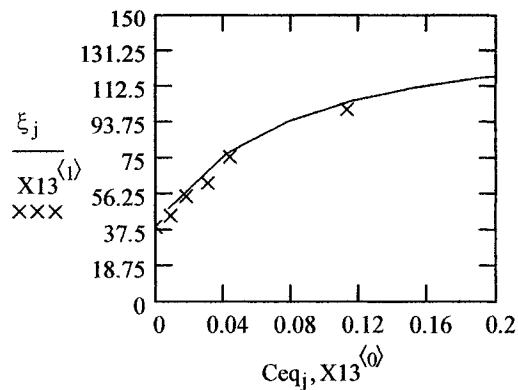
initial oil conc vs. optimum salinity

$$X10 := \begin{pmatrix} 0 & 6.3 \\ 0.0092 & 5.5 \\ 0.0182 & 3.8 \\ 0.03 & 3.1 \\ 0.044 & 2.59 \\ 0.113 & 1.15 \\ 0.2 & 0.6 \end{pmatrix}$$

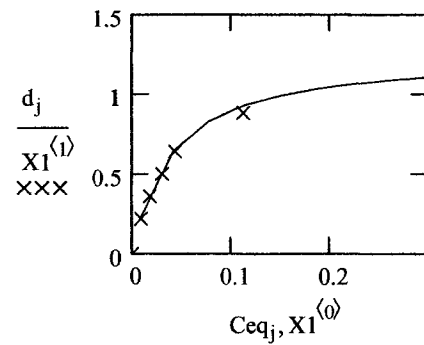
shell thickness at larger droplet sizes vs. initial dodecanol concentration

$$X1 := \begin{pmatrix} 0 & 0 \\ 0.0092 & 0.22 \\ 0.0183 & 0.36 \\ 0.031 & 0.5 \\ 0.044 & 0.64 \\ 0.113 & 0.88 \end{pmatrix}$$

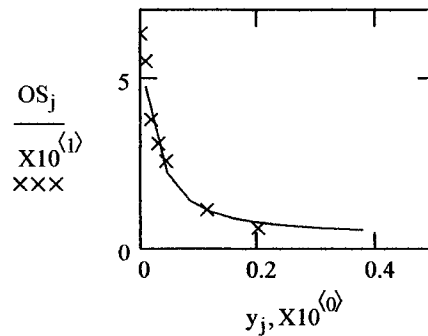
Plot model and experimental data:



Characteristic length vs. equilibrium excess oil concentration



Shell thickness vs. equilibrium excess oil concentration



Optimum salinity vs. equilibrium excess oil concentration

Calculate x1 and x2:

x1 is lower critical salinity and x2 is upper critical salinity

$$x1_j := e^{-\left[\ln(OS_j) - \left(\frac{2 \cdot L}{\xi_j}\right) + \left(\frac{2 \cdot L}{Rw}\right)\right]}$$

$$x2_j := e^{-\left[\ln(OS_j) - \left(\frac{2 \cdot L}{Ro}\right) + \left(\frac{2 \cdot L}{\xi_j}\right)\right]}$$

Calculate the droplet radii as a function of salinity

Discretize salinity variable for easier computations: n := 15 i := 0..n

The salinity scale is made dependent on the optimum salinity, which is dependent on the initial dodecanol concentration in the oil

salinity variable $x_{i,j} := 0.0588 + i \cdot \left[\frac{(1.5OS)_j}{n}\right]$

the core oil radius $(RRc_{i,j}) := \frac{1}{\left(\frac{1}{L}\right) \cdot \ln\left(\frac{OS_j}{x_{i,j}}\right) + \frac{1}{Rw}}$ Type I

characteristic length $RRRc_{i,j} := \frac{1}{\left(\frac{1}{2 \cdot L}\right) \cdot \ln\left(\frac{OS_j}{x_{i,j}}\right) + \frac{1}{\xi_j}}$ Type III

the water radius $RRw_{i,j} := \frac{1}{\left(\frac{1}{\xi_j}\right) - \left(\frac{1}{2 \cdot L}\right) \cdot \ln\left(\frac{OS_j}{x_{i,j}}\right)}$ Type III

$$RRRw_{i,j} := \frac{1}{\left(\frac{1}{Ro}\right) - \left(\frac{1}{L}\right) \cdot \ln\left(\frac{OS_j}{x_{i,j}}\right)}$$

Type II

Combined oil core radius function:

$$rc_{i,j} := \begin{cases} RRC_{i,j} & \text{if } x_{i,j} < x1_j \\ RRRc_{i,j} & \text{if } x1_j \leq x_{i,j} \leq x2_j \\ Ro & \text{otherwise} \end{cases}$$

Combined water radius function:

$$rw_{i,j} := \begin{cases} Rw & \text{if } x_{i,j} < x1_j \\ RRw_{i,j} & \text{if } x1_j \leq x_{i,j} \leq x2_j \\ RRRw_{i,j} & \text{otherwise} \end{cases}$$

Calculate the equilibrium excess oil phase concentration:

Initial guess for solve block: $Ceq_{i,j} := 0.02$

Solve block:

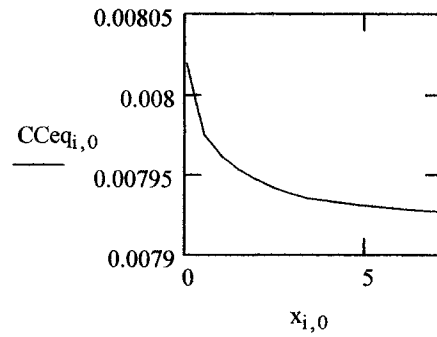
Given

$$Ceq_{i,j} = \frac{Vo \cdot y_j - \left[rc_{i,j} + K \cdot \left(\frac{Ceq_{i,j}}{B + Ceq_{i,j}} \right) \right] \cdot \left(\frac{A}{3} \right) \cdot \left[1 + \frac{(rc_{i,j})^3 \cdot (Ceq_{i,j} - 1)}{\left[rc_{i,j} + K \cdot \left(\frac{Ceq_{i,j}}{B + Ceq_{i,j}} \right) \right]^3} \right]}{\left[Vo - \left[rc_{i,j} + K \cdot \left(\frac{Ceq_{i,j}}{B + Ceq_{i,j}} \right) \right] \right] \cdot \frac{A}{3}}$$

$$FF_{i,j} := \text{Find}(Ceq_{i,j})$$

$$CCeq_{i,j} := FF_{i,j}$$

The excess oil concentration at equilibrium as a function of salinity at 0.009 initial dodecanol volume fraction, model prediction:

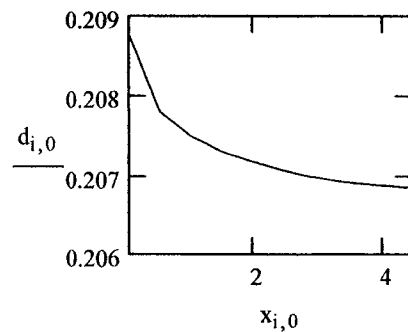
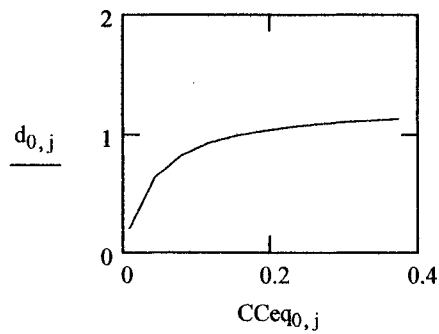


Shell thickness:

$d_{i,j}$ is the shell thickness as a function of both salinity and initial oil composition:

$$d_{i,j} := \frac{K \cdot CCeq_{i,j}}{B + CCeq_{i,j}}$$

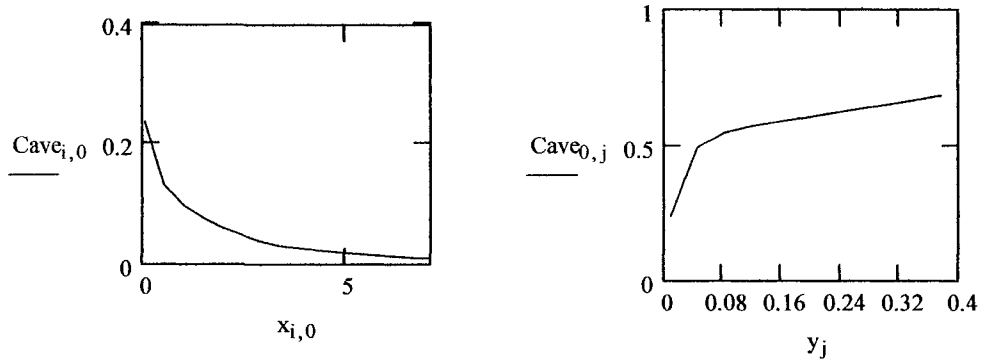
Plot of model shell thickness as a function of equilibrium dodecanol concentration in the excess oil (left), and as a function of salinity:



Average dodecanol volume fraction in the solubilized oil (Cave):

$$Cave_{i,j} := \left[1 + \frac{(rc_{i,j})^3 \cdot (CCeq_{i,j} - 1)}{\left[rc_{i,j} + K \cdot \left(\frac{CCeq_{i,j}}{B + CCeq_{i,j}} \right) \right]^3} \right]$$

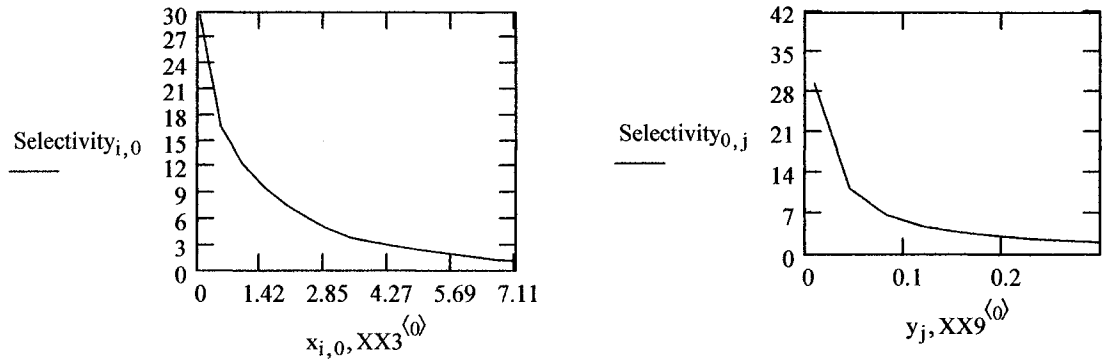
Plot of model Cave as a function of salinity (left), and initial dodecanol concentration in the excess oil (right):



Selectivity:

$$Selectivity_{i,j} := \frac{Cave_{i,j}}{CCeq_{i,j}}$$

Plot of model selectivity as a function of salinity (left), and initial dodecanol concentration in the excess oil:



Total solubilized water in surfactant phase:

$$vw_{i,j} := rw_{i,j} \cdot \frac{A}{3}$$

Total solubilized oil in surfactant phase:

$$vo_{i,j} := (rc_{i,j} + d_{i,j}) \cdot \frac{A}{3}$$

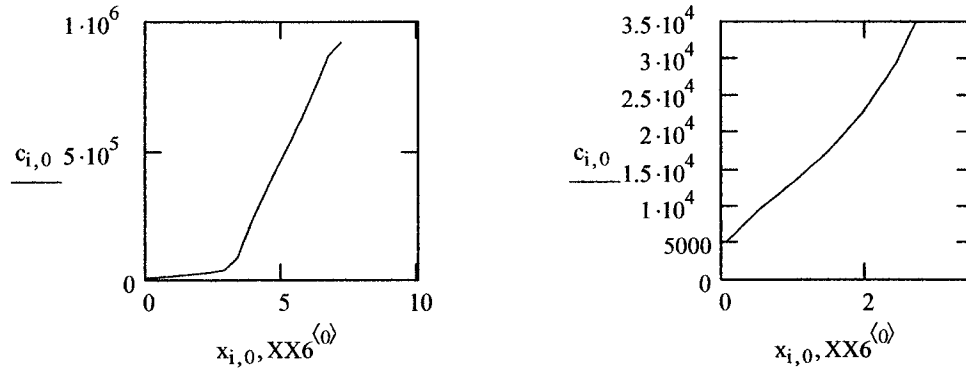
Total volume of surfactant phase:

$$vs_{i,j} := vw_{i,j} + vo_{i,j} + Vs$$

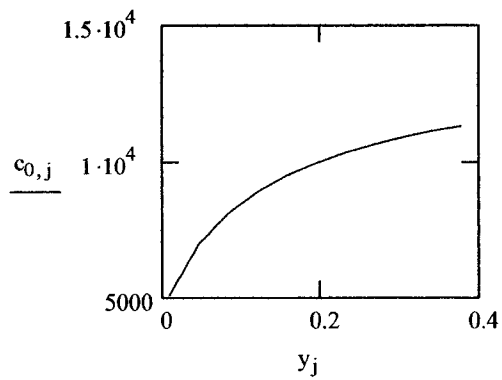
Combined oil concentration in surfactant phase:

$$c_{i,j} := \frac{vo_{i,j} \cdot 10^6}{vs_{i,j}}$$

Plot of model surfactant phase total oil concentrations in vol ppm as a function of salinity at fixed initial dodecanol concentration:

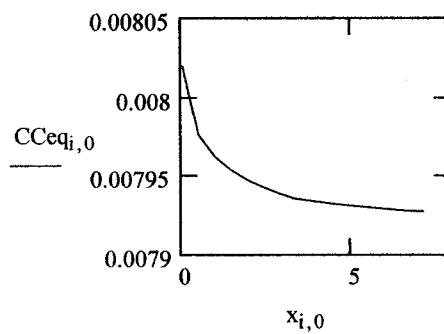


Plot of model results at fixed salinity (no added salt):



Excess oil phase equilibrium concentration:

Plot of model as a function of salinity at no added salt:



Appendix D

Example Mathcad Program to Calculate Dodecanol-Limonene Mixture Solubilization as a Function of Salinity

Mathcad model example to calculate dodecano-Limonene solubilization at fixed initial dodecanol concentration and **varying salinity**.

The initial dodecanol concentration is **0.03 volume fraction** in the oil.

Data

<u>Surfactant properties:</u>	Area per surfactant molecule (Angstroms ²)	a := 100
	Molecular weight of surfactant (g/mole)	MWs := 388
	Concentration in water (g/100ml)	Cs := 4
	CMC (%)	CMC := 0.0588
	Length parameter (angstroms)	L := 10

Water phase initial data: Initial surfactant+water volume (ml) Vw0 := 5

Oil phase properties:

Component 1 (Dodecanol)	density (g/ml)	ρ1 := 0.82
	molecular weight (g/mole)	MWo1 := 186
	length of hydrophylic segment (Angstroms)	Ra := 3
	length of hydrophobic segment (Angstroms)	Rb := 15

Component 2 (Limonene)	density (g/ml)	ρ2 := 0.842
	molecular weight (g/mole)	MWo2 := 136.24
	Optimum salinity (%)	S2 := 6.3
	Characteristic length (Angstroms)	ξ2 := 29

Initial concentration c1ini := 0.03

Initial oil volume (ml) Vo0 := 5

Adsorption parameters:

Saturation thickness (angstroms): $K := 1.25$

Slope denominator: $B := 0.04$

Parameters evaluated at intermediate salinity

Conversions

Initial surfactant volume (angstroms³):

$$V_s := V_w \cdot 10^{24} \cdot \frac{C_s}{100} \quad V_s = 2 \times 10^{23}$$

Initial water volume (angstroms³):

$$V_w := V_w \cdot 10^{24} \cdot \frac{100 - C_s}{100} \quad V_w = 4.8 \times 10^{24}$$

Total surfactant surface area (angstroms²):

$$A := V_w \cdot \left(\frac{C_s}{100} \right) \cdot \left(\frac{1}{MW_s} \right) \cdot 6.022 \cdot 10^{23} \cdot a \quad A = 3.104 \times 10^{22}$$

$$V_o := V_o \cdot 10^{24}$$

Radius of total oil in system (Angstroms): $R_o := 3 \cdot \frac{V_o}{A}$

Radius of total water in system (Angstroms): $R_w := 3 \cdot \frac{V_w}{A}$

Calculations

Calculate optimum salinity (OS) and characteristic length (ξ):

Use manual iteration instead of the iteration program to show how the equilibrium oil concentration value converges.

bending rigidity with limonene only (reference) $\kappa_2 := \frac{\ln\left(\frac{\xi^2 + L}{L}\right)}{2 \cdot \pi}$ $\kappa_2 = 0.217$

First iteration step:

use initial oil concentration as the equilibrium oil concentration (c1ini)

shell thickness $d := \frac{K \cdot c1ini}{B + c1ini}$ $d = 0.536$

number density $\sigma := d \cdot 10^{-24} \cdot \left(\frac{\rho_1}{MW_{o1}}\right) \cdot 6.022 \cdot 10^{23}$ $\sigma = 1.422 \times 10^{-3}$

bending constant $\kappa := \kappa_2 + \left(\frac{1}{12}\right) \cdot \left(1 + \frac{\pi}{2}\right) \cdot (Ra^2 + Rb^2) \sigma$ $\kappa = 0.288$

characteristic length $\xi := (L + d) \cdot e^{(2 \cdot \pi \cdot \kappa)}$ $\xi = 64.311$

optimum salinity $OS := e^{\left[\ln(S_2) + \left(\frac{1}{4}\right) \cdot \sqrt{\frac{\pi}{6}} \cdot (Ra - Rb) \cdot \left(\frac{\sigma \cdot \xi}{\kappa}\right)\right]}$ $OS = 3.161$

Calculate equilibrium bulk oil concentration at optimum:

$RRo := \xi - L + d$ $RRo = 54.846$

$v_o := \frac{A \cdot RRo}{3}$ $d = 0.5357$

$C_{eq} := \frac{V_o \cdot c1ini - v_o \cdot \left[1 - \frac{(\xi - L)^3}{(RRo)^3}\right]}{V_o - v_o \cdot \left[1 - \frac{(\xi - L)^3}{(RRo)^3}\right]}$ $\xi = 64.311$
 $C_{eq} = 0.027$

Second iteration:

Use the end result of C_{eq} from first iteration to compute shell thickness, and the other variables

$$\text{shell thickness} \quad d := \frac{K \cdot C_{eq}}{B + C_{eq}} \quad d = 0.501$$

$$\text{number density} \quad \sigma := d \cdot 10^{-24} \cdot \left(\frac{\rho l}{M W_{o1}} \right) \cdot 6.022 \cdot 10^{23} \quad \sigma = 1.331 \times 10^{-3}$$

$$\text{bending constant} \quad \kappa := \kappa_2 + \left(\frac{1}{12} \right) \cdot \left(1 + \frac{\pi}{2} \right) \cdot (R_a^2 + R_b^2) \sigma \quad \kappa = 0.283$$

$$\text{characteristic length} \quad \xi := (L + d) \cdot e^{(2 \cdot \pi \cdot \kappa)}$$

$$\text{optimum salinity} \quad OS := e^{-\left[\ln(S_2) + \left(\frac{1}{4} \right) \cdot \sqrt{\frac{\pi}{6}} \cdot (R_a - R_b) \cdot \left(\frac{\sigma \cdot \xi}{\kappa} \right) \right]} \quad OS = 3.338$$

equilibrium oil concentration at optimum

$$RR_o := \xi - L + d$$

$$v_o := \frac{A \cdot RR_o}{3}$$

$$C_{eq} := \frac{V_o \cdot c_{1ini} - v_o \cdot \left[1 - \frac{(\xi - L)^3}{RR_o^3} \right]}{V_o - v_o \cdot \left[1 - \frac{(\xi - L)^3}{RR_o^3} \right]} \quad C_{eq} = 0.027$$

Compute difference between previous and new C_{eq} (in absolute value), and if it is less than an error limit, (say 1% of old value) stop iteration here, and accept OS and characteristic length values.

Third iteration step

Use the new C_{eq} value to recalculate shell thickness, and other stuff.
 C_{eq} should now oscillate around a certain value

shell thickness $d := \frac{K \cdot C_{eq}}{B + C_{eq}} \quad d = 0.504$

number density $\sigma := d \cdot 10^{-24} \cdot \left(\frac{\rho_1}{MW_{o1}} \right) \cdot 6.022 \cdot 10^{23}$

bending constant $\kappa := \kappa_2 + \left(\frac{1}{12} \right) \cdot \left(1 + \frac{\pi}{2} \right) \cdot (Ra^2 + Rb^2) \sigma$

characteristic length $\xi := (L + d) \cdot e^{(2 \cdot \pi \cdot \kappa)}$

optimum salinity $OS := e^{\left[\ln(S_2) + \left(\frac{1}{4} \right) \cdot \sqrt{\frac{\pi}{6}} \cdot (Ra - Rb) \cdot \left(\frac{\sigma \cdot \xi}{\kappa} \right) \right]} \quad OS = 3.326$

equilibrium oil concentration at optimum:

$$RRo := \xi - L + d$$

$$v_o := \frac{A \cdot RRo}{3}$$

$$C_{eq} := \frac{V_o \cdot c_{1ini} - v_o \cdot \left[1 - \frac{(\xi - L)^3}{RRo^3} \right]}{V_o - v_o \cdot \left[1 - \frac{(\xi - L)^3}{RRo^3} \right]} \quad C_{eq} = 0.027$$

check difference between new and old C_{eq} .

If difference is greater than 1% of old C_{eq} , go to fourth iteration step. Otherwise stop, and accept new OS and new ξ .

Fourth iteration step:

I found that 4 iteration was enough.

shell thickness $d := \frac{K \cdot C_{eq}}{B + C_{eq}} \quad d = 0.504$

number density $\sigma := d \cdot 10^{-24} \cdot \left(\frac{\rho l}{M W_{o1}} \right) \cdot 6.022 \cdot 10^{23}$

bending constant $\kappa := \kappa_2 + \left(\frac{1}{12} \right) \cdot \left(1 + \frac{\pi}{2} \right) \cdot (R_a^2 + R_b^2) \sigma$

characteristic length $\xi := (L + d) \cdot e^{(2 \cdot \pi \cdot \kappa)}$

optimum salinity $OS := e^{\left[\ln(S_2) + \left(\frac{1}{4} \right) \cdot \sqrt{\frac{\pi}{6}} \cdot (R_a - R_b) \cdot \left(\frac{\sigma \cdot \xi}{\kappa} \right) \right]}$

Results: $OS = 3.326$ $\xi = 62.414$

Calculate water and oil droplet radii

Droplet radii is a function of both salinity (x) and initial oil concentration (c).

calculate x1 and x2:

x1 is lower critical salinity and x2 is upper critical salinity

x1 and x2 depends only on initial oil concentration (c).

$$x1 := e^{\left[\ln(OS) - \left(\frac{2 \cdot L}{\xi - L} \right) + \left(\frac{2 \cdot L}{R_w} \right) \right]} \quad x1 = 2.371$$

$$x2 := e^{\left[\ln(OS) - \left(\frac{2 \cdot L}{R_o} \right) + \left(\frac{2 \cdot L}{\xi - L} \right) \right]} \quad x2 = 4.674$$

Calculate droplet radii:

the core oil radius $RRc(x) := \frac{1}{\left(\frac{1}{L}\right) \cdot \ln\left(\frac{OS}{x}\right) + \frac{1}{Rw}}$ Type I

$RRRc(x) := \frac{1}{\left(\frac{1}{2 \cdot L}\right) \cdot \ln\left(\frac{OS}{x}\right) + \frac{1}{\xi - L}}$ Type III

the water radius $RRw(x) := \frac{1}{\left(\frac{1}{\xi - L}\right) - \left(\frac{1}{2 \cdot L}\right) \cdot \ln\left(\frac{OS}{x}\right)}$ Type III

$RRRw(x) := \frac{1}{\left(\frac{1}{Ro}\right) - \left(\frac{1}{L}\right) \cdot \ln\left(\frac{OS}{x}\right)}$ Type II

Combined oil core radius function: $rc(x) := \begin{cases} RRc(x) & \text{if } x < x1 \\ RRRc(x) & \text{if } x1 \leq x \leq x2 \\ Ro & \text{otherwise} \end{cases}$

Combined water radius function: $rw(x) := \begin{cases} Rw & \text{if } x < x1 \\ RRw(x) & \text{if } x1 \leq x \leq x2 \\ RRRw(x) & \text{otherwise} \end{cases}$

Calculate equilibrium oil concentration (CCeq):

Initial guess for solve block:

$CCeq := c1ini$

Solve block:

Given

$$CC_{eq} = \frac{V_o \cdot c_{1ini} - \left[rc(x) + K \cdot \left(\frac{CC_{eq}}{B + CC_{eq}} \right) \right] \cdot \left(\frac{A}{3} \right) \cdot \left[1 + \frac{rc(x)^3 \cdot (CC_{eq} - 1)}{\left[rc(x) + K \cdot \left(\frac{CC_{eq}}{B + CC_{eq}} \right) \right]^3} \right]}{\left[V_o - \left[rc(x) + K \cdot \left(\frac{CC_{eq}}{B + CC_{eq}} \right) \right] \cdot \frac{A}{3} \right]}$$

$$FF(x) := \text{Find}(CC_{eq})$$

$$CC_{Ceq}(x) := FF(x)$$

This is the dodecanol concentration in the excess oil phase at equilibrium:

Calculate shell thickness:

$$d(x) := \frac{K \cdot CC_{Ceq}(x)}{B + CC_{Ceq}(x)}$$

Results

Calculate the average dodecanol concentration in the micellar oil:

$$C_{ave}(x) := \left[1 + \frac{rc(x)^3 \cdot (CC_{Ceq}(x) - 1)}{\left[rc(x) + K \cdot \left(\frac{CC_{Ceq}(x)}{B + CC_{Ceq}(x)} \right) \right]^3} \right]$$

Calculate selectivity :

$$\text{Selectivity}(x) := \frac{C_{ave}(x)}{CC_{Ceq}(x)}$$

Total solubilized water volume in surfactant macro phase:

$$vw(x) := rw(x) \cdot \frac{A}{3}$$

Total solubilized oil volume in surfactant macro phase:

$$vo(x) := (rc(x) + d(x)) \cdot \frac{A}{3}$$

Total volume of microemulsion phase:

$$vs(x) := vw(x) + vo(x) + Vs$$

Solubilized oil concentration (ppm) in microemulsion phase:

$$C(x) := \frac{vo(x) \cdot 10^6}{vs(x)} \quad C(0.1) = 6.872 \times 10^3$$

This is what we measure with GC from a sample, taken from the microemulsion phase

counter for salinity

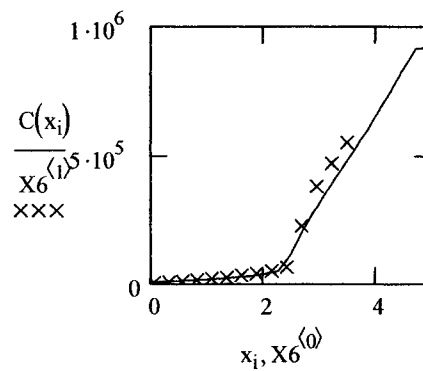
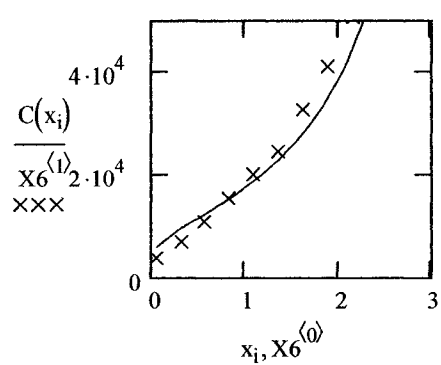
i := 0..30

Salinity and concentration is discretized only for easier plotting!

$$x_i := CMC + \frac{2OS \cdot i}{30}$$

Total oil concentration (ppm) in the microemulsion phase:

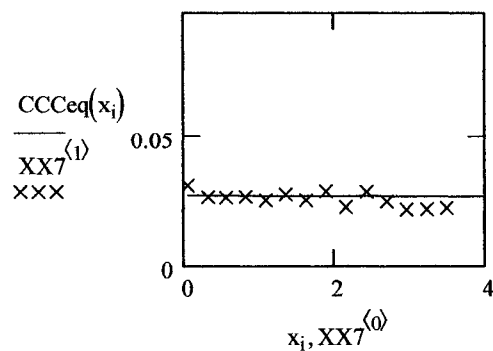
	0.058	3897.56938
	0.326674716	7180.734786
	0.566349432	11046.02147
	0.825357481	15563.80575
	1.089198864	20283.94706
	1.35497358	24691.46797
	1.621714962	32910.1422
X6 :=	1.889008726	41237.42895
	2.156647727	50697.59554
	2.424516888	66037.66395
	2.692547159	227225.5675
	2.960694602	381824.8147
	3.228929924	472629.8225
	3.497232846	552618.6786



Excess oil phase equilibrium concentration:

XX7 :=

0.058	0.031239474
0.326674716	0.026672697
0.566349432	0.026378399
0.825357481	0.02679057
1.089198864	0.025491009
1.35497358	0.027646053
1.621714962	0.025426535
1.889008726	0.028921601
2.156647727	0.022916996
2.424516888	0.028704496
2.692547159	0.024969846
2.960694602	0.021965461
3.228929924	0.022081579
3.497232846	0.02255636

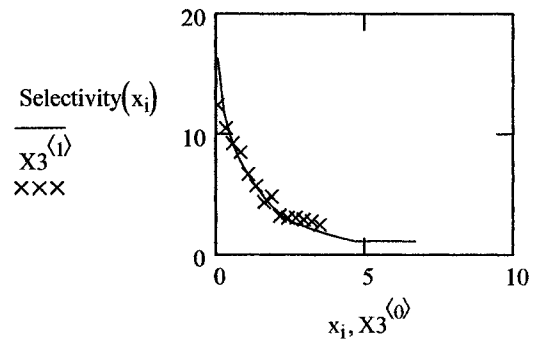


Selectivity:

Experimental

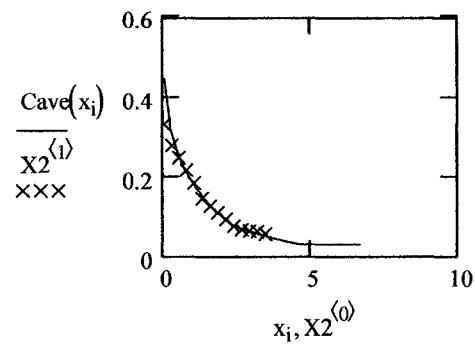
X3 :=

0.058	12.40787871
0.326674716	10.50607606
0.566349432	9.225216172
0.825357481	8.464081822
1.089198864	6.64090895
1.35497358	5.673450309
1.621714962	4.320092321
1.889008726	4.774157199
2.156647727	3.217293407
2.424516888	3.035490343
2.692547159	3.046510608
2.960694602	2.884291442
3.228929924	2.765303727
3.497232846	2.464085273



Average dodecanol concentration in the micellar oil:

$X_2 :=$	0.058	0.330951594
	0.326674716	0.277133467
	0.566349432	0.247148801
	0.825357481	0.215757984
	1.089198864	0.183594918
	1.35497358	0.144256183
	1.621714962	0.124943986
	1.889008726	0.10940934
	2.156647727	0.092350784
	2.424516888	0.075795728
	2.692547159	0.066918008
	2.960694602	0.063689709
	3.228929924	0.062375185
	3.497232846	0.055698324



Appendix E

Example Mathcad Program to Calculate Dodecanol-Limonene Mixture Solubilization as a Function of Oil Composition

Mathcad code to calculate solubilization of dodecanol-limonene oil mixture at constant salinity, with **varying initial oil phase composition**. Example calculations are shown for the **no added salt** case, where the salinity was taken equal to the Na⁺ contribution from the surfactant at the CMC. The surfactant concentration is constant.

Data

<u>Surfactant properties:</u>	Area per surfactant molecule (Angstroms ²)	a := 100	
	Molecular weight of surfactant (g/mole)	MWs := 388	
	Concentration in water (g/100ml)	Cs := 4	
	CMC (%)	CMC := 0.0588	
	Length parameter (angstroms)	L := 10	
<u>Water phase initial data:</u>	Initial surfactant+water volume (ml)	Vw0 := 5	
<u>Oil phase properties:</u>			
Component 1 (Dodecanol)	density (g/ml)	ρ1 := 0.82	
	molecular weight (g/mole)	MWo1 := 186	
	length of hydrophylic segment (Angstroms)	Ra := 3	
	length of hydrophobic segment (Angstroms)	Rb := 1	
Component 2 (Limonene)	density (g/ml)	ρ2 := 0.842	
	molecular weight (g/mole)	MWo2 := 136.24	
	Optimum salinity (%)	S2 := 6.2	
	Characteristic length (Angstroms)	ξ2 := 29	
Initial oil volume (ml)	Vo0 := 5		

Adsorption parameters:

Saturation thickness (angstroms): $K := 1.25$

Slope denominator: $B := 0.04$

Parameters evaluated at no added salt

Conversions

Initial surfactant volume (angstroms³):

$$V_s := V_w0 \cdot 10^{24} \cdot \frac{C_s}{100} \quad V_s = 2 \times 10^{23}$$

Initial water volume (angstroms³):

$$V_w := V_w0 \cdot 10^{24} \cdot \frac{100 - C_s}{100} \quad V_w = 4.8 \times 10^{24}$$

Total surfactant surface area (angstroms²):

$$A := V_w0 \cdot \left(\frac{C_s}{100} \right) \cdot \left(\frac{1}{MW_s} \right) \cdot 6.022 \cdot 10^{23} \cdot a \quad A = 3.104 \times 10^{22}$$

Total volume of oil in the system (angstroms³):

$$V_o := V_o0 \cdot 10^{24}$$

Radius of total oil in system (Angstroms):

$$R_o := 3 \cdot \frac{V_o}{A}$$

Radius of total water in system (Angstroms):

$$R_w := 3 \cdot \frac{V_w}{A}$$

Calculations

Calculate optimum salinity (OS) and characteristic length (ξ):

Optimum salinity (OS), and the optimum characteristic length (ξ) are not dependent on salinity (x), they are functions of only the equilibrium oil composition (C_{eq}) at the optimum. C_{eq} is not known, only the initial oil composition is known.

C_{eq} is dependent on the initial oil composition (c). So the optimum salinity and the optimum characteristic length are calculated iteratively. Manual iteration is used here instead of the iteration program to demonstrate C_{eq} convergence.

$$\text{bending rigidity with limonene only (reference rigidity)} \quad \kappa_2 := \frac{\ln\left(\frac{\xi_2 + L}{L}\right)}{2 \cdot \pi} \quad \kappa_2 = 0.217$$

First iteration step:

use initial oil concentration as the equilibrium oil concentration ($C_{eq}=c$)

$$\text{shell thickness} \quad d(c) := \frac{K \cdot c}{B + c} \quad d(0.0092) = 0.234$$

$$\text{number density} \quad \sigma(c) := d(c) \cdot 10^{-24} \cdot \left(\frac{\rho_1}{MW_{o1}}\right) \cdot 6.022 \cdot 10^{23} \quad \sigma(0.0092) = 6.205 \times 10^{-4}$$

$$\text{bending constant} \quad \kappa(c) := \kappa_2 + \left(\frac{1}{12}\right) \cdot \left(1 + \frac{\pi}{2}\right) \cdot (Ra^2 + Rb^2) \sigma(c) \quad \kappa(0.0092) = 0.248$$

$$\text{characteristic length} \quad \xi(c) := (L + d(c)) \cdot e^{(2 \cdot \pi \cdot \kappa(c))} \quad \xi(0.0092) = 48.527$$

$$\text{optimum salinity} \quad OS(c) := e^{\left[\ln(S_2) + \left(\frac{1}{4}\right) \cdot \sqrt{\frac{\pi}{6}} \cdot (Ra - Rb) \cdot \left(\frac{\sigma(c) \cdot \xi(c)}{\kappa(c)}\right) \right]} \quad OS(0.0092) = 4.762$$

Calculate equilibrium bulk oil concentration at optimum:

$$RRo(c) := \xi(c) - L + d(c) \quad RRo(0.0092) = 38.761$$

$$vo(c) := \frac{A \cdot RRo(c)}{3} \quad d(0.0092) = 0.2337$$

$$Ceq(c) := \frac{Vo \cdot c - vo(c) \cdot \left[1 - \frac{(\xi(c) - L)^3}{(RRo(c))^3} \right]}{Vo - vo(c) \cdot \left[1 - \frac{(\xi(c) - L)^3}{(RRo(c))^3} \right]} \quad Ceq(0.0092) = 7.769 \times 10^{-3}$$

Second iteration:

Use the end result of Ceq from first iteration to compute shell thickness, and the other variables.

shell thickness $d(c) := \frac{K \cdot Ceq(c)}{B + Ceq(c)} \quad d(0.0092) = 0.203$

number density $\sigma(c) := d(c) \cdot 10^{-24} \cdot \left(\frac{\rho 1}{MWo1} \right) \cdot 6.022 \cdot 10^{23} \quad \sigma(0.0092) = 5.397 \times 10^{-}$

bending constant $\kappa(c) := \kappa 2 + \left(\frac{1}{12} \right) \cdot \left(1 + \frac{\pi}{2} \right) \cdot (Ra^2 + Rb^2) \sigma(c) \quad \kappa(0.0092) = 0.244$

characteristic length $\xi(c) := (L + d(c)) \cdot e^{(2 \cdot \pi \cdot \kappa(c))}$

optimum salinty $OS(c) := e^{\left[\ln(S2) + \left(\frac{1}{4} \right) \cdot \sqrt{\frac{\pi}{6}} \cdot (Ra - Rb) \cdot \left(\frac{\sigma(c) \cdot \xi(c)}{\kappa(c)} \right) \right]}$

equilibrium oil concentration at optimum (Ceq)

$RRo(c) := \xi(c) - L + d(c)$ radius of total solubilized oil

$vo(c) := \frac{A \cdot RRo(c)}{3}$ volume of total solubilized oil

$$Ceq(c) := \frac{Vo \cdot c - vo(c) \cdot \left[1 - \frac{(\xi(c) - L)^3}{RRo(c)^3} \right]}{Vo - vo(c) \cdot \left[1 - \frac{(\xi(c) - L)^3}{RRo(c)^3} \right]} \quad Ceq(0.0092) = 7.955 \times 10^{-3}$$

Compute difference between previous and new C_{eq} (in absolute value), and if it is less than an error limit, (say 1% of old value) stop iteration here, and accept OS and characteristic length values.

Third iteration step

Use the new C_{eq} value to recalculate shell thickness, and other variables.
 C_{eq} should now oscillate around a certain value

$$\text{shell thickness} \quad d(c) := \frac{K \cdot C_{eq}(c)}{B + C_{eq}(c)} \quad d(0.0092) = 0.207$$

$$\text{number density} \quad \sigma(c) := d(c) \cdot 10^{-24} \cdot \left(\frac{\rho_1}{MW_{o1}} \right) \cdot 6.022 \cdot 10^{23}$$

$$\text{bending constant} \quad \kappa(c) := \kappa_2 + \left(\frac{1}{12} \right) \cdot \left(1 + \frac{\pi}{2} \right) \cdot (Ra^2 + Rb^2) \sigma(c)$$

$$\text{characteristic length} \quad \xi(c) := (L + d(c)) \cdot e^{(2 \cdot \pi \cdot \kappa(c))}$$

$$\text{optimum salinity} \quad OS(c) := e^{\left[\ln(S_2) + \left(\frac{1}{4} \right) \cdot \sqrt{\frac{\pi}{6}} \cdot (Ra - Rb) \cdot \left(\frac{\sigma(c) \cdot \xi(c)}{\kappa(c)} \right) \right]}$$

equilibrium oil concentration at optimum:

$$RRo(c) := \xi(c) - L + d(c)$$

$$vo(c) := \frac{A \cdot RRo(c)}{3}$$

$$C_{eq}(c) := \frac{Vo \cdot c - vo(c) \cdot \left[1 - \frac{(\xi(c) - L)^3}{RRo(c)^3} \right]}{Vo - vo(c) \cdot \left[1 - \frac{(\xi(c) - L)^3}{RRo(c)^3} \right]}$$

$$\text{check difference between new and old } C_{eq} \quad C_{eq}(0.0092) = 7.93 \times 10^{-3}$$

If difference is greater than 1% of old C_{eq} , go to fourth iteration step. Otherwise stop, and accept new OS and new ξ .

Fourth iteration step:

shell thickness $d(c) := \frac{K \cdot C_{eq}(c)}{B + C_{eq}(c)}$ $d(0.0092) = 0.207$

number density $\sigma(c) := d(c) \cdot 10^{-24} \cdot \left(\frac{\rho l}{MW_{ol}} \right) \cdot 6.022 \cdot 10^{23}$

bending constant $\kappa(c) := \kappa_2 + \left(\frac{1}{12} \right) \cdot \left(1 + \frac{\pi}{2} \right) \cdot (Ra^2 + Rb^2) \sigma(c)$

characteristic length $\xi(c) := (L + d(c)) \cdot e^{(2 \cdot \pi \cdot \kappa(c))}$

optimum salinity $OS(c) := e^{\left[\ln(S_2) + \left(\frac{1}{4} \right) \cdot \sqrt{\frac{\pi}{6}} \cdot (Ra - Rb) \cdot \left(\frac{\sigma(c) \cdot \xi(c)}{\kappa(c)} \right) \right]}$

Four iteration is enough.

For easier calculations discretize concentration:

$$j := 0..20 \quad c_j := j \cdot 0.02$$

Model results:

$OS(c_j) =$	$C_{eq}(c_j) =$	$\xi(c_j) =$	ξ with surfactant length
6.2	0	39	
3.913	0.018	55.789	
2.814	0.036	68.032	
2.215	0.056	76.905	
1.852	0.075	83.505	
1.614	0.095	88.564	
1.448	0.115	92.546	
1.326	0.135	95.755	

(These range variables contain more elements than shown here.)

Experimental data:

X15 is the shell thickness in Angstroms (2nd column) at intermediate salinity versus initial dodecanol concentration in volume fraction (1st column)

$$X15 := \begin{pmatrix} 0 & 0 \\ 0.0092 & 0.22 \\ 0.0183 & 0.36 \\ 0.031 & 0.5 \\ 0.044 & 0.64 \\ 0.12 & 0.87 \end{pmatrix}$$

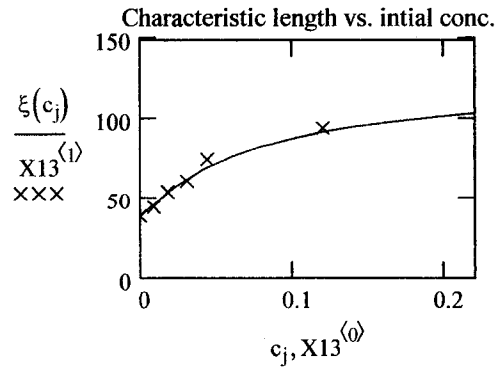
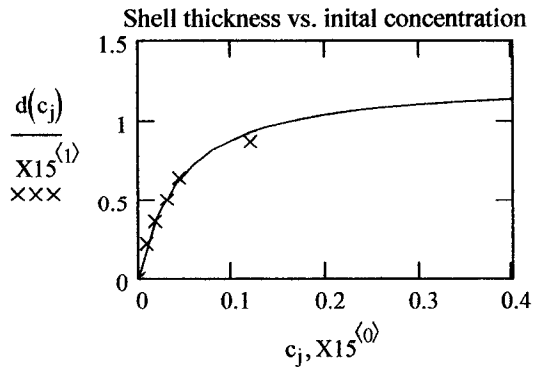
X13 is the characteristic length in Angstroms (2nd column) versus initial dodecanol concentration in volume fraction (1st column)

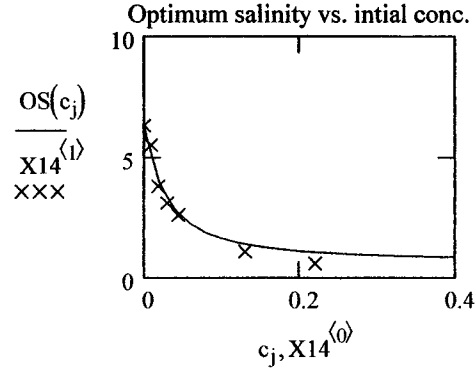
$$X13 := \begin{pmatrix} 0 & 39 \\ 0.0092 & 44.7 \\ 0.0183 & 54.8 \\ 0.031 & 61.6 \\ 0.044 & 75.2 \\ 0.12 & 95 \end{pmatrix}$$

X14 is the optimum salinity in wt % (2nd column) versus initial dodecanol concentration in volume fraction (1st column)

$$X14 := \begin{pmatrix} 0 & 6.3 \\ 0.0092 & 5.5 \\ 0.0182 & 3.8 \\ 0.03 & 3.1 \\ 0.044 & 2.59 \\ 0.13 & 1.08 \\ 0.22 & 0.6 \end{pmatrix}$$

Plot of experimental data and model results:





Calculate water and oil droplet radii

Droplet radii is a function of both salinity (x) and initial oil concentration (c). Here the salinity is fixed, but the same salinity induces different curvature for the different oil compositions.

Calculate x1 and x2:

x1 is lower critical salinity and x2 is upper critical salinity

x1 and x2 depends only on initial oil concentration (c).

$$x1_j := e^{-\left[\ln(OS(c_j)) - \left(\frac{2 \cdot L}{\xi(c_j) - L} \right) + \left(\frac{2 \cdot L}{Rw} \right) \right]}$$

$$x2_j := e^{-\left[\ln(OS(c_j)) - \left(\frac{2 \cdot L}{Ro} \right) + \left(\frac{2 \cdot L}{\xi(c_j) - 10} \right) \right]}$$

for limonene only:

$$x1_0 = 3.248$$

$$x2_0 = 11.856$$

Calculate droplet radii:

Fixed salinity: no added salt (with a constant CMC)

$$x := 0.0588$$

if CMC increases, the value of no added salt would increase, but this is not accounted for in the model

the core oil radius

$$RRc_j := \frac{1}{\left(\frac{1}{L}\right) \cdot \ln\left(\frac{OS(c_j)}{x}\right) + \frac{1}{Rw}} \quad \text{Type I}$$

$$RRRc_j := \frac{1}{\left(\frac{1}{2 \cdot L}\right) \cdot \ln\left(\frac{OS(c_j)}{x}\right) + \frac{1}{\xi(c_j) - L}} \quad \text{Type III}$$

the water radius

$$RRw_j := \frac{1}{\left(\frac{1}{\xi(c_j) - L}\right) - \left(\frac{1}{2 \cdot L}\right) \cdot \ln\left(\frac{OS(c_j)}{x}\right)} \quad \text{Type III}$$

$$RRRw_j := \frac{1}{\left(\frac{1}{Ro}\right) - \left(\frac{1}{L}\right) \cdot \ln\left(\frac{OS(c_j)}{x}\right)} \quad \text{Type II}$$

Combined oil core radius function:

$$rc_j := \begin{cases} RRc_j & \text{if } x < x1_j \\ RRRc_j & \text{if } x1_j \leq x \leq x2_j \\ Ro & \text{otherwise} \end{cases}$$

Combined water radius function:

$$rw_j := \begin{cases} Rw & \text{if } x < x1_j \\ RRw_j & \text{if } x1_j \leq x \leq x2_j \\ RRRw_j & \text{otherwise} \end{cases}$$

Calculate equilibrium oil concentration (CCeq):

Choose a concentration. Fix that concentration, and calculate CCeq for different salinity values
 Choose the next concentration and calculate CCeq for different salinity values.
 Than you will end up with a matrix for CCeq(x,c).

In Mathcad use solve block to calculate CCeq(x,c) matrix:

Initial guess for solve block: $CCeq_j := 0.0092$

Variables: CCeq depends on both x and c, both are range variables, but now we fixed x (i.e. no added salt). In the general model both variables has to be allowed to change.

Solve block:

Given

$$CCeq_j = \frac{Vo \cdot c_j - \left[rc_j + K \cdot \left(\frac{CCeq_j}{B + CCeq_j} \right) \right] \cdot \left(\frac{A}{3} \right) \cdot \left[1 + \frac{(rc_j)^3 \cdot (CCeq_j - 1)}{\left[rc_j + K \cdot \left(\frac{CCeq_j}{B + CCeq_j} \right) \right]^3} \right]}{\left[Vo - \left[rc_j + K \cdot \left(\frac{CCeq_j}{B + CCeq_j} \right) \right] \cdot \frac{A}{3} \right]}$$

FF_j := Find(CCeq_j) This is the solution vector.

CCeq_j := FF_j

Here CCeq(c) is the calculated equilibrium oil concentration when only c is allowed to change.

This is the dodecanol concentration in volume fraction in the excess oil phase at equilibrium.

Calculate shell thickness at no added salt:

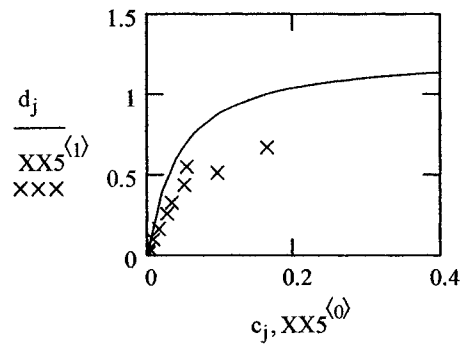
$$d_j := \frac{K \cdot CCeq_j}{B + CCeq_j}$$

XX 5 below is the experimental shell thickness at no added salt as a function of bulk dodecanol concentration . The 1st column in the bulk dodecanol concentration in the excess oil at equilibrium in volume fraction, and the 2nd column is the shell thickness.

XX5 :=

0.001036686	0.015429983
0.00143622	0.019243586
0.002408895	0.017829763
0.003708469	0.040515928
0.008270321	0.098653441
0.016201195	0.164149733
0.027596736	0.261321904
0.034052494	0.328705988
0.051347483	0.436418218
0.054480404	0.549566452
0.096268679	0.513851052
0.163711777	0.668928334

Plot of experimental and model shell thickness as a function of bulk dodecanol concentration at equilibrium:



Oil Solubilization Results

Calculate the average dodecanol concentration in the micellar oil:

$$Cave_j := \left[1 + \frac{(rc_j)^3 \cdot (CCCe_{q_j} - 1)}{\left[rc_j + K \cdot \left(\frac{CCCe_{q_j}}{B + CCCe_{q_j}} \right) \right]^3} \right]$$

Calculate selectivity :

$$\text{Sel}_j := \frac{\text{Cave}_j}{\text{CCCeq}_j}$$

Total solubilized water volume in surfactant macro phase:

$$vw_j := rw_j \cdot \frac{A}{3}$$

Total solubilized oil volume in surfactant macro phase:

$$vo_j := (rc_j + d_j) \cdot \frac{A}{3}$$

Total volume of microemulsion phase:

$$vs_j := vw_j + vo_j + Vs$$

Total solubilized oil concentration in microemulsion phase in ppm units:

$$C_j := \frac{vo_j \cdot 10^6}{vs_j}$$

This is what we get from measured dodecanol and limonene concentration using GC from a sample, taken from the microemulsion phase

Experimental data:

XX11 is the total oil solubilization in the microemulsion phase in ppm units as a function of the equilibrium dodecanol concentration in the excess oil phase.

X3 is the selectivity as a function of the equilibrium dodecanol concentration in the excess oil phase.

X2 is the average dodecanol volume fraction in the solubilized oil as a function of the equilibrium dodecanol concentration in the excess oil phase.

Total solubilization

XX11 :=

0	1885.016924
0.071496922	7564.719109
0.096435709	8329.816025
0.113382675	9384.090287
0.135018278	10331.85386
0.153976036	10884.32402
0.173805225	11139.36086
0.177388414	11160.02541
0.207655279	12500.12932
0.409192486	7185.167749
1	2415.398993
0.001134744	1867.585563
0.001565172	1948.597943
0.002558927	1785.271173
0.00404519	2157.960992
0.00908518	2695.302386
0.017615349	3365.025362
0.02977632	4542.174349
0.036817302	5240.330024
0.054643735	6396.40852
0.059131622	7427.409985
0.099597909	8128.942586
0.166759174	11522.39463

Selectivity

X3 :=

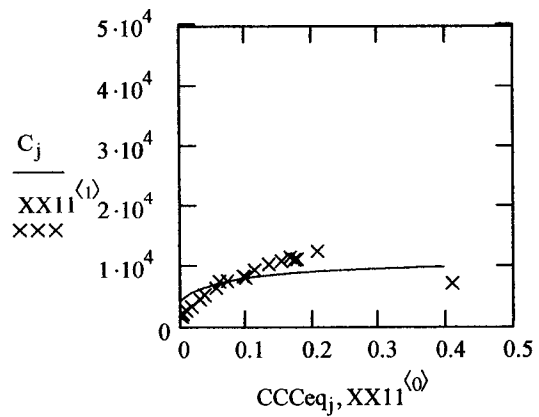
0.071496922	5.241836391
0.096435709	4.014293468
0.113382675	3.567957619
0.135018278	2.966093441
0.153976036	2.633013425
0.173805225	2.359110225
0.177388414	2.402764927
0.207655279	2.191537776
0.409192486	1.367812151
1	1
0.001036686	49.54511026
0.00143622	42.74067914
0.002408895	26.16570119
0.003708469	31.16168261
0.008270321	26.38304856
0.016201195	17.81780374
0.027596736	12.41682634
0.034052494	10.9698872
0.051347483	8.100162406
0.054480404	8.161261798
0.096268679	4.541303435
0.163711777	2.927901631

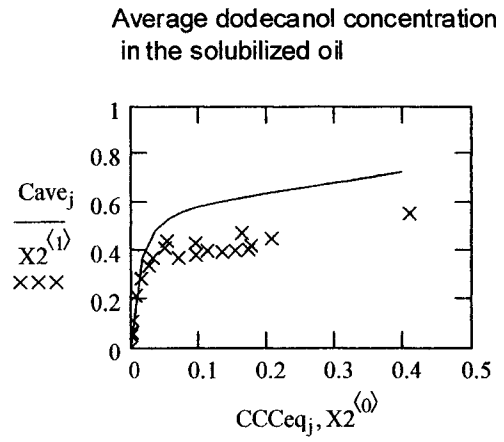
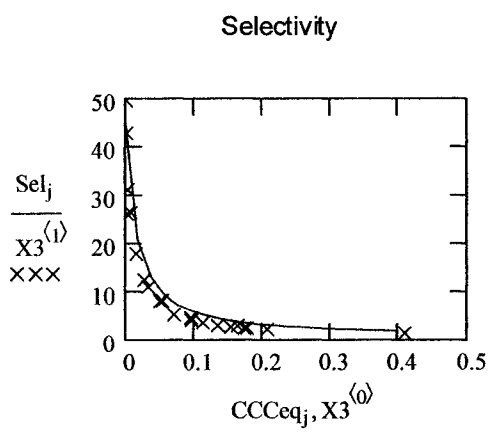
Cave

	0	0
	0.071496922	0.374775167
	0.096435709	0.387121235
	0.113382675	0.404544578
	0.135018278	0.400476829
	0.153976036	0.40542097
	0.173805225	0.410025683
	0.177388414	0.426222661
	0.207655279	0.455084389
	0.409192486	0.559698454
	1	1
X2 :=	0.001036686	0.051362699
	0.00143622	0.061385
	0.002408895	0.063030415
	0.003708469	0.115562122
	0.008270321	0.218196292
	0.016201195	0.28866971
	0.027596736	0.342663877
	0.034052494	0.373552018
	0.051347483	0.415922949
	0.054480404	0.444628841
	0.096268679	0.437185283
	0.163711777	0.479331979

Plot of experimental data and model results:

total oil solubilization in the microemulsion





Fractional decrease of dodecanol concentration in excess oil phase vs. initial concentration:

Model prediction :
$$\frac{c_j - CCCeq_j}{c_j}$$

Experimental data:

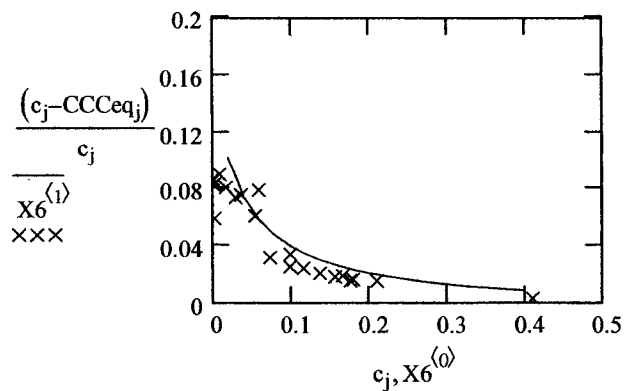
X6; 1st column is the fractional dodecanol concentration decrease in the excess oil phase between initial and equilibrium states, and the 2nd column is the initial dodecanol concentration in the oil phase in volume fraction

fractional dodecanol loss
from excess oil phase

0.073808624	0.031320217
0.098877404	0.024694174
0.116140847	0.023748514
0.13778959	0.020112635
0.15674296	0.017652622
0.176466211	0.015079298
0.180196752	0.01558484
0.210787326	0.014858801
0.410281723	0.002654851
1	0
0.001134744	0.086414495
0.001565172	0.082388842
0.002558927	0.05863098
0.00404519	0.08324005
0.00908518	0.089690981
0.017615349	0.080279663
0.02977632	0.073198567
0.036817302	0.075095357
0.054643735	0.06032261
0.059131622	0.078658717
0.099597909	0.033426707
0.166759174	0.018274237

X6 :=

Plot of model and data:



Initial versus bulk oil composition

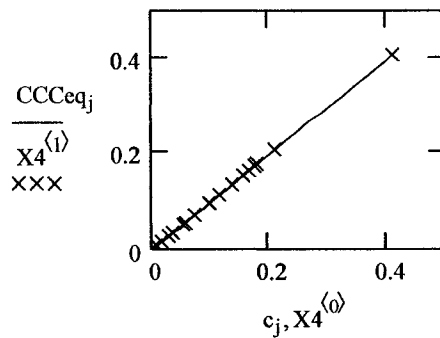
Experimental data: X4.

The 1st column is the initial dodecanol concentration in equilibrium, the 2nd column is the dodecanol volume fraction in the excess oil at equilibrium

Initial vs. equilibrium oil phase volume fraction

	0	0
	0.073808624	0.071496922
	0.098877404	0.096435709
	0.116140847	0.113382675
	0.13778959	0.135018278
	0.15674296	0.153976036
	0.176466211	0.173805225
	0.180196752	0.177388414
	0.210787326	0.207655279
	0.410281723	0.409192486
	1	1
X4 :=	0.001134744	0.001036686
	0.001565172	0.00143622
	0.002558927	0.002408895
	0.00404519	0.003708469
	0.00908518	0.008270321
	0.017615349	0.016201195
	0.02977632	0.027596736
	0.036817302	0.034052494
	0.054643735	0.051347483
	0.059131622	0.054480404
	0.099597909	0.096268679
	0.166759174	0.163711777

Model and data plotted: equilibrium vs. initial dodecanol volume fraction in the oil phase



APPENDIX F

ACETONE-TCE MIXTURE EXPERIMENTAL DATA

Partitioning of acetone and TCE in acetone-TCE-water mixtures without surfactant:

Total volume of acetone +TCE mixture is 5 ml, and total volume of water is 5 ml. All of the mixtures reached 2 phase equilibrium. The two phases are the water phase and the oil phase. Concentration of acetone is measured in both phases, concentration of TCE is measured only in the water phase.

Acetone concentration in oil phase, ppm	Acetone concentration in water phase, ppm	TCE concentration in oil phase, ppm
0	0	924
3746	3945	955
7186	7381	908
19726	20137	714
27205	30118	598
34901	36897	824
57347	60212	899
84633	87152	795
3587	3029	1109
16521	15733	1085
33489	32006	1001
54348	59072	935
64700	72856	1020

Partitioning of acetone and TCE in water / TCE-acetone oil mixture / surfactant systems:

The surfactant is sodium dihexyl sulfosuccinate, at constant aqueous concentration of 2 wt %. The aqueous surfactant solution also contains NaCl at constant concentration of 0.8948 wt%.

Acetone concentration in oil phase, ppm	Acetone concentration in water phase, ppm	TCE concentration in oil phase, ppm
0	0	15000
4241	3506	25022
7867	5858	21495
20331	19809	21716
31139	28381	17487
31244	28078	16282
66366	57644	10958
108583	95850	4931

Concentration of acetone and TCE in the various phases as a function of salinity:

The initial acetone concentration was constant, 5 volume % in the TCE-acetone oil mixture. The sodium dihexyl sulfosuccinate surfactant concentration was also constant in the aqueous phase, 2 wt%. The aqueous phase salinity was varied. The water-to-oil ratio was 1. Two and three phase equilibria were reached depending on the salinity.

Salinity wt %	Acetone concentration in the oil phase, ppm	Acetone concentration in the middle phase, ppm	TCE concentration in the middle phase, ppm	Acetone concentration in the water phase, ppm	TCE concentration in the water phase, ppm
0.038	14820			15980	2327
0.2233	11008			8362	1528
0.4466	13793			13352	3146
0.6699	14381			14679	5580
0.8932	15946			15180	7968
1.1165	14726			15053	5592
1.3398	10474	11443	154787	13111	2789
1.5631	12772	26105	718036	15909	465
1.7864	13373			15262	431
2.0097	12229			14634	832

Phase behavior data with varying salinity and initial acetone concentration:

The aqueous sodium dihexyl sulfosuccinate surfactant concentration was constant, 2 wt%. The oil-to-water ratio was 1, constant in each samples.

Initial acetone concentration in the oil, volume %	Experimental optimum salinity, aqueous NaCl wt %	Middle phase volume measured in vial closest to optimum, % total system volume
0	1.56	11.43
1	1.43	8.57
2	1.34	10.00
7.5	1.34	7.86
15	1.56	8.57
25	1.82	5.71
10	1.39	7.50

Interfacial tension data:

The aqueous surfactant solution contained 0.89 wt% NaCl in each vials. The water-to-oil ratio was 1, constant in each vial. The temperature was 27 C.

Surfactant concentration, wt %	IFT (dyne / cm)				
	0 % acetone	1 % acetone	5% acetone	15% acetone	25% acetone
2	0.1500	0.2031	0.2104	0.1500	0.4583
1.6	0.1645	0.2062	0.1082	0.1459	0.3203
1.2	0.1443	0.2120	0.2594	0.1279	0.6556
0.8	0.1944	0.2235	0.2420	0.5185	0.8845
0.4	2.0067	0.7518	1.2785	2.9252	3.0142
0.2	7.3183	4.6974	5.6970	6.5962	4.0553
0.1	12.7565	9.2720	9.9825	9.3072	5.8692
0.06	17.2232	13.1018	14.1867	12.6727	8.7139
0.00001	31.9798	32.1016	27.4006	19.6285	14.5164

APPENDIX G

Benzene-Limonene Mixture Experimental Data

Partitioning of benzene and limonene in benzene-limonene-water mixtures

Initial benzene volume fraction in oil	Benzene concentration in water phase, ppm	Limonene concentration in water phase, ppm
0	0	16.7
0.021	30	30
0.033	62	2.7
0.09	170	4
0.19	358	16
0.39	736	24.8
0.64	1208	0
0.78	1466	26
1	1410	0

Benzene and limonene concentration in benzene-limonene-water-surfactant mixtures

Data for 0 initial benzene volume fraction in the oil phase

Added aqueous NaCl concentration, wt %	Benzene concentration in surfactant phase, ppm	Limonene concentration in surfactant phase, ppm	Benzene concentration in excess oil phase, ppm	Limonene concentration in excess oil phase, ppm
0	0	2049.234651	0	1
0.78	0	5640.289752	0	1
1.56	0	9959.611634	0	1
2.34	0	9591.693193	0	1
3.12	0	29670.14959	0	1
3.9	0	98935.11032	0	1
4.68	0	237502.266	0	1
5.46	0	354086.331	0	1
6.24	0	454990.1748	0	1
7.02	0	537944.0364	0	1
7.8	0	507982.6845	0	1
8.58	0	705349.102	0	1

Data for 0.021 initial benzene volume fraction in the oil phase

Added aqueous NaCl concentration, wt %	Benzene concentration in surfactant phase, ppm	Limonene concentration in surfactant phase, ppm	Benzene concentration in excess oil phase, ppm
0.00	210.49	1861.91	21031.82
0.62	286.94	5130.66	18888.17
1.24	421.05	10859.95	20154.30
1.85	610.76	16133.31	20866.99
2.47	694.45	20937.98	20386.84
3.09	881.12	29650.25	19191.29
3.71	2989.29	98013.45	
4.33	6875.69	266131.31	21566.05
4.95	6590.30	327539.91	23549.93
5.56	8070.87	342969.66	
6.18	10026.74	427736.34	18156.18
6.80	13733.20	532748.66	21479.13
7.42	12142.22	539009.93	18134.03
8.04	13141.19	525087.68	

Data for 0.033 initial benzene volume fraction in the oil phase

Added aqueous NaCl concentration, wt %	Benzene concentration in surfactant phase, ppm	Limonene concentration in surfactant phase, ppm	Benzene concentration in excess oil phase, ppm	Limonene concentration in excess oil phase, ppm
0	289.1250554	2340.889874	32950.77299	979306.4168
0.595886484	417.673621	4834.856766	32943.92439	1009720.827
1.191772968	292.1794946	4619.464156	32770.5467	1016373.839
1.787659452	682.2393838	11878.34359	32770.5467	1016373.839
2.383545936	470.2634908	9824.145114	33921.29157	1052181.476
2.97943242	1157.44677	24086.11251	35507.46317	1058433.826
3.575318905	1349.297586	31604.85845	32848.40446	1009049.129
4.171205389	5489.666545	139775.7526	33399.53646	975241.9966
4.767091873	9548.674075	244691.7948	33002.13748	964177.7728
5.362978357	12760.89144	347848.4285	31334.86406	936685.8393
5.958864841	14130.82248	378597.7762	35437.17492	1088994.136
6.554751325	15317.36769	409301.2985	30920.34358	909325.2153
7.150637809	16259.9402	434176.2908	32458.21453	1041822.62
7.746524293	16636.10239	427650.5412	32507.41631	1001987.599

Data for 0.09 initial benzene volume fraction in the oil phase

Added aqueous NaCl concentration, wt %	Benzene concentration in surfactant phase, ppm	Limonene concentration in surfactant phase, ppm	Benzene concentration in excess oil phase, ppm	Limonene concentration in excess oil phase, ppm
0.00	748.67	1754.51	90917.58	1014314.73
0.54	1486.51	6100.61	94090.68	869244.53
1.08	2032.97	10730.51	102974.88	899942.06
1.61	2463.88	14037.52	100677.65	969810.58
2.15	3092.66	19116.37	103731.52	998846.90
2.69	3652.15	22533.85	93443.52	876575.72
3.23	4411.64	31870.46	105230.40	1085594.86
3.77	17062.76	140198.18	95276.78	1083859.16
4.30	30163.90	239448.29	106131.68	1104185.79
4.84	33425.53	271396.19	110279.53	1171437.39
5.38	40065.78	342089.33	110280.80	1341410.97
5.92	44733.20	360030.33	114033.29	1242096.72
6.46	53117.01	468413.23	104028.21	944873.45
6.99	51721.23	455443.47	91892.76	973147.62

Data for 0.19 initial benzene volume fraction in the oil phase

Added aqueous NaCl concentration, wt %	Benzene concentration in surfactant phase, ppm	Limonene concentration in surfactant phase, ppm	Benzene concentration in excess oil phase, ppm	Limonene concentration in excess oil phase, ppm
0.00	1626	2831	181582	833840
0.44	2441	4435	158636	670645
0.88	3471	8319	179943	749559
1.32	4115	11273	183660	859114
1.75	6056	20439	205003	970602
2.19	7205	22426	186617	867153
2.63	9474	33649	181933	847268
3.07	10960	38138	190543	822766
3.51	58192	225025	193544	884745
3.95	97188	427043	194312	960158
4.38	87668	312424	189082	877766
4.82	114954	505485	156450	1170356
5.26	118708	436027	203879	1023083
5.70	117759	423612	176482	837934

Data for 0.39 initial benzene volume fraction in the oil phase

Added aqueous NaCl concentration, wt %	Benzene concentration in surfactant phase, ppm	Limonene concentration in surfactant phase, ppm	Benzene concentration in excess oil phase, ppm	Limonene concentration in excess oil phase, ppm
0.00	3107	1962	328696	533231
0.36	4621	3472	336086	503091
0.71	6503	5731	333884	545956
1.07	9241	10474	328028	529138
1.43	12731	13875	348170	551075
1.79	13650	10730	338519	532370
2.14	19511	24809	338021	562357
2.50	23436	26619	344372	539537
2.86	93249	126487	344875	600210
3.22	144637	189634	343820	501313
3.57	287227	390875	325077	571301
3.93	201329	293803	334251	510111
4.29	222570	322368	345242	487500
4.64	268553	382416	331592	549961

Data for 0.64 initial benzene volume fraction in the oil phase

Added aqueous NaCl concentration, wt %	Benzene concentration in surfactant phase, ppm	Limonene concentration in surfactant phase, ppm	Benzene concentration in excess oil phase, ppm	Limonene concentration in excess oil phase, ppm
0.00	3295	1219	524746	333018
0.29	5238	2107	565184	387672
0.58	7353	3281	534885	302060
0.87	12373	6280	540914	314027
1.16	15661	8060	569581	390182
1.46	18490	10603	551056	390297
1.75	28947	15526	547297	346332
2.04	39171	20452	534270	301441
2.33	155727	81803	530714	310821
2.62	248392	139308	528449	351127
2.91	331196	197816	551092	369018
3.20	339564	174621	540207	336325
3.49	578920	311276		
3.78	565741	353029		

Data for 0.78 initial benzene volume fraction in the oil phase

Added aqueous NaCl concentration, wt %	Benzene concentration in surfactant phase, ppm	Limonene concentration in surfactant phase, ppm	Benzene concentration in excess oil phase, ppm	Limonene concentration in excess oil phase, ppm
0	5804	1483	615514	150553
0.26	5881	1563	636821	145855
0.53	9746	2130	630431	180066
0.79	12350	3081	637067	211539
1.05	17345	4440	615284	176301
1.31	23541	4413	557734	150254
1.58	29504	6743	603327	151751
1.84	39909	8470	564916	154931
2.10	160612	38092	535888	153604
2.37	243527	62800	567620	147205
2.63	356316	91688	578500	139622
2.89	392015	116918	573026	147274
3.15	149580	247990	548980	174211
3.42	244410	34635		

Data for 1.0 initial benzene volume fraction in the oil phase

Added aqueous NaCl concentration, wt %	Benzene concentration in surfactant phase, ppm	Limonene concentration in surfactant phase, ppm	Benzene concentration in excess oil phase, ppm	Limonene concentration in excess oil phase, ppm
0	7200.731843	0	1	0
0.237263227	10631.85319	0	1	0
0.474526453	15025.39511	0	1	0
0.71178968	20089.02784	0	1	0
0.949052907	27883.68868	0	1	0
1.186316133	34276.95635	0	1	0
1.42357936	53806.60226	0	1	0
1.660842587		0	1	0
1.898105814	339249.1949	0	1	0
2.13536904	515052.6159	0	1	0
2.372632267	715805.7717	0	1	0
2.609895494	903714.8476	0	1	0

Optimum salinity and optimum middle phase volume, and shell thickness data

Initial benzene volume fraction in oil	Equilibrium average benzene volume fraction in excess oil	Optimum salinity, NaCl wt %	Optimum middle phase volume, ml	Average shell thickness, Angstroms
0	0	6.2	0.714	0
0.021	0.018	6	0.786	0.05
0.033	0.0315	5.9	0.857	0.06
0.09	0.086	5.37	0.929	0.18
0.19	0.16	4.5	1.002	0.35
0.39	0.362	3.57	1.143	0.5
0.64	0.617	2.7	1.357	0.6
0.78	0.76	2.57	1.429	0.61
1	1	2.04	1.457	0.7

APPENDIX H

DODECANOL-LIMONENE MIXTURE EXPERIMENTAL DATA

Dodecanol and Limonene Concentration data

Initial dodecanol concentration in oil phase 0.0092 volume fraction

Added aqueous NaCl concentration, wt %	Dodecanol concentration in excess oil, ppm	Dodecanol concentration in surfactant phase, ppm	Limonene concentration in surfactant phase, ppm
0	8733	415	1895
0.49	9154	865	4835
0.97	8030	1049	7987
1.46	9497	1211	11633
1.94	8365	1487	16407
2.43	8120	1564	23086
2.91	8093	1532	28926
3.40	8049	1583	37649
3.88	8093	2234	48982
4.37	8014	8690	233059
4.85	6469	9307	298662
5.34	8538	10759	359509
5.82	7726	14588	405160
6.31	7486	14193	473881

Initial dodecanol concentration in the oil phase 0.0183 volume fraction

Added aqueous NaCl concentration, wt %	Dodecanol concentration in excess oil, ppm	Dodecanol concentration in surfactant phase, ppm	Limonene concentration in surfactant phase, ppm
0	18493	899	2488
0.36	16624	1355	5453
0.72	15837	1994	9371
1.08	16738	2520	13732
1.45	15577	2405	19086
1.81	13815	2735	26310
2.17	14634	2909	34904
2.53	17830	3836	41828
2.89	16094	3853	58666
3.25	14801	15768	261072
3.61	15084	21891	354201
3.97	15980	22696	424522
4.34	15472	20944	496244
4.70	15616	23387	577559

Initial dodecanol concentration in the oil phase 0.03 volume fraction

Added aqueous NaCl concentration, wt %	Dodecanol concentration in excess oil, ppm	Dodecanol concentration in surfactant phase, ppm	Limonene concentration in surfactant phase, ppm
0	26673	1290	2608
0.27	26378	1990	5191
0.54	26791	2730	8316
0.81	25491	3358	12206
1.07	27646	3724	16560
1.34	25427	3562	21130
1.61	28922	4112	28798
1.88	22917	4512	36726
2.15	28704	4682	46016
2.42	24970	5005	61032
2.69	21965	15205	212020
2.96	22082	24318	357507
3.22	22556	29480	443149
3.49	22604	30780	521839

Initial dodecanol concentration in the oil phase 0.044 volume fraction

Added aqueous NaCl concentration, wt %	Dodecanol concentration in excess oil, ppm	Dodecanol concentration in surfactant phase, ppm	Limonene concentration in surfactant phase, ppm
0	40616	1960	3209
0.20	41986	2218	5106
0.40	40901	3117	7577
0.60	39582	3737	10900
0.80	39149	4397	13392
1.00	38829	4595	18785
1.20	40618	4600	24390
1.40	37529	4909	28684
1.60	36121	5129	37085
1.79	37099	6850	49271
1.99	40904	6950	60128
2.19	34235	7868	75235
2.39	35413	27464	286404
2.59	34208	34421	408623

Initial dodecanol concentration in the oil phase 0.113 volume fraction

Added aqueous NaCl concentration, wt %	Dodecanol concentration in excess oil, ppm	Limonene concentration in excess oil, ppm	Dodecanol concentration in surfactant phase, ppm	Limonene concentration in surfactant phase, ppm
0	116126	1050088	2806	5846
0.11	124260	1086881	4648	9554
0.22	123915	1020345	6184	13642
0.33	103789	988873	7120	17931
0.43	120093	1090364	6434	19687
0.54	100265	1039264	10465	28354
0.65	105686	1059002	7816	30557
0.76	110780	1102077	10415	46553
0.87	98690	990509	12716	57491
0.98	98892	1006752	13999	79518
1.09	90473	1007775	41283	304357
1.20	93401	939943	90952	913796
1.30	96179	1006324	83319	1006560
1.41	95595	960317	95779	941780

Dodecanol adsorption study data

Initial aqueous surfactant concentration was 4 wt % in each vial, with no added NaCl. Experiments were carried out at room temperature.

Dodecanol and limonene concentration results:

Initial dodecanol concentration in oil phase, volume fraction	Equilibrium dodecanol concentration in excess oil, volume fraction	Dodecanol concentration in surfactant phase, ppm	Limonene concentration in surfactant phase, ppm
0	0	0	1885
0.08142	0.07150	2835	4730
0.11114	0.09644	3225	5105
0.13139	0.11338	3796	5588
0.15413	0.13502	4138	6194
0.17034	0.15398	4413	6472
0.19238	0.17381	4567	6572
0.20675	0.17739	4757	6403
0.26547	0.20766	5689	6812
0.54789	0.40919	4022	3164
1	1	2415	0
0.00113	0.00104	96	1772
0.00157	0.00144	120	1829
0.00256	0.00241	113	1673
0.00405	0.00371	249	1909
0.00909	0.00827	588	2107
0.01762	0.01620	971	2394
0.02978	0.02760	1556	2986
0.03682	0.03405	1958	3283
0.05464	0.05135	2660	3736
0.05913	0.05448	3302	4125
0.09960	0.09627	3554	4575
0.16676	0.16371	5523	5999

Surfactant concentration and interfacial tension data:

These measurements were carried out using the adsorption experiment sample series. Surfactant concentration was measured only at higher dodecanol concentrations.

Equilibrium dodecanol concentration in excess oil, volume fraction	Surfactant concentration in the aqueous phase, ppm	Interfacial tension, dyne/cm
0	40933	3.5302
0.07150	40547	1.0326
0.09644	40933	0.8086
0.11338	40504	0.6684
0.13502	40135	0.6217
0.15398	40166	0.5699
0.17381	39871	0.4657
0.17739	39433	0.4144
0.20766	37450	0.3013
0.40919	22121	0.1450
1	12102	0.8435
0.00104		3.2400
0.00144		3.2123
0.00241		3.1630
0.00371		2.9164
0.00827		2.5923
0.01620		2.3046
0.02760		1.9116
0.03405		1.6176
0.05135		1.3174
0.05448		1.2004
0.09627		1.0996
0.16371		0.7254

APPENDIX I

BENZENE-LIMONENE COLUMN STUDY EXPERIMENTAL DATA

Column study parameters

Column diameter (cm)	2.5
Column length (cm)	15
Packing material	Glass beads
Experimental effective pore volume (ml)	37.4
Experimental porosity	0.508
Column study flow rate (ml/min)	2.0
Maximum pre-column study flow rate (ml/min)	21
Experimental water permeability (up to 21 ml/min flow rate)	

Column study breakthrough curves

Column is contaminated with 0.1 volume fraction benzene – 0.9 volume fraction limonene mixture in upward flow mode. After complete organic saturation the flow direction is switched to downward flush mode. The column is flushed with DI water with variable flow rate for 3 hours. The flow rate is increased stepwise between 1 ml/min to 21 ml/min. Each flow rate steps are continued until no two-phase flow is detected. After the highest flow rate, 21 ml/min is reached, and the separate organic phase flow stopped the column was flushed for 1 more hour to ensure that the organic phase saturation of the column is close to the residual saturation. Next the surfactant flush was started with 2 ml/min flow rate.

Organic concentrations were measured 24 hours after the column study was finished.

Pore volume (ml)	Effluent limonene concentration, ppm	Effluent benzene concentration, ppm
0.00	0.10	64.34
0.08	0.10	33.61
0.16	0.10	59.62
0.21	0.10	27.84
0.27	0.10	39.05
0.32	0.10	35.56
0.37	0.10	36.80
0.43	0.10	33.73
0.75	0.10	26.96
0.80	0.10	32.00
0.85	0.10	60.12
0.91	0.10	37.62
0.96	0.10	46.56
1.01	585.65	49.04
1.07	1113.82	90.42
1.12	1464.92	115.53
1.17	1248.11	117.83
1.23	1611.73	156.58
1.28	1422.88	144.85
1.33	1317.16	150.68
1.39	1387.49	129.53
1.44	1368.10	109.93
1.49	1546.38	105.99
1.55	1182.83	87.32
1.60	1266.39	100.02
1.65	1099.44	97.83
1.71	1149.96	69.93
1.76	1102.05	68.57
1.81	1129.66	92.61
1.87	1277.29	109.00
1.92	1005.89	92.37
1.97	1034.54	86.64
2.03	1095.30	99.87
2.08	1183.08	91.29
2.13	1332.53	101.45
2.19	1238.62	95.72
2.24	1239.17	105.66
2.29	1414.50	117.88
2.35	1184.31	95.65